AGARD-AG-300 Vol.3 Part 2

AGARD

ADVISORY GROUP FOR AEROSPACE RESEARCH & DEVELOPMENT
7 RUE ANCELLE 92200 NEUILLY SUR SEINE FRANCE

AGARDograph 300
Flight Test Techniques Series - Volume 3

on

Identification of Dynamic Systems – Applications to Aircraft Part 2: Nonlinear Analysis and Manoeuvre Design

(L'Identification des Systèmes Dynamiques – Applications aux aéronefs Titre 2: L'analyse non-linéaire et la conception de la manoeuvre)

This AGARDograph has been sponsored by the Flight Mechanics Panel of AGARD.

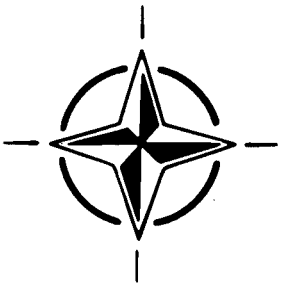

NORTH ATLANTIC TREATY ORGANIZATION

Published May 1994

AGARD-AG-300 Vol.3 Part 2

AGARD
ADVISORY GROUP FOR AEROSPACE RESEARCH & DEVELOPMENT
7 RUE ANCELLE 92200 NEUILLY SUR SEINE FRANCE

AGARDograph 300
Flight Test Techniques Series - Volume 3

on

Identification of Dynamic Systems – Applications to Aircraft Part 2: Nonlinear Analysis and Manoeuvre Design

(L'Identification des Systèmes Dynamiques –
Applications aux aéronefs
Titre 2: L'analyse non-linéaire et la conception de la manoeuvre)

by

J.A. Mulder and **J.K. Sridhar**
Faculty of Aerospace Engineering
Delft University of Technology
Kluyverweg 1, 2629 HS Delft
The Netherlands

J.H. Breeman
Flight Instrumentation Division
National Aerospace Laboratory
Anthony Fokkerweg 2, 1059 CM Amsterdam
The Netherlands

This AGARDograph has been sponsored by the Flight Mechanics Panel of AGARD.

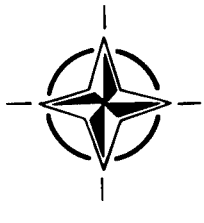

North Atlantic Treaty Organization
Organisation du Traité de l'Atlantique Nord

The Mission of AGARD

According to its Charter, the mission of AGARD is to bring together the leading personalities of the NATO nations in the fields of science and technology relating to aerospace for the following purposes:

- Recommending effective ways for the member nations to use their research and development capabilities for the common benefit of the NATO community;
- Providing scientific and technical advice and assistance to the Military Committee in the field of aerospace research and development (with particular regard to its military application);
- Continuously stimulating advances in the aerospace sciences relevant to strengthening the common defence posture;
- Improving the co-operation among member nations in aerospace research and development;
- Exchange of scientific and technical information;
- Providing assistance to member nations for the purpose of increasing their scientific and technical potential;
- Rendering scientific and technical assistance, as requested, to other NATO bodies and to member nations in connection with research and development problems in the aerospace field.

The highest authority within AGARD is the National Delegates Board consisting of officially appointed senior representatives from each member nation. The mission of AGARD is carried out through the Panels which are composed of experts appointed by the National Delegates, the Consultant and Exchange Programme and the Aerospace Applications Studies Programme. The results of AGARD work are reported to the member nations and the NATO Authorities through the AGARD series of publications of which this is one.

Participation in AGARD activities is by invitation only and is normally limited to citizens of the NATO nations.

Published May 1994

ISBN 92-835-0748-7

Printed by Specialised Printing Services Limited
40 Chigwell Lane, Loughton, Essex IG10 3TZ

Preface

Since its founding in 1952, the Advisory Group for Aerospace Research and Development has published, through the Flight Mechanics Panel, a number of standard texts in the field of flight testing. The original Flight Test Manual was published in the years 1954 to 1956. The Manual was divided into four volumes:

1. Performance
2. Stability and Control
3. Instrumentation Catalog, and
4. Instrumentation Systems.

As a result of developments in the field test instrumentation, the Flight Test Instrumentation Group of the Flight Mechanics Panel was established in 1968 to update Volumes 3 and 4 of the Flight Test Manual by the publication of the Flight Test Instrumentation Series, AGARDograph 160. In its published volumes AGARDograph 160 has covered recent developments in flight test instrumentation.

In 1978, the Flight Mechanics Panel decided that further specialist monographs should he published covering aspects of Volumes 1 and 2 of the original Flight Test Manual, including the flight testing of aircraft systems. In March 1981, the Flight Test Techniques Group was established to carry out this task. The monographs of this series (with the exception of AG 237 which was separately numbered) are being published as individually numbered volumes of AGARDograph 300.

In 1993 the FTTG was disbanded, and the Flight Test Editorial Committee was formed to continue sponsoring and editing volumes in the AG 160 and AG 300 series.

At the end of each volume of both AGARDograph 160 and AGARDograph 300 an Annex gives a list of volumes published in the Flight Test Instrumentation Series (AG 160) and in the Flight Test Techniques Series (AG 300).

The present Volume is a sequel to two previous AGARDographs published in the AGARD Flight Test Techniques Series, Volume 2 on "Identification of Dynamic Systems" and Volume 3 on "Identification of Dynamic Systems – Applications to Aircraft, Part 1: The Output Error Approach" both written by R.E. Maine and K.W. Iliff. The intention of the present document is to cover some of those areas which were either absent or only briefly mentioned in these volumes. These areas are Flight Path Reconstruction, Nonlinear Model Identification, Optimal Input Design and Flight Test Instrumentation.

The theoretical developments are illustrated with examples taken from an actual flight test program.

Préface

Depuis sa création en 1952, le Groupe Consultatif pour la Recherche et les Réalisations Aérospatiales (AGARD), a publié, par l'intermédiaire du Panel de la Mécanique du Vol, un certain nombre de textes normatifs dans le domaine des essais en vol. Le premier Manuel d'Essais en Vol a été publié entre les années 1954 et 1956. Ce manuel est composé de quatre volumes à savoir:

1. Performances
2. Stabilité et Contrôle
3. Catalogue d'Instrumentation
4. Systèmes d'Instrumentation.

Suite aux développements dans le domaine de l'instrumentation des essais en vol, le Groupe de Travail sur l'Instrumentation des Essais en Vol du Panel de la Mécanique du Vol a été créé en 1968 avec pour mandat de mettre à jour les volumes 3 et 4 du Manuel des Essais en Vol, sous la forme de la série AGARDographie 160 sur l'Instrumentation des Essais en Vol. Les différents volumes de l'AGARDographie 160 publiés jusqu'à ce jour couvrent les derniers développements dans ce domaine.

En 1978, le Panel AGARD de la Mécanique du Vol a décidé d'éditer d'autres monographies spécialisées, couvrant les volumes 1 et 2 du Manuel des Essais en Vol d'origine, y compris les Essais en Vol des systèmes de bord. Au mois de mars 1981, le Groupe de Travail sur les Techniques des Essais en Vol a été constitué pour mener à bien cette tâche. Les monographies dans cette série, à l'exception de l'AG 237 qui porte un numéro distinct, sont numérotées individuellement dans la série AG 300.

Le groupe a été dissout en 1993, et le Comité de Rédaction des Essais en Vol a été créé afin d'assurer la publication de volumes dans les séries AG 160 et AG 300.

A la fin de chacun de ces volumes, un annexe donne la liste des volumes publiés dans la série "Instrumentation des Essais en Vol" (AG 160) et dans la série "Techniques des Essais en Vol" (AG 300).

Le présent volume représente la suite de deux AGARDographies publiées dans la série "Techniques des Essais en Vol"; il s'agit du volume 2 sur "L'Identification des Systèmes Dynamiques" et du Volume 3 sur "L'Identification des Systèmes Dynamiques – Applications aux Aéronefs" Titre 1: "La Méthode des Ecarts de Performances" rédigés par R.E. Maine et K.W. Iliff. Ce document a pour objet de traiter certains sujets qui ont été peu ou pas abordés dans ces volumes, c'est-à-dire, la reconstitution de la trajectoire de vol, l'identification des modèles non-linéaires, l'optimalisation des éléments de conception et l'instrumentation des essais en vol.

Les développements théoriques sont illustrés par des exemples tirés d'un programme d'essais en vol réel.

Acknowledgements

ACKNOWLEDGEMENT TO WORKING GROUP 11 MEMBERS

In the preparation of the present volume the members of the Flight Test Techniques Group listed below took an active part. AGARD has been most fortunate in finding these competent people willing to contribute their knowledge and time in the preparation of this and other volumes.

La liste des membres du groupe de travail sur les techniques des essais en vol ont participé activement à la rédaction de ce volume figure ci-dessous. L'AGARD peut être fier que ces personnes compétentes aient bien voulu accepter de partager leurs connaissances et aient consacré le temps nécessaire à l'élaboration de ce et autres documents.

Appleford, J.K.	A&AEE/UK
Bever, G.	NASA/US
Bogue, R.K.	NASA/US
Bothe, H.	DLR/GE
Campos, L.M.B.	IST/PO
Delle Chiaie, S.	DASRS/IT
Russell, R.A.	NATC/US
van der Velde, R.L.	NLR/NE
Zundel, Y.	CEV/FR

R.R. HILDEBRAND, AFFTC
Member, Flight Mechanics Panel
Chairman, Flight Test Editorial Committee

ACKNOWLEDGEMENT BY THE AUTHORS

The authors are grateful to the following experts for their keen interest in reading the report and offering many constructive suggestions and useful comments:

Prof. Vladislav Klein, JIAFS/NASA Langley Research Center, The George Washington University, United States

Dr Richard Maine, NASA Dryden Flight Research Facility, Edwards, California, United States

Dr Jean Ross, Aircraft and Armament Evaluation Establishment, Salisbury, United Kingdom

Prof. Jaap De Leeuw, Institute of Aerospace Studies, University of Toronto, Canada

Dr Ralph Bach, NASA Ames Research Center, Moffett Field, California, United States

Dr Peter Hamel and Dr Ermin Plaetschke, German Aerospace Research Establishment (DLR), Braunschweig, Germany

Dr Mark Tischler, US Army Aero Flight Dynamics Directorate, NASA Ames Research Center, Moffett Field, California, United States.

The authors also express their gratitude to the staff of the Faculty of Aerospace Engineering of the Delft University of Technology and to the National Aerospace Laboratory, Amsterdam for support, encouragement and help received during the preparation of the report; in particular to Dr Chu Qi Ping and Research Fellow Ir C.A.A.M. van der Linden. The authors finally would like to thank the present and former members of Working Group 11 (presently called the Flight Test Editorial Committee) for their encouragement and support, in particular the chairman Mr R.R. Hildebrand and the Dutch representative Ing. R.L. van der Velde.

Contents

SYMBOL DEFINITIONS, ABBREVIATIONS AND REFERENCE FRAMES

Throughout this volume many different variables are introduced. Often the actual meaning of the symbol follows directly from the context of its use. Vectors will be generally underlined. Matrices and reference frames (reference axes) are denoted with capitals. Their use follows directly from the context.

0.1 Symbols, abbreviations, definitions

a	parameter vector; polynomial coefficient of $d(\omega)$ in denominator in $T(\omega)$
A_x, A_y, A_z	specific aerodynamic forces along the X-, Y- and Z-axis respectively
b	wing span; polynomial coefficient of $n(\omega)$ in numerator of $T(\omega)$
$\bar{c}$	mean aerodynamic chord
C	Cramer-Rao Lower Bound; rate of climb
C_{α_0}	parameter in angle of attack vane calibration formula
C_{β_0}	parameter in angle of side slip vane calibration formula
C_{si}	sidewash coefficient
C_{up}	upwash coefficient
C_ℓ	$\frac{L}{\frac{1}{2}\rho V^2 S b}$, coefficient of aerodynamic rolling moment (nondimensional moment about X_B-axis)
C_{ℓ_0}	constant part of C_ℓ
C_{ℓ_p}	$\frac{\partial C_\ell}{\partial \frac{pb}{2V}}$
C_{ℓ_r}	$\frac{\partial C_\ell}{\partial \frac{rb}{2V}}$
C_{ℓ_β}	$\frac{\partial C_\ell}{\partial \beta}$
$C_{\ell_{\dot{\beta}}}$	$\frac{\partial C_\ell}{\partial \frac{\dot{\beta} b}{V}}$
$C_{\ell_{\delta_a}}$	$\frac{\partial C_\ell}{\partial \delta_a}$
$C_{\ell_{\delta_r}}$	$\frac{\partial C_\ell}{\partial \delta_r}$
C_m	$\frac{M}{\frac{1}{2}\rho V^2 S \bar{c}}$, coefficient of aerodynamic pitching moment (nondimensional moment about Y_B-axis)
C_{m_0}	constant part of C_m
$C_{m_{\Delta p_t}}$	$\frac{\partial C_m}{\partial \frac{\Delta p_t}{\frac{1}{2}\rho V^2}}$
C_{m_q}	$\frac{\partial C_m}{\partial \frac{q\bar{c}}{V}}$
C_{m_u}	$2C_{m_0} + \frac{\partial C_m}{\partial V} V$
C_{m_α}	$\frac{\partial C_m}{\partial \alpha}$
$C_{m_{\alpha^2}}$	$\frac{\partial C_m}{\partial \alpha^2}$
$C_{m_{\dot{\alpha}}}$	$\frac{\partial C_m}{\partial \frac{\dot{\alpha}\bar{c}}{V}}$
$C_{m_{\delta_e}}$	$\frac{\partial C_m}{\partial \delta_e}$

C_n $\frac{N}{\frac{1}{2}\rho V^2 S b}$, coefficient of aerodynamic yawing moment (nondimensional moment about Z_B-axis)

C_{n_0} constant part of C_n

C_{n_p} $\frac{\partial C_n}{\partial \frac{pb}{2V}}$

C_{n_r} $\frac{\partial C_n}{\partial \frac{rb}{2V}}$

C_{n_β} $\frac{\partial C_n}{\partial \beta}$

$C_{n_{\dot{\beta}}}$ $\frac{\partial C_n}{\partial \frac{\dot{\beta} b}{V}}$

$C_{n_{\delta_a}}$ $\frac{\partial C_n}{\partial \delta_a}$

$C_{n_{\delta_r}}$ $\frac{\partial C_n}{\partial \delta_r}$

C_X $\frac{X}{\frac{1}{2}\rho V^2 S}$, coefficient of aerodynamic longitudinal force

C_{X_0} constant part of C_X

$C_{X_{\Delta p_t}}$ $\frac{\partial C_X}{\partial \frac{\Delta p_t}{\frac{1}{2}\rho V^2}}$

C_{X_q} $\frac{\partial C_X}{\partial \frac{q\bar{c}}{V}}$

C_{X_u} $2C_{X_0} + \frac{\partial C_X}{\partial V} V$

C_{X_α} $\frac{\partial C_X}{\partial \alpha}$

$C_{X_{\alpha^2}}$ $\frac{\partial C_X}{\partial \alpha^2}$

$C_{X_{\dot{\alpha}}}$ $\frac{\partial C_X}{\partial \frac{\dot{\alpha}\bar{c}}{V}}$

$C_{X_{\delta_e}}$ $\frac{\partial C_X}{\partial \delta_e}$

C_Y $\frac{Y}{\frac{1}{2}\rho V^2 S}$, coefficient of aerodynamic lateral force

C_{Y_0} constant part of C_Y

C_{Y_p} $\frac{\partial C_Y}{\partial \frac{pb}{2V}}$

C_{Y_r} $\frac{\partial C_Y}{\partial \frac{rb}{2V}}$

C_{Y_β} $\frac{\partial C_Y}{\partial \beta}$

$C_{Y_{\dot{\beta}}}$ $\frac{\partial C_Y}{\partial \frac{\dot{\beta} b}{V}}$

$C_{Y_{\delta_a}}$ $\frac{\partial C_Y}{\partial \delta_a}$

$C_{Y_{\delta_r}}$ $\frac{\partial C_Y}{\partial \delta_r}$

C_Z $\frac{Z}{\frac{1}{2}\rho V^2 S}$, coefficient of aerodynamic vertical force

C_{Z_0} constant part of C_Z

$C_{Z_{\Delta p_t}}$ $\frac{\partial C_Z}{\partial \frac{\Delta p_t}{\frac{1}{2}\rho V^2}}$

C_{Z_q} $\frac{\partial C_Z}{\partial \frac{q\bar{c}}{V}}$

C_{Z_u} $2C_{Z_0} + \frac{\partial C_Z}{\partial V} V$

C_{Z_α}	$\frac{\partial C_Z}{\partial \alpha}$
$C_{Z_{\dot{\alpha}}}$	$\frac{\partial C_Z}{\partial \frac{\dot{\alpha}\bar{c}}{V}}$
$C_{Z_{\delta_e}}$	$\frac{\partial C_Z}{\partial \delta_e}$
d	dimension of $\mathcal{R}_{\mathcal{M}}$
d(ω)	polynomial in denominator of T(ω)
$\underline{e}$	model residue vector in regression analysis
$\underline{e}_i$	model residual; elementary input signal; basis vector of $\mathcal{R}_{\mathcal{M}}$
E	mathematical expectation operator; energy
f	vector function
F	right handed rectangular reference frame; linear system matrix
g	gravitational acceleration
G	linear system input matrix
h	geometric altitude
H	matrix in linear system observation model
I	identity matrix
I_e	moment of inertia of propeller and rotating engine components
I_x, I_y, I_z	moments of inertia about the X-, Y- and Z-axis respectively
I_{xy}, I_{yz}, I_{zx}	corresponding products of inertia
j	imaginary number , $\sqrt{-1}$
J	matrix in linear system observation model; performance index
K	Kalman filter gain matrix
K_p	One stage prediction gain matrix
L	aerodynamic moment about the X-axis; likelihood function; orthogonal matrix
m	mass of the aircraft; integer
M	aerodynamic moment about the Y-axis; information matrix
$\bar{M}$	M/N, average information matrix
$M^{(k)}$	point-input information matrix from $\underline{u}^{(k)}$
$\mathcal{M}$	set of average information matrices from power constrained input signals
n	integer
n(ω)	polynomial in numerator of T(ω)
N	aerodynamic moment about the Z-axis
O	origin of frame of reference
p	angular rate about the X-axis (roll rate)
p_{st}	static pressure of air
p_t	total pressure in propeller slipstream
P_u	total power of input signals
q	angular rate about the Y-axis (pitch rate); integer
q_c	impact pressure of air
r	angular rate about the Z-axis (yaw rate)
R	radius of hypersphere; multiple regression coefficient
R^*	partial correlation coefficient
R^n	n-dimensional Euclidean space
$\mathcal{R}_{\mathcal{M}}$	information space
s	integer
S	wing surface area; sensitivity matrix
$S_{uu}(\omega)$	power spectral density matrix of input signals
t	time (continuous)
t_i	time (discrete)
T	observation time interval; state transformation matrix; temperature
T(ω)	frequency response matrix
u	component of airspeed along the X-axis
$\underline{u}$	vector of input signals
$\underline{u}^{(k)}$	vector of harmonic signal in input signals
$\underline{U}(\omega)$	Fourier transform of vector of input signals
U	state transformation matrix
v	component of airspeed along the Y-axis
$\underline{v}$	vector of measurement errors
V	true airspeed
$V(\hat{\underline{a}})$	covariance matrix
V_{vv}, V_{ww}	covariance matrices
w	component of airspeed along the Z-axis; measurement noise
W_x, W_y, W_z	components of aircraft weight along the X-, Y- and Z-axis respectively; components of atmospheric wind
x_α	x-coordinate of the α-vane in the body fixed reference frame
x_β	x-coordinate of the β-vane in the body fixed reference frame

x_E	position of the aircrafts centre of gravity with respect to an earth fixed reference frame along the X-axis
$\underline{x}$	system state vector; row vector of independent variables in regression analysis
$\underline{X}(\omega)$	Fourier transform of system state vector
X	aerodynamic longitudinal force along the X-axis; matrix of independent variables in regression analysis
$\underline{y}$	observation vector
y_α	y-coordinate of the α-vane in the body fixed reference frame
y_E	position of the aircrafts centre of gravity with respect to an earth fixed reference frame along the Y-axis
$\underline{Y}(\omega)$	Fourier transform of observation vector
Y	aerodynamic lateral force along the Y-axis
z_β	z-coordinate of the β-vane in the body fixed reference frame
z_E	position of the aircrafts centre of gravity with respect to an earth fixed reference frame along the Z-axis
Z	aerodynamic vertical force along the Z-axis

Greek symbols

α	angle of attack; power ratio of a harmonic signal in the input signals
α_v	angle of attack measured by a vane
β	angle of side slip; cartesian coordinates
β_v	angle of side slip measured by a vane
γ	flight path angle
δ_{ij}	Kronecker delta
δ_a	aileron deflection angle $\delta_a=\delta_{a_r}-\delta_{a_\ell}$
δ_{a_ℓ}	left aileron deflection (aileron down is positive)
δ_{a_r}	right aileron deflection (aileron down is positive)
δ_e	elevator deflection angle (elevator down is positive)
δ_r	rudder deflection angle (rudder left is positive)
Δ	increment
ε	aerodynamic model error
θ	pitch angle; phase of a harmonic signal in the input signals
$\underline{\theta}$	parameter vector
$\underline{\lambda}$	vector containing bias errors
Γ	discrete system input matrix
μ	amplitude of a harmonic signal in the input signals
μ_b	$\frac{m}{\rho S b}$
μ_c	$\frac{m}{\rho S \bar{c}}$
ν	Kalman filter innovation
ψ	angle of yaw
$\underline{\psi}$	information vector, vector representation of M
ρ	air density
σ	standard deviation
ϕ	angle of roll
ω	angular frequency

Superscripts

*	reconstructible state variable or identifiable parameter
^	estimated value; normalized value
-	mean value
~	small deviation from nominal value
H	matrix conjugate transpose
(k)	harmonic signal in the input signals
o	optimal value
T	matrix transpose
·	derivative with respect to time
-1	matrix inverse

subscripts

m	measured quantity
B	body fixed reference frame F_B
D	datum fixed reference frame F_D
E	Earth fixed vertical reference frame F_E
e	engine
S	stability reference frame F_S
0	nominal value

0.2 Abbreviations

cg	centre of gravity
CRLB	Cramer Rao Lower Bound
cov $\underline{a}$	covariance matrix of $\underline{a}$
det A	determinant A
DME	Distance Measuring Equipment
DUT	Delft University of Technology
ln	logarithm to base e
LHS	Left Hand Side
ML	Maximum likelihood
NLR	National Aerospace Laboratory
TAS	V , True Air Speed
tr A	trace of square matrix A

0.3 reference frames

A number of different reference frames will be referred in this volume. Their definitions will be given below. Within this volume, the translational equations and the rotational equations are both referred to the body axes. The aircraft attitude is defined by the Euler angles ψ, θ and ϕ and for this reason the vehicle carried vertical reference frame is introduced. The aircraft position is defined with respect to the earth fixed reference frame.

Datum reference frame F_D
The location of characteristic points relative to the aircraft - as for instance the centre of gravity - is expressed in terms of coordinates in a body fixed, rectangular and left handed reference frame which is named here the datum reference frame (see fig. 0-1). The X_D-axis is in the plane of symmetry of the aircraft. The Y_D-axis is perpendicular to this plane of symmetry and points to port. The direction of the Z_D-axis is upwards in normal flight. For the particular aircraft used in the present flight tests, the origin O_D coincides with the projection on the plane of symmetry of a reference point on the starboard wing leading edge at 1.4 m distance from the plane of symmetry. The direction of the X_D-axis is chosen parallel to a reference wing chord connecting the leading edge and the trailing edge at the same distance from the plane of symmetry.

Body-fixed reference frame F_B
The body-fixed reference frame of the aircraft is a right-handed orthogonal system $O_BX_BY_BZ_B$. The origin O_B lies in the centre of gravity of the aircraft (see fig. 0-1). The $X_BO_BZ_B$ plane coincides with the aircraft's plane of symmetry if it is symmetric, or is located in a plane, approximating what would be the plane of symmetry. The X_B-axis is directed towards the nose of the aircraft, the Y_B-axis points to starboard and the Z_B-axis points towards the bottom of the aircraft.
The positive directions for the body axis rates (p, q, and r respectively), the body axis velocities (u, v, and w), the body axis forces (X, Y, and Z), and the body axis moments (L, M, and N) are shown in figure 0-2.

Stability reference frame F_S
The stability reference frame $O_SX_SY_SZ_S$ is a special body-fixed reference frame, used in the study of small deviations from a nominal flight condition. The reference frames F_B and F_S differ in the orientation of the X-axis. The X_S-axis is chosen parallel to the true airspeed V. In the case of a non symmetrical nominal flight condition the X_S-axis is chosen parallel to the projection of $\underline{V}$ on the aircraft's plane of symmetry.

Earth-fixed reference frame F_E
The earth-fixed reference frame is a right-handed orthogonal system $O_EX_EY_EZ_E$, which is considered to be fixed in space. Its origin can be placed at an arbitrary position, but it will be chosen to coincide with the aircraft's centre of gravity at the start of a flight test manoeuvre. The Z_E-axis points downwards, parallel to the local direction of the gravitation. The X_E-axis is directed north, the Y_E-axis east (fig. 0-3).

Vehicle-carried vertical reference system F_V
The origin of the vehicle carried vertical reference frame is attached to the aircraft's centre of gravity. Except for this difference, F_V is identical to the earth fixed vertical reference F_E (fig. 0-3).

Vehicle carried vertical reference frame F_T
The reference frame F_T was found to be convenient in the analysis of the linearized flight path reconstruction problem. The origin is attached to the aircraft's centre of gravity. The Z_T-axis points downwards parallel to the local direction of gravitation. The X_T-axis coincides with the projection of the X_B-axis at the start of a flight test manoeuvre on the local horizontal plane (fig. 0-4).

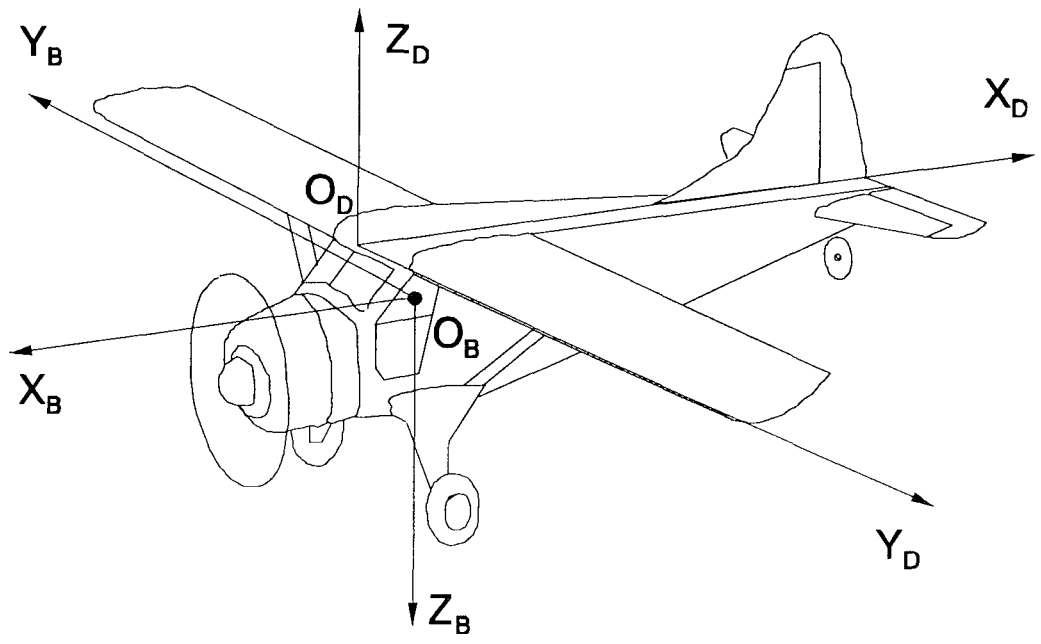

Figure 0-1: *The datum reference frame F_D and body-fixed reference frame F_B.*

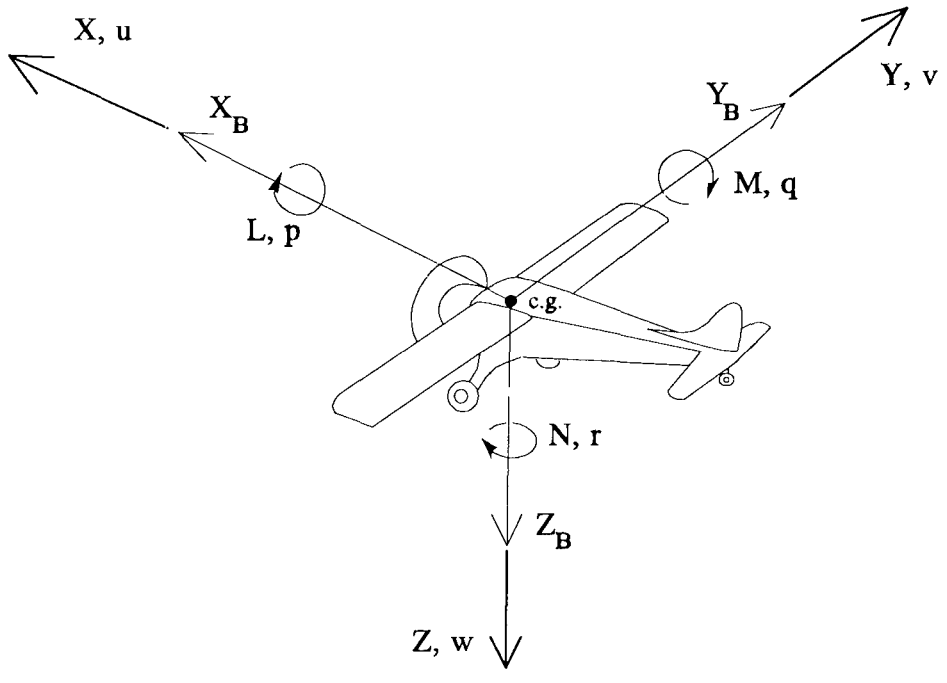

Figure 0-2: *The body-fixed reference frame F_B. X, Y, Z, L, M and N denote the forces along and moments about the body-axis; u, v, w, p, q and r denote the linear and angular velocities.*

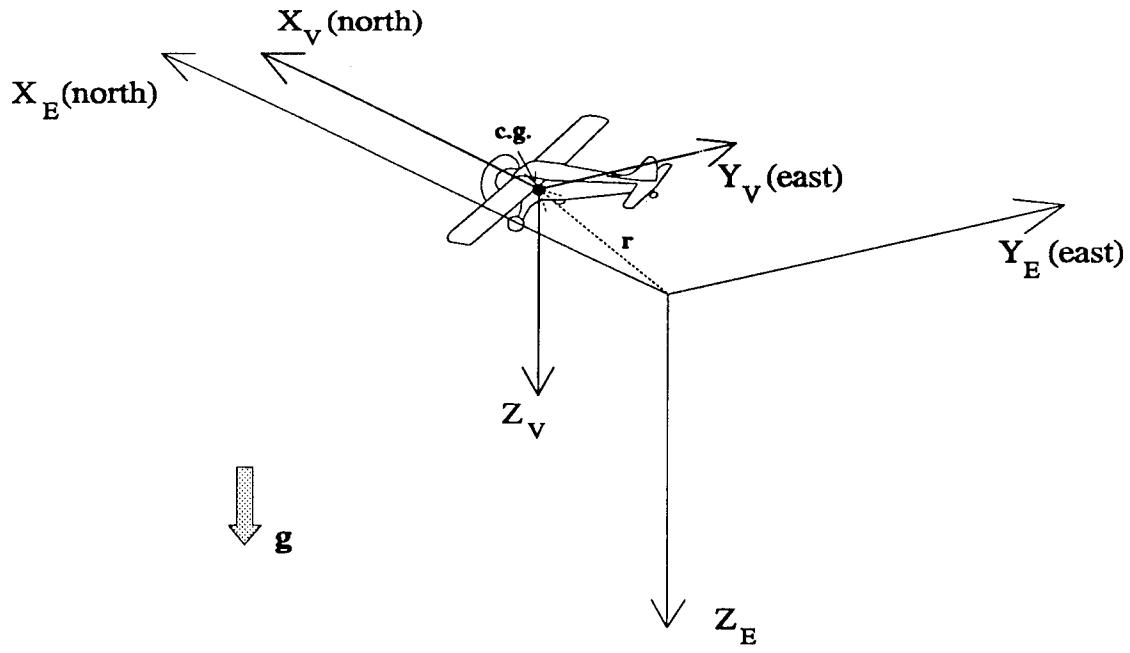

Figure 0-3: *Relationships between earth-fixed reference frame and vehicle-carried vertical reference frame. The vector r denotes the position of the aircraft c.g. with respect to F_E.*

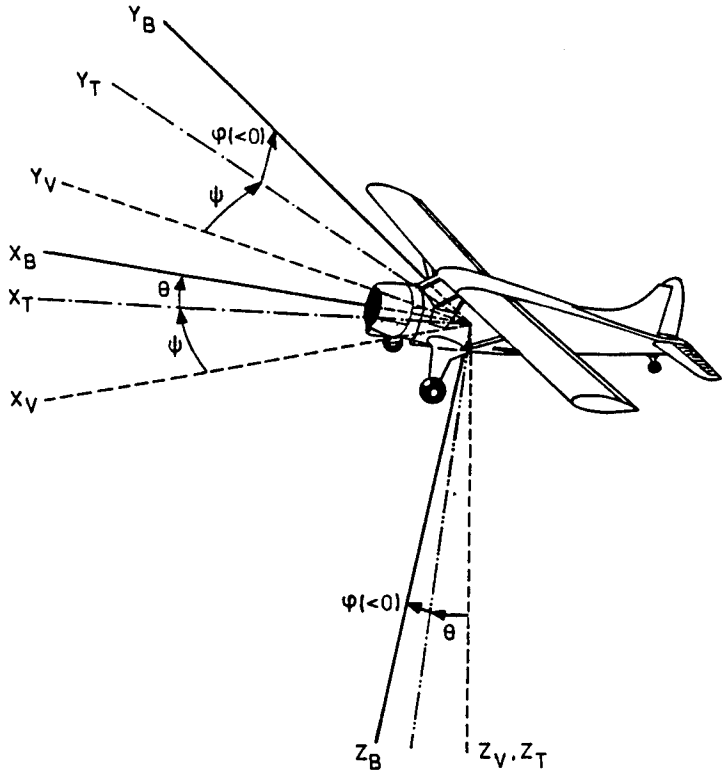

Figure 0-4: *The body-fixed reference frame F_B and the vehicle-carried vertical reference frames F_V and F_T at the start of a flight test manoeuvre.*

Synopsis

This AGARDograph is a sequel to the previous AGARDographs published in the AGARD *Flight Test Techniques Series*, Volume 2 on *'Identification of Dynamic Systems'* and Volume 3 on *'Identification of Dynamic Systems - Applications to Aircraft Part - 1: The Output Error Approach'* both written by R.E. Maine and K.W. Iliff. The intention of the present document is to cover some of those areas which were either absent or only briefly mentioned in these volumes. These areas are *Flight Path Reconstruction, Nonlinear Model Identification, Optimal Input Design* and *Flight Test Instrumentation*. Just like Maine and Iliff the present authors will stay close to those techniques with which they are most familiar. The present approach to identification is rather different from that presented in the earlier AGARDographs in the sense that the identification problem is decomposed into a state estimation and a parameter identification part. This approach is referred to as the *Two-Step Method* (TSM), although one will find other names like *Estimation Before Modelling* (EBM) in the literature. It will be shown in the present AGARDograph that this approach has significant practical advantages over methods in which no attempt is made to decompose the joint parameter-state estimation problem. The two-step method is generally applicable to flight vehicles such as fixed wing aircraft and rotorcraft which are equipped with state of the art inertial reference systems. The theoretical developments in the present AGARDograph will be illustrated with examples of a flight test program with the De Havilland DHC-2 Beaver aircraft, the experimental aircraft of the Delft University of Technology which has been used for almost two decades to test new ideas in the science of aircraft parameter identification.

1 INTRODUCTION

The primary goals of most flight test programs of civil and military aircraft are the certification for air worthiness and the estimation of performance and stability and control characteristics. While certain characteristics can be measured directly in flight such as rate of climb in stationary rectilinear flight or damping ratio's and time constants of eigen motions a much more efficient approach is to *identify* a mathematical model of the aerodynamic forces and moments acting on the aircraft from measurements of dynamic flight test manoeuvres. Identification implies the development of an adequate mathematical model structure as well as estimation of the numerical values of the parameters in the model. When applied to aircraft this process is often referred to as *aircraft parameter identification*. After successful identification of aerodynamic models for different aircraft configurations and flight conditions they may be exploited in numerous different ways. It is possible now to compute a variety of performance and stability and control characteristics, to compile tables and graphs for Aircraft Operations Manuals and compare actual aerodynamic characteristics with theoretical predictions or wind tunnel results. A very interesting application is in the enhancement of the fidelity of mathematical models for flight simulation. During the last two decades, the advent of the digital computer and improvement in flight measurement techniques has made a tremendous impact on theory and practice of aircraft parameter identification. Working Group 11 (WG 11) of the Flight Mechanics Panel of AGARD has defined as one of its missions to stimulate the development and applications of aircraft parameter identification techniques in its series on *Flight Test Techniques*. In this series, an excellent overview of identification of dynamic systems has been written by R.E. Maine and K.W. Iliff in volume 2 [1]. In the succeeding volume, the same authors gave an exhaustive, practical and elegant treatment of one of the primary parameter identification technique namely the *Output Error Method* used at NASA Dryden for the problem of estimating aircraft stability and control derivatives [2]. The report examines this one single approach with lucid presentation of results and discussion right from flight test planning to evaluation of results carried out at their NASA Dryden Flight Research facility. This material formed the main theme of part - 1 of volume 3.

The purpose of the present AGARDograph which

is part - 2 of volume 3, is to present and discuss in detail a successful and practical method for aircraft parameter identification that has originated at the Delft University of Technology. This method is referred to here as the *Two-Step Method*, although one may find other names like *Estimation Before Modelling (EBM)* in the literature. The report goes into some detail on the application of accurate *Flight Test Instrumentation* sensors and systems which has revolutionized the identification process and in particular has made the two-step method an attractive and efficient identification tool. The report also examines and focuses attention on some new emerging areas of technology namely the *Optimal Input Design* for excitation of aircraft manoeuvres which can lead to more accurate parameter estimates and reduction of expensive flight test time. The problems, results and discussions addressed in this report are based mainly on the investigations at the Delft University of Technology (DUT) and the National Aerospace Laboratory (NLR), Amsterdam.

1.1 Flight Testing and Identification Background of Delft TU and NLR

Since the early sixties the Faculty of Aerospace Engineering of the Delft University of Technology and the National Aerospace Laboratory, Amsterdam have been engaged in the development of methods to derive aircraft performance as well as stability and control characteristics from dynamic flight test data. Traditional methods of performance testing employed measurements in steady straight flight conditions in which the aircraft experienced neither translational nor angular accelerations. Attention was focused on the analysis and design of 'hybrid' flight test manoeuvres consisting of quasi-steady as well as nonsteady flight conditions for the derivation of all aircraft performance- and stability and control characteristics of interest. The emphasis on the simultaneous measurement of performance- and stability and control characteristics dictated development and application of high accuracy flight test measurement techniques and transducers. Key to success proved to be what was called *flight path reconstruction*, i.e. the technique to accurately reconstruct the time history of the aircraft's state during the flight test manoeuvre. The results of these investigations were reported in references [3 to 14].

Between 1967 and 1968, a number of flight test programs were carried out to evaluate the quality and performance of the flight test methods, the flight test measurement system and the data reduction procedures developed for the derivation of aircraft performance, stability and control characteristics from measurements in nominally symmetric nonsteady manoeuvring flight. Symmetric flight trials flown with the DHC-2 Beaver aircraft of the Delft University of Technology yielded most encouraging results.

It was decided to extend these investigations to high subsonic jet flight. In the early seventies proposals were made for flight test programs with the Hawker Hunter MK 7 experimental aircraft of the National Aerospace Laboratory. A new high accuracy flight test instrumentation system was built which was small enough to be installed in a wing mounted pod [16]. During 1973 and 1974 several successful flight tests were conducted. The higher speeds and different propulsion system required new aerodynamic models. Also, the flight path reconstruction needed an extended model which included the effects of curvature and rotation of the earth. This gave birth to a new concept namely, the calibration of engine gross thrust and mass flow sensor systems in dynamic flight simultaneously with the identification of aerodynamic parameters and independent of any data of the engine manufacturer. An overview of the results of these very successful flight tests is given in ref. [12].

Around 1978, further flight test programs were planned to aim at the aircraft model identification both in symmetric and asymmetric nonsteady manoeuvring flight as an international cooperative program with DLR in Braunschweig, Germany. The results of these investigations are reported in ref. [19]. The method for parameter identification developed at DUT was by then dubbed the *Two-Step Method*: in the first step, the flight path is reconstructed, followed by the second step in which the parameters are identified. Based upon the confidence and experience gained in methods and analysis, further flight test programs were carried out by the National Aerospace Laboratory (NLR) to investigate the applicability for the case of a twin engined transport type aircraft, the Fokker F-28 Fellowship. Initial results of the

assessment of performance and stability and control characteristics are reported in ref. [21]. The techniques as developed in the course of these flight test programs were subsequently applied with high degree of success during the testing and development phase of Fokker 50 and Fokker 100 type aircraft [22]. In 1987 flight simulation models were developed for the Cessna Citation 500 of the Dutch Government civil aviation flying school (RLS) flight simulator [23].
The National Aerospace Laboratory and Delft TU are currently cooperating in a flight test program with the Fairchild Metro II experimental aircraft of NLR. These experiments have demonstrated that estimation of the aircraft state, as well as the identification of longitudinal and lateral aerodynamic model parameters can be performed on-board in real time [24 to 26]. In the same flight test program, attention is focused on different measurement and analysis methods to identify propeller thrust in dynamic flight test manoeuvres [27].

Thus, this successful chain of experiments and analyses amply demonstrated that nonsteady flight test techniques as developed and tested at the Delft University of Technology and the National Aerospace Laboratory was a proven, cost effective and well established technique for the measurement of performance and stability and control characteristics as required for the certification of aircraft. The results and discussions of the two-step identification procedure presented in this report are based on this nonsteady flight test technique.

1.2 Requirements for Nonsteady Flight Test Techniques

The successful application of the nonsteady flight test technique developed at the Delft University of Technology depends on a well chosen combination of the aircraft to be tested, the flight test instrumentation system, the signals applied to excite the aircraft, the models selected for identification and the procedure devised to analyze test data. The nonsteady flight test technique in particular hinges on accurate measurement of several inertial- and barometric variables.

The flight test method includes:
1. Utilization of a high accuracy flight test instrumentation system, comprising high quality inertial and barometric sensors, see ref. [13].
2. Careful calibration of all transducers to be used in the flight test instrumentation system, ref. [16,17,28].
3. Analytic or computer aided development of optimal manoeuvre shapes, i.e.,optimal time histories for the control surface deflections required to excite the aircraft, so as for example to maximize the amount of information in the measurements, concerning the characteristic parameters of interest, ref. [3,29].
4. Excitation of the aircraft manually or under servo control (according to the optimal test signals developed) during test flights flown in fine weather.
5. Off-line analysis of the measurements recorded in flight, using advanced state and parameter estimation techniques [30].

1.3 Motivation for Nonlinear Analysis

Stability and control derivatives are the parameters in a linear aerodynamic model of the aircraft. Linear aerodynamic models can be represented by homogeneous polynomials of the first degree in the state and control input variables of the linearized equations of motion. Such polynomials are widely used as linear approximations of aerodynamic forces and moments acting on the aircraft in dynamic flight conditions. In general the domain in which linear models are valid is restricted to small deviations from a nominal flight condition which is stationary.

The advantage of using nonlinear models is that such models should be valid for a larger range of flight conditions. In addition dynamic flight test manoeuvres are much less constrained with respect to the amplitudes of angle of attack and air speed excursions.

One specific form of representing nonlinear models is by using higher order polynomials in state and control input variables. In principle, the domain of nonlinear models covers larger deviations from a given nominal flight condition, as compared to linear models.

1.4 Motivation for Manoeuvre Design

The importance of choosing appropriate control inputs and exciting specific aircraft modes for extraction of stability and control derivatives from dynamic flight test data was first noted by Gerlach [3]. Subsequent research focused on design techniques for optimal control input signals. Optimal input signals may be designed to either maximize the information contents contained in the flight test data or minimize the necessary length of the flight test manoeuvre for a specified level of accuracy of the parameters to be estimated. After a review of the literature attention is focused in the present AGARDograph on two techniques for the optimization of control input signals as developed at the Delft University of Technology.

1.5 Two-Step Method

Analysis of dynamic flight test data, in the sense of estimating stability and control derivatives from measurements of the dynamic response of the aircraft to control input signals, can be formulated in the theoretical frame work of maximum likelihood estimation theory [53]. This requires the stability and control derivatives to be interpreted as unknown parameters in a dynamical system of a given form. It is assumed that the response of the system to precisely known input signals has been observed by measuring the outputs of the system at discrete instants of time. The measurements are assumed to be corrupted by additive, mutually independent and normally distributed random errors. It is known that the likelihood function of these measurements depends on the parameters as well as on the initial state vector components. Optimizing the likelihood function with respect to these parameters and the initial state vector components constitutes a nonlinear optimization problem. The optimum values are called the maximum likelihood estimates of the system parameters and initial condition. In this form the maximum likelihood method is a so-called *Output Error Method* and probably the most frequently used method to date for estimating stability and control derivatives from measurements in dynamic flight test manoeuvres [54,55]. The maximum likelihood method has been extensively discussed in the preceding part - 1 of the present volume 3 in the AGARD Flight Test Techniques Series.

In the present volume it is shown that, if certain conditions concerning accuracy and type of the variables measured in flight are met, the original maximum likelihood estimation problem can be decomposed into two separate estimation problems which can be solved in two consecutive steps. Each of the two separate estimation problems is much easier to solve than the original estimation problem. These two steps are called *step 1* and *step 2*. In the general case of nonlinear equations of motion, *step 1* corresponds to a nonlinear state reconstruction problem known as the *Flight Path Reconstruction* problem [7,10]. The next *step 2* can be formulated as a 'linear-in-the-parameters' estimation problem. This is of great practical importance, as it allows the systematic and step wise development of adequate nonlinear models of the aerodynamic forces and moments during the flight test manoeuvre.

1.6 Organization of the Report

In chapter 2 we will discuss mathematical models which will be useful for the analysis of flight path reconstruction and aerodynamic model identification. The nonlinear equations will be used for the practical implementations, while the linear models will be used for the study of reconstructibility and identifiability. In chapter 3 we will treat flight path reconstruction in a detailed way in its own right. We discuss identification of nonlinear aerodynamic models using regression techniques in chapter 4. Next we present two approaches in chapter 5 for the optimization of multi dimensional input signals which can be of great use in the design of flight test manoeuvres. Practical examples of different types of longitudinal and lateral control input signals, several of which evaluated in real flight are presented in chapter 6. The detailed aspects of flight test instrumentation, design, execution and flight data processing are covered in chapter 7. Conclusions drawn from the previous sections are presented in chapter 8.

2 AIRCRAFT AND INSTRUMENTATION MODELS

In this chapter we present some mathematical models which will be used in the later chapters. These models can be broadly classified as *Kinematic models, Observation models* and *Aerodynamic models*. Kinematic models are in fact a special form of the customary equations of motion in which specific aerodynamic forces (the outputs of 'ideal' accelerometers in the centre of gravity) and angular rates serve as inputs. Kinematic models can conveniently be written in state space form. Observation models describe the relations between several observed variables as airspeed and side slip angle and the state vector components of the kinematic model. Kinematic and observation models are instrumental for *flight path reconstruction.*

As discussed in chapter 3 flight path reconstruction refers to techniques to compute the time histories of the components of the state vector (including the 'flight path') from onboard inertial, barometric and other sensors.

Aerodynamic models describe the aerodynamic forces and aerodynamic moments which act on the aircraft during the dynamic flight test manoeuvre to be analyzed. In the linearized form of the equations of motion the models of these aerodynamic forces and moments are also linearized and contain well known sets of parameters called *stability-* and *control derivatives.* It is possible to apply the identification techniques discussed in chapter 4 to estimate the values of these stability- and control derivatives from dynamic flight test measurements. The two-step method as discussed in the present document, however, allows also the estimation of so called *aerodynamic derivatives* in *nonlinear aerodynamic models*, be it that these nonlinear models should be of a special form in which the derivatives appear linearly in the output (the aerodynamic force- and moment coefficients). A question of theoretical and practical interest is whether one should estimate stability- and control derivatives at all flight conditions of interest (as defined by nominal angle of attack, Mach number, power setting, etc.) or estimate aerodynamic derivatives in one nonlinear aerodynamic model valid for the same set of flight conditions. In any case nonlinear aerodynamic models become mandatory when linear models turn out to be inadequate, and in those applications where interest is focused on the modelling of aircraft performance characteristics, e.g. see Mulder and van Sliedregt [12].

Although nonlinear forms of kinematic and observation models are used for actual flight path reconstruction, linearized versions of these models are developed also below to allow discussion of certain state reconstructibility topics in chapter 3. The linearized forms of aerodynamic models shown below serve the same purpose in a fundamental discussion of identifiability in chapter 4. In addition the design of optimal input signals for dynamic flight test manoeuvres as discussed in chapter 5 is based on linear forms of all mathematical aircraft models.

2.1 Kinematic Models

2.1.1 Aircraft Equations of Motion

In this volume we restrict ourselves to the simplified case of rigid and symmetrical aircraft moving through an atmosphere which moves with uniform constant speed over a flat earth. Using a body fixed reference frame with origin in the centre of gravity this results in equations of motion as presented below.

In flight path reconstruction, see chapter 3, the quality of the sensor systems employed may in some cases warrant accounting for the effects of curvature and rotation of the earth, ref. [13].

Aircraft equations of motion take the form of three sets of first order differential equations for respectively translational velocities, angular velocities and attitude angles, e.g. Etkin [57]. Using the customary body-fixed reference frame F_B the equations for the components u, v and w of true air speed $\underline{V}_a$ along the body axes X_B, Y_B and Z_B take the following form:

$$\begin{aligned} X &= m(\dot{u} + qw - rv) + mg\sin\theta \\ Y &= m(\dot{v} + ru - pw) - mg\cos\theta\sin\phi \\ Z &= m(\dot{w} + pv - qu) - mg\cos\theta\cos\phi \end{aligned} \quad , \qquad (2.1\text{-}1)$$

where p, q and r denote the rates of rotation about the axes of F_B; θ and ϕ denote pitch and roll angle respectively; m denotes aircraft mass and g denotes the local acceleration due to gravity. X, Y and Z

represent the components of the *total aerodynamic force*, including the aerodynamic effects of propulsion systems.

The rotational dynamics of the aircraft are represented by a second set of first order differential equations for the angular rates p, q and r about the body axes X_B, Y_B and Z_B respectively. For an aircraft with a geometrical plane of symmetry, these equations are given by:

$$\begin{aligned} L &= I_x\dot{p} - (I_y - I_z)qr - I_{xz}(\dot{r} + pq) , \\ M &= I_y\dot{q} - (I_z - I_x)rp - I_{zx}(r^2 - p^2) + I_e\omega_e r , \\ N &= I_z\dot{r} - (I_x - I_y)pq - I_{zx}(\dot{p} - qr) - I_e\omega_e q . \end{aligned} \qquad (2.1\text{-}2)$$

where L, M and N denote the *total aerodynamic moments* (including again any aerodynamic effects of the propulsion system) about the body axes X_B, Y_B and Z_B. I_x, I_y and I_z denote the moments of inertia and I_{zx} the only (due to symmetry) non-zero product of inertia in F_B. Gyroscopic effects of rotating propellers or turbines can easily be taken into account. For the case of a spin axis parallel to X_B this leads to additional terms with $I_e\omega_e$ as shown in (2.1-2).

The orientation of F_B with respect to the earth-fixed vertical reference frame F_E is governed by a third set of first order differential equations for the Euler angles ϕ, θ and ψ:

$$\begin{aligned} \dot{\phi} &= p + q\sin\phi\tan\theta + r\cos\phi\tan\theta , \\ \dot{\theta} &= q\cos\phi - r\sin\phi , \\ \dot{\psi} &= q\sin\phi\sec\theta + r\cos\phi\sec\theta . \end{aligned} \qquad (2.1\text{-}3)$$

The three sets of equations (2.1-1), (2.1-2) and (2.1-3) may be written in standard state space form by solving for the derivatives with respect to time and defining a state vector with u, v, w, p, q, r, ϕ, θ, ψ as components. By adjoining an aerodynamic model (a set of models of the total aerodynamic forces X, Y, and Z and the total aerodynamic moments L, M and N) these equations can be solved by means of numerical integration given the aircraft mass, moments and product of inertia and an initial value of the state vector. It is worth noting here that the 'physical' input variables such as control surface deflections and engine thrust or power changes also serve as inputs to the above set of differential equations as they should appear as independent variables in the aerodynamic model. The solution consists of the time histories of translational and angular velocity components u, v, w and p, q, r, and the Euler angles ϕ, θ, ψ. Next we will write the model in a slightly different form and define a set of alternative input signals.

2.1.2 Nonlinear Kinematic Models

Kinematic models of aircraft motion consist of a set of first order ordinary differential equations in which not the 'physical inputs' but rather measured variables as *specific aerodynamic forces* and *body rotation rates* appear as forcing functions.
A specific force is defined here as the external non-gravitational field force per unit of mass. Specific forces are the variables measured by 'ideal' accelerometers in the body's centre of gravity, irrespective of whether the body is influenced by a gravitational field or not. In flight tests such ideal accelerometers would measure the specific aerodynamic forces according to:

$$\begin{aligned} X &= A_x m , \\ Y &= A_y m , \\ Z &= A_z m , \end{aligned} \qquad (2.1\text{-}4)$$

in which A_x, A_y and A_z denote the specific aerodynamic forces along the body axes X_B, Y_B and Z_B respectively. Substitution of (2.1-4) into (2.1-1) and dividing by m leads to the following set of relations:

$$\begin{aligned} \dot{u} &= A_x - g\sin\theta - qw + rv , \\ \dot{v} &= A_y + g\cos\theta\sin\phi - ru + pw , \\ \dot{w} &= A_z + g\cos\theta\cos\phi - pv + qu . \end{aligned} \qquad (2.1\text{-}5)$$

As mass m has been eliminated we may take the view point that (2.1-5) represents a set of what might be called *kinematical* relations. The two sets of equations (2.1-5) and (2.1-3) may again be solved numerically if now the specific aerodynamic forces A_x, A_y and A_z and the angular rates p, q and r are taken as input variables. The solution consists of the time histories of the translational velocity components u, v and w and the Euler angles ϕ, θ, ψ.
The position of the aircraft's centre of gravity relative to the earth fixed frame of reference F_E can

be computed as well by numerically integrating the following set of equations simultaneously with equations (2.1-5) and (2.1-3):

$$\begin{bmatrix} \dot{x}_E \\ \dot{y}_E \\ \dot{z}_E \end{bmatrix} = L_{EB} \begin{bmatrix} u \\ v \\ w \end{bmatrix} + \begin{bmatrix} W_{x_E} \\ W_{y_E} \\ W_{z_E} \end{bmatrix}, \tag{2.1-6}$$

where L_{EB} denotes an orthogonal matrix of the form:

$$L_{EB} = \begin{bmatrix} \cos\theta\cos\psi & \sin\phi\sin\theta\cos\psi - \cos\phi\sin\psi & \cos\phi\sin\theta\cos\psi + \sin\phi\sin\psi \\ \cos\theta\sin\psi & \sin\phi\sin\theta\sin\psi + \cos\phi\cos\psi & \cos\phi\sin\theta\sin\psi - \sin\phi\cos\psi \\ -\sin\theta & \sin\phi\cos\theta & \cos\phi\cos\theta \end{bmatrix}, \tag{2.1-7}$$

and W_{x_E}, W_{y_E} and W_{z_E} denote the components of a constant atmospheric wind vector $\underline{W}_E$ along the axes of F_E.

Remark In cases of relatively long flight path's in particular during climb or descent as in typical performance flight tests, it can no longer be assumed that the atmospheric wind components are constant. For the case of varying wind components Eq. (2.1-5) may still be used if u, v and w are replaced by the corresponding components u_E, v_E and w_E of $\underline{V}_E$, speed with respect to the earth fixed reference frame F_E. Eq. (2.1-6) then takes the form:

$$\begin{bmatrix} \dot{x}_E \\ \dot{y}_E \\ \dot{z}_E \end{bmatrix} = L_{EB} \begin{bmatrix} u_E \\ v_E \\ w_E \end{bmatrix}$$

Next the components u, v and w of $\underline{V}_a$ follow from $\underline{V}_a = \underline{V}_E - \underline{W}_E$. It may be attractive from the estimation theoretic point of view to add a model of the varying wind components to the kinematical model. The reason is that a model will have much less parameters than the total number of unknown values of the three components of the wind at the (discrete) time instants of the flight test manoeuvre. A simple model which seems to work well in practice describes the wind components as a linear trend in time and proportional to altitude. A more sophisticated alternative would be a stochastic model driven by 'white noise'.

Equations (2.1-5), (2.1-3) and (2.1-6) represent a *kinematic model* for the motion (speed, attitude and position) of F_B with respect to a flat and non rotating earth. If the effects of the curvature and rotation of earth are to be included then we must express the geographical positions in terms of longitude and latitude and decompose the local atmospheric wind along the axes of the vehicle carried vertical reference frame F_V or F_T [13]. In the case of flexible aircraft, the specific aerodynamic forces and the quantities sensed by accelerometers can in principle no longer be assumed identical. Even then, however, the kinematical relations (2.1-5), (2.1-3) and (2.1-6) would still be valid. To see this, we might interpret equations (2.1-1) as equations of motion of just an inertial reference system fixed at the centre of gravity. Then the components X, Y, Z would represent *external suspension forces*. A_x, A_y and A_z in (2.1-5) would represent *specific suspension forces* and still be identical to the quantities sensed by ideal accelerometers.

We may now interpret (2.1-5), (2.1-3) and (2.1-6) as to represent a dynamical system, and define a *state vector* $\underline{x}$ and an *input vector* $\underline{u}$ as follows:

$$\begin{aligned} \underline{x} &= \mathrm{col}(u, v, w, \phi, \theta, \psi, x_E, y_E, z_E), \\ \underline{u} &= \mathrm{col}(A_x, A_y, A_z, p, q, r). \end{aligned} \tag{2.1-8a}$$

The system *state equation* may be written as:

$$\dot{\underline{x}} = \underline{f}(\underline{x}, \underline{u}). \tag{2.1-8b}$$

$\underline{f}$ denoting a nonlinear vector function of $\underline{x}$ and $\underline{u}$. While accelerometers and rate gyro's serve to measure the components of the input vector $\underline{u}$, barometric and other sensors may be used to measure the components of an *observation vector*, see section 2.3 below.

2.1.3 Linearized Kinematic Models

In the present section we derive a set of linearized kinematical relations starting again from equations of motion as in section 2.1.2 above, but this time in their linearized form.

The linearized form of the equations of motion is derived in two steps. First the nonlinear equations of motion (2.1-1) and (2.1-2) for variables in the body fixed reference frame F_B are written in terms

of variables in a (body fixed) stability reference frame F_S. Next we may linearize these equations for small deviations from a nominal flight condition of steady, rectilinear flight with side slip angle equal to zero. It is readily ascertained that in the nominal flight condition the components of air speed along and the rates of rotation about the axes of F_S have the following values:

$$u_{0_S} = V_0 , \quad v_{0_S} = 0 , \quad w_{0_S} = 0 ,$$
$$p_{0_S} = 0 , \quad q_{0_S} = 0 , \quad r_{0_S} = 0 ,$$

while the nominal pitch angle is equal to the nominal flight path angle:

$$\theta_{0_S} = \gamma_0 ,$$

the subscript $_0$ referring to the nominal flight condition. The linearized versions of the equations of motion (2.1-1) and (2.1-2) may now be written as:

$$\begin{aligned} \tilde{X}_S &= m\dot{\tilde{u}}_S + mg\cos\gamma_0\tilde{\theta}_S , \\ \tilde{Y}_S &= m(\dot{\tilde{v}}_S + V_0\tilde{r}_S) - mg\cos\gamma_0\tilde{\phi}_S , \\ \tilde{Z}_S &= m(\dot{\tilde{w}}_S - V_0\tilde{q}_S) + mg\sin\gamma_0\tilde{\theta}_S , \end{aligned} \tag{2.1-9}$$

$$\begin{aligned} \tilde{L}_S &= I_{x_S}\dot{\tilde{p}}_S - I_{zx_S}\dot{\tilde{r}}_S - I_e\omega_e\sin\alpha_0\tilde{q}_S , \\ \tilde{M}_S &= I_{y_S}\dot{\tilde{q}}_S + I_e\omega_e\sin\alpha_0\tilde{p}_S + I_e\omega_e\cos\alpha_0\tilde{r}_S , \\ \tilde{N}_S &= I_{z_S}\dot{\tilde{r}}_S - I_{zx_S}\dot{\tilde{p}}_S - I_e\omega_e\cos\alpha_0\tilde{q}_S . \end{aligned} \tag{2.1-10}$$

where the superscript $\tilde{}$ indicates small deviations from the steady, rectilinear nominal flight condition mentioned above. The side slip angle in the nominal flight condition is defined to be zero. (This means that if the nominal aerodynamic flow field is asymmetrical due to for example propeller slipstream swirl the nominal roll angle will have a value different from zero. Below, this value is assumed to be small enough to be negligible.)
From section 2.1.2 it follows that we may write the external aerodynamic force increments $\tilde{X}_S$, $\tilde{Y}_S$ and $\tilde{Z}_S$ in terms of corresponding increments of accelerometer readings according to:

$$\begin{aligned} \tilde{X}_S &= \tilde{A}_{x_S} m , \\ \tilde{Y}_S &= \tilde{A}_{y_S} m , \\ \tilde{Z}_S &= \tilde{A}_{z_S} m . \end{aligned} \tag{2.1-11}$$

The linearized forms of the kinematical relations for the Euler angles of F_S are:

$$\begin{aligned} \dot{\tilde{\phi}}_S &= \tilde{p}_S + \tan\theta_0\tilde{r}_S , \\ \dot{\tilde{\theta}}_S &= \tilde{q}_S , \\ \dot{\tilde{\psi}}_S &= \frac{\tilde{r}_S}{\cos\gamma_0} . \end{aligned} \tag{2.1-12}$$

Now it is convenient to express the geographical position in terms of coordinates x_T, y_T, z_T along the axes of the vertical reference frame F_T. Equation (2.1-6) is then written as:

$$\begin{pmatrix} \dot{x}_T \\ \dot{y}_T \\ \dot{z}_T \end{pmatrix} = L_{TS} \begin{pmatrix} u_S \\ v_S \\ w_S \end{pmatrix} + \begin{pmatrix} W_{x_T} \\ W_{y_T} \\ W_{z_T} \end{pmatrix} , \tag{2.1-13}$$

where the transformation matrix L_{TS} can be written as:

$$L_{TS} = \begin{bmatrix} \cos\theta_S\cos\tilde{\psi}_S & \sin\phi_S\sin\theta_S\cos\tilde{\psi}_S - \cos\phi_S\sin\tilde{\psi}_S & \cos\phi_S\sin\theta_S\cos\tilde{\psi}_S + \sin\phi_S\sin\tilde{\psi}_S \\ \cos\theta_S\sin\tilde{\psi}_S & \sin\phi_S\sin\theta_S\sin\tilde{\psi}_S + \cos\phi_S\cos\tilde{\psi}_S & \cos\phi_S\sin\theta_S\sin\tilde{\psi}_S - \sin\phi_S\cos\tilde{\psi}_S \\ -\sin\theta_S & \sin\phi_S\cos\theta_S & \cos\phi_S\cos\theta_S \end{bmatrix} ,$$

Linearization of (2.1-13) results in:

$$\begin{aligned} \dot{\tilde{x}}_T &= \cos\gamma_0\tilde{u}_S + \sin\gamma_0\tilde{w}_S - V_0\sin\gamma_0\tilde{\theta}_S + W_{x_T} \\ \dot{\tilde{y}}_T &= \tilde{v}_S + V_0\cos\gamma_0\tilde{\psi}_S + W_{y_T} \\ \dot{\tilde{z}}_T &= -\sin\gamma_0\tilde{u}_S + \cos\gamma_0\tilde{w}_S - V_0\cos\gamma_0\tilde{\theta}_S + W_{z_T} \end{aligned} \tag{2.1-14}$$

Because of the definition of the nominal flight condition given above, it follows that:

$$\tilde{v}_S = v_S \,, \qquad \tilde{w}_S = w_S \,,$$
$$\tilde{p}_S = p_S \,, \qquad \tilde{q}_S = q_S \,, \qquad \tilde{r}_S = r_S$$
$$\tilde{\phi}_S = \phi_S \,.$$

with:

$$\tilde{\alpha} \cong \frac{w_S}{V_0} \,, \qquad \tilde{\beta} \cong \frac{v_S}{V_0} \,.$$

Equations (2.1-9), (2.1-12) and (2.1-14) may be written as the following sets of linear first order differential equations for the longitudinal variables:

$$\begin{aligned}
\dot{\tilde{u}}_S &= -\cos\gamma_0 \tilde{\theta} + \tilde{A}_{x_S} \,, \\
\dot{\tilde{\alpha}} &= \frac{-g\sin\gamma_0 \tilde{\theta} + \tilde{A}_{z_S}}{V_0} + \tilde{q}_S \,, \\
\dot{\tilde{\theta}}_S &= \tilde{q}_S \,, \\
\dot{\tilde{x}}_T &= \cos\gamma_0 \tilde{u}_S + V_0 \sin\gamma_0 \tilde{\alpha} - V_0 \sin\gamma_0 \tilde{\theta} + W_{x_T} \,, \\
\dot{\tilde{z}}_T &= -\sin\gamma_0 \tilde{u}_S + V_0 \cos\gamma_0 \tilde{\alpha} - V_0 \cos\gamma_0 \tilde{\theta} + W_{z_T} \,,
\end{aligned} \tag{2.1-15}$$

and lateral variables:

$$\begin{aligned}
\dot{\tilde{\beta}} &= \frac{g\cos\gamma_0 \tilde{\phi}_S + \tilde{A}_{y_S}}{V_0} - \tilde{r}_S \,, \\
\dot{\tilde{\psi}} &= \frac{\tilde{r}_S}{\cos\gamma_0} \,, \\
\dot{\tilde{\phi}} &= \tilde{p}_S + \tan\gamma_0 \tilde{r}_S \,, \\
\dot{\tilde{y}}_T &= V_0 \tilde{\beta} + V_0 \cos\gamma_0 \tilde{\psi} + W_{y_T} \,.
\end{aligned} \tag{2.1-16}$$

Eqs. (2.1-15) and (2.1-16) are a linearized form of the nonlinear kinematical relations (2.1-5), (2.1-3) and (2.1-6) derived in section 2.1.2. As said above, they will not be used in actual flight path reconstructions but rather will serve to analyze the reconstructibility characteristics of flight path reconstruction problems in chapter 3.

2.2 Aerodynamic Models

Aerodynamic models are defined in the present context as mathematical models of the aerodynamic force- and moment components in a body-fixed or wind-axes reference frame. The development of aerodynamic models from (dynamic) flight test data requires an initial 'guess' of the mathematical structure of the model. This initial guess is referred to here as the *a priori model*, indicating that no flight data was yet incorporated in the model. A priori models can be based on *physical knowledge*, *(semi) empirical databases*, results from *Computational Fluid Dynamics* or on *wind tunnel measurements*.

The form of the a priori model will strongly depend on the ultimate goal of the flight test program. If the goal would be to develop an in essence *phenomenological model*, to be used in for example control system design or simulation it would 'suffice' to select a set of suitable variables 'explaining' the observed phenomena (the time histories of aerodynamic force- and moment components). If, however, the flight test program is aimed at an analysis of aircraft performance characteristics, a *physical model* would be needed showing minute details in (sub)models of thrust, lift and drag, e.g. Mulder and Van Sliedregt [12].

If the atmosphere is in uniform motion with respect to earth and the effects of elastic deformations of the airframe are neglected, the total aerodynamic force and moment depend on not only the present values of variables such as control surface deflections, angle of attack and side slip angle but also on the past trajectory with respect to the surrounding air mass. This leads to aerodynamic models consisting of integrals of 'indicial functions' [58]. A more practical and well proven alternative is to expand each of the above mentioned variables as a (truncated) Taylor series backwards in time. This results in aerodynamic models in the form of (nonlinear) algebraic functions of the above mentioned variables and their derivatives with respect to time.

Below in section 2.2.1 an example is given of an aerodynamic model for the case of a low-subsonic, propeller driven aircraft. The model consists of three polynomials for the aerodynamic force components, three polynomials for the components of the aerodynamic moment and an expression relating engine power to a measure of propeller

thrust. The linearized version of the model, which will be referred to in chapter 4 and 5, is derived in section 2.2.2.

2.2.1 A Nonlinear Aerodynamic Model for Low Speed Propeller Driven Flight

In this section an aerodynamic model is developed for the case of low speed propeller driven flight. The first part of the model describes the (dimensionless) aerodynamic force and moment coefficients while the second part expresses a measure of propeller thrust in terms of engine power.

For a given aircraft configuration the components of the aerodynamic force and aerodynamic moment depend on the present flight condition as defined by variables as angle of attack, side slip angle, body rotation rates, control surface deflections, engine power setting, dynamic pressure, true air speed, Mach number and Reynolds number. By considering dimensionless force and moment coefficients dynamic pressure disappears from the list of variables. On the other hand, in nonstationary flight conditions the past values of in particular the angle of attack and the side slip angle are known to also have a nonnegligible effect on the force and moment coefficients. This is usually accounted for by including derivatives with respect to time in the list of variables. In the present case of low speed flight we may assume the effect of compressibility to be so small that it can be neglected. Also, scale effects can probably be ignored, as Reynolds number variations occurring in flight are relatively small in the present case.

If the propeller is represented as an ideal pulling disc, it is possible to derive the following relation:

$$\frac{\Delta p_t}{\tfrac{1}{2}\rho V^2} = a + b\frac{P}{\tfrac{1}{2}\rho V^2} \qquad (2.2\text{-}1)$$

where Δp_t denotes the increase of total air pressure in the propeller slip-stream and P denotes engine power. It can also be shown that $\Delta p_t/\tfrac{1}{2}\rho V^2$ is a direct 'measure' for propeller thrust [3]. In the case of propeller driven aircraft, neglecting compressibility and scale effects, variations of air speed V and engine power settings (engine speed and manifold pressure in the case of a piston engined aircraft) affect the aerodynamic force and moment coefficients only indirectly through changes of $\Delta p_t/\tfrac{1}{2}\rho V^2$. Consequently, the effect of true air speed and engine power setting can be represented by one single variable $\Delta p_t/\tfrac{1}{2}\rho V^2$ in the list of variables above [195]. Assuming that the aerodynamic force and moment coefficients are analytic functions of the remaining variables then they can be expanded in the form of a Taylor series. If the effects of the lateral variables β, p, r, $\dot{\beta}$, δ_a and δ_r on the longitudinal coefficients C_X, C_Z and C_m and vice versa, the effects of the longitudinal variables $\Delta p_t/\tfrac{1}{2}\rho V^2$, α, q, $\dot{\alpha}$ and δ_e on the lateral coefficients C_Y, C_l and C_n are neglected, then first order models for the longitudinal and lateral aerodynamic force and moment coefficients can be written in terms of dimensionless variables in the following form:

$$\begin{aligned}
C_X &= C_{X_0} + C_{X_{\Delta p_t}}\frac{\Delta p_t}{\tfrac{1}{2}\rho V^2} + C_{X_\alpha}\alpha + C_{X_q}\frac{q\bar{c}}{V} + \\
&\quad + C_{X_{\dot{\alpha}}}\frac{\dot{\alpha}\bar{c}}{V} + C_{X_{\delta_e}}\delta_e , \\
C_Z &= C_{Z_0} + C_{Z_{\Delta p_t}}\frac{\Delta p_t}{\tfrac{1}{2}\rho V^2} + C_{Z_\alpha}\alpha + C_{Z_q}\frac{q\bar{c}}{V} + \\
&\quad + C_{Z_{\dot{\alpha}}}\frac{\dot{\alpha}\bar{c}}{V} + C_{Z_{\delta_e}}\delta_e , \\
C_m &= C_{m_0} + C_{m_{\Delta p_t}}\frac{\Delta p_t}{\tfrac{1}{2}\rho V^2} + C_{m_\alpha}\alpha + C_{m_q}\frac{q\bar{c}}{V} + \\
&\quad + C_{m_{\dot{\alpha}}}\frac{\dot{\alpha}\bar{c}}{V} + C_{m_{\delta_e}}\delta_e ,
\end{aligned} \qquad (2.2\text{-}2)$$

and:

$$\begin{aligned}
C_Y &= C_{Y_0} + C_{Y_\beta}\beta + C_{Y_p}\frac{pb}{2V} + C_{Y_r}\frac{rb}{2V} + \\
&\quad + C_{Y_{\dot{\beta}}}\frac{\dot{\beta}b}{V} + C_{Y_{\delta_a}}\delta_a + C_{Y_{\delta_r}}\delta_r , \\
C_l &= C_{l_0} + C_{l_\beta}\beta + C_{l_p}\frac{pb}{2V} + C_{l_r}\frac{rb}{2V} + \\
&\quad + C_{l_{\dot{\beta}}}\frac{\dot{\beta}b}{V} + C_{l_{\delta_a}}\delta_a + C_{l_{\delta_r}}\delta_r , \\
C_n &= C_{n_0} + C_{n_\beta}\beta + C_{n_p}\frac{pb}{2V} + C_{n_r}\frac{rb}{2V} + \\
&\quad + C_{n_{\dot{\beta}}}\frac{\dot{\beta}b}{V} + C_{n_{\delta_a}}\delta_a + C_{n_{\delta_r}}\delta_r .
\end{aligned} \qquad (2.2\text{-}3)$$

In cases where an aerodynamical plane of

symmetry exists (coinciding with the geometrical plane of symmetry) it follows that these 'cross coupling' effects can be neglected in first order aerodynamic models.

It can be seen here that the relations (2.2-2) and (2.2-3) result in nonlinear relations for the dimensional aerodynamic forces and moments. For example, using equation (2.2-1) in the model for C_X in (2.2-2) we get:

$$C_X = (C_{X_0} + a C_{X_{\Delta p_t}}) + b C_{X_{\Delta p_t}} \frac{P}{\frac{1}{2}\rho V^3} +$$

$$+ C_{X_\alpha}\alpha + C_{X_q}\frac{q\bar{c}}{V} + C_{X_{\dot{\alpha}}}\frac{\dot{\alpha}\bar{c}}{V} + C_{X_{\delta_e}}\delta_e .$$

For constant engine power P the expression for the dimensional aerodynamic force X:

$$X = C_X \tfrac{1}{2}\rho V^2 S$$

may then be written as the following nonlinear expression:

$$X = X_{V^2}V^2 + X_{V^{-1}}V^{-1} + X_{\alpha V^2}\alpha V^2 +$$

$$+ X_{qV}qV + X_{\dot{\alpha}V}\dot{\alpha}V + X_{\delta_e V^2}\delta_e V^2 .$$

In line with what was stated above concerning the development of a priori aerodynamic models systematic wind tunnel evaluations were made to verify the postulated relations between the force and moment coefficients and the following variables in the right hand side of (2.2-2) and (2.2-3): α, β, $\Delta p_t/\frac{1}{2}\rho V^2$, δ_e, δ_a and δ_r. The evaluations were made in a high quality low subsonic wind tunnel with a 1:11 scale model of the De Havillland DHC-2 Beaver [14]. The model was equipped with an engine driven propeller to simulate slipstream effects. Some of the results are shown in fig. 2-1. These wind tunnel results indicated that the a priori models (2.2-2) and (2.2-3) would fail to describe several significant nonlinear characteristics. For example, it follows from fig. 2-1(a) that C_X and C_m depend in a nonlinear fashion on α. Further, a pronounced lateral to longitudinal aerodynamic *cross coupling* exists in the sense that C_m also depends on β. Fig. 2-1(b) shows that while the C_Y-β and C_l-β relations are approximately linear, this is certainly not true for the relation C_n-β. In addition the same figure shows that C_Y, C_l and C_n all depend on $\Delta p_t/\frac{1}{2}\rho V$and α, an example of longitudinal to lateral aerodynamic cross coupling. Finally, from Fig. 2-1(c) it follows that the lateral control derivatives with respect to δ_r depend on $\Delta p_t/\frac{1}{2}\rho V^2$. In retrospect this is not surprising since at least part of the vertical tailplane is submerged in the propeller slip stream.

The wind tunnel results can be exploited next to extend the a priori model with additional terms accounting for the observed (static) nonlinearities and cross coupling effects. However, as we are inclined to add only a limited number of additional terms for reasons discussed in chapter 4, the resulting a priori model will still only be capable to approximate the observed static aerodynamic characteristics. The resulting a priori model accounts for the nonstationarity of actual flight conditions with simple terms containing first order derivatives of α and β. We must expect this to lead to rather crude approximations of the actual complex aerodynamic phenomena of nonsteady flight.

Finally, the resulting a priori model describes only the *deterministic* components of the aerodynamic force and moment coefficients. This means that stochastic contributions as generated by turbulent boundary layers, turbulence in the propeller slipstream and local flow separations are not included. The effect of such random fluctuations on aircraft motion is discussed in Jones [63].

2.2.2 Linearized Aerodynamic Models

For small deviations from a stationary rectilinear flight condition, well known linear models may be derived of the aerodynamic force and moment coefficients [57].

The linear nondimensional models of the longitudinal force and moment coefficients $\tilde{C}_X$, $\tilde{C}_Z$ and $\tilde{C}_m$ may be written as:

$$\begin{bmatrix}\tilde{C}_X\\ \tilde{C}_Z\\ \tilde{C}_m\end{bmatrix} = \begin{bmatrix} C_{X_u} & C_{X_\alpha} & C_{X_q} & C_{X_{\dot{\alpha}}} & C_{X_{\delta_e}}\\ C_{Z_u} & C_{Z_\alpha} & C_{Z_q} & C_{Z_{\dot{\alpha}}} & C_{Z_{\delta_e}}\\ C_{m_u} & C_{m_\alpha} & C_{m_q} & C_{m_{\dot{\alpha}}} & C_{m_{\delta_e}}\end{bmatrix} \cdot \begin{bmatrix}\tilde{u}/V_0\\ \tilde{\alpha}\\ \tilde{q}\bar{c}/V_0\\ \tilde{\dot{\alpha}}\bar{c}/V_0\\ \tilde{\delta}_e\end{bmatrix} . \qquad (2.2\text{-}4)$$

where:

$$\tilde{C}_X = \frac{\tilde{X}}{\frac{1}{2}\rho_0 V_0^2 S}, \quad \tilde{C}_Z = \frac{\tilde{Z}}{\frac{1}{2}\rho_0 V_0^2 S}, \quad \tilde{C}_m = \frac{\tilde{M}}{\frac{1}{2}\rho_0 V_0^2 S\bar{c}}. \tag{2.2-5}$$

and C_{X_u}, C_{X_α}, etc. denote the *longitudinal stability and control derivatives* in the body fixed reference frame F_B. The models in the stability reference frame F_S can be written as:

$$\begin{bmatrix} \tilde{C}_{X_S} \\ \tilde{C}_{Z_S} \\ \tilde{C}_{m_S} \end{bmatrix} = \left[C_{X,Z,m}\right]_S \cdot \begin{bmatrix} \tilde{u}_S/V_0 \\ \tilde{\alpha} \\ \tilde{q}_S\bar{c}/V_0 \\ \dot{\tilde{\alpha}}\bar{c}/V_0 \\ \tilde{\delta}_e \end{bmatrix} \tag{2.2-6}$$

where:

$$\left[C_{X,Z,m}\right]_S = \begin{bmatrix} C_{X_{u_S}} & C_{X_{\alpha_S}} & C_{X_{q_S}} & C_{X_{\dot{\alpha}_S}} & C_{X_{\delta_{e_S}}} \\ C_{Z_{u_S}} & C_{Z_{\alpha_S}} & C_{Z_{q_S}} & C_{Z_{\dot{\alpha}_S}} & C_{Z_{\delta_{e_S}}} \\ C_{m_{u_S}} & C_{m_{\alpha_S}} & C_{m_{q_S}} & C_{m_{\dot{\alpha}_S}} & C_{m_{\delta_{e_S}}} \end{bmatrix}.$$

The linear nondimensional models of the lateral force and moment coefficient $\tilde{C}_Y$, $\tilde{C}_l$ and $\tilde{C}_n$ may be written as:

$$\begin{bmatrix} \tilde{C}_Y \\ \tilde{C}_l \\ \tilde{C}_n \end{bmatrix} = \begin{bmatrix} C_{Y_\beta} & C_{Y_p} & C_{Y_r} & C_{Y_{\dot{\beta}}} & C_{Y_{\delta_a}} & C_{Y_{\delta_r}} \\ C_{l_\beta} & C_{l_p} & C_{l_r} & C_{l_{\dot{\beta}}} & C_{l_{\delta_a}} & C_{l_{\delta_r}} \\ C_{n_\beta} & C_{n_p} & C_{n_r} & C_{n_{\dot{\beta}}} & C_{n_{\delta_a}} & C_{n_{\delta_r}} \end{bmatrix} \cdot \begin{bmatrix} \tilde{\beta} \\ \tilde{p}b/2V_0 \\ \tilde{r}b/2V_0 \\ \dot{\tilde{\beta}}b/V_0 \\ \tilde{\delta}_a \\ \tilde{\delta}_r \end{bmatrix} \tag{2.2-7}$$

where:

$$\tilde{C}_Y = \frac{\tilde{Y}}{\frac{1}{2}\rho_0 V_0^2 S}, \quad \tilde{C}_l = \frac{\tilde{L}}{\frac{1}{2}\rho_0 V_0^2 Sb}, \quad \tilde{C}_n = \frac{\tilde{N}}{\frac{1}{2}\rho_0 V_0^2 Sb}. \tag{2.2-8}$$

and C_{Y_β}, C_{Y_p}, etc. denote the *lateral stability* and *control derivatives* in the body fixed reference frame F_B. The corresponding models in stability frame of reference F_S can be written as:

$$\begin{bmatrix} \tilde{C}_{Y_S} \\ \tilde{C}_{l_S} \\ \tilde{C}_{n_S} \end{bmatrix} = \left[C_{Y,l,n}\right]_S \cdot \begin{bmatrix} \tilde{\beta} \\ \tilde{p}_S b/2V_0 \\ \tilde{r}_S b/2V_0 \\ \dot{\tilde{\beta}}b/V_0 \\ \tilde{\delta}_a \\ \tilde{\delta}_r \end{bmatrix} \tag{2.2-9}$$

where:

$$\left[C_{Y,l,n}\right]_S = \begin{bmatrix} C_{Y_{\beta_S}} & C_{Y_{p_S}} & C_{Y_{r_S}} & C_{Y_{\dot{\beta}_S}} & C_{Y_{\delta_{a_S}}} & C_{Y_{\delta_{r_S}}} \\ C_{l_{\beta_S}} & C_{l_{p_S}} & C_{l_{r_S}} & C_{l_{\dot{\beta}_S}} & C_{l_{\delta_{a_S}}} & C_{l_{\delta_{r_S}}} \\ C_{n_{\beta_S}} & C_{n_{p_S}} & C_{n_{r_S}} & C_{n_{\dot{\beta}_S}} & C_{n_{\delta_{a_S}}} & C_{n_{\delta_{r_S}}} \end{bmatrix}.$$

Some computer programs are available for the linearization of aerodynamic models. In particular NASA Dryden has developed an interactive Fortran program 'linear' that provides the user with a powerful and flexible tool for the linearization of aircraft aerodynamic models [64]. The program numerically determines a linear system model from a nonlinear aerodynamic model supplied by the user.

2.3 Observation Models

Observation models relate certain measured variables such as airspeed and barometric altitude, to the components of the state vector and input

vector as defined in (2.1-8). Observation models take the form of nonlinear algebraic relations between the observed variables and the state- and input vector components, see section 2.3.1. A linearized version, used in the reconstructibility analysis of chapter 3 is given in section 2.3.2.

2.3.1 Nonlinear Observation Models

In this section the models are derived for observations of true air speed V, angle of attack α, side slip angle β, barometric altitude variations and geographical position measurements.
True air speed V can be derived from differential and absolute barometric and temperature transducers. The observation model for V follows directly from its definition as the resultant of the air velocity components u, v and w along the axes of F_B:

$$V = \sqrt{u^2 + v^2 + w^2} \ . \tag{2.3-1}$$

By definition, the angle of attack is:

$$\alpha = \arctan\frac{w}{u} \ , \tag{2.3-2}$$

which is different from α_v, the angle of attack measured by an angle of attack vane. This is due to a number of effects, such as aircraft induced air velocity components, the rotation of F_B about the X_B and Y_B axes, vane dynamics and boom bending. The first two effects can be described by:

$$\alpha_v = \arctan\frac{w - x_\alpha q + y_\alpha p}{u} + C_{up}\alpha + C_{\alpha_o} \ , \tag{2.3-3}$$

where C_{up} is the upwash coefficient and C_{α_o} is the zero shift of the angle of attack vane. It is assumed that the measured angle of attack depends linearly on α [36]. In practice, the actual upwash may also depend on engine power settings.

The side slip angle is defined as:

$$\beta = \arctan\frac{v}{\sqrt{u^2 + w^2}} \ , \tag{2.3-4}$$

which is again different from what a side slip vane would measure, as shown in fig. 2-2. When the vane axis of rotation is parallel to the Z_B axis and the effects of an aircraft induced side velocity components and the rotation of F_B about the X_B and Z_B axes are taken into account, the side slip vane angle is:

$$\beta_v = \arctan\frac{v + x_\beta r - z_\beta p}{u} + C_{si}\beta + C_{\beta_o} \ , \tag{2.3-5}$$

where x_β and z_β are the coordinates of the wind vane relative to F_B, C_{si} is the sidewash coefficient of the wind vane and C_{β_o} accounts for the vane being positioned outside the aircraft's geometrical plane of symmetry as well as for any asymmetry of the air flow due to for example rotation in the propeller slipstream. The aircraft induced part of the measured sideslip angle is assumed to be a linear function of β. The quantities C_{si} and C_{β_o} should either be given or estimated from the flight test data.

Altitude variations can accurately be measured with differential pressure transducers as long as the flight condition is 'quasi stationary'. The corresponding observation model is:

$$\Delta h = -z_E \ . \tag{2.3-6}$$

In principle any navigation system (e.g. inertial platform, doppler radar, OMEGA or DME) may be used for the measurement of the geographical position. In the case of a flat earth approximation, it is often convenient to express the geographical position in terms of coordinates x_E and y_E in a vertical earth fixed reference frame F_E.

V, Δh, α_v and β_v are components of an observation vector $\underline{y}$:

$$\underline{y} = \mathrm{col}\left(V, \Delta h, \alpha_v, \beta_v\right) \ . \tag{2.3-7}$$

The observation vector $\underline{y}$ above reflects the configuration of the flight measurement system as used in the flight test program discussed in the following chapters. If for example the measurement system would include an Inertial Reference System (IRS) then pitch, roll and yaw attitude angles could have been included in $\underline{y}$ as well.
Equations (2.3-1) to (2.3-6) may be written in the form of the following observation equation:

$$\underline{y} = \underline{h}(\underline{x}, \underline{u}) \tag{2.3-8}$$

2.3.2 Linearized Observation Models

In the stability reference frame F_S, the equation for resultant velocity V is given by:

$$V = \sqrt{u_S^2 + v_S^2 + w_S^2} \,. \tag{2.3-9}$$

The corresponding linearized from is:

$$\tilde{V} = \tilde{u}_S \,. \tag{2.3-10}$$

The linearized form of the observation model of the angle of attack vane for small deviations from the nominal stationary and rectilinear flight condition is given by:

$$\begin{aligned}
\alpha_{v_0} + \tilde{\alpha}_v &= \arctan\frac{w_0}{u_0} + \\
&+ \frac{1}{1 + \left(\frac{w_0}{u_0}\right)^2}\left(\frac{\tilde{w}}{u_0} - \frac{x_\alpha}{u_0}\tilde{q} + \frac{y_\alpha}{u_0}\tilde{p}\right) + \\
&+ C_{up}(\alpha_0 + \tilde{\alpha}) + C_{\alpha_0} \\
&= (1 + C_{up})\alpha_0 + C_{\alpha_0} + (1 + C_{up})\tilde{\alpha} + \\
&- \frac{x_{\alpha_S}}{V_0}\tilde{q}_S + \frac{y_{\alpha_S}}{V_0}\tilde{p}_S \,.
\end{aligned} \tag{2.3-11}$$

In the nominal flight condition, the vane angle is:

$$\alpha_{v_0} = (1 + C_{up})\alpha_0 + C_{\alpha_0} \,.$$

Subtraction of α_{v_0} from both sides of equation (2.3-11) results in the following linearized observation model:

$$\tilde{\alpha}_v = C_{\alpha_1}\tilde{\alpha} - \frac{x_{\alpha_S}}{V_0}\tilde{q}_S + \frac{y_{\alpha_S}}{V_0}\tilde{p}_S \,, \tag{2.3-12}$$

where:

$$C_{\alpha_1} = (1 + C_{up})$$

The observation model of the sideslip vane can be linearized in a similar way resulting in:

$$\begin{aligned}
\beta_{v_0} + \tilde{\beta}_v &= \arctan\frac{v_0}{u_0} + \\
&+ \frac{1}{1 + \left(\frac{v_0}{u_0}\right)^2}\left(\frac{\tilde{v}}{u_0} + \frac{x_\beta}{u_0}\tilde{r} - \frac{z_\beta}{u_0}\tilde{p}\right) \\
&+ C_{si}(\beta_0 + \tilde{\beta}) + C_{\beta_0} \\
&= \frac{\tilde{v}}{u_0} + \frac{x_\beta}{u_0}\tilde{r} - \frac{z_\beta}{u_0}\tilde{p} + C_{si}\tilde{\beta} + C_{\beta_0}
\end{aligned}$$

since $v_0=\beta_0=0$. Substitution of $u_0=V_0\cos\alpha_0$ and transformation of x_β, z_β, $\tilde{r}$ and $\tilde{p}$ from F_B to F_S results in:

$$\begin{aligned}
\beta_{v_0} + \tilde{\beta}_v &= C_{\beta_1}\tilde{\beta} + \frac{x_{\beta_S}}{V_0\cos\alpha_0}\tilde{r}_S - \\
&- \frac{z_{\beta_S}}{V_0\cos\alpha_0}\tilde{p}_S + C_{\beta_0} \,,
\end{aligned} \tag{2.3-13}$$

in which:

$$C_{\beta_1} = \frac{1}{\cos\alpha_0} + C_{si}$$

It is very difficult to determine C_{β_o} in flight. This can be seen as follows. Assume first a stationary rectilinear flight condition with roll angle equal to zero. Then, for a strictly symmetrical airflow condition, the sideslip must be zero. For propeller driven aircraft, however, the airflow cannot be assumed to be symmetrical due to the rotation in the propeller slipstream. Consequently, a stationary rectilinear flight with zero roll angle does no longer imply a zero sideslip angle (in addition, if the side slip vane is not mounted in the aircraft's symmetry plane, there will also be an offset in β_v). Let the side slip then be equal to β_0 and the vane indicate a value β_{v_o} in this condition of zero roll angle. In the nominal flight condition with zero roll angle mentioned above it then follows from equation (2.3-13) that:

$$C_{\beta_0} = \beta_{v_0} - C_{\beta_1}\beta_0 \,,$$

and because β_0 is unknown, C_{β_o} is unknown also. The consequence of this is that the linearized observation model of the side slip vane, comprises an unknown constant C_{β_o} according to:

$$\tilde{\beta}_v = C_{\beta_1}\tilde{\beta} + \frac{x_{\beta_S}}{V_0\cos\alpha_0}\tilde{r}_S - \frac{z_{\beta_S}}{V_0\cos\alpha_0}\tilde{p}_S + C_{\beta_0} \tag{2.3-14}$$

where $\tilde{\beta}_v$ indicates a deviation of the vane angle with respect to β_{v_o}. The fact that C_{β_o} is unknown actually affects the reconstructibility of the sideslip angle. This is discussed in detail in section 3.1.2.

2.4 Models of Measurement Errors

The outputs of the sensors used for measurement of the system input and output signal components are corrupted with time dependent errors.

The components of the *input vector* $\underline{u}$ are measured by the accelerometer and rate gyroscopes. These measurements are assumed to be contaminated with constant bias errors as well as with random errors. By careful pre-flight calibration the scale factor and misalignment errors can be neglected, although these can become important for recordings of long duration. The error model is expressed as:

$$\underline{u}_m = \begin{pmatrix} A_x(i) \\ A_y(i) \\ A_z(i) \\ p(i) \\ q(i) \\ r(i) \end{pmatrix}_m = \begin{pmatrix} A_x(i) \\ A_y(i) \\ A_z(i) \\ p(i) \\ q(i) \\ r(i) \end{pmatrix} - \underline{\lambda} - \underline{w}(i) \ , \tag{2.4-1}$$

where the index i refers to a discrete time t_i,

$$\underline{\lambda} = \mathrm{col}\left(\lambda_x, \lambda_y, \lambda_z, \lambda_p, \lambda_q, \lambda_r\right)$$

represents a vector of *bias error corrections* which are unknown but assumed to be constant during each dynamic flight test manoeuvre and:

$$\underline{w} = \mathrm{col}\left(w_x, w_y, w_z, w_p, w_q, w_r\right)$$

represents a vector of additive stochastic measurement errors. These errors are assumed to be zero mean and uncorrelated, i.e.:

$$\begin{aligned} E\{\underline{w}(i)\} &= \underline{0} \\ E\{\underline{w}(i)\,\underline{w}^T(j)\} &= V_{ww}\cdot\delta_{ij} \ . \end{aligned} \tag{2.4-2}$$

The measurements of the *observation vector* are the barometric and the vane measurements. The barometric measurements V and Δh are assumed to be corrupted only with random measurement errors. The bias of these differential barometric measurements can be measured by short circuiting of the pneumatic sensor systems prior and posterior to each flight test manoeuvre, which allows an accurate post flight compensation of the bias errors. The absolute static pressure measurement defines the reference condition and therefore its bias is usually not important for parameter identification.

Usually, the bias and scale factor errors in the vane angle transducers are small enough to be negligible, because these transducers are relatively stable and can be calibrated very well before flight. In addition in flight these transducer errors are indistinguishable from the much larger upwash and sidewash calibration coefficients discussed in section 2.3. Therefore only random errors are assumed.

In summary the measurement errors of the observation vector $\underline{y}$ are all assumed to be:

$$\underline{y}_m = \underline{y} + \underline{v} \ , \tag{2.4-3}$$

where the measured variable is denoted by $\underline{y}_m$, and $\underline{y}$ is assumed to be free of bias errors. The stochastic measurement errors $\underline{v}$ are assumed to be additive, zero mean and uncorrelated according to:

$$\begin{aligned} E\{\underline{v}(i)\} &= \underline{0} \\ E\{\underline{v}(i)\,\underline{v}^T(j)\} &= V_{vv}\cdot\delta_{ij} \ . \end{aligned} \tag{2.4-4}$$

The final set of measurements are not in the observation model presented in section 2.3, because they are not used in flight path reconstruction, but in *parameter identification.*

The total pressure increase Δp_t in the propeller slipstream was measured with a differential pressure transducer of the same type and quality as used for the measurement of V and Δh. Therefore, zero mean and uncorrelated measurement errors can also be assumed for this variable. The control surface deflections δ_a, δ_e and δ_r transducers are also stable sensors, which can be well calibrated on the ground, so again zero mean and uncorrelated measurement errors can be assumed.

The above modelling of the measurement errors is only valid if the utmost care is devoted to the quality of the transducers as well as of the data

logging part of the instrumentation system and to careful and repeated calibration of all measuring channels. The typical accuracies of the measurement system used in the flight experiments is shown in chapter 7 by the results of extensive laboratory calibrations.

In the design phase of the above measurement system much attention was given to the 'quality' of the transducers to be used in the system. Perhaps one of the most significant benefits of using such high quality transducers is that models of the measurement error characteristics can assume relatively simple forms, a typical example of this are the inertial measurement errors.

2.5 Conclusions

In this chapter, different kinds of mathematical models were presented, namely kinematic, aerodynamic, observation and error models. Nonlinear as well as linear versions of these models were derived. The nonlinear versions of the models are used for the actual analysis of dynamic flight test measurements. Their linearized counterparts are used in chapter 3 and 4 for analysis of state reconstructibility and identifiability of stability and control derivatives, and in chapter 5 for the optimization of control inputs of dynamic flight test manoeuvres.

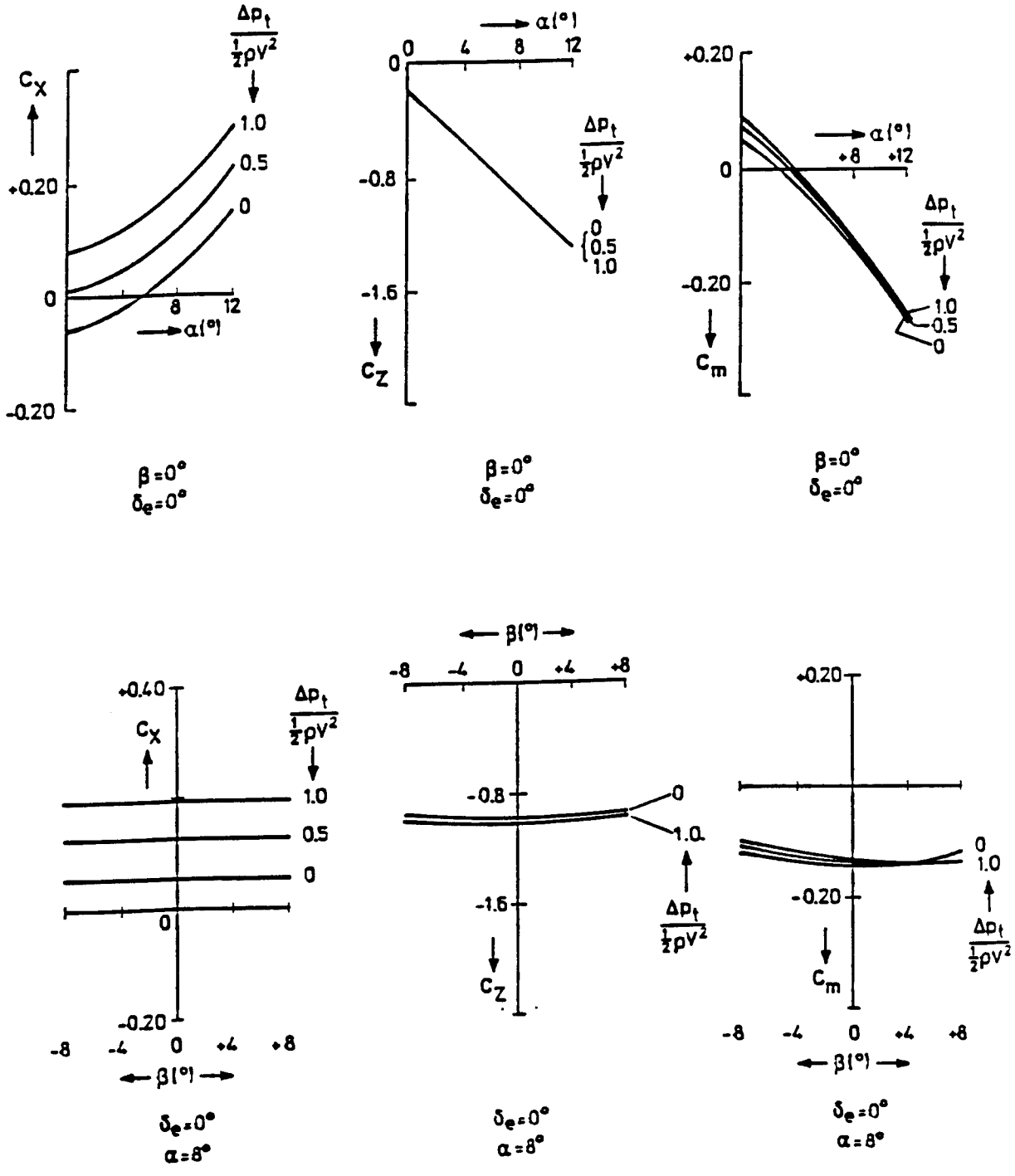

Figure 2-1(a): *Longitudinal aerodynamic force and moment coefficients of the DHC-2 Beaver aircraft as a function of angle of attack α and side slip angle β for three different values $\Delta p_t/\frac{1}{2}\rho V^2$ as measured at a Reynolds number of 0.47×10^6 on a 1:11 scale model in the wind-tunnel.*

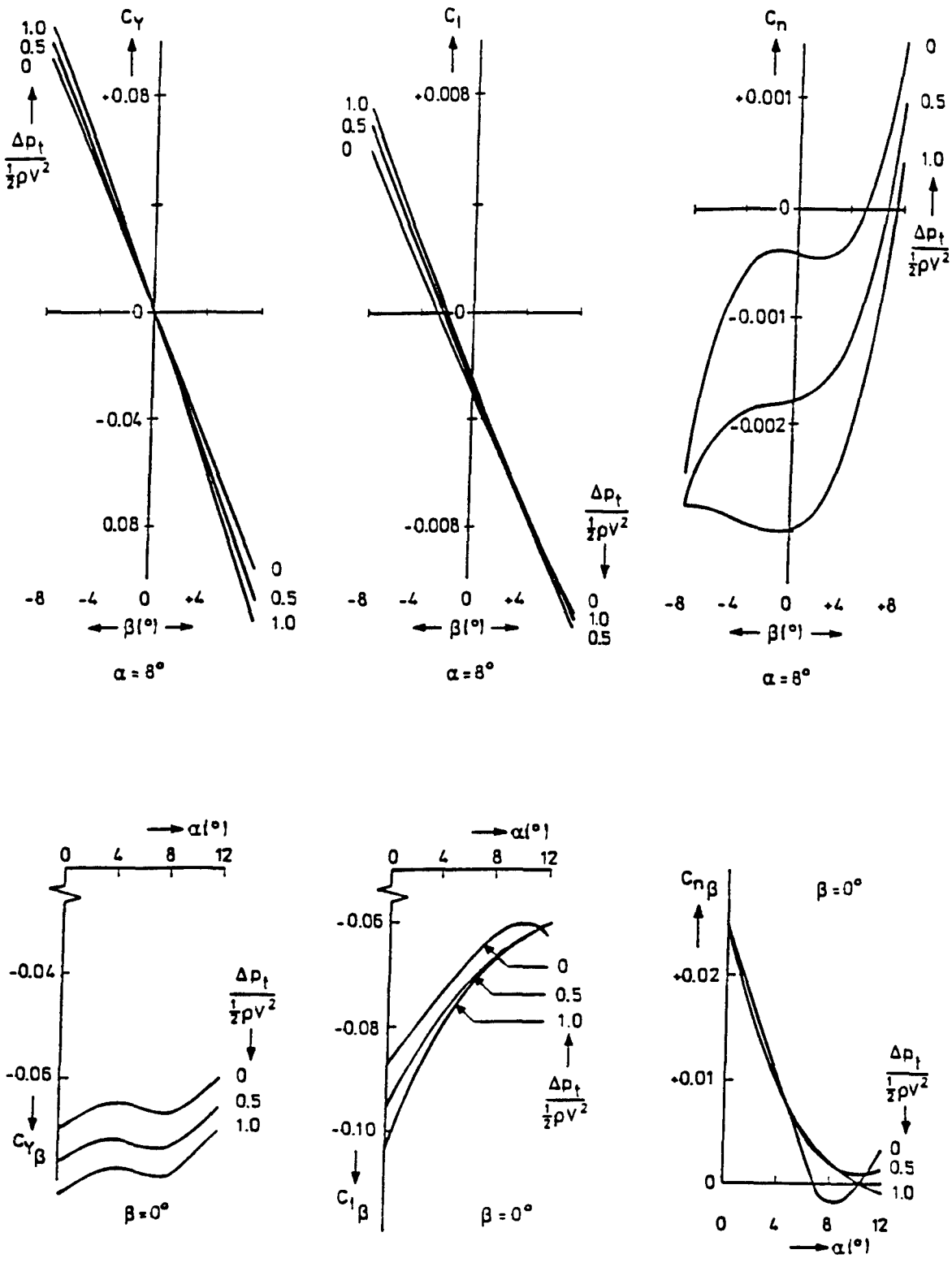

Figure 2-1(b): *Lateral aerodynamic force and moment coefficients as a function of side slip angle β, for three different values of* $\Delta p_t/\frac{1}{2}\rho V^2$.

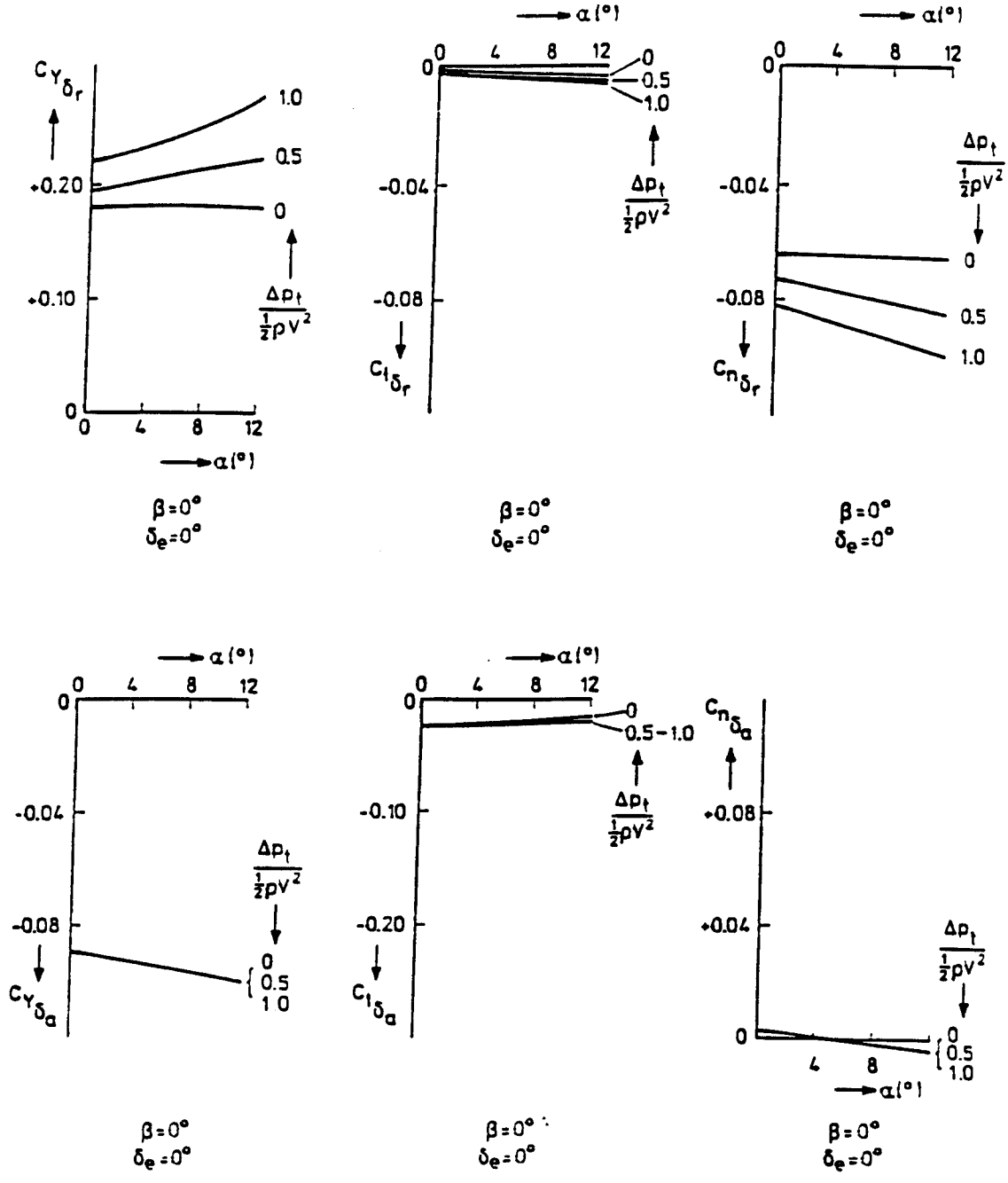

Figure 2-1(c): *Lateral aileron and rudder control derivatives as a function of angle of attack α, for three different values of* $\Delta p_t/\frac{1}{2}\rho V^2$.

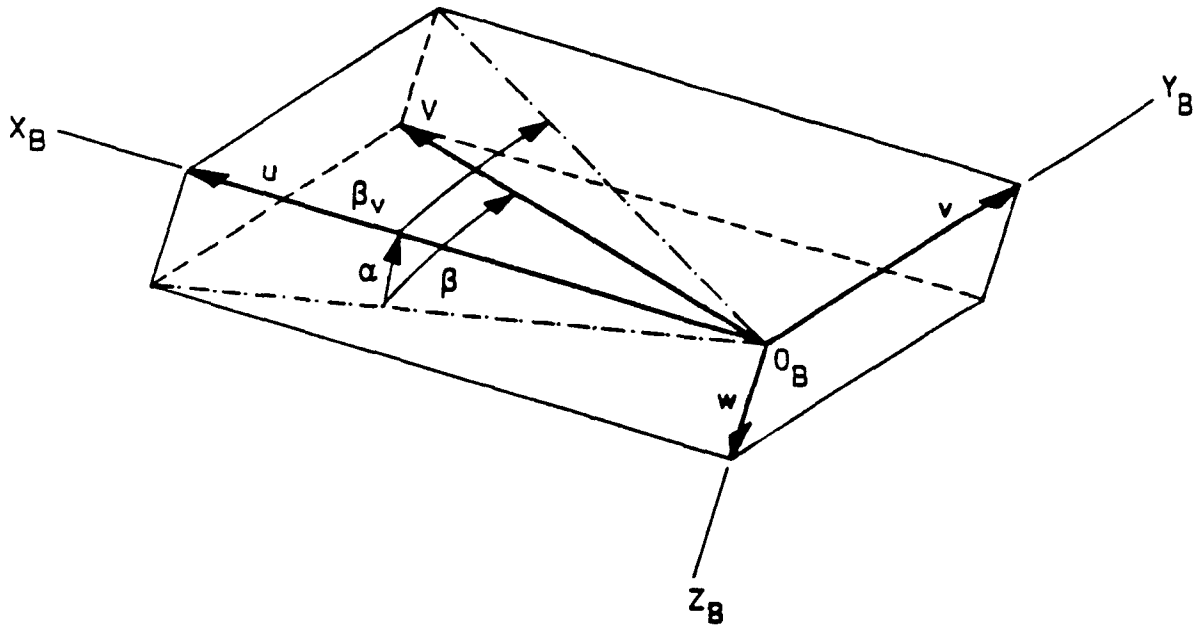

Figure 2-2: *Definition of side slip angle* β *and side slip vane angle* β_v.

3 FLIGHT PATH RECONSTRUCTION

The problem of flight path reconstruction from onboard measurements studied in this volume centres around properly combining the kinematic model of the aircraft's state trajectory (and so implicitly the aircraft's flight path) as discussed in chapter 2, with a compatible set of transducers such as inertial, barometric and flow angle transducers for the measurement of the input and output signals, see chapter 7. The calculation of the aircraft's state trajectory from the recorded input- and output measurements is what is called a state estimation or state reconstruction problem in the system theoretical literature. The term estimation is used if the calculation of the state vector is based on the measurements up to and including the present time. The term reconstruction indicates that all available measurements of a complete flight test manoeuvre are used to calculate the state vector. Reconstruction can only be used for post-manoeuvre data analysis. However, as a 'reconstructed' state vector is based on past as well as future measurements it will be intuitively clear that reconstructed state vectors are in principle more accurate than 'estimated' state vectors.

The earliest aircraft state reconstructions used barometric airspeed and altitude output measurements, e.g. Gerlach [3]. As airspeed and altitude measurements define a 'flight path' the aircraft state reconstruction problem was subsequently called '*flight path reconstruction*' by Jonkers [6].

The initial motive behind the development of flight path reconstruction methods was to reconstruct certain variables which are difficult to measure directly in dynamic flight conditions. One typical examples of such a variable is the angle of attack. It soon followed that several transducer bias errors could be (and in fact had to be) estimated simultaneously.

Following a flight path reconstruction, the reconstructed state variables are used for the identification of the aerodynamic model as described in chapter 4. Several performance and stability and control characteristics of interest may subsequently be derived either directly from the aerodynamic model or by correcting the reconstructed aircraft states of the actual flight condition of nonstationary flight to a 'corresponding' stationary flight condition, also using the identified aerodynamic model [5,11].

Historical Background

The first application of state estimation to post flight data analysis was made by Gerlach around 1960 at the Delft University of Technology. While early attempts to measure aircraft performance in quasi-steady and nonsteady flight conditions suffered from inadequate instrumentation, he applied high accuracy instrumentation techniques and showed that the need for direct measurement of the angle of attack could be eliminated. This stimulated research in and development of so called flight path reconstruction methods.

This early invention was primarily concerned with the accurate determination of the angle of attack and airspeed during dynamic symmetrical flight test manoeuvres. The difficult problem of measuring the angle of attack directly in dynamic flight conditions by means of vanes was circumvented by deriving it instead as the difference between the pitch angle and the flight path angle. Airspeed and flight path angle could be derived from horizontal and vertical speed. Pitch angle, horizontal and vertical speed as well as altitude were all obtained by integrating functions of measurements from a high accuracy pitch rate gyro and high accuracy normal and longitudinal accelerometers. The initial conditions for the integration were determined from airspeed and altitude measurements at the steady state initial part of the manoeuvre. It soon turned out that the results of the integration suffered from imprecise initial conditions and the effect of small unknown bias errors of the pitch rate gyro and the longitudinal and vertical accelerometers. This led to the idea to 'compare' computed airspeed and altitude with high accuracy barometric measurements of these variables. Regression techniques were used next in an iterative loop to compute least squares estimates of the initial conditions and of the unknown bias errors, see [4, 5,66]. Later, Jonkers [6] used the *Extended Kalman Filter and Kalman Smoother* to solve the same problem. Since the barometric airspeed and altitude measurements define a flight path he introduced the name flight path reconstruction. Mulder [10] compared Maximum Likelihood solutions with those from the extended Kalman Filter and Kalman

Smoother.

Except for probably being the first to demonstrate the feasibility of flight path reconstruction methods Gerlach also pointed out that these methods may serve also to provide a check on instrument accuracy and data consistency apart from generating estimates of unmeasured or poorly measured variables. These items were the primary objectives in most of the studies that followed Gerlach's original work [3 to 5]. All results of Gerlach were obtained in low speed symmetrical flight conditions. Subsequently the technique was applied successfully to high speed flight and asymmetrical flight conditions.
Subsequently, probably the earliest uses of state estimation techniques for flight path reconstruction elsewhere were Wingrove [31 to 33] at NASA Ames, Eulrich and Weingarten [34] at Calspan, and Molusis [35] at Sikorsky Aircraft and later Klein [36] at JIAFS, NASA Langley. Over the past few years, the work in this field has been evolving towards the use of more detailed kinematic models, the development of more sophisticated algorithms, and new applications [31].

The flight path reconstruction problem can be solved by a number of different methods. Several important techniques are:

Weighted Least-Squares - This method solves the case where the random error is assumed to be present only in the inputs of the kinematic model as used for flight path reconstruction. This means that only system state noise is considered. The resulting algorithm, which is of the so-called *Equation Error* type, see Maine and Iliff [1] and chapter 4 later, is relatively simple and very efficient from the numerical point of view.

Extended Kalman Filter/Smoother - A standard Kalman filter [190] estimates the state of a linear system with an error model which allows noise in the inputs (system state noise) as well as noise in the observations. The Kalman algorithm is a recursive formula, which proceeds sequentially (filters) through the data. For a fixed time interval a substantial improvement in accuracy can be obtained by adding a smoothing step in the reverse time direction. Nonlinear kinematic equations are handled by linearizing around a nominal trajectory (usually the current best estimate of the trajectory is used) and bias and scale factors can be estimated by including them as undriven states with unknown initial condition, see section 3.1 below and Jonkers [6].

Output Error - This method applies in the case where all errors are assumed to be in the observations, i.e. there is no state noise. In principle the method compares a simulation of the actual system with the measurements, while integrating so-called sensitivity functions, which describe the influence of the model parameters on the state. After one simulation run, a Gauss-Newton (or alternative) optimization algorithm is used to find new estimates of the model parameters. In practice this process has to be repeated for several iterations, which makes this method relatively expensive in computer time. In addition the number of sensitivity equations can be large, which adds to the computer memory requirements. The sensitivity equations can be derived analytically. An alternative is compute sensitivities directly via finite differences. This results in very flexible software programs.

Filter Error - This method solves in principle the same problem formulation as the Extended Kalman Filter/Smoother i.e. with system state noise as well as observation noise. In principle it is a combination of a Kalman Filter and an Output Error method. The Filter Error method is the most expensive with respect to computer time of the above methods. In addition it is the most complex with respect to implementation and therefore seldomly used for practical flight path reconstructions.

Flight path reconstruction as a means of checking instrument accuracy and data consistency is now used by many flight test groups [37 to 49] and [235]. Once a consistent, smoothed set of time histories is obtained from the data, other analyses, such as estimation of aerodynamic model parameters can be readily performed, see chapter 4. The data consistency application is now more or less a routine matter and has been extensively treated in the literature. Some of the various other applications of flight path reconstruction have been in the area of aircraft accident analyses [50], estimation of wind vector components from high

altitude turbulence measurements [51], testing of high performance aircraft involving high angle of attack and spin manoeuvres [52], aircraft modelling [9 to 12,61,119] and stall speed determination. A good number of additional citations on this subject can be found in the papers of Chapman and Yates [189].

A number of computer programs are available for state estimation, but a particular reference must be made to the package SMACK (SMoothing for AirCraft Kinematics) [69] developed at NASA Ames research centre, DEKFIS (Discrete Extended Kalman Filter Smoother) developed at the Systems Control [44], FTDA (Flight Test Data Analysis) [30] developed at the Delft University of Technology and FPR (Flight Path Reconstruction) package developed at NLR Amsterdam [217].

Although it is possible in principle to apply any of the methods discussed above to the solution of the flight path reconstruction problem a choice is made in the remaining part of this chapter for the Extended Kalman Filter/Smoother for the following reasons. First the Extended Kalman Filter/Smoother allows to account for system noise as well as observation noise. The second reason is that this method has been well proven in many actual applications to flight path reconstruction problems. We first start discussing the application of the Extended Kalman Filter/Smoother to the flight path reconstruction problem in section 3.1, and then analyze some of the *reconstructibility characteristics* in section 3.2. This analysis is based on the linearized form of the kinematical model for flight path reconstruction as derived in section 2.1. We continue with a practical example in section 3.3 and conclusions in section 3.4.

The Extended Kalman Filter/Smoother algorithms used for flight path reconstruction are listed in full in appendix C. More details can be found in the extensive Kalman filter literature, for instance Sage and Melsa [71] for theoretical background or Brown and Hwang [234] for practical implementation details.

3.1 Nonlinear Flight Path Reconstruction

In this section, extended Kalman filtering and smoothing algorithms are applied to the solution of the nonlinear flight path reconstruction problem. First we will discuss the basic linear Kalman filter in section 3.1.1. Subsequently in section 3.1.2 it is shown that the problem must be re-formulated to fit the Kalman filter model. The application to the nonlinear flight path reconstruction is discussed in section 3.1.3 and the estimation of the unknown parameter vector is discussed in section 3.1.4. For convenience a summary of the Kalman filter and smoother algorithms is given in appendix C, together with a description of the application of Maximum Likelihood estimation to deterministic nonlinear flight path reconstruction. Finally section 3.1.5 describes how some additional quantities, which are needed for aerodynamic model identification, can be derived from the reconstructed flight path.

3.1.1 Basic Kalman Filter

This subsection discusses the basic linear Kalman filter as first published by Kalman [190]. This filter is based on the linear stochastic differential equations:

$$\begin{aligned} \dot{\underline{x}}(t) &= F\cdot\underline{x}(t) + G_u\cdot\underline{u}(t) + G_w\cdot\underline{w}(t) \ , \\ \underline{y}(t) &= H\cdot\underline{x}(t) + J\cdot\underline{u}(t) \ , \\ \underline{y}_m(i) &= \underline{y}(i) + \underline{v}(i) \ . \end{aligned} \tag{3.1-1}$$

In practice all measurements are sampled with a fixed time step Δt and the data processing is done by sequentially processing these samples. This means that the discrete form of (3.1-1) is required. The discrete form of the linearized state equations is:

$$\begin{aligned} \underline{x}(i+1) &= \Phi\cdot\underline{x}(i) + \Gamma_u\cdot\underline{u}(i) + \Gamma_w\cdot\underline{w}(i) \ , \\ \underline{y}_m(i) &= H\cdot\underline{x}(i) + J\cdot\underline{u}(i) + \underline{v}(i) \ . \end{aligned} \tag{3.1-2}$$

In which the transition matrix Φ, the deterministic input distribution matrix Γ_u and the stochastic input distribution matrix Γ_w can be calculated from F, G_u and G_w as shown in appendix C. The process noise $\underline{w}(i)$ and the measurement noise $\underline{v}(i)$ are assumed to be zero mean and white gaussian noise with covariances V_{ww} and V_{vv} respectively.

The Kalman filter that produces the optimal estimate of the state of this system is described in the following. When the estimate of the state at time step t_i, $\hat{\underline{x}}(i|i)$, is known, the estimate at time step t_{i+1}, $\hat{\underline{x}}(i+1|i)$, is:

$$\hat{\underline{x}}(i+1|i) = \Phi \cdot \hat{\underline{x}}(i|i) + \Gamma_u \cdot \underline{u}(i) \ . \tag{3.1-3}$$

This is called the *propagation step*. The covariance matrix $P(i+1|i)$ of the state at time step t_{i+1} follows from a known $P(i|i)$ as:

$$P(i+1|i) = \Phi P(i|i) \Phi^T + \Gamma_w V_{ww} \Gamma_w^T \ . \tag{3.1-4}$$

At this moment the measurements at t_{i+1} can be used in the *update step* to improve the state estimate at time step t_{i+1} by:

$$\hat{\underline{x}}(i+1|i+1) = \hat{\underline{x}}(i+1|i) + \\ + K(i+1) \left[\underline{y}_m(i+1) - H\hat{\underline{x}}(i+1|i) - J\underline{u}(i+1) \right] , \tag{3.1-5}$$

where the gain matrix $K(i+1)$ is calculated from the covariance matrix $P(i+1|i)$ by:

$$K(i+1) = P(i+1|i) H^T \left[HP(i+1|i) H^T + V_{vv} \right]^{-1} \ . \tag{3.1-6}$$

The covariance matrix of the improved estimate $P(i+1|i+1)$ is calculated as:

$$P(i+1|i+1) = \left[I - K(i+1) H \right] P(i+1|i) \ . \tag{3.1-7}$$

These relations are applied recursively, starting from the first time step t_0 by using the initial values for the estimate and the covariance matrix:

$$\hat{\underline{x}}(0|0) = \underline{0} \ , \\ P(0|0) = P_0 \ . \tag{3.1-8}$$

The estimate of the state vector at the final time t_N $\hat{\underline{x}}(N|N)$ is based on all measurements between t_0 and t_N, but for all earlier times the estimate $\hat{\underline{x}}(i|i)$ is based on only a part of the available measurements. The filter estimate can be improved by adding a *Smoother* step to the algorithm. One implementation of a Smoother is to start at the final time t_N and then work backwards towards t_0, all the while correcting the estimates for the information contained in the measurement after the current time, resulting in a smoother estimate $\hat{\underline{x}}(i|N)$, which for all t_i has a lower covariance $P(i|N)$ than the filter estimate $\hat{\underline{x}}(i|i)$ with $P(i|i)$.

3.1.2 Treatment of Input Noise

The standard Kalman filter is based on the linear stochastic differential equation given by (3.1-1). In section 2.1 a set of differential equations was derived that relates the aircraft state vector to the input vector of specific forces and angular rates (2.1-8b), repeated here:

$$\dot{\underline{x}} = \underline{f}(\underline{x}, \underline{u}) \ , \\ \underline{x}(0) = \underline{x}_0 \ . \tag{3.1-9}$$

where the state vector and input vector were defined in (2.1-8a) as:

$$\underline{x} = \mathrm{col}\left(u, v, w, \phi, \theta, \psi, x_E, y_E, z_E \right) \ , \\ \underline{u} = \mathrm{col}\left(A_x, A_y, A_z, p, q, r \right) \ . \tag{3.1-10}$$

If the input vector $\underline{u}$ and the initial value of the state vector $\underline{x}_0$ are precisely known then the state vector can be reconstructed by simple integration. In reality not all components of the initial value of the state are measured and the measurements are corrupted with errors. The input vector $\underline{u}$ is usually completely available, but its measurement is corrupted by errors such as bias error and random noise.

In sections 2.3 and 2.4 observation models and measurement error models were derived leading to equation (2.4-1) for the measurements $\underline{u}_m$ of the input vector and to equation (2.4-3) for the measurements of the state vector. The total observation vector is then:

$$\underline{z}_m = \begin{pmatrix} \underline{u}_m \\ \underline{y}_m \end{pmatrix} = \underline{h}'(\underline{x}, \underline{u}, \underline{\theta}) + \begin{pmatrix} \underline{w} \\ \underline{v} \end{pmatrix} \ , \tag{3.1-11}$$

where the vector $\underline{\theta}$ includes all the unknown parameters like biases, scale factors, vane calibration coefficients, wind components, etc. The vector $\underline{w}$ accounts for the noise on the measurements of the input vector $\underline{u}_m$ and $\underline{v}$ accounts for the noise on the measurements of the observation vector $\underline{y}_m$.

The problem with this formulation is that the 'true' input vector $\underline{u}$ is not available for use in equation (3.1-1). It is therefore convenient to transform the formulation into an equivalent form by not using

the 'true' but the 'measured' input vector $\underline{u}_m$ in (3.1-1). Using (2.4-1) this means that the system error model is now considered to be driven by $\underline{u}_m+\underline{w}+\underline{\lambda}$ instead of by $\underline{u}$, where

$$\underline{u}_m = \mathrm{col}\left(A_{x_m}, A_{y_m}, A_{z_m}, p_m, q_m, r_m\right) , \qquad (3.1\text{-}12)$$

and $\underline{\lambda}$ is the bias error error correction on the measurements of the original $\underline{u}$. (It should be noted that $\underline{\lambda}$ forms part of $\underline{\theta}$.) The new input vector $\underline{u}_m$ is by definition known exactly, but the noise vector $\underline{w}$ and the the bias error correction are now seen to be driving the system, e.g. that $\underline{w}$ is treated as system noise in (3.1-1), as was already implied by choice of name. The system differential equation now becomes:

$$\begin{aligned} \dot{\underline{x}} &= \underline{f}\left(\underline{x}, \underline{u}_m, \underline{w}, \underline{\theta}\right) , \\ \underline{x}(0) &= \underline{x}_0 . \end{aligned} \qquad (3.1\text{-}13)$$

and the observation equation becomes:

$$\underline{y}_m = \underline{h}\left(\underline{x}, \underline{u}_m, \underline{\theta}\right) + \underline{v} . \qquad (3.1\text{-}14)$$

The observation vector $\underline{y}_m$ now no longer includes direct measurements of the input vector $\underline{u}_m$, but $\underline{u}_m$ is still needed in the observation equation, because the angular rates and specific forces still appear in the observation models derived in section 2.3.

The equations are now in a form which is suitable for the application of Kalman filter theory. It should be added here that there are other approaches for this problem, see for instance Bach [40 to 43].

3.1.3 Linearized Kalman Filter

Now that the system equations are in the proper form the implementation of the nonlinear Kalman filter will be discussed. Initially, the estimation of the unknown parameter vector will be postponed to the next subsection.

The general flight path reconstruction problem is nonlinear. However, in order to apply Kalman filter techniques, the differential equations describing the errors must be linear. Three approaches will be discussed in the following.

In the first approach the kinematic and observation equation are linearized around a nominal steady-state flight condition. The problem is usually defined in the stability axis system using perturbation variables referred to the steady-state condition. This necessitates the calculation of the matrices of partial derivatives F, G_u, G_w, H and J which in this case are *constant*. This approach is assumed in appendix C.1 and is also used in the reconstructibility analysis in section 3.2. This approach is not used for practical flight path reconstruction, because for linearity reasons only small deviations from the steady-state flight condition are allowed.

In the second approach it is assumed that there is a nominal trajectory $\underline{x}^{nom}$ which is close to the true solution and in addition satisfies the system differential equation. This can be done by integrating (3.1-9) using $\underline{u}_m$ instead of $\underline{u}$. If the errors in $\underline{u}_m$ are small this will be reasonable. Then the perturbation $\tilde{\underline{x}}$ can be defined as:

$$\tilde{\underline{x}} = \underline{x} - \underline{x}^{nom} . \qquad (3.1\text{-}15)$$

By linearizing the system equations we obtain:

$$\begin{aligned} \dot{\tilde{\underline{x}}} &= F\cdot\tilde{\underline{x}} + G_w\cdot\underline{w} , \\ \tilde{\underline{y}} &= H\cdot\tilde{\underline{x}} + \underline{v} , \end{aligned} \qquad (3.1\text{-}16)$$

where F, G_w and H now are time-varying matrices of partial vector derivatives of the functions $\underline{f}(\underline{x},\underline{u},\underline{w})$ and $\underline{h}(\underline{x},\underline{u})$ with respect to the state vector $\underline{x}$ and the noise vector $\underline{w}$. Since the nominal trajectory satisfies the differential equations $\underline{u}_m$ does not affect the perturbation $\tilde{\underline{x}}$ and so no longer appears in these equations.
This approach has been succesfully applied to the updating of inertial navigation systems. The INS output can be directly used as a nominal trajectory, which will be reasonably close to the true trajectory, because the sensor errors of an INS are very small, see Brown and Hwang [234].

In order for the linearization to be accurate, it is important that the nominal trajectory $\underline{x}^{nom}$ is close to the actual trajectory. This is very difficult to achieve with flight test sensors. The third approach is then to use the *Extended Kalman Filter* (*EKF*) where in each update step the nominal trajectory is set equal to the last estimate of the state vector and

the error estimate is reset to zero. In practice the update correction is applied directly to the prediction of the actual system state $\hat{\underline{x}}(i+1|i)$ instead of to the estimate of the perturbation $\hat{\underline{x}}(i+1|i)$, see equation (C.2-8). Because the error estimate is reset to zero, the propagation equation (3.1-3) now becomes trivial and it is possible to directly integrate the system differential equations to the next time step using (C.2-2). This has the additional advantage that it is no longer necessary to pre-calculate a nominal trajectory before starting the Kalman filter procedure.

When the solution has converged this will ensure that the linearization will remain valid. However, the EKF may diverge when the estimate of the state is too far from the true solution, for example because of a poor initial estimate for the state $\underline{x}$.

In all the presented approaches, it is necessary to calculate matrices of partial derivatives. Analytical differentation can be done by hand which must be done with extreme care to prevent human errors. Here it is preferable to use a symbolic algebra package such as Maple or Mathematica, which will give correct answers, as long as the problem is entered correctly. A good alternative to analytical differentation is to calculate numerical derivatives during each step of the algorithm. Although this is expensive in computer time, this has the advantage of much flexibility if the system equations are changed frequently, because it can eliminate the need to change the software.

3.1.4 Estimation of Unknown Parameters

As stated earlier the system equations also contain a vector of unknown parameters $\underline{\theta}$, which includes biases, scale factors etc. If this is taken into account the flight path reconstruction problem becomes a *joint state and parameter estimation problem*. This can be handled in the Kalman filter approach by *augmenting* the state vector with the unknown parameter vector as:

$$\underline{x}' = \begin{pmatrix} \underline{x} \\ \underline{\theta} \end{pmatrix} \tag{3.1-17}$$

and adding

$$\dot{\underline{\theta}} = \underline{0} \tag{3.1-18}$$

to the differential equations. If one (or more) of the unknown parameters is not constant, but varies with time in an unpredictable manner, this component θ_k can be modelled as a Markov process:

$$\dot{\theta}_k = -\frac{1}{\tau_k}\theta_k + w_{\theta_k} . \tag{3.1-19}$$

Here τ_k is the correlation time that governs the temporal evolution of θ_k. If τ_k is large with respect to the observation time the evolution of θ_k will approximate a random walk. These models have been used to describe accelerometer and gyroscope drift, where τ_k turns out to be large (1 to 10 hours), see Brown and Hwang [234].

The same Markov model can also be used to describe the variation of the wind vector components with time and the change in the barometric pressure reference. In combination with absolute position measurements (e.g. GPS) this allows succesful Flight Path Reconstruction in less favorable wheather conditions, for flight tests with large changes in altitude and for longer flight recordings.

Adding unknown parameters must be done with great care, because too much added parameters will soon lead to nonreconstructible components in the augmented state. This is analyzed in detail in section 3.2. Furthermore, adding many constant parameters makes the Extended Kalman filter very prone to divergence. The reason for this is that when a parameter is modelled as a constant, the Kalman filter covariance of this parameter will converge to zero and this will cause the gain matrix K(i) also to converge to zero. In effect the Kalman filter will start to ignore the observations after a certain amount of time. This can be avoided by adding some artificial noise by using a Markov model instead of a constant parameter, since now the filter covariance and consequently the gain will no longer converge to zero.

For convenience the prime on the augmented state $\underline{x}$ will be dropped in the following discussions.

The Extended Kalman filter and smoother gives a solution of the nonlinear system state reconstruction problem, which takes the stochastic

measurement errors of accelerometers and rate gyros into account. However, in practice these measurement errors are very small. If these errors are assumed equal to zero (i.e. $\underline{w}=\underline{0}$) the flight path reconstruction problem becomes an *Output Error* problem. This makes it possible to formulate the flight path reconstruction problem in terms of the problem of calculating Maximum Likelihood estimates of the unknown parameters. This is described in more detail in appendix C.3.

In earlier work [10], extended Kalman filtering and smoothing solutions of the nonlinear flight path reconstruction problem have been compared to the corresponding solution resulting from the Output Error method. For the case of a flight test measurement system which was (with respect to accuracy) equivalent to the system used in the present study, both solutions proved to be virtually identical.

The actual application of the extended Kalman filter and smoother to flight path reconstruction in an actual flight test program is presented in section 3.3, together with some characteristic results.

3.1.5 Calculation of Additional Quantities

The results of the flight path reconstruction are used for the calculation of quantities needed for aerodynamic model identification as discussed in chapter 4.

With (2.3-1) airspeed is calculated as:

$$\hat{V} = \sqrt{\hat{u}^2 + \hat{v}^2 + \hat{w}^2} \quad , \tag{3.1-20}$$

in which the superscript $\hat{}$ indicates a reconstructed variable. Angle of attack and side slip angle are determined with (2.3-2) and (2.3-4) as:

$$\hat{\alpha} = \arctan\frac{\hat{w}}{\hat{u}} \quad , \tag{3.1-21}$$

$$\hat{\beta} = \arctan\frac{\hat{v}}{\sqrt{\hat{u}^2 + \hat{w}^2}} \quad . \tag{3.1-22}$$

Reconstructed bias error corrections are used to correct A_{z_m}, p_m and q_m. Aerodynamic forces are calculated according to (2.1-4) as:

$$\begin{aligned} X &= m(A_{x_m} + \hat{\lambda}_x) \ , \\ Y &= m(A_{y_m} + \hat{\lambda}_y) \ , \\ Z &= m(A_{z_m} + \hat{\lambda}_z) \ , \end{aligned} \tag{3.1-23}$$

and subsequently, the dimensionless aerodynamic force coefficients C_X, C_Y and C_Z are calculated by division by $\frac{1}{2}\rho\hat{V}^2S$.

Aerodynamic moments can be calculated with (2.1-2). This requires differentiation of the measured angular rotation rates since angular accelerations are not measured directly. Furthermore, the moments and products of inertia must be known. The relations used for the calculation of the aerodynamic moments read:

$$\begin{aligned} L &= I_x\dot{p}_m - (I_y - I_z)(q_m + \hat{\lambda}_q)r_m - \\ &\quad - I_{zx}(\dot{r}_m + (p_m + \hat{\lambda}_p)(q_m + \hat{\lambda}_q)) \ , \\ M &= I_y\dot{q}_m - (I_z - I_x)r_m(p_m + \hat{\lambda}_p) - \\ &\quad - I_{zx}(r_m^2 - (p_m + \hat{\lambda}_p)^2) + I_e\omega_e(r_m + \hat{\lambda}_r) \ , \\ N &= I_z\dot{r}_m - (I_x - I_y)(p_m + \hat{\lambda}_p)(q_m + \hat{\lambda}_q) - \\ &\quad - I_{zx}(\dot{p}_m - (q_m + \hat{\lambda}_q)r_m) - I_e\omega_e(q_m + \hat{\lambda}_q) \ . \end{aligned} \tag{3.1-24}$$

The dimensionless moment coefficients C_m, C_l and C_n are calculated by division by $\frac{1}{2}\rho\hat{V}^2S\bar{c}$ and $\frac{1}{2}\rho\hat{V}^2Sb$ respectively.

For aerodynamic model development, see section 4.2, it is necessary to know the time histories of $\dot{\alpha}$ and $\dot{\beta}$. These variables can be calculated by numerical differentiation from $\hat{\alpha}$ and $\hat{\beta}$. Alternately, these variables can also determined by differentiation of (3.1-21), resulting in:

$$\dot{\hat{\alpha}} = \frac{\hat{u}\dot{\hat{w}} - \hat{w}\dot{\hat{u}}}{\hat{u}^2 + \hat{w}^2} \quad , \tag{3.1-25}$$

and by differentiation of (3.1-22), resulting in:

$$\dot{\hat{\beta}} = \frac{(\hat{u}^2 + \hat{w}^2)\dot{\hat{v}} - \hat{v}(\hat{u}\dot{\hat{u}} + \hat{w}\dot{\hat{w}})}{(\hat{u}^2 + \hat{v}^2 + \hat{w}^2)\sqrt{\hat{u}^2 + \hat{v}^2}} \quad . \tag{3.1-26}$$

With (2.1-5), $\dot{\hat{v}}$, $\dot{\hat{u}}$ and $\dot{\hat{w}}$ can be found according to:

$$
\begin{aligned}
\dot{\hat{u}} &= A_{x_m} - g\sin\hat{\theta} - (q_m + \hat{\lambda}_q)\hat{w} + r_m\hat{v} \,, \\
\dot{\hat{v}} &= A_{y_m} + \hat{\lambda}_y + g\cos\hat{\theta}\sin\hat{\phi} - (r_m + \hat{\lambda}_r)\hat{u} + \\
&\quad + (p_m + \hat{\lambda}_p)\hat{w} \,, \\
\dot{\hat{w}} &= A_{z_m} + \hat{\lambda}_z + g\cos\hat{\theta}\cos\hat{\phi} - (p_m + \hat{\lambda}_p)\hat{v} + \\
&\quad + (q_m + \hat{\lambda}_q)\hat{u} \,.
\end{aligned}
\tag{3.1-27}
$$

3.2 Reconstructibility Analysis

In the case of 'small' perturbations the kinematic system model and the observation models for flight path reconstruction as developed in chapter 2 may be linearized, see (2.1-15), (2.3-11) and (2.3-13). In this case, flight path reconstruction constitutes a linear reconstruction problem. Furthermore it follows that in the linear case the reconstruction of the longitudinal and of the lateral state vector components become independent reconstruction problems. In general, it may not be possible to reconstruct all components of the state vector. The ultimate objective of the present analysis will be to determine which 'parts' of the state vectors are reconstructible whether longitudinal or lateral.

In section 3.2.1. it is shown how to derive the reconstructible subspaces (so called the reconstructible 'parts' of the state vector) corresponding to a particular linear system and observation model. Reconstructibility depends of course on the number and particular type of transducers used in the reconstruction, and so depends on the 'observation configuration', as expressed in terms of an observation model. The results are applied in section 3.2.2, resulting in reconstructible subspaces for the longitudinal and for the lateral flight path reconstruction problem for different observation configurations.

It is to be noted here that the analysis presented in this section is a tutorial introduction meant to explain the principles of reconstructibility analysis. In the actual practice of flight testing, the instrument configurations can be much more elaborate than the simple configuration described here. Nevertheless, the same reconstructibility concept can be used to analyze more realistic configurations.

3.2.1 Reconstructible Subspaces

Let us discuss the reconstructible and nonreconstructible subspace of state vector from input and observation measurements [70]. Consider the linear stochastic system:

$$
\dot{\underline{x}} = F\cdot\underline{x} + G_u\cdot\underline{u} + G_w\cdot\underline{w} \,,
\tag{3.2-1}
$$

with the observation model:

$$
\begin{aligned}
\underline{y}_m &= \underline{y} + \underline{v} \\
&= H\cdot\underline{x} + J\cdot\underline{u} + \underline{v} \,,
\end{aligned}
\tag{3.2-2}
$$

in which $\underline{x}$, $\underline{u}$ and $\underline{y}$ denote the state, input and observation vector of dimension n, s and m respectively. The vectors $\underline{w}$ and $\underline{v}$ denote system or process noise and additive measurement noise respectively. The elements of the system matrix F, the input matrix G and the observation matrices H and J are known. Starting from an initial condition $\underline{x}(t_0)=\underline{x}_0$ which is unknown, the system is excited by a known input signal $\underline{u}(t)$, $t\in[t_0,t_1]$. In order to find a basis for the reconstructible subspace of $\underline{x}$, the so called reconstructibility matrix Q is formed according to:

$$
Q = \begin{bmatrix} H \\ H\cdot F \\ H\cdot F^2 \\ \vdots \\ H\cdot F^{n-1} \end{bmatrix} \,.
\tag{3.2-3}
$$

Assume that the maximum number of independent rows in Q is equal to n_1. Then the dimension of the reconstructible subspace is n_1 and a set of independent rows of Q forms a basis for this subspace. Now it is possible to construct a matrix U of rank n, which can be partitioned as:

$$
U = \begin{bmatrix} U_1 \\ \cdots\cdots \\ U_2 \end{bmatrix} \,,
\tag{3.2-4}
$$

in which U_1 contains the independent rows of Q. The matrix U_2 forms a basis for the nonreconstructible subspace. The matrix U transforms the state vector $\underline{x}$ into a reconstructible

part $\underline{x}_1^*$ and a nonreconstructible part $\underline{x}_2^*$ according to:

$$\underline{x}^* = \begin{pmatrix} \underline{x}_1^* \\ \cdots\cdots \\ \underline{x}_2^* \end{pmatrix} = \begin{bmatrix} U_1 \\ \cdots\cdots \\ U_2 \end{bmatrix} \underline{x} \; . \tag{3.2-5}$$

The components $\underline{x}_1^*$ can be reconstructed to a high precision from exact recordings of the input signal $\underline{u}(t)$ and observation signal $\underline{y}(t)$, $t \in [t_0, t_1]$ [70]. The obvious choice for an algorithm to solve the linear longitudinal and lateral flight path reconstruction problems is a Kalman filter and smoother [70 and 71].

We study now the linear flight path reconstruction in the context of state reconstruction. The associated system and observation models (3.2-1) and (3.2-2) are derived from the linearized kinematical model of section 2.1.3. This model can then be divided into two independent models, governing the longitudinal and lateral motion respectively. This means that for the linear case, the reconstruction of the longitudinal motion is independent of the reconstruction of the lateral motion.

3.2.2 Longitudinal Case

In the stability reference frame F_S, the longitudinal and vertical accelerometer and pitch rate gyro measurements can be written as:

$$\begin{aligned} \tilde{A}_{x_{S_m}} &= \tilde{A}_{x_S} - \lambda_{x_S} - w_{x_S} \; , \\ \tilde{A}_{z_{S_m}} &= \tilde{A}_{z_S} - \lambda_{z_S} - w_{z_S} \; , \\ \tilde{q}_{S_m} &= \tilde{q}_S - \lambda_{q_S} - w_{q_S} \; , \end{aligned} \tag{3.2-6}$$

where the superscript $\tilde{}$ denotes deviations from nominal values belonging to the nominal flight condition of steady straight flight, λ denotes (small) bias error corrections and w denotes random measurement noise. Substitution of $\tilde{A}_{x_S}$, $\tilde{A}_{z_S}$ and $\tilde{q}_S$ in the linearized kinematical relations of the longitudinal motion (2.1-15), results in:

$$\begin{aligned} \dot{\tilde{u}}_S &= -g\cos\gamma_0 \cdot \tilde{\theta} + \lambda_{x_S} + \tilde{A}_{x_{S_m}} + w_{x_S} \; , \\ \dot{\tilde{\alpha}} &= -\frac{g}{V_0}\sin\gamma_0 \cdot \tilde{\theta} + \frac{1}{V_0}\lambda_{z_S} + \lambda_{q_S} + \frac{1}{V_0} \cdot \tilde{A}_{z_{S_m}} + \\ &\quad + \tilde{q}_{S_m} - \frac{1}{V_0} \cdot w_{z_S} + w_{q_S} \; , \\ \dot{\tilde{\theta}} &= \lambda_{q_S} + \tilde{q}_{S_m} + w_{q_S} \; , \\ \dot{\tilde{x}}_T &= \cos\gamma_0 \cdot \tilde{u}_S + V_0 \sin\gamma_0 \cdot \tilde{\alpha} - V_0 \sin\gamma_0 \cdot \tilde{\theta} + W_{x_T} \; , \\ \dot{\tilde{z}}_T &= -\sin\gamma_0 \cdot \tilde{u}_S + V_0 \cos\gamma_0 \cdot \tilde{\alpha} - V_0 \cos\gamma_0 \cdot \tilde{\theta} + W_{z_T} \; . \end{aligned} \tag{3.2-7}$$

The unknown bias error corrections λ_{x_S}, λ_{z_S} and λ_{q_S}, and the longitudinal components of the atmospheric wind W_{x_T} and W_{z_T}*, are assumed to be constant in the course of one flight test manoeuvre. This assumption may be expressed in terms of the following constraints:

$$\begin{aligned} \dot{\lambda}_{x_S} &= 0 \; , \\ \dot{\lambda}_{z_S} &= 0 \; , \\ \dot{\lambda}_{q_S} &= 0 \; , \\ \dot{W}_{x_T} &= 0 \; , \\ \dot{W}_{z_T} &= 0 \; . \end{aligned} \tag{3.2-8}$$

Eqs. (3.2-7) and (3.2-8) may be interpreted to represent the following linear dynamical system:

$$\dot{\underline{x}} = F \cdot \underline{x} + G_u \cdot \underline{u} + G_w \cdot \underline{w} \; , \tag{3.2-9}$$

where $\underline{x}$ represents a so-called augmented state vector, composed of the variables $\tilde{u}_S$, $\tilde{\alpha}$, $\tilde{\theta}$, $\tilde{x}_T$ and $\tilde{z}_T$ of equations (3.2-7) and the parameters λ_{x_S}, λ_{z_S}, λ_{q_S}, W_{x_T} and W_{z_T} of equations (3.2-8):

$$\begin{aligned} \underline{x} = \mathrm{col}\big(& \tilde{u}_S, \tilde{\alpha}, \tilde{\theta}, \tilde{x}_T, \tilde{z}_T, \ldots \\ & \lambda_{x_S}, \lambda_{z_S}, \lambda_{q_S}, W_{x_T}, W_{z_T} \big) \; , \end{aligned} \tag{3.2-10}$$

$\underline{u}$ represents the input vector to the system:

$$\underline{u} = \mathrm{col}\left(\tilde{A}_{x_{S_m}}, \tilde{A}_{z_{S_m}}, \tilde{q}_{S_m} \right) \; , \tag{3.2-11}$$

---

* Note that lower case w is used to indicate measurement noise, while upper case W is used to indicate atmospheric wind components.

and $\underline{w}$ represents system noise [70]:

$$\underline{w} = \mathrm{col}\left(w_{x_S}, w_{z_S}, w_{q_S}\right) . \tag{3.2-12}$$

From section 2.3 and the list of measured variables given in table 3-5, it follows that the available observations pertaining to the system (3.2-7) and (3.2-8) are airspeed, angle of attack, geographical position and altitude variations with respect to a nominal altitude. The corresponding observation vector is:

$$\underline{y} = \mathrm{col}\left(\tilde{u}_S, \tilde{\alpha}_v, \tilde{x}_T, \tilde{z}_T\right) . \tag{3.2-13}$$

From section 2.3.2. it follows that the corresponding linearized observation model may be written as:

$$\underline{y} = H \cdot \underline{x} + J \cdot \underline{u} . \tag{3.2-14}$$

For reasons explained below, the observation matrix H is partitioned into 4 matrices of dimension 1×n, n denoting the dimension of the augmented state vector defined above:

$$H = \begin{bmatrix} H_1 \\ H_2 \\ \vdots \\ H_3 \\ H_4 \end{bmatrix} . \tag{3.2-15}$$

It may be ascertained that H is empty except for the following non-zero elements:

$$\begin{aligned} h_{1,1} &= 1 , \\ h_{2,2} &= C_{\alpha_1} , \\ h_{3,4} &= 1 , \\ h_{4,5} &= 1 . \end{aligned} \tag{3.2-16}$$

Now it is assumed that the angle of attack vane has been calibrated prior to the flight tests, so that C_{α_1} is known. For each individual row of H, it is possible to define a corresponding reconstructibility matrix. This leads to the reconstructibility matrices Q_i, for each row H_i of the observation matrix H. It is possible to derive from each matrix Q_i the reconstructible subspace of the state vector $\underline{x}$ which corresponds to a scalar observation y_i. Knowledge of the reconstructible subspaces of $\underline{x}$ corresponding to individual elements y_i of the observation vector $\underline{y}$, allows an easy comparison of different feasible observation configurations, i.e. combinations of elements of $\underline{y}$, with respect to the resulting reconstructible subspace of $\underline{x}$, as shown below. For example, the reconstructibility matrix Q_i corresponding to a particular row H_i is:

$$Q_i = \begin{bmatrix} H_i \\ H_i \cdot F \\ H_i \cdot F^2 \\ \vdots \\ H_i \cdot F^{n-1} \end{bmatrix} . \tag{3.2-17}$$

Let U_{1_i} denote the matrix of independent rows in Q_i and $\underline{x}^*_{1_i} = U_{1_i} \cdot \underline{x}$ the corresponding reconstructible state vector. The reconstructible state vector of an observation configuration consisting of a set of two or more rows of H, i.e. two or more elements of $\underline{y}$, may then be constructed from the independent rows in the corresponding set of matrices U_{1_i}. This procedure allows a comparison of different observation configurations with respect to the corresponding reconstructible subspaces of the state vector.

The system matrix F of the linear longitudinal flight path reconstruction model (3.2-7) and (3.2-8) is rather sparse. This makes it easy to derive the analytical form of the reconstructibility matrices Q_i corresponding to each of the elements y_i of $\underline{y}$. The matrices Q_i are shown in Appendix B for the case of a nominal flight condition of stationary, rectilinear flight. Using these matrices, it is possible to determine the set of independent rows U_{1_i} and the corresponding components of $\underline{x}^*_{1_i}$ for each of the matrices Q_i. The reconstructible parts of the state vector $\underline{x}$ are shown in table 3-1, for the case of nominally horizontal flight conditions., i.e. $\gamma_0 = 0$.

Next, the reconstructible state vectors $\underline{x}^*_1$ for three different extended observation vectors are shown in table 3-2. It is seen from the first column that an observation configuration consisting of airspeed and angle of attack observations results in an error $-\frac{1}{g} \cdot \lambda_{x_S}$ in the reconstructed trajectory of $\tilde{\theta}$. The cause for this error is that λ_{x_S} cannot be reconstructed. Because of the assumption made in (3.2-8) this error is constant. Inspection of the second column shows that the same error is also

present in an observation configuration consisting of airspeed and altitude observations. Addition of observations of the longitudinal geographical position, as in the observation configuration of the third column, has no effect in this respect.
It appears that for any observation configuration, λ_{x_S} is nonreconstructible. The practical implication is that the quality of the longitudinal accelerometer should be such that λ_{x_S} is small enough to be negligible.

At first sight, the second column of table 3-2, corresponding to the observation configuration with airspeed and altitude observations, seems to compare unfavourably to the first column, corresponding to airspeed and angle of attack observations, because of an error $-\frac{1}{g}\cdot\lambda_{x_S} + \frac{1}{V_0}\cdot W_{z_T}$ in the reconstructed trajectory of the angle of attack $\tilde{\alpha}$. This is because λ_{x_S} as well as W_{z_T} cannot be reconstructed. As mentioned above, however, the effect of λ_{x_S} can be kept small by using a high quality accelerometer, see section 3.3. The magnitude of W_{z_T}, on the other hand, depends on atmospheric weather conditions. In general, dynamic flight tests are made in fair weather dominated by anti cyclonic atmospheric pressure patterns. In such weather conditions, vertical winds are associated with a downward motion of the atmosphere called subsidence, which is of the order of 0.1 to 0.2 m/s. Consequently, in general, the term $\frac{1}{V_0}\cdot W_{z_T}$ can be neglected when V_0 is not too small.

The advantage of using the observation configuration of the second column, rather than the observation configuration of the first column, is that while altitude variations can be accurately measured with barometric pressure transducers, it is much more difficult to measure the angle of attack. In general, angle of attack measurements must be corrected for aircraft induced air velocity components. This necessitates a time consuming and cumbersome calibration of the angle of attack sensor in a series of strictly stationary rectilinear flight conditions. Furthermore, the results of such a calibration apply, at least in principle only to stationary flight conditions. This means that additional and unknown errors may be associated with the extrapolation of the results of the calibration to dynamic flight conditions.
From the third column, it follows that addition of longitudinal geographical position measurements in the observation model does not change the reconstructibility of the angle of attack $\tilde{\alpha}$ of the observation configuration of the second column. Although $\tilde{x}_T$ and W_{x_T} have become reconstructible, they are not of interest for aerodynamic model identification, see chapter 4.
The above arguments show that the use of second observation configuration is more appropriate than the other two configurations for flight path reconstruction of actual flight test data, see sections 3.2 and 3.3. The above analysis should also lay some foundation to derive criteria for the formulation of observation configuration.

3.2.3 Lateral Case

Analogous to (3.2-6) the lateral accelerometer, roll and yaw rate gyro measurements along and about the axes of F_S respectively, may be written as:

$$\begin{aligned}
\tilde{A}_{y_{S_m}} &= \tilde{A}_{y_S} - \lambda_{y_S} - w_{y_S}\,,\\
\tilde{p}_{S_m} &= \tilde{p}_S - \lambda_{p_S} - w_{p_S}\,,\\
\tilde{r}_{S_m} &= \tilde{r}_S - \lambda_{r_S} - w_{r_S}\,.
\end{aligned} \qquad (3.2\text{-}18)$$

Again, the superscript $\tilde{}$ denotes deviations from a nominal flight condition of steady rectilinear flight. Substitution in (2.1-16) results in:

$$\begin{aligned}
\dot{\tilde{\beta}} &= \frac{g\cos\gamma_0}{V_0}\cdot\tilde{\phi}_S + \frac{1}{V_0}\cdot\lambda_{y_S} - \lambda_{r_S} + \frac{1}{V_0}\cdot\tilde{A}_{y_{S_m}} -\\
&\quad - \tilde{r}_{S_m} + \frac{1}{V_0}\cdot w_{y_S}\,,\\
\dot{\tilde{\psi}} &= \frac{1}{\cos\gamma_0}\cdot\lambda_{r_S} + \frac{1}{\cos\gamma_0}\cdot\tilde{r}_{S_m} + \frac{1}{\cos\gamma_0}\cdot w_{r_S}\,,\\
\dot{\tilde{\phi}} &= \lambda_{p_S} + \tan\gamma_0\cdot\lambda_{r_S} + \tilde{p}_{S_m} + \tan\gamma_0\cdot\tilde{r}_{S_m} +\\
&\quad + w_{p_S} + \tan\gamma_0\cdot w_{r_S}\,,\\
\dot{\tilde{y}}_T &= V_0\cdot\tilde{\beta} + V_0\cos\gamma_0\cdot\tilde{\psi} + W_{y_T}\,.
\end{aligned} \qquad (3.2\text{-}19)$$

Equation (3.2-19) represents a linear system with state vector components $\tilde{\beta}$, $\tilde{\psi}$, $\tilde{\varphi}_S$ and $\tilde{y}_T$. In principle the bias error corrections λ_{y_S}, λ_{p_S} and λ_{r_S}

and the lateral component of the atmospheric wind W_{y_T} are unknown, but may be assumed to be constant in the course of one flight test manoeuvre. This assumption can be expressed in terms of the following constraints:

$$\begin{aligned} \dot{\lambda}_{y_S} &= 0 \,, \\ \dot{\lambda}_{p_S} &= 0 \,, \\ \dot{\lambda}_{r_S} &= 0 \,, \\ \dot{W}_{y_T} &= 0 \,. \end{aligned} \tag{3.2-20}$$

An additional parameter C_{β_o} appears in the linearized observation model of the side slip vane, see equation (2.3-13). This parameter is also assumed to be constant in the course of one flight test manoeuvre, resulting in the following additional constraint:

$$\dot{C}_{\beta_0} = 0 \,. \tag{3.2-21}$$

Analogous to the longitudinal case discussed above, an augmented state vector may now be composed of the variables $\tilde{\beta}$, $\tilde{\psi}$, $\tilde{\varphi}_S$ and $\tilde{y}_T$ in equations (3.2-19) and the parameters λ_{y_S}, λ_{p_S}, λ_{r_S}, W_{y_T} and C_{β_o} in (3.2-20) and (3.2-21) according to:

$$\underline{x} = \mathrm{col}\left(\tilde{\beta}, \tilde{\psi}, \tilde{\phi}_S, \tilde{y}_T, \lambda_{y_S}, \lambda_{p_S}, \lambda_{r_S}, C_{\beta_0}, W_{y_T}\right) . \tag{3.2-22}$$

Next, equations (3.2-19), (3.2-20) and (3.2-21) may be interpreted to represent the following linear dynamical system:

$$\dot{\underline{x}} = F \cdot \underline{x} + G_u \cdot \underline{u} + G_w \cdot \underline{w} \,, \tag{3.2-23}$$

in which $\underline{u}$ denotes the following system input vector:

$$\underline{u} = \mathrm{col}\left(\tilde{A}_{y_{S_m}}, \tilde{p}_{S_m}, \tilde{r}_{S_m}\right) , \tag{3.2-24}$$

and the vector $\underline{w}$ represents again system noise, accounting for the effects of input signal measurement errors:

$$\underline{w} = \mathrm{col}\left(w_{y_S}, w_{p_S}, w_{r_S}\right) . \tag{3.2-25}$$

From section 2.3 and the list of measured variables shown in table 3-5 it follows that the available observations pertaining to the time dependent variables and constant parameters in equations (3.2-19), (3.2-20) and (3.2-21) respectively, are sideslip vane angle, yaw angle and lateral geographical position. The corresponding linearized observation variables constitute the following observation vector:

$$\underline{y} = \mathrm{col}\left(\tilde{\beta}_v, \tilde{\psi}, \tilde{y}_T\right) . \tag{3.2-26}$$

Using equation (2.3-14), the corresponding linearized observation model can be written as:

$$\underline{y} = H \cdot \underline{x} + J \cdot \underline{u} \,. \tag{3.2-27}$$

Analogous to equation (3.2-14), the observation matrix H may be partitioned into 3 matrices of dimension 1×n, n denoting the dimension of the augmented state vector defined above:

$$H = \begin{bmatrix} H_1 \\ H_2 \\ H_3 \end{bmatrix} . \tag{3.2-28}$$

The observation matrix H is empty except for the following non-zero elements:

$$\begin{aligned} h_{1,1} &= C_{\beta_1} \,, \\ h_{1,8} &= 1 \,, \\ h_{2,2} &= 1 \,, \\ h_{3,4} &= 1 \,. \end{aligned} \tag{3.2-29}$$

The reconstructibility matrices Q_i corresponding to the rows H_i in the observation matrix H, have been derived in appendix B. Subsequently, analogous to the longitudinal case discussed above, the components of the reconstructible state vectors $\underline{x}^*_{1_i}$ can be determined. The reconstructible parts of the state vector are shown in table 3-3, for nominally horizontal flight conditions, i.e. γ_0=0. The reconstructible state vectors $\underline{x}^*_{1_i}$ for three different feasible extended observation configurations are shown in table 3-4.

From table 3-4, it follows that all these observation configurations generate a constant error in the reconstructed side slip angle. In this respect, there is no improvement as compared to the first column of table 3-3, where only the sideslip vane observations are employed. The only advantage of adding yaw angle and lateral geographical position observations as in the third column of table 3-4, is the reconstructibility of the bias error correction λ_{r_S}. In the flight path reconstruction of actual flight

test data, however, no attempt was made to estimate λ_r, and only sideslip vane observations were included in the observation model, see section 3.3.

3.3 Practical Flight Path Reconstruction

The analysis in section 3.2 of the longitudinal and lateral flight path reconstruction problem was based on linearized versions of the kinematic and the observation model. The significance of this analysis lies in the possibility to determine reconstructible subspaces in the augmented state space for different observation model configurations. For actual flight path reconstruction, however, the more precise nonlinear kinematical relations (2.1-3), (2.1-5) and (2.1-6) are used. In addition these relations are extended to include the effects of the curvature and rotation of the earth, see ref [13].

In this section the results of the reconstructibility analysis are applied in 3.3.1 to define the model for an example measurement configuration. Subsequently the initialization of the Kalman filter is discussed in 3.3.2. Finally some actual results from flight tests are presented.

The example of a successful flight path reconstruction and the associated high accuracy flight test measurement system is taken from a flight program of the DHC-2 Beaver [14,16]. A list of measured variables is shown in table 3-5.

Flight path reconstruction may be interpreted as a particular example of the reconstruction of the state vector of a nonlinear, dynamical system model. Table 3-6 presents the elements of the state vector $\underline{x}$, input vector $\underline{u}_m$ and observation vector $\underline{y}$ of the system model.

Application of the extended Kalman filter and smoother requires a priori specification of the covariance matrices of the process noise V_{ww} and the observation noise V_{vv}. In flight path reconstruction, process noise is due to random errors of accelerometer and rate gyro measurements.

The flight test measurement system consist of separate channels for each of the variables to be measured. It may therefore be assumed that measurement errors of different variables are uncorrelated. This means that V_{ww} and V_{vv} are diagonal, see also section 2.4. Their elements can be estimated from the residuals of laboratory calibrations.

Perhaps one of the most important design considerations of the flight test measurement system was the minimization of parasitic sensitivities of recorded flight test data to 'environmental factors' which occur in actual flight, such as mechanical vibrations, temperature and pressure variations and electro-magnetic interference [16 and 17]. It is impossible, however, to build an instrumentation system which is completely insensitive in this respect. Parasitic sensitivities lead to additional contributions to the measurement errors of the instrumentation system during flight. In the present application of the Kalman filter and smoother these extra measurement errors were taken into account by substituting for the diagonal elements of the covariance matrices V_{ww} and V_{vv}, substantially larger values than the corresponding estimates obtained from laboratory calibrations.

The values as used in the present state reconstruction problem are listed in table 3-6 in terms of standard deviations, i.e. square roots of the diagonal elements of V_{ww} and V_{vv}.

3.3.1 Flight Path Reconstruction Model

The system and observation model for the nonlinear flight path reconstruction problem is derived as follows. With (2.4-1) the specific aerodynamic force along X_B can be written as:

$$A_x = A_{x_m} + \lambda_x + w_x \,. \qquad (3.3\text{-}1)$$

Similar expressions hold for the specific forces A_y and A_z as well as for the angular rates p, q and r. Substitution in (2.1-5) defines with (2.1-3) and (2.1-6) a nonlinear stochastic system with state vector $\underline{x}$ as defined earlier in (2.1-8):

$$\underline{x} = \mathrm{col}\left(u, v, w, \psi, \theta, \phi, x_E, y_E, z_E\right), \qquad (3.3\text{-}2)$$

input vector $\underline{u}_m$:

$$\underline{u}_m = \mathrm{col}\left(A_{x_m}, A_{y_m}, A_{z_m}, p_m, q_m, r_m\right), \qquad (3.3\text{-}3)$$

and process noise $\underline{w}$ due to the stochastic

accelerometer and rate gyro measurement errors as defined in (2.4-2):

$$\underline{w} = \mathrm{col}\left(w_x, w_y, w_z, w_p, w_q, w_r\right), \tag{3.3-4}$$

From inspection of the list of variables determined in flight as given in table 3-5, it follows that the most complete observation vector would include airspeed, change of altitude, angle of attack, side slip angle, yaw angle and geographical position:

$$\underline{y} = \mathrm{col}\left(V, \Delta h, \alpha_v, \beta_v, \psi, x_E, y_E\right). \tag{3.3-5}$$

The corresponding nonlinear system and observation models contain a relatively large number of unknown parameters: the components of the constant atmospheric wind in (2.1-6), the accelerometer and rate gyro bias error corrections in (2.4-1) and the parameters in the observation models of the vane measurements α_v and β_v. This results in the augmented state vector to consist of 26 elements:

$$\begin{aligned}\underline{x} = \mathrm{col}\big(&u, v, w, \psi, \theta, \phi, x_E, y_E, z_E, \ldots \\ &W_{x_E}, W_{y_E}, W_{z_E}, \lambda_x, \lambda_y, \lambda_z, \lambda_p, \lambda_q, \lambda_r, \ldots \\ &C_{up}, C_{\alpha_0}, x_\alpha, y_\alpha, C_{si}, C_{\beta_0}, x_\beta, z_\beta\big).\end{aligned} \tag{3.3-6}$$

Additionally one can think of scale factors for vane measurements, accelerometers, rate gyros to be included in the state vector. Because of its high dimension, the reconstruction of this augmented state vector would be rather expensive in terms of computing time. Furthermore, as shown in section 3.2, $\underline{x}$ is not completely reconstructible, at least for the case of small amplitude flight test manoeuvres for which linearized kinematical and observation models are valid. For aerodynamic model identification, however, not all elements of $\underline{x}$ need to be known. This leads to the possibility to reduce the dimension of $\underline{x}$ as shown below.

1. If the horizontal distance traversed in the course of a flight test manoeuvre is small compared to the scale of the prevailing atmospheric pressure pattern, and if the flight test manoeuvre is executed at some nominal altitude, then W_{x_E} and W_{y_E}, the components of the horizontal wind can be assumed to be constant. It is shown in section 3.2 that in this case, neither W_{x_E} and W_{y_E} nor the geographical position coordinates x_E and y_E are needed for aerodynamic model identification. These variables may, therefore, be removed from the system and observation model.

2. The reconstructibility analysis of section 3.2 is based on the assumption that the angle of attack vane is calibrated in separate measurements in stationary rectilinear flight conditions. Here, the parameters of the angle of attack vane calibration model (2.3-3) have been included as elements of $\underline{x}$ to indicate that this calibration can in principle also be made in nonstationary flight conditions as part of a flight path reconstruction. In the context of the present section, however, following the arguments in section 3.2, α_v was removed from the observation model. This implies of course also removal of the parameters C_{up}, C_{α_o}, x_α and y_α in $\underline{x}$.

3. As mentioned in section 3.2, the quality of the heading gyro in terms of rate of drift was low compared to the quality of rate gyros in terms of bias error corrections. For this reason, ψ is removed from the observation model.

4. The position coordinates x_β and z_β can be interpreted as unknown parameters in the calibration model of the sideslip vane (2.3-5), and be determined as part of a flight path reconstruction. However, these coordinates can also be calculated directly for a given location of the aircraft's mass centre since the position of the vane is known.

Now, the resulting observation model configuration corresponds to the second column of table 3-2 and the first column of table 3-3:

$$\underline{y} = \mathrm{col}\left(V, \Delta h, \beta_v\right). \tag{3.3-7}$$

This means that, at least for small amplitude flight test manoeuvres, it is impossible to reconstruct the bias error corrections λ_x, λ_y and λ_r. This has the effect of introducing bias errors in the reconstructed angle of attack α, pitch angle θ and roll angle ϕ. However, the quality of the accelerometers and rate gyros is such that these bias error corrections can be assumed to be very small. Consequently, the corresponding bias errors in the reconstructions of α, θ and ϕ are small enough to be negligible. Since the angle of attack vane observations are discarded, the vertical

component of the atmospheric wind is also not reconstructible. The corresponding error in the reconstructed angle of attack can be relatively large as compared to the bias error introduced by the nonreconstructibility of λ_x. If the vertical wind is due to subsidence and anti-cyclonic (high) atmospheric pressure distributions, a representative value is 0.1 m/s. At a nominal TAS of V_0=45 m/s the corresponding error in the reconstruction of α is of the order of 0.1°, which is approximately 10 times the error introduced by λ_x.

In section 2.3.2 it was argued that C_{β_0}, the constant term in the sideslip vane calibration model, cannot in principle be determined directly in stationary rectilinear flight. Furthermore, according to section 3.2, C_{β_0} is also not reconstructible. This means that C_{β_0} must be set equal to β_{v_0}, the sideslip vane angle in the nominal flight condition preceding the flight test manoeuvre.

The state vector resulting from the discussion above is:

$$\underline{x} = \mathrm{col}\left(u, v, w, \psi, \theta, \phi, z_E, \lambda_z, \lambda_p, \lambda_q, C_{si}\right) . \tag{3.3-8}$$

In order to avoid the introduction of different bias errors in the reconstructed time history of the side slip angle, one value of C_{β_0} was used in the flight path reconstruction of all flight test manoeuvres at each nominal flight condition.
An important remark is necessary at this stage. The state vector (3.3-8) and the observation vector (3.3-7) may look very simple. In practice much more measurements are available for example, attitude angles, geographical positions, etc. which obviously improve the reconstructibility. However, the additional measurements also introduce additional noise, bias and scale factor errors thus complicating the analysis. For the purpose of the current exposition, a full analysis would go too far.

3.3.2 Filter Initialization

Next, an a priori estimate of the state vector at the start of the flight test manoeuvre and the corresponding covariance matrix must be specified. Let $\hat{\underline{x}}(i|j)$ denote an estimate of the state vector at time t_i, as calculated from the set of all measured observation vectors $\underline{y}_m$ from the start of the flight test manoeuvre at time t_0 up to and including time t_j. The corresponding covariance matrix is denoted by P(i|j). The reconstruction of the state vector is started from an a priori estimate of the state vector $\hat{\underline{x}}(0|0)$ with covariance matrix P(0|0). In the case of a nonlinear system model, as in flight path reconstruction, the accuracy of $\hat{\underline{x}}(0|0)$ determines to a certain degree the magnitude of the linearization errors in the extended Kalman filter and smoother. For this reason, it is advantageous to start each flight test manoeuvre from a condition of nominally stationary and rectilinear flight. As shown below, in such flight conditions it is relatively easy to calculate fairly accurate values of the components of the state vector $\underline{x}$ mentioned in table 3-6, from the stationary outputs of the instrumentation system. Nowadays accurate measurements of the attitude angles can be obtained from the Inertial Navigation Systems or Attitude Heading Reference System, but if these are not available the following procedure can still be used.

The yaw angle ψ cannot be calculated from the stationary outputs of the instrumentation system. So a direct measurement of ψ is always necessary, if only to provide an initial value. It is based on the integration of the angular rate measurements. It plays no direct role in the aerodynamic model identification and its main importance lies in the calculation of the centripetal and coriolis terms in the full kinematic equations.
A good choice for the a priori estimate $\hat{\psi}(0|0)$ of ψ is its measured value at time $t=t_0$:

$$\hat{\psi}(0|0) = \psi_m(0) . \tag{3.3-9}$$

Although not measured directly by the measurement system, it is nevertheless possible to derive a priori estimates for the remaining two attitude angles, i.e. the pitch angle θ and the roll angle ϕ, as follows [66].

Since the initial flight condition at time $t=t_0$ is nominally stationary and rectilinear, the components u, v, and w of airspeed $\underline{V}$ are constant in time, i.e.:

$$\dot{u}(0) = \dot{v}(0) = \dot{w}(0) = 0 , \tag{3.3-10}$$

and furthermore, the three body rotation rates p, q and r, are zero:

$$p(0) = q(0) = r(0) = 0 \ . \tag{3.3-11}$$

Substitution of (3.3-10) and (3.3-11) in the equations of motion (2.1-5) results in:

$$g\sin\theta = A_x \ , \tag{3.3-12}$$

$$g\cos\theta\sin\phi = -A_y \ , \tag{3.3-13}$$

$$g\cos\theta\cos\phi = -A_z \ . \tag{3.3-14}$$

Elimination of θ in (3.3-13) by substituting for $\cos\theta$ from (3.3-14) results in the following expression for ϕ:

$$\phi = \arctan\frac{A_y}{A_z} \ . \tag{3.3-15}$$

Equations (3.3-12) and (3.3-15) show that in stationary rectilinear flight conditions, it is possible to estimate the attitude angles θ and ϕ from the specific aerodynamic forces A_x, A_y and A_z. The specific aerodynamic forces are measured in flight with accelerometers. This makes it possible to calculate the a priori estimates $\hat{\theta}(0|0)$ and $\hat{\phi}(0|0)$ of the pitch and roll angle respectively, from the accelerometer outputs $A_{x_m}(0)$, $A_{y_m}(0)$ and $A_{z_m}(0)$ according to:

$$\hat{\theta}(0|0) = \arcsin\frac{A_{x_m}(0)}{g} \ , \tag{3.3-16}$$

$$\hat{\psi}(0|0) = \arctan\frac{A_{y_m}(0)}{A_{z_m}(0)} \ . \tag{3.3-17}$$

Next, the a priori estimates of the three velocity components u, v and w of airspeed V must be determined. Much like θ and ϕ above, these velocity components are also not measured directly in the measurement system. It is possible, however, to estimate these velocity components in an indirect way as follows.

In the initial nominal flight condition, the roll angle ϕ is kept equal to zero as closely as possible. The flight condition is, therefore, nominally symmetrical, see section 2.3.2. This means that the velocity vector $\underline{V}$ is approximately parallel to the plane of symmetry, see fig. 2-2.

Due to the absence of additional information, the only rational estimate of v(0), the component of V in the initial flight condition, is zero, i.e.:

$$\hat{v}(0|0) = 0 \ . \tag{3.3-18}$$

The remaining two velocity components could readily be estimated from $V_m(0)$, the measured airspeed at time $t=t_0$, and $\hat{\alpha}(0|0)$, the a priori estimate of the angle of attack, if this latter estimate were known. Fig. 2-2 shows that in symmetrical flight conditions, u and w can then be estimated with the following relations:

$$\hat{u}(0|0) = V_m(0)\cdot\cos\hat{\alpha}(0|0) \ , \tag{3.3-19}$$

$$\hat{w}(0|0) = V_m(0)\cdot\sin\hat{\alpha}(0|0) \ . \tag{3.3-20}$$

The angle of attack is measured directly in the measurement system by means of a vane, see table 3-5. The use of this measurement as an a priori estimate of $\alpha(0)$, however, depends on C_{α_o} and C_{up}, the parameters in the vane calibration formula, see (2.3-3). These parameters can be determined in a separate flight test program consisting of measurements in stationary rectilinear flight conditions, e.g. ref [9]. It is possible, however, to avoid execution of such an additional flight test program by calculating an a priori estimate of $\alpha(0)$ in an alternative way as follows. From fig. 2-2 it can be deduced that in strictly symmetrical rectilinear flight conditions the following relation exists between the angle of attack α, the flight path angle γ and pitch angle θ:

$$\alpha = \theta - \gamma \ . \tag{3.3-21}$$

Using (3.3-21) the a priori estimate $\hat{\alpha}(0|0)$ follows from:

$$\hat{\alpha}(0|0) = \hat{\theta}(0|0) - \hat{\gamma}(0|0) \ . \tag{3.3-22}$$

In (3.3-22) $\hat{\theta}(0|0)$ is calculated with (3.3-16). The a priori estimate of the flight path angle can be based on the following relation, see fig. 2-2:

$$\gamma = \arcsin\frac{C}{V} \ , \tag{3.3-23}$$

in which C denotes the rate of climb. Assuming for the present $\hat{C}(0|0)$ to be known and substituting the measured airspeed for V, then the a priori estimate $\hat{\gamma}(0|0)$ can be determined with:

$$\hat{\gamma}(0|0) = \arcsin\frac{\hat{C}(0|0)}{V_m(0)} \ . \tag{3.3-24}$$

Rate of climb belongs also to the group of variables which is not measured directly in the measurement system, see table 3-5. It is possible, however, to calculate rate of climb in stationary flight conditions from altitude measurements at different instants of time according to:

$$C(0) = \frac{\Delta h(\Delta t) - \Delta h(0)}{\Delta t} , \qquad (3.3\text{-}25)$$

in which Δh denotes the change of altitude with respect to a certain reference altitude and Δt denotes a suitable time interval with a length in the order of seconds. As can be seen from table 3-5 the altitude variation Δh is not directly measured, but it can be calculated from static pressure and total temperature measurements. By substituting the results at time $t=t_0$ and $t=t_0+\Delta t$ in (3.3-25), an a priori estimate of $C(0)$ can be calculated with:

$$C(0|0) = \frac{\Delta h_m(\Delta t) - \Delta h_m(0)}{\Delta t} . \qquad (3.3\text{-}26)$$

The change of altitude as derived from static pressure and total temperature measurements constitutes the best-possible a priori estimate of $z_E(0)$, the vertical distance from the horizontal plane corresponding to the static pressure at the start of the recording:

$$\hat{z}_E(0|0) = -\Delta h_m(0) . \qquad (3.3\text{-}27)$$

Finally, due to lack of any information, the initial estimates of the bias error corrections λ_z, λ_p and λ_q and of the sidewash correction factor C_{si}, see section 2.3.1, are set equal to zero.

According to table 3-6, the diagonal elements of $P(0|0)$ were given numerical values which were approximately two orders of magnitude larger than the values resulting from taking account only of the errors of the measurement system. The reason is that the assumption of stationarity of the initial nominal flight condition, on which several of the above estimates of the components of the initial state vector are based, is - in general - not fully satisfied in practice. This means that these estimates are corrupted by errors which depend on the 'degree of stationarity' of the initial flight condition. The large numerical values of the diagonal elements $P(0|0)$ above, are a reflection of the possibility that in some cases the initial flight condition might deviate significantly from a stationary flight condition, introducing additional errors in the estimates of the components of the initial state vector. A more refined estimation of the initial condition, taking into account possible deviations from the nominally stationary flight condition is given in [13].

3.3.3 Results

Some results of an actual flight path reconstruction are presented in figs. 3-1, 3-2 and 3-3.

Fig. 3-1 shows the time histories of the difference between the measured values V_m, Δh_m and β_{v_m} and the corresponding extended Kalman smoother estimates.
The dynamic longitudinal and lateral flight test manoeuvres, with a length of 10 and 16 seconds respectively, are preceded and followed by sections of quasi-steady flight. It can be seen in fig. 3-1, that the accuracy of the V and Δh measurements during these dynamic sections of the flight test manoeuvre, is generally considerably lower than in the remaining quasi-steady sections. This phenomenon is thought to be caused by the dynamic response of the air in the pneumatic pressure tubes connecting the total and static pressure orifices with the pressure transducers. Due to the complexity of these responses, they can only partially be accounted for in a practical way. As a result, the remaining measurement errors are no longer expected to be uncorrelated in time.
This problem was circumvented by discarding all total and static pressure measurements in the dynamic sections of the flight test manoeuvre. This means that in these sections the V and Δh observations are not used, which reduces the observation vector to $y=\beta_v$. In simulation experiments with uncorrelated measurement errors in every section of the flight test manoeuvre, such a temporary reduction of the observation measurements proved to result in only a small increase of the theoretical Kalman smoother estimation variances.

Fig. 3-2 shows the reconstruction of the bias error corrections and the side wash correction factor by the extended Kalman filter. The estimated bias error corrections $\hat{\lambda}_p(N|N)$ and $\hat{\lambda}_q(N|N)$ at $t=t_N$, N denoting the total number of observation vector measurement and t_N denoting the time instant of

the last measurement, of the roll and pitch rate gyro respectively, are in the order of 0.004 deg/s. This is equivalent to 1 mV, the resolution of the data logging part of the instrumentation system. The estimated value of λ_z, the bias error correction of the vertical accelerometer, at $t=t_N$ is approximately equal to 0.036 m/s^2. This is considered to be an extremely large value for high quality force balance type accelerometers as used in the present instrumentation system. Our experience is that large bias error corrections of such accelerometers can be caused by microscopic defects in the pendulum bearings in the transducer. The accelerometer in question was subsequently replaced.

The reduction of the bias estimation error variance with time confirms the validity of the linear reconstructibility analysis as carried out in section 3.2. In this analysis the reconstruction of the side wash correction factor C_{si} had to be left out of consideration since it would imply a nonlinear reconstruction analysis. Fig. 3-2 shows that, although C_{si} is reconstructible, the accuracy of its reconstruction remains relatively low.

The time intervals of the longitudinal and lateral dynamic manoeuvres during which the airspeed and altitude observation measurements are discarded, are evident particularly in figs. 3-2(a) and (b). During these time intervals there appears to be virtually no reduction of the standard deviations of the bias estimation errors. Finally, it must be noted that smoothing cannot improve the accuracy of bias estimates. This is the reason that Fig. 3.2 only shows filter results.

Characteristic examples of the theoretical extended Kalman filter and smoother reconstruction accuracies of the dynamic state vector components are shown in Fig. 3-3. They are expressed in terms of standard deviations. These standard deviations are the square roots of the diagonal elements of $P(i|i-1)$ and $P(i|N)$, i.e. the covariance matrices of estimation errors resulting from the Kalman filter and Kalman smoother respectively.

Fig. 3-3 also confirms the conclusions of the linear reconstructibility analysis of section 3.2. The theoretical reconstruction errors of the extended Kalman smoother of all state vector components, except yaw angle ψ, are shown to be very small. Since only side slip vane measurements were used here as lateral observations, the lateral observation model corresponds to the first column in table 3-3. According to section 3.2, this will leave ψ nonreconstructible. It is not surprising, therefore, that the a priori estimation error of ψ remains approximately equal to the a priori value during filtering as well as smoothing. Since ψ is not used quantitatively further on, this does not affect the results of the second step of the data analysis procedure. It must be remarked that the use of yaw angle measurements, see table 3-5, and side slip measurements as lateral observations, does allow reconstruction of the yaw angle ψ. In addition, it is also possible to reconstruct the bias error correction λ_r of the yaw rate gyro, see table 3-3.

Figs. 3-3(a), (b), (c), (e) and (g) clearly show time intervals during which standard deviations of the extended Kalman filter increase, rather than decrease with time. These time intervals correspond again to the time intervals of the longitudinal and lateral dynamic manoeuvres during which airspeed and altitude observation measurements are discarded. However, in the standard deviation curves of the extended Kalman smoother, these time intervals become virtually indiscernible from the quasi-steady sections of the flight test manoeuvre. This shows clearly the great advantage of the Kalman smoother step.

In general it can be said that experience with the extended Kalman filtering and smoothing algorithms for flight path reconstruction of the flight test manoeuvres as carried out in the course of the present flight test program has been very good. All manoeuvres to which the algorithms were applied could successfully be reconstructed in the sense that the residuals were of approximately the same magnitude as shown in fig. 3-1. In addition, the estimated bias error corrections were of the same order of magnitude as during the laboratory calibrations.

3.4 Conclusions

Flight path reconstruction is an important tool for the analyst of flight test data. This is true irrespective whether one applies it as a first step of the two step method, as an independent

compatibility check as a precursor to the one step method or just as a method to reconstruct trajectories.

The emphasis in this section has been on the detailed analysis of one relatively simple measurement configuration. There are no reasons why this configuration cannot be extended with any number of additional transducers and this is in fact what is being done in most flight test projects. However, in the present exposition there are some good reasons for our emphasis.

Firstly, the measurement configuration treated in this section is the minimum necessary for aerodynamic parameter identification. As such it is essential to be familiar with its characteristics and limitations.

Secondly, under normal circumstances there are no additional measurements which will dramatically improve the accuracy of the parameter identification results achievable with this minimum configuration. This is not always the case, however. For example the addition of absolute position (e.g. GPS) to the observation vector will improve the accuracy of the reconstructed wind vector, which can be of great importance in less favourable weather conditions (varying winds). It should be noted, however, that GPS will not help much for the vertical wind component. To estimate the vertical wind component one could in principle us an angle of attack vane, at the cost of having to identify the vane calibration coefficients as well.

Finally, all the essential characteristics of the flight path reconstruction problem are exhibited by the configuration treated in this section. This is true in particular for the reconstructibility analysis. It should be no problem for the reader to apply this analysis to his own perhaps more extensive measurement configuration.

As noted before, flight path reconstruction has many more applications than just for aerodynamic model identification, such as stall speed determination and accident analysis. Ideally a flight path reconstruction software package should be flexible enough to handle these other applications as well.

There are other aspects involved in the application of flight path reconstruction, not the least among which is the choice of the instrumentation error model. Some of these aspects will be further discussed in chapter 7.

This concludes our discussion of the first step in the two step method. Now that we have an accurate estimate of the state trajectory of the aircraft, we will turn our attention in the following section to the determination of the aerodynamic model.

$y_1 = \tilde{u}_S$	$y_2 = \tilde{\alpha}_v$	$y_3 = \tilde{x}_T$	$y_4 = \tilde{z}_T$
$\tilde{u}_S$	$\tilde{\alpha}$	$\tilde{u}_S + W_{x_T}$	$\tilde{\alpha} - \tilde{\theta} + \frac{1}{V_0} \cdot W_{z_T}$
$\tilde{\theta} - \frac{1}{g} \cdot \lambda_{x_S}$	$\frac{1}{V_0} \cdot \lambda_{z_S} + \lambda_{q_S}$	$\tilde{\theta} - \frac{1}{g} \cdot \lambda_{x_S}$	$\tilde{z}_T$
λ_{q_S}		$\tilde{x}_T$	λ_{z_S}
		λ_{q_S}	

Table 3-1: *Reconstructible state vectors $\underline{x}_{l_i}^*$ of individual observations y_i of the linear longitudinal flight path reconstruction problem, applicable to horizontal nominal flight conditions.*

$\underline{y} = \text{col}(\tilde{u}_S, \tilde{\alpha}_v)$	$\underline{y} = \text{col}(\tilde{u}_S, \tilde{z}_T)$	$\underline{y} = \text{col}(\tilde{u}_S, \tilde{x}_T, \tilde{z}_T)$
$\tilde{u}_S$	$\tilde{u}_S$	$\tilde{u}_S$
$\tilde{\alpha}$	$\tilde{\alpha} - \frac{1}{g} \cdot \lambda_{x_S} + \frac{1}{V_0} \cdot W_{z_T}$	$\tilde{\alpha} - \frac{1}{g} \cdot \lambda_{x_S} + \frac{1}{V_0} \cdot W_{z_T}$
$\tilde{\theta} - \frac{1}{g} \cdot \lambda_{x_S}$	$\tilde{\theta} - \frac{1}{g} \cdot \lambda_{x_S}$	$\tilde{\theta} - \frac{1}{g} \cdot \lambda_{x_S}$
λ_{z_S}	$\tilde{z}_T$	$\tilde{x}_T$
λ_{q_S}	λ_{z_S}	$\tilde{z}_T$
	λ_{q_S}	λ_{z_S}
		λ_{q_S}
		W_{x_T}

Table 3-2: *Reconstructible state vectors $\underline{x}_l^*$ for three different observation configurations of the linear longitudinal flight path reconstruction problem, applicable to horizontal nominal flight conditions.*

$\underline{y} = \tilde{\beta}_v$	$\underline{y}_2 = \tilde{\psi}$	$\underline{y}_3 = \tilde{y}_T$
$\tilde{\beta} + \frac{C_{\beta_0}}{C_{\beta_1}}$	$\tilde{\psi}$	$\tilde{\beta} + \tilde{\psi} + \frac{1}{V_0} \cdot W_{y_T}$
$\tilde{\phi}_S + \frac{1}{g} \cdot \lambda_{y_S} - \frac{V_0}{g} \cdot \lambda_{r_S}$	λ_{r_S}	$\tilde{\phi}_S + \frac{1}{g} \cdot \lambda_{y_S}$
λ_{p_S}		$\tilde{y}_T$
		λ_{p_S}

Table 3-3: *Reconstructible state vectors $\underline{x}_{1_i}^*$ of individual observations y_i of the linear lateral flight path reconstruction problem, applicable to horizontal nominal flight conditions.*

$\underline{y} = \mathbf{col}(\tilde{\beta}_v, \tilde{\psi})$	$\underline{y} = \mathbf{col}(\tilde{\psi}, \tilde{y}_T)$	$\underline{y} = \mathbf{col}(\tilde{\beta}_v, \tilde{\psi}, \tilde{y}_T)$
$\tilde{\beta} + \frac{C_{\beta_0}}{C_{\beta_1}}$	$\tilde{\beta} + \frac{1}{V_0} \cdot W_{y_T}$	$\tilde{\beta} + \frac{C_{\beta_0}}{C_{\beta_1}}$
$\tilde{\psi}$	$\tilde{\psi}$	$\tilde{\psi}$
$\tilde{\phi}_S + \frac{1}{g} \cdot \lambda_{y_S}$	$\tilde{\phi}_S + \frac{1}{g} \cdot \lambda_{y_S}$	$\tilde{\phi}_S + \frac{1}{g} \cdot \lambda_{y_S}$
λ_{p_S}	$\tilde{y}_T$	$\tilde{y}_T$
λ_{r_S}	λ_{p_S}	λ_{p_S}
	λ_{r_S}	λ_{r_S}
		$C_{\beta_0} - C_{\beta_1} \cdot \frac{W_{y_T}}{V_0}$

Table 3-4: *Reconstructible state vectors $\underline{x}_1^*$ for three different observation configurations of the linear lateral flight path reconstruction problem, applicable to horizontal nominal flight conditions.*

Channel Number		Measured Variable
1	A_x	specific force along X-axis
2	A_y	specific force along Y-axis
3	A_z	specific force along Z-axis
4	p	roll rate
5	q	pitch rate
6	r	yaw rate
7	ψ	yaw angle
8	n	engine speed
9	T_t	total temperature
10	δ_e	elevator angle
11	δ_{a_l}	port aileron angle
12	δ_{a_r}	starboard aileron flap angle
13	δ_r	rudder angle
14	δ_{f_l}	port wing flap angle
15	δ_{f_r}	starboard wing flap angle
16	δ_{t_e}	elevator trim angle
17	δ_{t_r}	rudder trim angle
18	α_v	α-vane angle
19	β_v	β-vane angle
20	Δp_t	increase in total pressure behind propeller disc
21	Δp_1	variation in static pressure
22	q_c	impact pressure
23	p_z	engine manifold pressure
24	p_{st}	static pressure
25	DME	Distance Measuring Equipment
26	T_{carb}	carburettor temperature

Table 3-5: *List of measured variables.*

state vector:

$$\underline{x} = \mathrm{col}\left(u, v, w, \psi, \theta, \phi, z_E, \lambda_z, \lambda_p, \lambda_q, C_{si}\right)$$

input vector:

$$\underline{u}_m = \mathrm{col}\left(A_{x_m}, A_{y_m}, A_{z_m}, p_m, q_m, r_m\right)$$

observation vector

$$\underline{y} = \mathrm{col}\left(V, \Delta h, \beta_v\right)$$

square roots of diagonal elements of V_{ww}:

$$\sigma_{A_{x_m}} = 0.0032 \quad m/s^2$$
$$\sigma_{A_{y_m}} = 0.0014 \quad m/s^2$$
$$\sigma_{A_{z_m}} = 0.0056 \quad m/s^2$$
$$\sigma_{p_m} = 0.0032 \quad deg/s$$
$$\sigma_{q_m} = 0.0032 \quad deg/s$$
$$\sigma_{r_m} = 0.0032 \quad deg/s$$

square roots of diagonal elements of V_{vv}:

$$\sigma_{V_m} = 0.30 \quad m/s$$
$$\sigma_{\Delta h_m} = 0.40 \quad m$$
$$\sigma_{\beta_{v_m}} = 0.86 \quad deg$$

Table 3-6: *State, input and observation vectors, and covariance matrices of process and observation noise of the extended Kalman filter and smoother.*

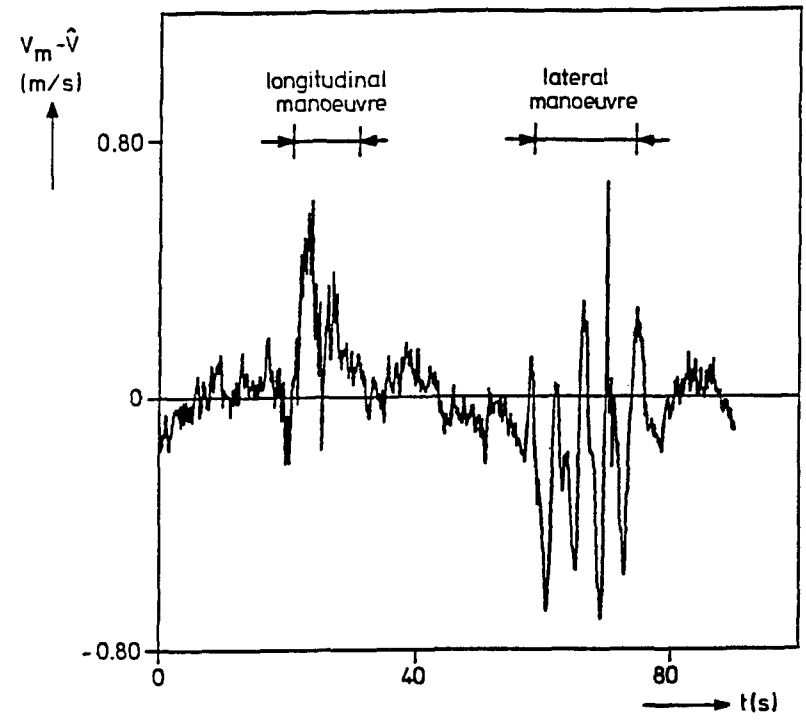

(a) *Residual of airspeed V*

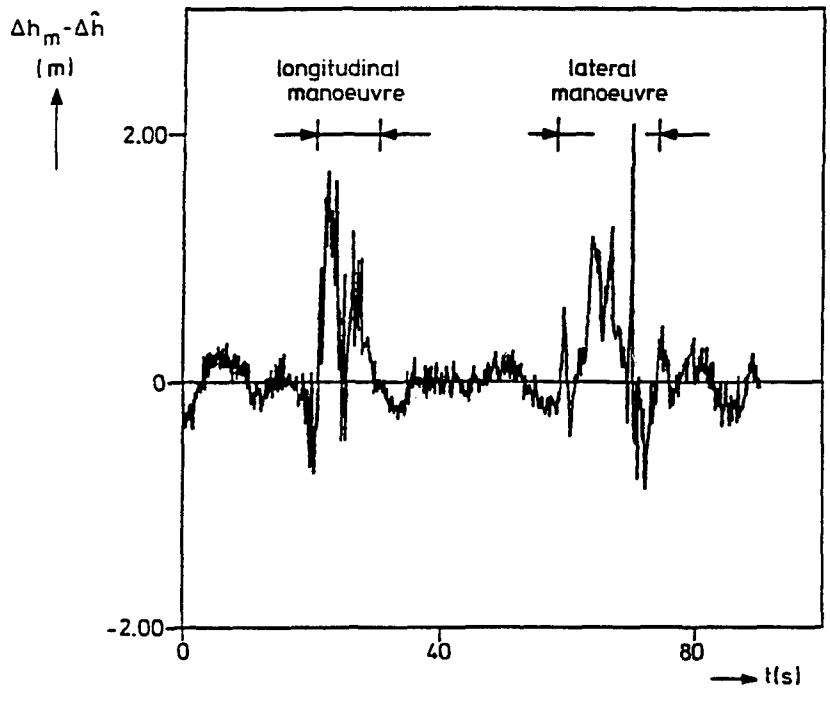

(b) *Residual of altitude variation Δh*

Figure 3-1: *Residuals of the extended Kalman smoother. Results of the reconstruction of an actual flight test manoeuvre.*

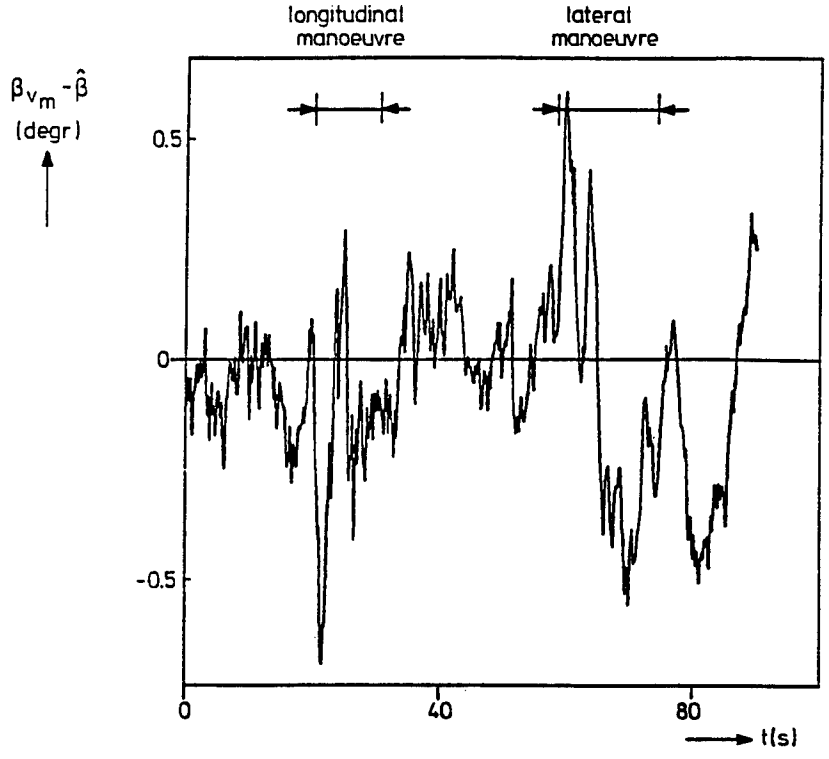

(c) *Residual of side slip vane angle* β

Figure 3-1: *Continued.*

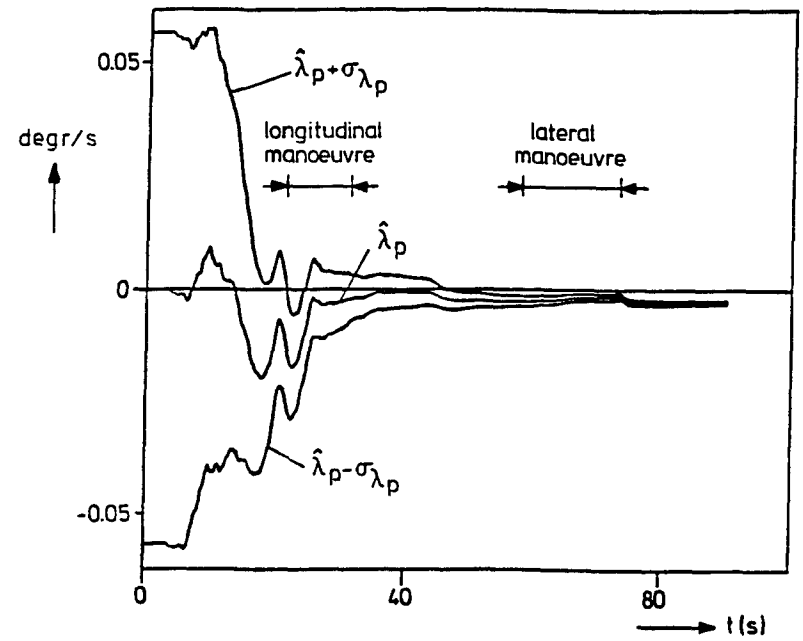

(a) *Estimate of bias error corrections λ_p of roll rate gyro*

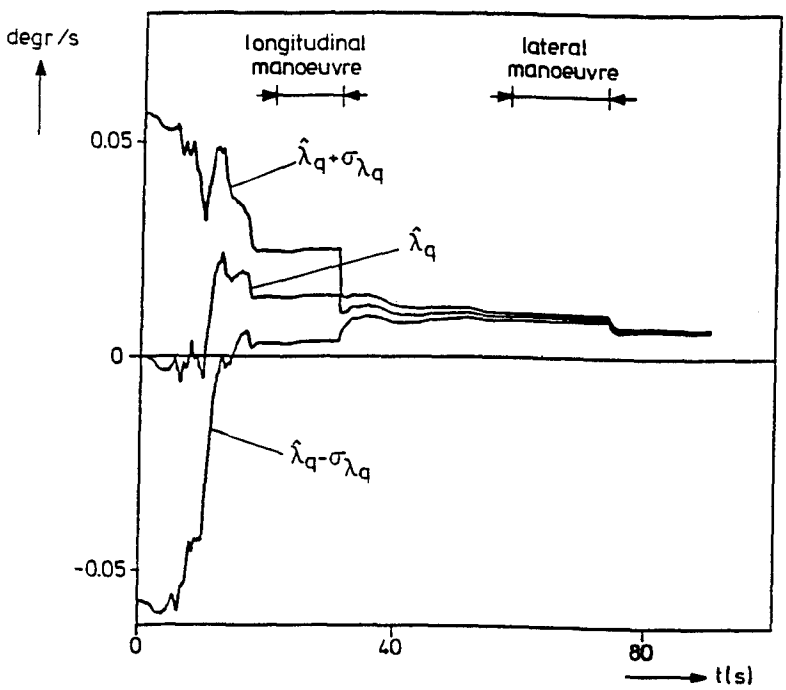

(b) *Estimate of bias error correction λ_q of pitch rate gyro*

Figure 3-2: *Extended Kalman filter estimates of bias error corrections λ_p, λ_q, λ_z, side wash correction factor C_{si} and corresponding standard deviations. Results of the reconstruction of an actual flight test manoeuvre.*

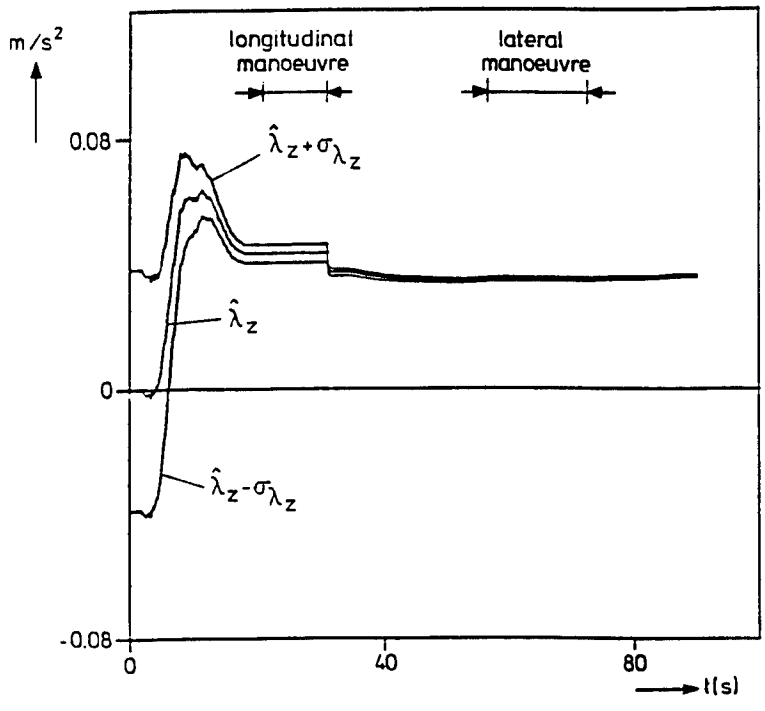

(c) *Estimate of bias error correction λ_z of vertical accelerometer*

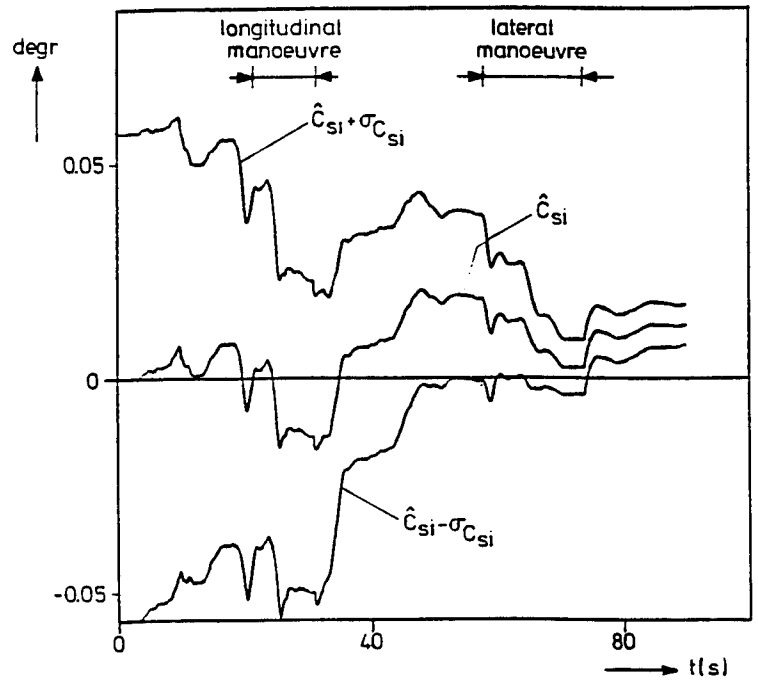

(d) *Estimate of side wash correction factor C_{si} of the side slip vane angle*

Figure 3-2: *Continued.*

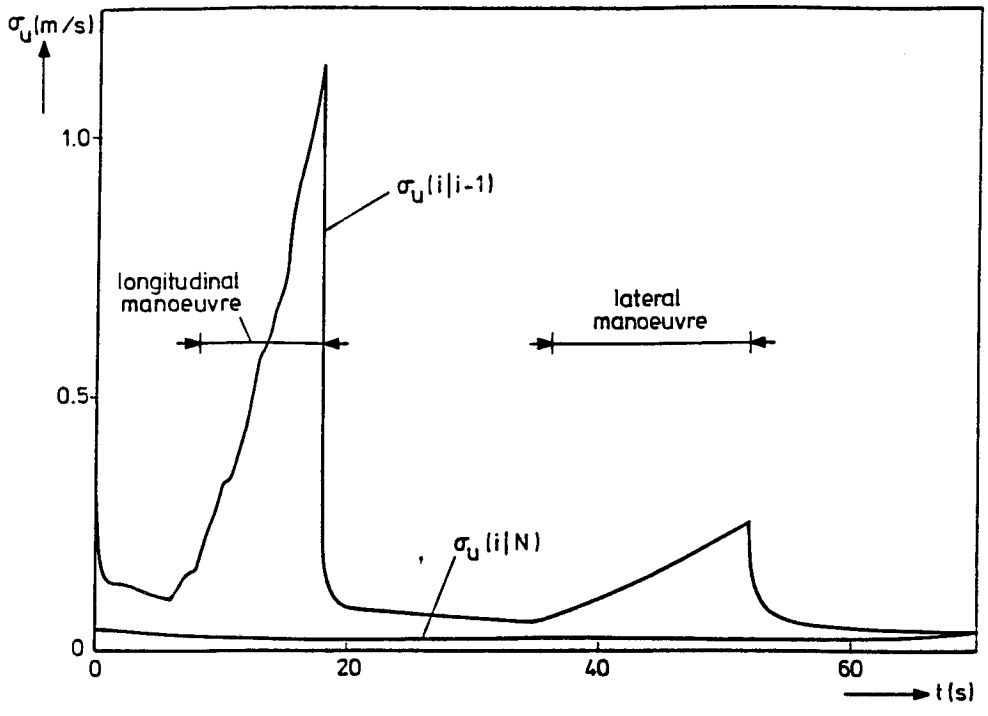

(a) *Standard deviations of $\hat{u}(i|i\text{-}1)$ and $\hat{u}(i|N)$, the estimates of the component of airspeed along the X_B-axis of the extended Kalman filter and the extended Kalman smoother respectively*

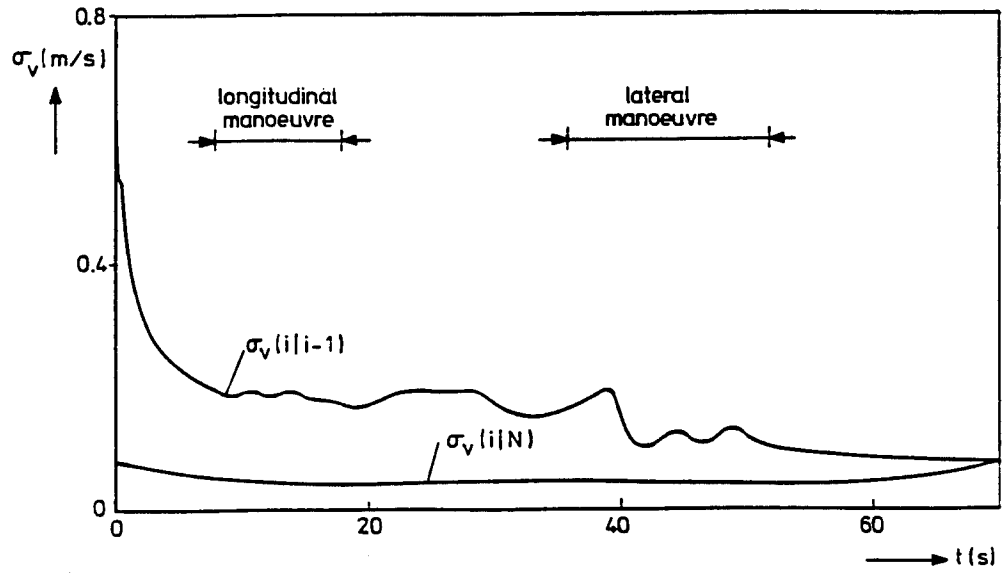

(b) *Standard deviations of $\hat{v}(i|i\text{-}1)$ and $\hat{v}(i|N)$, the estimatesc of the component of airspeed along the Y_B-axis of the extended Kalman filter and the extended Kalman smoother respectively*

Figure 3-3: *Theoretical standard deviations of the extended Kalman filter and -smoother. Results of the reconstruction of an actual flight test manoeuvre.*

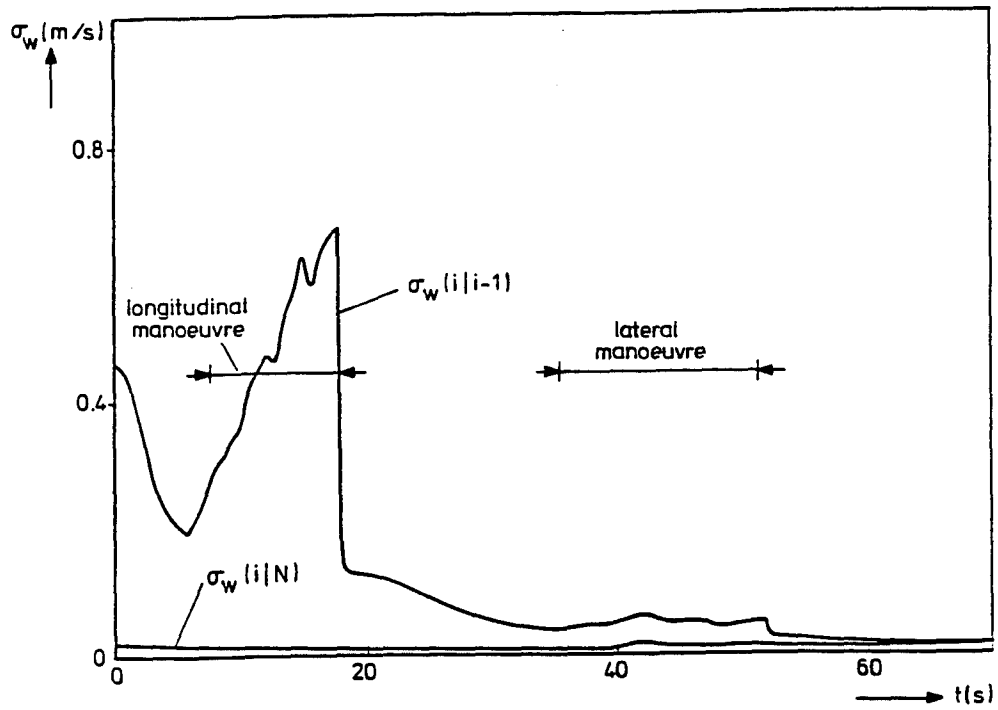

(c) *Standard deviations of $\hat{w}(i|i\text{-}1)$ and $\hat{w}(i|N)$, the estimates of the component of airspeed along the Z_B-axis of the extended Kalman filter and the extended Kalman smoother respectively*

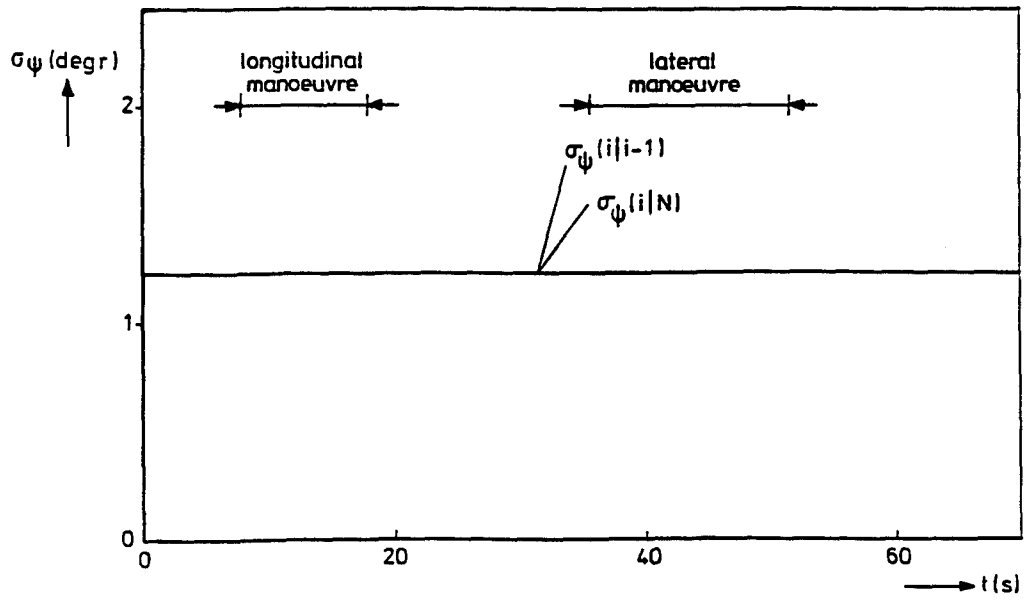

(d) *Standard deviations of $\hat{\psi}(i|i\text{-}1)$ and $\hat{\psi}(i|N)$, the estimates of the yaw angle of the extended Kalman filter and the extended Kalman smoother respectively*

Figure 3-3: *Continued.*

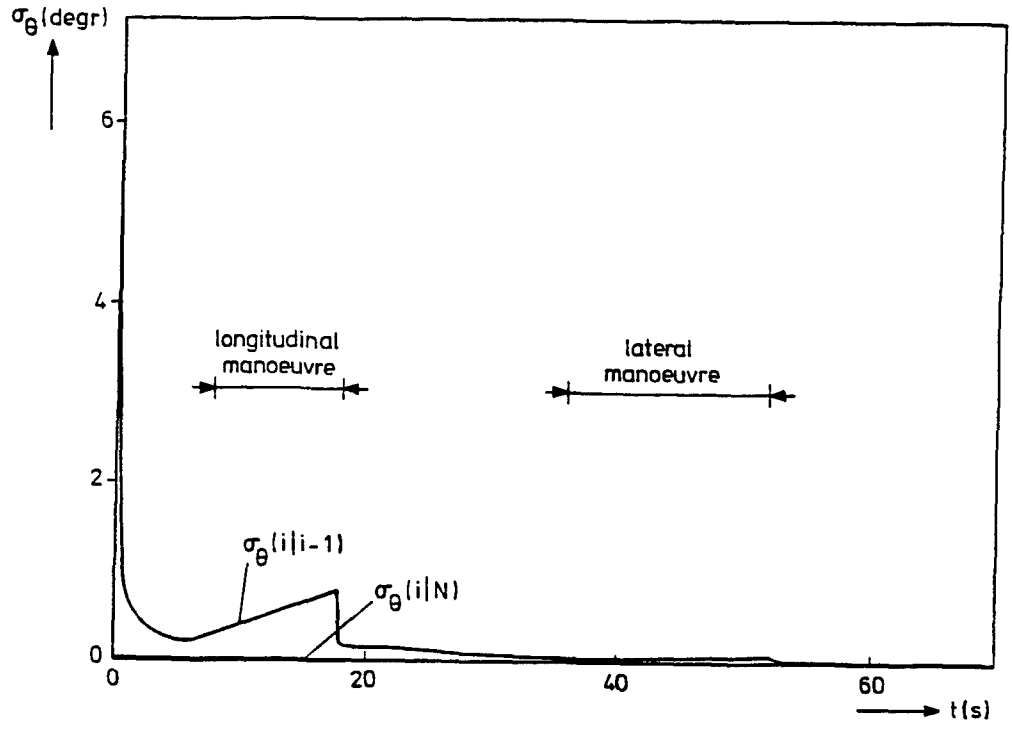

(e) *Standard deviations of $\hat{\theta}(i|i-1)$ and $\hat{\theta}(i|N)$, the estimates of the component of the pitch angle of the extended Kalman filter and the extended Kalman smoother respectively*

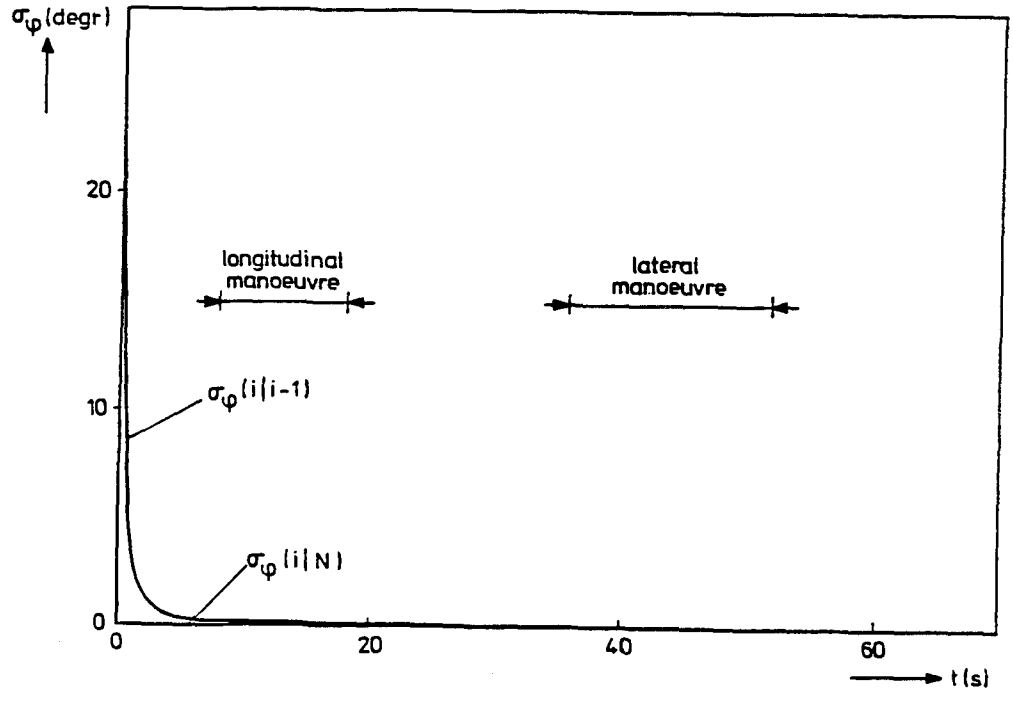

(f) *Standard deviations of $\hat{\phi}(i|i-1)$ and $\hat{\phi}(i|N)$, the estimates of the roll angle of the extended Kalman filter and the extended Kalman smoother respectively*

Figure 3-3: *Continued.*

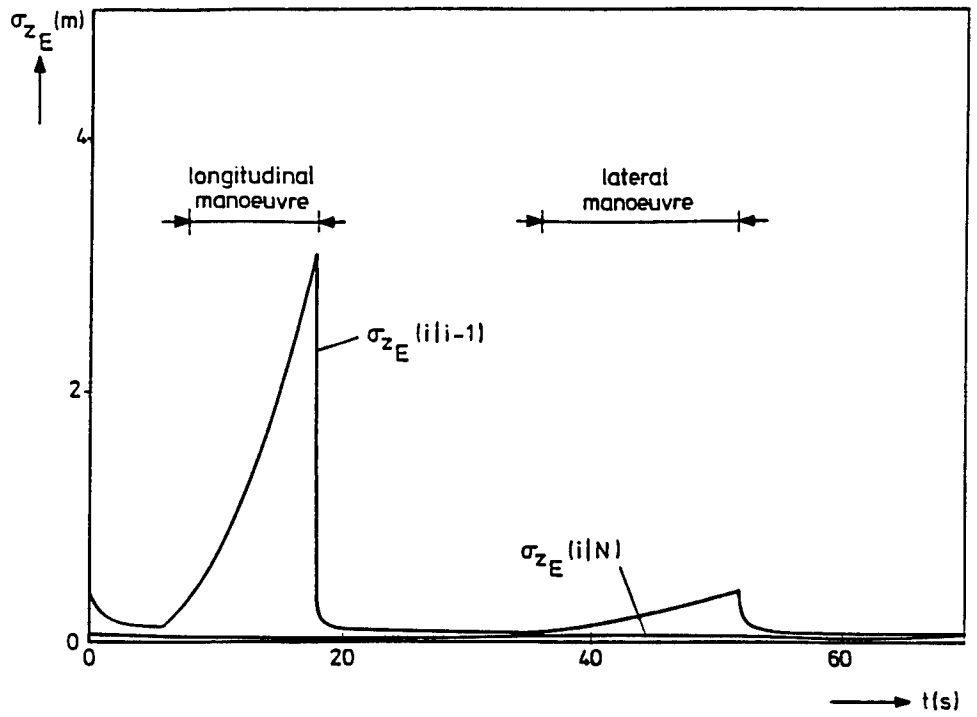

(g) *Standard deviations of $\hat{z}_E(i|i\text{-}1)$ and $\hat{z}_E(i|N)$, the estimates of the vertical displacement of the extended Kalman filter and the extended Kalman smoother respectively*

Figure 3-3: *Continued.*

4 AERODYNAMIC MODEL IDENTIFICATION

Aircraft aerodynamic model identification is the process of developing 'adequate' mathematical descriptions of the aerodynamic forces and moments acting on the aircraft from measurements in flight [1,2,78,125,189,199]. Model identification encompasses the selection of a mathematical model structure as well as the estimation of the numerical values of the parameters in those models. Model identification is often also referred to as parameter identification. Parameter estimation is the narrower problem of just estimating the numerical parameter values given the form or structure of the mathematical model.

The model identification procedure which is the subject of the present volume is the so-called two-step method, see chapter 1. In the first step, called flight path reconstruction, time histories are reconstructed of variables as airspeed, angle of attack and side slip angle. In addition to that, the occurrence of (small) zero shifts may be detected in transducers such as accelerometers and rate gyros. The outputs of these transducers may subsequently be corrected using estimated values of these zero shifts, see chapter 3.

The identification of the aerodynamic model is the second step of the two step method and is discussed in the present chapter. This second step uses the results of the first step, which consequently must be executed first.

Historical background

The aircraft model identification problem has been the interest of several researchers since more than four decades.

Perhaps one of the first approaches to the identification of aircraft *dynamic response models* can be traced back to the work of Milliken in 1947 [77]. His analysis centred around the use of frequency response data and simple graphical methods. Several years later Greenberg [78] and Shinbrot [79] established more general and rigorous ways for determining aerodynamic model parameters from transient manoeuvres. They introduced parameter estimation methods based on application of linear and nonlinear least squares methods. Shinbrot interpreted the equations of motion (a set of ordinary differential equations) as algebraic equations and assumed all of the variables in the equations of motion including derivatives with respect to time and the control input signals to be known functions of time. This enabled him to estimate parameter values by minimizing a criterion in the form of a sum of squares of equation errors. For some variables, for instance the angle of attack, this would require computing derivatives with respect to time, which Shinbrot avoided by transforming the measured responses by means of so called *Method Functions*. After the transformation the equation error is still a linear function of the unknown parameters, a remarkable fact which holds true for both linear as well as nonlinear forms of the equations of motion.

The advent of fast digital computers and also the rapid progress in system theory paved the way for substantial improvements and refinements in aircraft parameter estimation techniques towards the end of sixties and more so in the beginning of seventies. These techniques were generally classified into *equation error methods* [4,80] and *output-* and *prediction error methods* [2,81 to 113, 115,122,126,200]. Shinbrot's method mentioned above is a typical example of an equation error method.

Output error methods use numerical solutions of the equations of motion to compute the time histories of observed variables. Now parameter estimates are computed by minimizing the sum of squares of the differences between these computed variables and the corresponding measured values. Prediction error methods use 'Kalman Filter representations' [95] of the system dynamics to allow and account for process- or system noise resulting from measurement errors of the input signals (control surface deflections) or external disturbances (e.g. atmospheric turbulence). The highlights of the progress were in the areas of algorithms for the estimation of parameters in linear as well as nonlinear aerodynamic models and the determination of 'adequate' aerodynamic model structures.

As a result, the estimation of stability and control derivatives (i.e. parameters in a linearized form of the equations of motion) of fixed wing aircraft has now become more or less a routine procedure. This is not the case, however, for those flight regimes where nonlinear aerodynamic effects are significant

and aerodynamic characteristics cannot be described in linear terms only. The main problem becomes then to determine the 'adequate' form of the aerodynamic model for a 'proper' description of the observed airplane motion. In the literature a number of methods have been proposed for determining adequate models from dynamic response measurements. Unbehauen and Gohring [141] proposed a simple statistical method to select the order of linear models of single input, single output (SISO) systems. Genesio and Milanese [142] describe more advanced statistical methods for order selection of models of linear multiple input and multiple output (MIMO) systems. In aircraft parameter identification of fixed wing rigid aircraft the order of the system model is known from the equations of motion. The problem of determining an adequate model structure is strictly related to the models of the aerodynamic moments and the aerodynamic forces acting on the aircraft during the flight test manoeuvre at the particular set of nominal flight test conditions. Klein [143] may have been the first to use formal statistical techniques to test the correctness of models of aircraft responses. He formed an appropriate statistic as the ratio of two variance estimates from residuals and repeated measurements of frequency response curves. Klein [144] also recommended the analysis of residuals for checking the accuracy of the model and suggested the sensitivity of a response to parameter changes for finding the important parameters in the model. Stepner and Mehra [145] gave a criterion for fit error which combined the sum of squares of residuals and the number of parameters in the model. Later Taylor Jr. [146] developed a criterion for the optimal number of unknown parameters satisfying the expected model response error. Hall, Gupta et al [59,148] gave a comprehensive treatment of model structure determination based on stepwise regression and their use in real flight data was then investigated by Gupta and Hall [131], Vincent, Gupta et al [202], Stalford [203] and Klein et al [150,151].

The DUT approach

In the middle of the 1960's, Gerlach of the Delft University of Technology realized that for high parameter accuracy, the customary technique of analogue recordings of measurements in continuous time would not suffice. He developed a digital measurement system which sampled measurements at discrete times. Now if a quadratic criterion for the equation error is minimized with respect to the parameters in the aerodynamic model, it becomes possible to apply the well developed mathematical techniques of regression analysis [3]. He applied the concept of minimizing equation errors, not to the equations of motion as Shinbrot had done, but rather directly to the equations of aerodynamic model. This in fact marked the beginning of continuous investigations into what became known as the *two-step method for aircraft parameter identification* at the Delft University of Technology and the National Aerospace Laboratory, NLR. In a sense, flight path reconstruction, the first step of the two step method, may be seen as to have a similar function as the transformations in Shinbrot's method in that they both prepare for application of equation error methods. The objective of the present chapter is to go into the details of the second step of the method using equation errors for aerodynamic model identification.

The second step exploits regression analysis to determine the model structure and model parameters in the aerodynamic model. The model determination phase consists of selecting a restricted number of variables from a finite set of so-called *candidate variables*. This leads to the selection of an *adequate model structure.*

The organization of the present chapter is as follows. In section 4.1, we first discuss the issue of *identifiability* of the parameters in linear aerodynamic models (stability and control derivatives) from flight test data. This is an analogous effort to what we discussed as the issue of state reconstructibility of linearized kinematic models in section 3.2. Next we present the general regression technique, a model development procedure based on residual analysis and also briefly touch upon the collinearity problem [75] in section 4.2. In section 4.3 a practical investigation of nonlinear aerodynamic model identification from flight test data for both the longitudinal and lateral case is conducted. Flight tests with the DHC-2 Beaver aircraft are used again for illustration.

4.1 Linear Aerodynamic Model Identification

The purpose of the analysis in this section is to determine the identifiable part of the parameter vector of *linearized aerodynamic models*. This is in fact the case in which only 'small' perturbations from a nominal steady flight condition are considered. The parameters in our model correspond now to the so-called *stability and control derivatives*. Since the equation error method is used in the second step of the two-step method the estimation problem reduces to a *linear parameter estimation problem*. Well established regression techniques may be used to solve this linear estimation problem. These techniques will be discussed in section 4.2

In section 4.1.1 we define parameter identifiability and show as to how to construct the identifiable sub space of the parameter space. In section 4.1.2 we develop the appropriate aerodynamic model equations by taking account of the results of the reconstructibility analysis of chapter 3. Finally we analyze the identifiability of the parameters in the resulting equations in sections 4.1.3 for the longitudinal case and in 4.1.4 for the lateral case.

4.1.1 Parameter Identifiability

If small perturbations from nominal flight conditions are considered, then from chapter 2, the aerodynamic forces and moments can be expressed in terms of homogeneous polynomials of first order. A natural question is, can we estimate all parameters in these first order polynomials from the available flight test measurements. This question is answered in section 4.1.2 using the notion of *parameter identifiability*.
If aerodynamic forces and moments are expressed in terms of polynomials, then the corresponding aerodynamic models may be written in the following form:

$$y(i) = x(i)\underline{a} + e(i) \qquad (4.1\text{-}1)$$

in which i refers to a time instant t_i, y(i) is a scalar dependent variable representing measured aerodynamic force or moment, x(i) is a $1 \times r$ matrix of measured independent variables, $\underline{a}$ is the vector of parameters to be identified and e(i) denotes a stochastic equation error due to measurement and model errors. The model errors could come from atmospheric turbulence, propeller slipstream or jet interference effects or fuel sloshing, etc., all of which can add unmodelled contributions to force and moment coefficients. All of these errors are rather heuristically accounted for by e(i), a stochastic random variable with the following properties:

$$\begin{aligned} E\{e(i)\} &= 0 , \\ E\{e(i)e(j)\} &= V_e\delta_{ij} . \end{aligned} \qquad (4.1\text{-}2)$$

For N different sets of y(i) and x(i) it is customary to write (4.1-1) in the form:

$$\underline{Y} = X\underline{a} + \underline{e}$$

in which $\underline{Y}$=col[y(1),y(2),...,y(N)], $\underline{e}$=col[e(1), e(2),...,e(N)] and X denotes the following matrix of independent variables:

$$X = \begin{bmatrix} x(1) \\ x(2) \\ \vdots \\ x(N) \end{bmatrix} .$$

The least squares estimate $\hat{\underline{a}}$ may readily be calculated from $\underline{Y}$ and X as the solution of the so called normal equations [73]:

$$[X^T \cdot X]\hat{\underline{a}} = X^T \cdot \underline{Y} , \qquad (4.1\text{-}3)$$

If the matrix $[X^T \cdot X]$ is invertible, i.e. has full rank r, then X has rank r and $\hat{\underline{a}}$ is the unique solution of (4.1-3). If the actual rank of X is $r_1<r$, then it is impossible to compute independent estimates of all of the components of the parameter vector $\underline{a}$.
Completely analogous to the definition of reconstructible subspace in system state reconstruction problems as discussed in chapter 3, identifiable subspaces may be defined in parameter identification problems as follows.

If X is of rank r_1, it is always possible to arrange and partition X as:

$$X = [X_1 \quad X_2] = [X_1 \quad X_1 \cdot C] \qquad (4.1\text{-}4)$$

in which C denotes a constant $r_1 \times (r\text{-}r_1)$ matrix. The $Nx(r\text{-}r_1)$ matrix X_2 contains those columns of X which are dependent on the independent columns contained in the Nxr_1 matrix X_1. Substitution of (4.1-4) in (4.1-3) results in:

$$\begin{bmatrix} X_1^T \cdot X_1 & \vdots & X_1^T \cdot X_1 C \\ \cdots\cdots & \vdots & \cdots\cdots \\ C^T X_1^T \cdot X_1 & \vdots & C^T X_1^T \cdot X_1 C \end{bmatrix} \begin{pmatrix} \hat{\underline{a}}_1 \\ \cdots \\ \hat{\underline{a}}_2 \end{pmatrix} = \begin{bmatrix} X_1^T \\ \cdots\cdots \\ C^T X_1^T \end{bmatrix} \underline{Y} \,. \tag{4.1-5}$$

There exists no unique solution for $\hat{\underline{a}}_1$ and $\hat{\underline{a}}_2$ in (4.1-5). The minimum norm solution is found by selecting one of the solutions, indicated as $\hat{\underline{a}}_1^*$, $\hat{\underline{a}}_2^*$ by setting:

$$\hat{\underline{a}}_2^* = \underline{0} \tag{4.1-6}$$

If the value of any parameter in $\underline{a}_2$ or a relation between parameters involving components in $\underline{a}_2$ are known, it may be preferable to use this knowledge instead of simply putting $\hat{\underline{a}}_2^*$ to zero. The components in $\hat{\underline{a}}_1^*$ may then be calculated as:

$$\hat{\underline{a}}_1^* = \left[X_1^T \cdot X_1\right]^{-1} X_1^T \cdot \underline{Y} \,. \tag{4.1-7}$$

It is instructive to determine the expected value of $\hat{\underline{a}}_1^*$:

$$\begin{aligned} E(\hat{\underline{a}}_1^*) &= \left[X_1^T \cdot X_1\right]^{-1} X_1^T \cdot E(\underline{Y}) \\ &= \left[X_1^T \cdot X_1\right]^{-1} X_1^T \left(\left[X_1 \quad X_1\right] C \cdot \underline{a}\right) \\ &= \left[I \quad C\right] \underline{a} = \underline{a}_1 + C \cdot \underline{a}_2 \,. \end{aligned} \tag{4.1-8}$$

Equation (4.1-8) clearly shows that $\hat{\underline{a}}_1^*$ is a biased estimate of $\underline{a}_1$, but it can be interpreted as an unbiased estimate of the new parameter $\underline{a}_1^* = \underline{a}_1 + C \cdot \underline{a}_2$. Analogous to the treatment of the reconstructible part $\underline{x}_1^*$ of the state vector $\underline{x}$ in section 3.2, $\underline{a}_1^*$ is called the identifiable part of the parameter vector $\underline{a}$. In the same way as in section 3.2, we can now find a matrix U_1 which constitutes a basis for the identifiable subspace of the parameter space and a matrix U_2 which constitutes a basis for the unidentifiable subspace of the parameter space. The linear transformation:

$$\begin{pmatrix} \underline{a}_1^* \\ \cdots \\ \underline{a}_2^* \end{pmatrix} = \begin{bmatrix} U_1 \\ \cdots\cdots \\ U_2 \end{bmatrix} \underline{a} \tag{4.1-9}$$

transforms the parameter vector $\underline{a}$ into an identifiable part $\underline{a}_1^*$ and unidentifiable part $\underline{a}_2^*$. If the matrix X contains the maximum number of r independent columns, then the parameter vector $\underline{a}$ is *completely identifiable.*

4.1.2 Linear Aerodynamic Model Equations including Reconstructibility Analysis

In the present section, the linear aerodynamic model presented in chapter 2 is developed further by including the results of the reconstructibility analysis of chapter 3.

In the linear case, the parameters to be estimated are the stability and control derivatives of the longitudinal and lateral aerodynamic force and moment coefficients. In the stability reference frame F_S, used in the present section, these models are listed in (2.2-6) and (2.2-9).

Application of the least squares method of section 4.1.1 requires the availability of all variables in the equations (2.2-6) and (2.2-9) be known. That is to say, all the aerodynamic force and moment coefficients as well as all variables in the right hand side, i.e. $\tilde{u}_S/V_0$, $\tilde{\alpha}$, etc. to be known at discrete instants of time. These variables must either be measured directly or be reconstructed as part of a longitudinal or lateral flight path reconstruction.

The measured time histories of the specific aerodynamic forces and body rotation rates in F_S may be used to compute the aerodynamic force and moment coefficients in the left hand side of equations (2.2-6) and (2.2-9). The results are indicated by subscripts m. For example, $\tilde{C}_{X_{S_m}}$ and $\tilde{C}_{l_{S_m}}$ are obtained as follows.

Division of both sides of the first relation in (2.1-11) by $\frac{1}{2}\rho_0 V_0^2 S$ results in:

$$\tilde{C}_{X_S} = \frac{m \cdot \tilde{A}_{x_S}}{\frac{1}{2}\rho_0 V_0^2 S} \,, \tag{4.1-10}$$

in which aircraft mass m may be assumed to be known. The same may be assumed for the reference wing area S and the nominal values of air density ρ_0 and true airspeed V_0.

Using (3.2-6), $\tilde{A}_{x_S}$ can be written as:

$$\tilde{A}_{x_S} = \tilde{A}_{x_{S_m}} + \lambda_{x_S} + w_{x_S} \,, \tag{4.1-11}$$

where λ_{x_S} denotes an unknown bias error correction and w_{x_S} an unknown random measurement error. Substitution in (4.1-10) results in:

$$\tilde{C}_{x_{S_m}} = \tilde{C}_{x_S} - \frac{m \cdot \lambda_{x_S}}{\frac{1}{2}\rho_0 V_0^2 S} - \frac{m \cdot w_{x_S}}{\frac{1}{2}\rho_0 V_0^2 S} \qquad (4.1\text{-}12)$$

Similar expressions holds for $\tilde{C}_{Y_{Sm}}$ and $\tilde{C}_{Z_{Sm}}$.

Division of the first line in the moment equations (2.1-10) by $\frac{1}{2}\rho_0 V_0^2 Sb$ results in:

$$\tilde{C}_{l_S} = \frac{I_{x_S}}{\frac{1}{2}\rho_0 V_0^2 Sb} \cdot \dot{\tilde{p}}_S - \frac{I_{zx_S}}{\frac{1}{2}\rho_0 V_0^2 Sb} \cdot \dot{\tilde{r}}_S \qquad (4.1\text{-}13)$$

where, for simplicity, the effect of rotating components, such as propellers or jet engine turbines have been neglected. The wing span b is known. The moment of inertia I_{x_S} and the product of inertia I_{zx_S} can be calculated by book-keeping methods or estimated from free-oscillation rig measurements, ref. [223].

The angular accelerations $\dot{\tilde{p}}_S$ and $\dot{\tilde{r}}_S$ are not measured directly but derived by numerically differentiating $\tilde{p}_S$ and $\tilde{r}_S$. Since the rotation rate measurements are assumed to be contaminated by constant bias and random errors, differentiation will result in:

$$\begin{aligned} \dot{\tilde{p}}_S &= \dot{\tilde{p}}_{S_m} + w_{\dot{p}_S}, \\ \dot{\tilde{r}}_S &= \dot{\tilde{r}}_{S_m} + w_{\dot{r}_S}, \end{aligned} \qquad (4.1\text{-}14)$$

in which $w_{\dot{p}_S}$ and $w_{\dot{r}_S}$ denote random errors in $\dot{\tilde{p}}_S$ and $\dot{\tilde{r}}_S$ respectively. Substitution of (4.1-14) in (4.1-13) results in:

$$\tilde{C}_{l_{S_m}} = \tilde{C}_{l_S} - \frac{I_{x_S}}{\frac{1}{2}\rho_0 V_0^2 Sb} \cdot w_{\dot{p}_S} + \frac{I_{zx_S}}{\frac{1}{2}\rho_0 V_0^2 Sb} \cdot w_{\dot{r}_S} \qquad (4.1\text{-}15)$$

Similar expressions can be derived for $\tilde{C}_{m_S}$ and $\tilde{C}_{n_S}$.

In the right hand side of equations (2.2-6) and (2.2-9) several variables like $\tilde{u}_S$, $\tilde{\alpha}$ and $\tilde{\beta}$ are obtained from flight path reconstruction. As a result of actual flight path reconstructions using high accuracy instrumentation techniques, the stochastic estimation errors of the reconstructible parts of the state vector are relatively very small. Therefore, these errors are neglected in the present analysis and only the bias errors are taken into account. According to section 3.2, table 3-2, $\tilde{u}_S$ is reconstructible. However, $\tilde{\alpha}$ and $\tilde{\beta}$ have been shown to be non reconstructible. For the observation configuration analyzed in chapter 3 it follows from table 3-2 and table 3-3 that:

$$\begin{aligned} \tilde{\alpha} &= \tilde{\alpha}^* + \frac{1}{g} \cdot \lambda_{x_S} - \frac{1}{V_0} \cdot W_{z_T}, \\ C_{\beta_1} \cdot \tilde{\beta} &= C_{\beta_1} \cdot \tilde{\beta}^* - C_{\beta_0}. \end{aligned} \qquad (4.1\text{-}16)$$

Differentiation of both sides of these relations results in:

$$\begin{aligned} \dot{\tilde{\alpha}} &= \dot{\tilde{\alpha}}^* \\ \dot{\tilde{\beta}} &= \dot{\tilde{\beta}}^* \end{aligned} \qquad (4.1\text{-}17)$$

All remaining variables in the right hand side of equations (2.2-6) and (2.2-9) may be obtained from direct measurements. For example, according to (3.2-6):

$$\tilde{q}_S = \tilde{q}_{S_m} + \lambda_{q_S} + w_{q_S}, \qquad (4.1\text{-}18)$$

and according to section 2.4:

$$\tilde{\delta}_e = \tilde{\delta}_{e_m} - v_{\delta_e}, \qquad (4.1\text{-}19)$$

in which v_{δ_e} denotes the measurement error of the elevator deflection angle δ_e.

Substitution of the relations derived above in the linear aerodynamic models (2.2-6) and (2.2-9) results in models which may be used for estimation of linear stability and control derivatives. For example, substitution of (4.1-12), (4.1-16), (4.1-17), (4.1-18) and (4.1-19) in the linear aerodynamic model of $\tilde{C}_{X_S}$ in (2.2-6) results in:

$$\tilde{C}_{X_{S_m}} = -\frac{m\lambda_{x_S}}{\frac{1}{2}\rho_0 V_0^2 S} + C_{X_{\alpha_S}}\cdot\left(\frac{1}{g}\cdot\lambda_{x_S} - \frac{1}{V_0}\cdot W_{z_T}\right) +$$

$$+ C_{X_{q_S}}\cdot\frac{\lambda_{q_S}\bar{c}}{V_0} + C_{X_{u_S}}\cdot\frac{\tilde{u}_S}{V_0} + C_{X_{\alpha_S}}\cdot\tilde{\alpha}^* +$$

$$+ C_{X_{q_S}}\cdot\frac{\tilde{q}_{S_m}\bar{c}}{V_0} - C_{X_{\dot{\alpha}_S}}\cdot\frac{\dot{\tilde{\alpha}}^*\bar{c}}{V_0} + C_{X_{\delta_{e_S}}}\cdot\tilde{\delta}_{e_m} -$$

$$- \frac{m}{\frac{1}{2}\rho_0 V_0^2 S}\cdot w_{x_S} + C_{X_{q_S}}\cdot\frac{\bar{c}}{V_0} w_{q_S} - C_{X_{\delta_{e_S}}}\cdot v_{\delta_e},$$

which can be written more compactly:

$$\tilde{C}_{X_{S_m}} = C_{X_{0_S}} + C_{X_{u_S}}\cdot\frac{\tilde{u}_S}{V_0} + C_{X_{\alpha_S}}\cdot\tilde{\alpha}^* +$$

$$+ C_{X_{q_S}}\cdot\frac{\tilde{q}_{S_m}\bar{c}}{V_0} + C_{X_{\dot{\alpha}_S}}\cdot\frac{\dot{\tilde{\alpha}}^*\bar{c}}{V_0} + \qquad (4.1\text{-}20)$$

$$+ C_{X_{\delta_{e_S}}}\cdot\tilde{\delta}_{e_m} + \delta\tilde{C}_{X_S}.$$

The last term $\delta\tilde{C}_{X_S}$ in (4.1-20) represents the equation error resulting from several time-varying measurement errors. However, if high accuracy measurement techniques are used, these measurement errors are too small to explain the order of magnitude of equation errors found when analysing actual flight test data. Therefore, aerodynamic model errors rather than measurement errors are the cause of time-varying equation errors. Relations similar to (4.1-20) may be derived for $\tilde{C}_{Y_{Sm}}$, $\tilde{C}_{Z_{Sm}}$, $\tilde{C}_{l_{Sm}}$, $\tilde{C}_{m_{Sm}}$ and $\tilde{C}_{n_{Sm}}$. The difference with the relation (2.2-6) and (2.2-9) are supplementary constant terms accounting the existence of measurement bias error corrections and unreconstructible components in the longitudinal and lateral state vectors and terms representing equation errors.

4.1.3 Identifiability of Linear Longitudinal Aerodynamic Model

To begin the discussion, it may be seen from equation (4.1-20) that the linear models of the longitudinal aerodynamic force and moment coefficients contain the following set of independent variables:

$$1,\ \frac{\tilde{u}_S}{V_0},\ \tilde{\alpha}^*,\ \frac{\tilde{q}_{S_m}\bar{c}}{V_0},\ \frac{\dot{\tilde{\alpha}}^*\bar{c}}{V_0},\ \tilde{\delta}_e \qquad (4.1\text{-}21)$$

In the remaining part of the present section an index m indicates the presence of an unknown bias error in an otherwise perfectly measured variable. At any particular instant of time, these variables constitute one row in the matrix X of independent variables as defined in section 4.1.1.

The variables $\tilde{u}_S/V_0$, $\tilde{\alpha}$, $\tilde{\theta}$ and $\tilde{q}_S\bar{c}/V_0$ are state vector components of the longitudinal linear equations of motion [57]. It may be verified that these equations of motion with elevator control deflections $\tilde{\delta}_e$ as input signal represent a completely controllable system [70]. This means that in principle it is possible to design a longitudinal flight test manoeuvre such that the time histories of $\tilde{u}_S/V_0$, $\tilde{\alpha}$, $\tilde{\theta}$ and $\tilde{q}_S\bar{c}/V_0$ are linearly independent. This implies independence of 1, $\tilde{u}_S/V_0$, $\tilde{\alpha}^*$, $\tilde{q}_{S_m}\bar{c}/V_0$ and $\tilde{\delta}_e$ in (4.1-21). According to the linearized kinematical model in (2.1-15), the remaining variable $\dot{\tilde{\alpha}}\bar{c}/V_0$ can be written as:

$$\frac{\dot{\tilde{\alpha}}\bar{c}}{V_0} = -\frac{g\bar{c}}{V_0^2}\sin\gamma_0\,\tilde{\theta} + \frac{\bar{c}}{V_0^2}\tilde{A}_{z_S} + \frac{\tilde{q}_S\bar{c}}{V_0}. \qquad (4.1\text{-}22)$$

where:

$$\tilde{A}_{z_S} = \frac{1}{m}\,\frac{1}{2}\rho_0 V_0^2 S\,\tilde{C}_{z_S}$$

The linear aerodynamic model of $\tilde{C}_{z_S}$ may be written as:

$$\tilde{C}_{z_S} = C_{z_{u_S}}\cdot\frac{\tilde{u}_S}{V_0} + C_{z_{\alpha_S}}\cdot\tilde{\alpha} + C_{z_{q_S}}\cdot\frac{\tilde{q}_S\bar{c}}{V_0} +$$

$$+ C_{z_{\dot{\alpha}_S}}\cdot\frac{\dot{\tilde{\alpha}}\bar{c}}{V_0} + C_{z_{\delta_{e_S}}}\cdot\tilde{\delta}_e$$

It is clear now that $\dot{\tilde{\alpha}}\bar{c}/V_0$ depends linearly on the variables $\tilde{u}_S/V_0$, $\tilde{\alpha}$, $\tilde{\theta}$, $\tilde{q}_S\bar{c}/V_0$ and $\tilde{\delta}_e$ in the following fashion:

$$\frac{\dot{\tilde{\alpha}}\bar{c}}{V_0} = \frac{1}{2\mu_c - C_{Z_{\dot{\alpha}S}}} \left\{ C_{Z_{u_S}} \cdot \frac{\tilde{u}_S}{V_0} + C_{Z_{\alpha_S}} \cdot \tilde{\alpha} - \right.$$
$$- 2\mu_c \frac{g\bar{c}}{V_0^2} \sin\gamma_0 \tilde{\theta} + (2\mu_c + C_{Z_{q_S}}) \cdot \frac{\tilde{q}_S \bar{c}}{V_0} +$$
$$\left. + C_{Z_{\delta_{e_S}}} \cdot \tilde{\delta}_e \right\} . \qquad (4.1\text{-}23)$$

In general the stability derivatives $C_{Z_{\dot{\alpha}S}}$ and $C_{Z_{qS}}$ are small compared to $2\mu_c$ [57]. Equation (4.1-23) may, therefore, be simplified by neglecting $C_{Z_{\dot{\alpha}S}}$ and $C_{Z_{qS}}$.

In the reconstructibility analysis of the linear longitudinal flight path reconstruction model, it was shown that the selected observation configuration of the actual flight tests led to a constant error in the reconstructed version $\tilde{\alpha}^*$ of the angle of attack $\tilde{\alpha}$, see equation (4.1-16). This constant error vanishes after differentiation, see equation (4.1-17).
Using equations (4.1-16), (4.1-17), (4.1-18) and the simplifications above, (4.1-23) may now be written as:

$$\frac{\dot{\tilde{\alpha}}^*\bar{c}}{V_0} = \left[1 , \frac{\tilde{u}_S}{V_0} , \tilde{\alpha}^* , \frac{\tilde{q}_{S_m}\bar{c}}{V_0} , \tilde{\delta}_e \right] \cdot C - \qquad (4.1\text{-}24)$$
$$- \frac{g\bar{c}}{V_0^2} \sin\gamma_0 \tilde{\theta}$$

in which C denotes a 5×1 matrix as defined in (4.1-4), with elements:

$$C^T = \left[\frac{C_{Z_{\alpha_S}}}{2\mu_c} \cdot \left(\frac{1}{g}\lambda_{x_S} - \frac{1}{V_0} W_{z_T} \right) + \frac{\lambda_{q_S}\bar{c}}{V_0} , \ldots \right.$$
$$\left. \frac{C_{Z_{u_S}}}{2\mu_c} , \frac{C_{Z_{\alpha_S}}}{2\mu_c} , 1 , \frac{C_{Z_{\delta_{e_S}}}}{2\mu_c} \right] . \qquad (4.1\text{-}25)$$

If the nominal flight condition is horizontal then $\gamma_0=0$ and consequently the term with $\tilde{\theta}$ vanishes. According to section 4.1.1 this means that no unique solution exists for the longitudinal stability and control derivative estimation problem. If one of the solutions is selected, for instance by setting $C_{X_{\dot{\alpha}S}}=C_{Z_{\dot{\alpha}S}}=C_{m_{\dot{\alpha}S}}=0$ the remaining estimates will be biased as shown in equation (4.1-8).

The existence of unidentifiable longitudinal stability and control derivatives was noted earlier by Gerlach [3]. The linear dependence exists only in horizontal nominal flight conditions. This means that in principle non horizontal nominal flight conditions (i.e. climb or descent) allow complete identifiability of all longitudinal stability and control derivatives. In normal practice, however, nominal flight path angles are too small to result in an effective elimination of the above identifiability problem. If a large flight path angle is chosen, the engine power setting will be very different than in horizontal flight, which may affect the aerodynamic model through interference effects and may introduce errors due to the limited accuracy of the thrust calculation.

Another possibility is to consider a manoeuvre in rolling or turning flight. This will also remove the linear dependence in equation (4.1-24) via the previously dropped term $g\bar{c}/V_0^2 \cdot \cos\varphi_0 \cdot \sin\phi_0 \cdot \tilde{\phi}$ at the linearization of the kinematical equations (2.1-5), see [103,21]. The success of this approach is limited by the effect of the rolling or turning flight condition on the aerodynamic model, which can be very important, especially for aircraft with propellers.

4.1.4 Identifiability of Linear Lateral Aerodynamic Model

To begin the discussion, it can be seen that the independent variables in the models of $\tilde{C}_{Y_{Sm}}$, $\tilde{C}_{l_{Sm}}$ and $\tilde{C}_{n_{Sm}}$ are:

$$1 , \tilde{\beta}^* , \frac{\tilde{p}_{S_m} b}{2V_0} , \frac{\tilde{r}_{S_m} b}{2V_0} , \frac{\dot{\tilde{\beta}}^* b}{V_0} , \tilde{\delta}_a , \tilde{\delta}_r . \qquad (4.1\text{-}26)$$

The variables $\tilde{\beta}$, $\tilde{\phi}$, $\tilde{p}_S b/2V_0$ and $\tilde{r}_S b/2V_0$ are components of the state vector of the linear lateral equations of motion [57]. Analogous to the longitudinal case discussed above, it may be verified that these equations represent a completely controllable system with aileron and rudder control deflections $\tilde{\delta}_a$ and $\tilde{\delta}_r$ as input signals. This means that lateral flight test manoeuvres can be designed such that the time histories of $\tilde{\beta}$, $\tilde{\phi}$, $\tilde{p}_S b/2V_0$, $\tilde{r}_S b/2V_0$, $\tilde{\delta}_a$ and $\tilde{\delta}_r$ are linearly independent. This

implies independence of 1, $\tilde{\beta}^*$, $\tilde{p}_{S_m}b/2V_0$, $\tilde{r}_{S_m}b/2V_0$, $\tilde{\delta}_a$ and $\tilde{\delta}_r$ in equation (4.1-26).

Next it must be investigated whether $\dot{\tilde{\beta}}^* b/V_0$ is independent. This could be checked by rewriting $\dot{\tilde{\beta}}b/V_0$ using equation (2.1-16) as:

$$\frac{\dot{\tilde{\beta}}b}{V_0} = \frac{gb}{V_0^2}\cos\gamma_0\tilde{\phi}_S + \frac{b}{V_0^2}\tilde{A}_{y_S} - 2\frac{\tilde{r}_S b}{2V_0} . \quad (4.1\text{-}27)$$

where:

$$\tilde{A}_{y_S} = \frac{1}{m}\tfrac{1}{2}\rho_0 V_0^2 S\,\tilde{C}_{Y_S}$$

The linear aerodynamic model of $\tilde{C}_{Y_S}$ from equation (2.2-9) may be written as:

$$\tilde{C}_{Y_S} = C_{Y_\beta}\cdot\tilde{\beta} + C_{Y_{\dot\beta}}\cdot\frac{\dot{\tilde{\beta}}b}{V_0} + C_{Y_p}\cdot\frac{\tilde{p}_S b}{2V_0} + C_{Y_r}\cdot\frac{\tilde{r}_S b}{2V_0} + C_{Y_{\delta_a}}\cdot\tilde{\delta}_a + C_{Y_{\delta_r}}\cdot\tilde{\delta}_r .$$

Substitution for $\tilde{A}_{y_S}$ in (4.1-27) leads, for the case of a nominally horizontal flight condition, i.e. $\gamma_0=0$, to the following expression for $\dot{\tilde{\beta}}b/V_0$:

$$\frac{\dot{\tilde{\beta}}b}{V_0} = \frac{1}{2\mu_b - \tilde{C}_{Y_{\dot\beta S}}}\left\{C_{Y_{\beta S}}\cdot\tilde{\beta} + 2\mu_b\frac{gb}{V_0^2}\tilde{\phi}_S + C_{Y_{pS}}\cdot\frac{\tilde{p}_S b}{2V_0} + \left(C_{Y_{rS}} - 4\mu_b\right)\cdot\frac{\tilde{r}_S b}{2V_0} + C_{Y_{\delta_{aS}}}\cdot\tilde{\delta}_a + C_{Y_{\delta_{rS}}}\cdot\tilde{\delta}_r\right\} \quad (4.1\text{-}28)$$

In equation (4.1-28) the terms $C_{Y_{pS}}\tilde{p}_S b/2V_0$ and $C_{Y_{\delta aS}}\tilde{\delta}_a$ are relatively small and may be neglected. Also $C_{Y_{\dot\beta S}}$ and $C_{Y_{rS}}$ are usually negligible compared to $2\mu_b$ and $4\mu_b$ respectively.

According to the reconstructibility analysis of the lateral flight path reconstruction model it follows from equations (4.1-16) and (4.1-17) that the reconstructed angle of side slip $\tilde{\beta}^*$ has a constant error which vanishes after differentiation. Using equations (3.2-18), (4.1-16), (4.1-17) along with the simplifications above, equation (4.1-28) may be written as:

$$\frac{\dot{\tilde{\beta}}^* b}{V_0} = \left[1\ ,\ \tilde{\beta}^*\ ,\ \frac{\tilde{p}_{S_m}b}{2V_0}\ ,\ \frac{\tilde{r}_{S_m}b}{2V_0}\ ,\ \tilde{\delta}_a\ ,\ \tilde{\delta}_r\right]C + \frac{gb}{V_0^2}\tilde{\phi}_S \quad (4.1\text{-}29)$$

in which C denotes a 6×1 matrix as defined in (4.1-4), with elements:

$$C^T = \left[-\frac{C_{Y_{\beta S}}}{2\mu_b}\frac{C_{\beta_0}}{C_{\beta_1}} - \frac{\lambda_{r_S}b}{4V_0}\ ,\ \frac{C_{Y_{\beta S}}}{2\mu_b}\ ,\ \ldots\right. \quad (4.1\text{-}30)$$
$$\left. 0\ ,\ -\frac{1}{2}\ ,\ 0\ ,\ \frac{C_{Y_{\delta_{rS}}}}{2\mu_b}\right] .$$

The controllability of the lateral equations of motion guarantees the existence of flight test manoeuvres for which the time history of $\tilde{\phi}_S$ is linearly independent of the time histories of the remaining variables in (4.1-29).
Consequently, the same holds true for $\dot{\tilde{\beta}}^* b/V_0$. This means that in principle, all lateral stability and control derivatives in the chosen model are identifiable.

4.2 Nonlinear Aerodynamic Model Identification

Nonlinear aerodynamic models are preferred to linearized models for analysis of actual flight test data. The obvious reason for this is that the validity of nonlinear models, as for instance in the form of relations for the aerodynamic force and moment coefficients (2.2-2) and (2.2-3), is not restricted to small deviations from a nominal flight condition. Furthermore, in the context of the two step method, the aerodynamic model identification problem can be formulated as a Linear Regression problem.
Model identification implies the development of an adequate model structure. Since linear regression techniques are used, aerodynamic model development can be based on residual analysis in subsequent steps starting from a relatively simple model structure.
In section 4.2.1 a brief outline is given of classical regression analysis. section 4.2.2 discusses the properties of simplified models. The subject of section 4.2.3 is model development via residual

analysis. In section 4.2.4, we briefly touch upon the sources of collinearity problems, their detection and treatment. For a detailed introduction to regression analysis the reader is referred to the books of Draper and Smith [73], Montgomery and Peck [75], Sen and Srivastava [228].

4.2.1 Principles of Regression Analysis

Models of aerodynamic force and moment coefficients, as for instance in equations (2.2-2) and (2.2-3) can be restricted to the following general form:

$$y(i) = \sum_{k=1}^{r} a_k \cdot x_k(i) + \varepsilon(i) \ , \qquad (4.2\text{-}1)$$

for i=1(1)N, in which y(i) denotes an aerodynamic force or moment coefficient, a_k, k=1(1)r denote aerodynamic model parameters to be estimated and $x_k(i)$ are airplane state and control variables. The variable $\varepsilon(i)$ denotes modelling errors accounting for all unmodelled effects like turbulence in the propeller slipstream and in the boundary layer, fuel sloshing, atmospheric turbulence, etc. These errors are treated as stochastic contributions to the force and moment coefficients and satisfy

$$\begin{aligned} E\{\varepsilon(i)\} &= 0 \ , \\ E\{\varepsilon(i)\cdot\varepsilon(j)\} &= V_\varepsilon \cdot \delta_{ij} \ . \end{aligned} \qquad (4.2\text{-}2)$$

That is to say that we postulate some assumptions that the equation error diagnostics are of the type:

- $\varepsilon(i)$ is a stationary vector,
- $\varepsilon(i)$ is uncorrelated with $x_k(i)$,
- $\varepsilon(i)$ is identically distributed and uncorrelated with zero mean and variance σ^2,
- $\varepsilon(i)$ has normal distribution so that confidence intervals for the estimates can be found and regression hypothesis tests can be employed.

The integer i in equation (4.2-1) refers to a particular time instant $t=t_i$ during a dynamic flight test manoeuvre. Models of this form are the subject of classical regression analysis. The variables $x_k(i)$ are called independent variables. These variables are assumed to be known exactly while y(i), called the dependent variable, is assumed to be measured with finite accuracy according to:

$$y_m(i) = y(i) + v(i) \ , \qquad (4.2\text{-}3)$$

where v(i) represents a random measurement error whose characteristics are similar to $\varepsilon(i)$ with:

$$\begin{aligned} E\{v(i)\} &= 0 \ , \\ E\{v(i)\cdot v(j)\} &= V_v \cdot \delta_{ij} \ . \end{aligned} \qquad (4.2\text{-}4)$$

The problem of regression is to calculate an estimate of the parameters a_k given N sets of values of the independent variables $x_k(i)$ and measurements of the dependent variable $y_m(i)$.

Equation (4.2-1) can be written in terms of a parameter vector $\underline{a}=\mathrm{col}[a_1,a_2,...,a_r]$ and a 1×r matrix $x(i)=[x_1(i),x_2(i),...,x_r(i)]$ according to:

$$y(i) = x(i)\cdot\underline{a} + \varepsilon(i) \ , \qquad (4.2\text{-}5)$$

for i=1(1)N.

Equation (4.2-5) can be substituted in (4.2-3) which may then be written in the following compact form:

$$\underline{Y}_m = X\cdot\underline{a} + \underline{\varepsilon} + \underline{v} \ , \qquad (4.2\text{-}6)$$

where:

$$\begin{aligned} \underline{Y} &= \mathrm{col}\left(y_m(1), y_m(2), \ldots, y_m(N)\right) \ , \\ \underline{\varepsilon} &= \mathrm{col}\left(\varepsilon(1), \varepsilon(2), \ldots, \varepsilon(N)\right) \ , \\ \underline{v} &= \mathrm{col}\left(v(1), v(2), \ldots, v(N)\right) \end{aligned}$$

and X denotes a matrix of independent variables:

$$X = \begin{bmatrix} x(1) \\ x(2) \\ \vdots \\ x(N) \end{bmatrix} .$$

The vector of residuals corresponding to a particular estimate $\hat{\underline{a}}$ of the parameter vector $\underline{a}$ is defined as:

$$\underline{e} = \underline{Y}_m - X\cdot\hat{\underline{a}} \ . \qquad (4.2\text{-}7)$$

The least squares estimate $\hat{\underline{a}}$ minimizes the sum of the squares of the residuals e(i), i=1(1)N,

$$\begin{aligned} \hat{\underline{a}}: \quad & \min_{\hat{\underline{a}}} \sum_{i=1}^{N} e^2(i) = \min_{\hat{\underline{a}}} \underline{e}^T\cdot\underline{e} \\ &= \min_{\hat{\underline{a}}} \left(\underline{Y}_m - X\cdot\hat{\underline{a}}\right)^T \left(\underline{Y}_m - X\cdot\hat{\underline{a}}\right) \end{aligned} \qquad (4.2\text{-}6)$$

The necessary conditions for the existence of a minimum are:

$$\frac{\partial}{\partial \hat{\underline{a}}}\left(\underline{e}^T\cdot\underline{e}\right) = 2\cdot\frac{\partial \underline{e}^T}{\partial \hat{\underline{a}}}\cdot\underline{e} = \underline{0} \qquad (4.2\text{-}9)$$

Substitution of $\underline{e}$ results in the so called normal equations:

$$\left[X^T\cdot X\right]\hat{\underline{a}} = X^T\cdot\underline{Y}_m \ . \qquad (4.2\text{-}10)$$

A unique solution exists if and only if $[X^T\cdot X]$ is positive definite. That is if its inverse exists. Then:

$$\hat{\underline{a}} = \left[X^T\cdot X\right]^{-1} X^T\cdot\underline{Y}_m \ . \qquad (4.2\text{-}11)$$

An unbiased estimate of the variance of $(V_\varepsilon+V_v)$ can be calculated with:

$$\hat{V}_e = \frac{\underline{e}^T\cdot\underline{e}}{N-r} \ . \qquad (4.2\text{-}12)$$

It is not difficult to show that under the assumptions made above the least squares estimate in (4.2-11) is unbiased:

$$E(\hat{\underline{a}}) = \left[X^T\cdot X\right]^{-1} X^T\cdot E(\underline{Y}_m) = \underline{a} \ . \qquad (4.2\text{-}13)$$

The covariance matrix of parameter estimation errors is:

$$V(\hat{\underline{a}}) = E\left\{(\hat{\underline{a}} - E(\hat{\underline{a}}))\cdot(\hat{\underline{a}} - E(\hat{\underline{a}}))^T\right\} \ .$$

Substitution of (4.2-11) and (4.2-13) results in:

$$V(\hat{\underline{a}}) = V_e\left[X^T\cdot X\right]^{-1} \qquad (4.2\text{-}14)$$

Since V_e is usually unknown, it is customary to substitute instead $\hat{V}_e$ as calculated with (4.2-12).

The goodness of fit of the perfect model:

$$y(i) = \sum_{k=1}^{r} a_k\cdot x_k(i) \qquad (4.2\text{-}15)$$

to the measurements $y_m(i)$, i=1(1)N may be expressed in terms of the simple correlation coefficient between $y_m(i)$ and $\hat{y}(i)=x(i)\cdot\hat{\underline{a}}$. This correlation coefficient is usually referred to as the multiple correlation coefficient R and R^2 is called the measure of fit.
Now define $\Delta y_m(i)$ and $\Delta\hat{y}(i)$ as deviations of $y_m(i)$ and $\hat{y}(i)$ from the mean $\bar{y}$, i.e.

$$\Delta y_m(i) = y_m(i) - \bar{y}$$
$$\Delta\hat{y}(i) = \hat{y}(i) - \bar{y}$$
$$\bar{y} = \frac{1}{N}\sum_{i=1}^{N} y_m(i)$$

Then the multiple correlation coefficient R follows from:

$$R^2 = \frac{\left(\sum_{i=1}^{N}(y_m(i)-\bar{y})(\hat{y}(i)-\bar{y})\right)^2}{\sum_{i=1}^{N}(y_m(i)-\bar{y})^2\sum_{i=1}^{N}(\hat{y}(i)-\bar{y})^2} = \frac{\left(\Delta\underline{Y}_m^T\cdot\Delta\hat{\underline{Y}}\right)^2}{\left(\Delta\underline{Y}_m^T\cdot\Delta\underline{Y}_m\right)\left(\Delta\hat{\underline{Y}}^T\cdot\Delta\hat{\underline{Y}}\right)} \qquad (4.2\text{-}16)$$

where:

$$\Delta\underline{Y}_m = \mathrm{col}\left(\Delta y_m(1), \Delta y_m(2), \ldots, \Delta y_m(N)\right) \ ,$$
$$\Delta\hat{\underline{Y}} = \mathrm{col}\left(\Delta\hat{y}(1), \Delta\hat{y}(2), \ldots, \Delta\hat{y}(N)\right) \ .$$

It may easily be verified with (4.2-7) that $\Delta\underline{Y}_m=\Delta\hat{\underline{Y}}+\underline{e}$. Substitution of this result in (4.2-16) and using the fact that $\underline{e}$ and $\Delta\hat{\underline{Y}}$ are orthogonal, i.e. $\underline{e}^T\cdot\Delta\hat{\underline{Y}}=0$, R^2 can be written as:

$$R^2 = 1 - \frac{\underline{e}^T\cdot\underline{e}}{\Delta\underline{Y}_m^T\cdot\Delta\underline{Y}_m} \qquad (4.2\text{-}17)$$

based on the assumption that $\bar{\underline{e}}=\underline{0}$.

A general remark about the least squares at this stage is necessary. In an actual experiment, the above assumptions may not be generally met. Because of the measurement errors in the independent variables, the least squares estimates are asymptotically biased, inconsistent and inefficient [157,159]. However, as a result of high accuracy instrumentation used and independent variables reconstructed from state estimation, the experience shows that these errors are quite small. The computed least squares estimates are accurate and comparable to those obtained for example from an output error method.

4.2.2 Characteristics of Simplified Models

In Equation (4.2-1), each term $a_k x_k(i)$ corresponds to one term of a multiple Taylor series expansion representing the aerodynamic model (section 2.2). Under certain conditions these Taylor series expansions can be assumed to be close approximations to the actual aerodynamic phenomena.

Let r denote the corresponding number of terms. In practice, the maximum number of parameters which can be estimated from a given set of measurements is much smaller than r. Let r_1 denote this a priori number of parameters. The corresponding model is:

$$y(i) = \sum_{k=1}^{r_1} a_k \cdot x_k(i) \; . \tag{4.2-18}$$

Since (4.2-18) probably contains only a small subset of the set of parameters in the perfect model (4.2-15), it is called a *simplified model.* A characteristic property of simplified models is that, in general, their parameter estimates are biased. This can be shown as follows. For a given set of N data points, the perfect model (4.2-15) can be written as:

$$\underline{Y} = X \cdot \underline{a} = X_1 \cdot \underline{a}_1 + X_2 \cdot \underline{a}_2 \; . \tag{4.2-19}$$

in which $\underline{a}_1$ denotes an r_1 dimensional parameter vector of the simplified model and $\underline{a}_2$ an $(r\text{-}r_1)$ dimensional vector of the remaining parameters. Each column of the matrix X_2 can be decomposed in a vector contained in the column space of X_1 and a vector perpendicular to this column space. This means that X_2 can be written as:

$$X_2 = X_1 \cdot C + \Delta X_2 \tag{4.2-20}$$

in which C denotes an $r_1 \times (r\text{-}r_1)$ matrix. Let $\hat{\underline{a}}_1^*$ denote the least squares estimate of $\underline{a}_1$ in the simplified model $\underline{Y}=X \cdot \underline{a}_1$. According to (4.2-11):

$$\hat{\underline{a}}_1^* = \left[X_1^T \cdot X_1\right]^{-1} X_1^T \cdot \underline{Y}_m \; . \tag{4.2-21}$$

From equation (4.2-19), it can be shown that this estimate is biased:

$$\begin{aligned} E(\hat{\underline{a}}_1^*) &= \left[X_1^T \cdot X_1\right]^{-1} X_1^T \, E(\underline{Y}_m) \\ &= \left[X_1^T \cdot X_1\right]^{-1} X_1^T \left(X_1 \cdot \underline{a}_1 + X_2 \cdot \underline{a}_2\right) \\ &= \underline{a}_1 + \left[X_1^T \cdot X_1\right]^{-1} X_1^T \cdot X_2 \cdot \underline{a}_2 \; . \end{aligned}$$

It can be shown that:

$$C_j = \left[X_1^T \cdot X_1\right]^{-1} X_1^T \cdot \underline{X}_{2_j}$$

where the index j refers to the j-th column of C and X_2 respectively. The expected value of $\hat{\underline{a}}_1^*$ is therefore:

$$E(\hat{\underline{a}}_1^*) = \underline{a}_1 + C \cdot \underline{a}_2 \; . \tag{4.2-22}$$

In general $\underline{a}_2 \neq \underline{0}$ and $C \neq O$, thus $\hat{\underline{a}}_1^*$ is biased.
It is important to note here that this bias is not constant but rather depends on the *structure of the matrix X.* This means in the case of dynamic flight test manoeuvres, the parameter estimation *bias* of simplified models depend on the form of the *flight test manoeuvre.*

The covariance matrix of $\hat{\underline{a}}_1^*$ is:

$$V(\hat{\underline{a}}_1^*) = E\left\{\left(\hat{\underline{a}}_1^* - E(\hat{\underline{a}}_1^*)\right) \cdot \left(\hat{\underline{a}}_1^* - E(\hat{\underline{a}}_1^*)\right)^T\right\}$$

Substitution of (4.2-21) and (4.2-22) leads to an expression similar to (4.2-14):

$$V(\hat{\underline{a}}_1^*) = V_e \left[X_1^T \cdot X_1\right]^{-1} \; .$$

4.2.3 Model Development via Residual Analysis

In aerodynamic model identification it is often possible to specify an a priori model containing those terms which are known to be indispensable from experience or from theoretical considerations. Next, the *model fit* is improved by selecting additional terms from a set of so called *candidate variables.* This can be done in successive steps via residual analysis.

The procedure described below is called *forward selection* in the literature, because at each step one variable is added to the model. An alternative procedure is *backward elimination* where one starts

with a model with many variables already included and at each step the least important variable is eliminated. Finally one can combine the two procedures and at each step include the most important variable and subsequently eliminate the least important variable, this procedure is called *stepwise regression*. In actual practice all procedures work well, but they need not necessarily lead to the same model. For instance, it may occur that one variable has a high correlation early in the forward selection procedure and therefore is included, but its contribution may become insignificant after a few other variables have been included. The stepwise regression procedure will in this case eliminate this variable, while the forward selection procedure will retain it.

Let the initial model contain r_1 parameters. The corresponding least squares estimate $\hat{\underline{a}}_1^*$ can be calculated with (4.2-21). The remaining model residuals are:

$$\begin{aligned} \underline{e}_1 &= \underline{Y}_m - X_1 \cdot \hat{\underline{a}}_1^* \\ &= \left[I - X_1 \left[X_1^T \cdot X_1 \right]^{-1} X_1^T \right] \underline{Y}_m \, . \end{aligned} \tag{4.2-23}$$

Next, each member of the set of candidate variables is evaluated with respect to its capability to improve the fit of the model. Let such a variable be $x_c(i)$, i=1(1)N. Then a column vector $\underline{X}_2$ can be defined as $\underline{X}_2=\text{col}[x_c(1),x_c(2),...,x_c(N)]$. If one uses $\underline{X}_2$ as the vector of the independent variables in a model for the least squares residual vector $\underline{e}_1$ according to:

$$\underline{e}_1 = \underline{X}_2 \cdot a_2 + \underline{e}_2 \, , \tag{4.2-24}$$

the corresponding least squares estimate of a_2, indicated as $\hat{a}_2'$, is now

$$\hat{a}_2' = \left[\underline{X}_2^T \cdot \underline{X}_2 \right]^{-1} \underline{X}_2^T \cdot \underline{e}_1 \, , \tag{4.2-25}$$

and the 'new' least squares residuals $\underline{e}_2'$ are equal to:

$$\underline{e}_2' = \underline{e}_1 - \underline{X}_2 \cdot \hat{a}_2' \tag{4.2-26}$$

According to (4.2-20), $\underline{X}_2$ can always be decomposed into components along and perpendicular to the column space of X_1:

$$\underline{X}_2 = X_1 \cdot \underline{c} + \Delta \underline{X}_2 \tag{4.2-27}$$

in which $\underline{c}$ denotes a column vector. By substituting equations (4.2-27) in (4.2-25) it is noticed that if $\Delta\underline{X}_2=\underline{0}$, then also $\hat{a}_2'=0$, and from equation (4.2-26) we get $\underline{e}_2'=\underline{e}_1$. That is, adding this candidate variable does not improve the *goodness of fit*. In general, $\hat{a}_2'\neq 0$ and with equations (4.2-26) and (4.2-25) the following expression may be derived for $\underline{e}_2'^T\cdot\underline{e}_2'$:

$$\begin{aligned} \underline{e}_2'^T \cdot \underline{e}_2' &= \underline{e}_1^T \cdot \underline{e}_1 - \underline{e}_1^T \cdot \Delta \underline{X}_2 \left[\underline{X}_2^T \cdot \underline{X}_2 \right]^{-1} \Delta \underline{X}_2^T \cdot \underline{e}_1 \\ &= \underline{e}_1^T \cdot \underline{e}_1 - \underline{e}_1^T \cdot \Delta \underline{X}_2 \cdot \\ &\quad \cdot \left[\underline{c}^T \underline{X}_1^T \cdot \underline{X}_1 \underline{c} + \Delta \underline{X}_2^T \cdot \Delta \underline{X}_2 \right]^{-1} \Delta \underline{X}_2^T \cdot \underline{e}_1 \, . \end{aligned} \tag{4.2-28}$$

In the analysis here, $\Delta\underline{X}_2$ is used as a candidate variable instead $\underline{X}_2$. The reason for this can be ascertained from equation (4.2-28). Since $X_1^TX_1$ is positive definite, we have:

$$\underline{e}_2^T \cdot \underline{e}_2 < \underline{e}_2'^T \cdot \underline{e}_2' \, .$$

where $\underline{e}_2$ denotes the vector of the smaller residuals:

$$\underline{e}_2 = \underline{e}_1 - \Delta \underline{X}_2 \cdot \hat{a}_2^*$$

The least squares estimate $\hat{a}_2^*$ is calculated as:

$$\hat{a}_2^* = \left[\Delta \underline{X}_2^T \cdot \underline{X}_2 \right]^{-1} \Delta \underline{X}_2^T \cdot \underline{e}_1 \tag{4.2-29}$$

The vector $\underline{c}$ in equation (4.2-27) is equal to:

$$\underline{c} = \left[X_1^T \cdot X_1 \right]^{-1} X_1^T \cdot \underline{X}_2 \, . \tag{4.2-30}$$

This is easily proved by showing that:

$$X_1^T \cdot \Delta \underline{X}_2 = X_1^T \left(\underline{X}_2 - X_1 \cdot \underline{c} \right) = \underline{0} \, .$$

The procedure for model development via residual analysis is to calculate from a given set of candidate variables (stored in the form of column vectors $\underline{X}_2$) the orthogonal components with respect to the columns of X_1. Next, one of the orthogonal candidate variables, in general the one which generates the smallest value of $\underline{e}_2^T\cdot\underline{e}_2$, is included in the model. Then this selection procedure is repeated for the set of remaining candidate variables, where the orthogonal components of the

candidate variables are calculated with respect to the new (extended) matrix of independent variables of the form $[X_1 \cdot \Delta \underline{X}_2]$. This only requires orthogonalization with respect to the new column $\Delta \underline{X}_2$, since all candidate variables were already orthogonal with respect to the columns of X_1.

The improvement of the goodness of fit in the subsequent steps of the model development can be described by the multiple correlation coefficient given in equation (4.2-17):

$$R_\ell^2 = 1 - \frac{\underline{e}_\ell^T \cdot \underline{e}_\ell}{\Delta \underline{Y}_m^T \cdot \Delta \underline{Y}_m} , \qquad (4.2\text{-}31)$$

in which ℓ refers to the ℓ-th step.

Each addition of a new candidate variable, results in a reduction of the sum of squares of model residuals $\underline{e}_\ell^T \cdot \underline{e}_\ell$ and a corresponding increase of multiple correlation coefficient R_ℓ. This makes it difficult to decide when to stop the process of adding candidate variables to the model. Therefore, we need to define additional statistical criteria to decide this issue.

One possibility is to test the statistical significance of each new parameter estimate by the *sequential F-test* and to test the statistical significance of all model parameters simultaneously by the *total F-test*. The feature of sequential F-test is that it can be used as a criterion for adding or removing terms from the model when it is being 'built'. For application of the sequential F-test one calculates:

$$F_{seq} = \frac{\underline{e}_{\ell-1}^T \cdot \underline{e}_{\ell-1} - \underline{e}_\ell^T \cdot \underline{e}_\ell}{\underline{e}_\ell^T \cdot \underline{e}_\ell} \cdot (N - r_\ell) ,$$

in which r_ℓ denotes the total number of parameters in the new model. F_{seq} can also be written in terms of multiple correlation coefficients according to:

$$F_{seq} = \frac{R_\ell^2 - R_{\ell-1}^2}{1 - R_\ell^2} \cdot (N - r_\ell) . \qquad (4.2\text{-}32)$$

At this stage it is convenient to introduce the *partial correlation coefficient* R_ℓ^* being the simple correlation coefficient between $\underline{e}_{\ell-1}$ and $\Delta \underline{X}_2$. The partial correlation coefficient can be written as:

$$R_\ell^{*2} = 1 - \frac{\underline{e}_\ell^T \cdot \underline{e}_\ell}{\underline{e}_{\ell-1}^T \cdot \underline{e}_{\ell-1}} . \qquad (4.2\text{-}33)$$

The relation between the multiple correlation coefficients R_ℓ and $R_{\ell-1}$ and the partial correlation coefficient R_ℓ^* is:

$$R_\ell^2 = 1 - (1 - R_{\ell-1}^2) \cdot (1 - R_\ell^{*2}) . \qquad (4.2\text{-}34)$$

Substitution of (4.2-34) in (4.2-32) results in:

$$F_{seq} = \frac{R_\ell^{*2}}{1 - R_\ell^{*2}} \cdot (N - r_\ell) . \qquad (4.2\text{-}35)$$

The null hypothesis $H_0: a_\ell = 0$ is rejected at a chosen confidence level α in favour of the alternative hypothesis $H_1: a_\ell \neq 0$ if:

$$F_{seq} > F_\alpha(1 , N - r_\ell) , \qquad (4.2\text{-}36)$$

in which F_α denotes the value of *Fisher's distribution function* with 1 and $N\text{-}r_\ell$ degrees of freedom; $\alpha = Pr\{H_1 | H_0\}$.

The combination of equations (4.2-35) and (4.2-36) allows us to bring the sequential F-test in the following form:

accept H_1 if :

$$R_\ell^{*2} > \frac{k}{1 + k} , \qquad (4.2\text{-}37)$$

where $k = \frac{1}{N - r_\ell} \cdot F_\alpha(1 , N - r_\ell)$.

This is depicted in fig. 4-1.

For application of the total F-test one calculates:

$$F_{tot} = \frac{\underline{e}_0^T \cdot \underline{e}_0 - \underline{e}_\ell^T \cdot \underline{e}_\ell}{\underline{e}_\ell^T \cdot \underline{e}_\ell} \cdot \frac{(N - r_\ell)}{(r_\ell - 1)} , \qquad (4.2\text{-}38)$$

in which $\underline{e}_0$ denotes the residuals of the most simple model with only one parameter a_0 and independent variable $x_0(i)=1$, $i=1(1)\,N$. F_{tot} can also be written as:

$$F_{tot} = \frac{R_\ell^2}{1 - R_\ell^2} \cdot \frac{(N - r_\ell)}{(r_\ell - 1)} . \qquad (4.2\text{-}39)$$

The null hypothesis $H_0: a_i = 0$, $i=1(1)r_\ell$ is rejected

and the alternative hypothesis H_1 is accepted at a chosen confidence level α if:

$$F_{tot} > F_\alpha(r_\ell - 1 \ , \ N - r_\ell) \ , \qquad (4.2\text{-}40)$$

where F_α denotes the value of Fisher's distribution function with r_ℓ-1 and N-r_ℓ degrees of freedom; $\alpha=Pr\{H_1|H_0\}$.

Combining equations (4.2-39) and (4.2-40) allows us to bring the total F-test in the following form:

accept H_1 if :

$$R_\ell^2 > \frac{k}{1+k} \ , \qquad (4.2\text{-}41)$$

$$\text{where } k = \frac{r_\ell - 1}{N - r_\ell} \cdot F_\alpha(r_\ell - 1 \ , \ N - r_\ell) \ .$$

An important characteristic of a model is its capability to predict aerodynamic force and moment coefficients for other data sets then was used in the determination procedure itself. The *Prediction Sum of Squares* (PRESS) criterion is often used to test for this characteristic, see Allen [229]. The prediction error for one data point is calculated by omitting this data point from the regression and then calculating the difference between this data point and the prediction by the model based on the remaining data points. The PRESS criterion is then calculated by repeating this procedure for all data points and summing the squared prediction errors. This criterion is recommended by Klein [150]. A disadvantage of this criterion is that if sequential correlation is present in the data, as is often the case with actual flight test data, this criterion will not be effective.

In order to negate the shortcomings of the PRESS criterion, the *Predict criterion* was introduced by Mulder [14]. This criterion uses a second dataset, which is not used in the parameter estimation at all. The model as estimated from the first data set is used to predict the model output for the second data set. The Predict criterion is then defined as:

$$\text{PREDICT} = \sum_{i=1}^{N} V(\hat{y}(i)) + \sum_{i=1}^{N} \left(y_m(i) - \hat{y}(i)\right)^2 \ . \qquad (4.2\text{-}42)$$

If $\hat{y}_{21}(i)$ denotes the estimate of $y_2(i)$ of the second data set, then $\hat{y}_{21}(i)$ can be calculated according to:

$$\hat{y}_{21}(i) = X_2(i) \cdot \hat{\underline{a}}_1^* \ ,$$

where $\hat{\underline{a}}_1^*$ is the parameter estimate based on the first data set and X_2 is the data matrix for the second data set. The first term in equation (4.2-42) is the estimated value of the prediction RSS calculated from the parameter estimation errors of $\hat{\underline{a}}_1^*$ calculated as $V(\hat{y}_{21}(i))=X_2(i)\cdot V(\hat{\underline{a}}_1^*)\cdot X_2^T(i)$, while the second term is the actual prediction RSS. When the number of included variables increases in the aerodynamic model the fit error in the first data set will decrease and as a consequence the first term in equation (4.2-42), which is the predicted fit error for the second data set, will decrease as well. As long as variables are added which improve the prediction the second term and the criterion as a whole will decrease as well, but soon variables will be added which happen to improve the fit to the first data set, but which actually degrade the prediction error for the second data set. In that case the second term will usually cause the Predict criterion to increase rapidly and thus give a good indication of the predictive capability of the model.

For more details on statistical tests the reader is referred again to [73,75,228]. In section 4.3 we will discuss the application of sequential and total F-tests and of the Predict criterion while developing longitudinal and lateral aerodynamic models from dynamic flight test data.

The final step in the model determination procedure is the *validation* of the model using independent data sets. It is very important to set aside extra recordings dedicated for validation during the planning of a flight test program. This is of course closely linked to the Predict criterion approach, although strictly speaking the second data sets used in this criterion are not independent any more.

4.2.4 Data Collinearity

If there is a high correlation between measured variables in the data matrix, this condition is called data collinearity. The matrix $[X^T \cdot X]$ in the normal equations (4.1-3) or (4.2-10) becomes very ill-conditioned and as a result some parameters or combination of parameters become nearly

unidentifiable. An example of collinearity is a highly manoeuvrable aircraft whose stability augmentation system deflects various control surfaces in concert thus causing near linear dependence among their deflections. One should recognise the collinearity problems as a data problem rather than as a statistical problem.

The condition may even further degrade when actually computing numerical values due to round-off and truncation errors in digital computation. Conversely, the same type of errors may also make a singular matrix appear to be just ill-conditioned. This points out the need for accurate numerical methods.

Some well-known numerical methods which are successful in dealing with ill-conditioned matrices are Householder's transformation, Given's rotation and singular value decomposition. For more details the reader is referred to Lawson and Hanson [72].

Some of the sources of collinearity problems can result from:

a) a flight experiment where certain independent characteristic modes determined by some of the regressors are not excited by the input signals,
b) over parameterization of the model or
c) constraints in the data, e.g. due to stability augmentation systems.

The detection of these collinearities can be made by inspecting:

a) correlation matrix $[X^T \cdot X]$,
b) eigen system analysis and singular value decomposition or
c) parameter variance decomposition.

A good theoretical discussion on these topics can be found in [74,75 and 228]. Some very interesting discussions with respect to sources of collinearity, diagnostics and adverse effects in the light of estimating parameters of modern high performance aircraft with high augmentation can be found in Klein [62,125,156 and 157].

4.3 Practical Aerodynamic Model Identification

In section 4.2, aerodynamic model development from flight test data begins from relatively simple a priori models containing only those variables which are known to be *indispensable* from theory or from experience. Next, a set of *candidate variables* is postulated, from which a limited number is selected to be included in more refined versions of the aerodynamic model.

To begin with, a priori models of the longitudinal and lateral aerodynamic force and moment coefficients are shown in table 4-1. The aerodynamic force and moment coefficients are initially assumed to depend linearly on the selected sets of independent variables, except for the terms with α^2 in the models of C_X and C_m, which were known to be indispensable from earlier flight test experience [14,15]. In addition, it is initially assumed that no aerodynamic '*cross coupling*' effects are present. That is to say, the longitudinal aerodynamic force and moment coefficients are assumed to depend only on variables related to strictly longitudinal manoeuvres, while the lateral aerodynamic force and moment coefficients are assumed to depend only on variables related to strictly lateral manoeuvres.

The result of the wind tunnel experiments as presented in fig. 2-1, however, indicate that aerodynamic cross coupling effects do exist and in fact are rather pronounced. The longitudinal coefficients C_Z and C_m depend on β and the lateral coefficients C_Y, C_l and C_n depend on α as well as on $\Delta p_t/\frac{1}{2}\rho V^2$. The cross coupling effects and also the relation between C_n and β as seen from fig. 2-1 are clearly *nonlinear*.

In this case it appears that the aerodynamic coefficients are continuous functions of $\Delta p_t/\frac{1}{2}\rho V^2$, α and β. It is possible therefore to approximate these functions by means of truncated Taylor series expansions. The models in table 4-1 are in fact examples of such approximations in which, except for the quadratic terms in α, only terms up to the first order are retained. More accurate approximations will result if terms of higher order than the first are added to these a priori models. This leads, therefore, to the so-called *candidate variables*.

For example, it is important to notice the form of the term $(\Delta p_t/\frac{1}{2}\rho V^2)^i \cdot \alpha^j \cdot \beta^k$. In the present section all these variables, up to the third order, i.e. $i+j+k \leq 3$, were included in the set of candidate variables. Also included in the set of candidate variables, were the control surface deflections δ_a, δ_e and δ_r as well as products of these control surface

deflections and first and second order powers of $\Delta p_t/\frac{1}{2}\rho V^2$,$\alpha$ and β. These latter products were included to account for the variation of control derivatives, as was already indicated by the wind tunnel experiments (fig. 2-1(c)). The set of candidate variables was extended further by adding the dimensionless body rotation rates pb/2V, $q\bar{c}/V$ and rb/2V and the dimensionless time derivatives $\dot{\alpha}\bar{c}/V$ and $\dot{\beta}b/V$. In general, body rotation rates are included in aerodynamic models to account for the effect of *curvature* of the streamlines on the aerodynamic force and moment coefficients [10]. The body rotation rates in the aerodynamic models of table 4-1 are used to model the effects of the dimensionless body rotation rate $q\bar{c}/V$ related to longitudinal manoeuvres on the longitudinal force and moment coefficients, and to model the effects of the dimensionless body rotation rates pb/2V and rb/2V related to lateral manoeuvres on the lateral force and moment coefficients. By including all dimensionless body rotation rates in the set of candidate variables, it is possible to account for hypothetical aerodynamic cross coupling effects. That is, the effect of $q\bar{c}/V$ on the lateral, and the effects of pb/2V and rb/2V on the longitudinal aerodynamic force and moment coefficients. The dimensionless time derivatives $\dot{\alpha}\bar{c}/V$ and $\dot{\beta}b/V$ were included in the set of candidate variables to account for nonstationary aerodynamic effects and the effects of the finite time needed for the vertical and lateral air velocity components induced by the wing and the fuselage to reach the horizontal and vertical aircraft tail surfaces [10].
The nonlinear dependence of the aerodynamic force and moment coefficients on $\Delta p_t/\frac{1}{2}\rho V^2$, α, and β, the variation of the control derivatives, and the hypothetical effects of the body rotation rates and the time delays as described above, all amounted to a total number of 40 candidate variables.

The above considerations clearly illustrate that the selection of candidate variables is to a certain extent *arbitrary*, even if supported by results from quite extensive wind tunnel experiments, as in the present case.

The process of sequential selection of candidate variables for improved model fit will be demonstrated now. Rather than a single longitudinal or lateral flight test manoeuvre, a data set consisting of 3 longitudinal and 3 lateral manoeuvres at 3 different values of nominal True Air Speeds of 35, 45 and 55 m/s respectively, will be used for this purpose. In such a data set, the range of variations of variables such as $\Delta p_t/\frac{1}{2}\rho V^2$, α and β is considerably larger than in a single longitudinal or lateral manoeuvre, as can be seen from fig. 4-2. The longitudinal and lateral manoeuvres lasted 10 and 16 seconds respectively. Combined with a sample rate of 10 Hz, this resulted in a joint data set of 786 data points.

Starting from the a priori models above, the models are sequentially extended with those candidate variables corresponding to the largest value of the partial correlation coefficient R^*_ℓ, which is equivalent to minimizing the residual sum of squares $\underline{e}_\ell^T \underline{e}_\ell$.

Fig. 4-3 shows two typical examples of the variation of the different criteria for model development as a function of the number of candidate variables added to the a priori model. The criteria shown are the performance index (P.I.) $\underline{e}_\ell^T \underline{e}_\ell$, the total F-value F_{tot}, the partial correlation coefficient R^*_ℓ and the PREDICT function. In these examples, both the total and the sequential F-tests lead to inclusion of at least 6 additional terms. Acceptance by the F-tests means that each of these terms yielded a significant contribution to the goodness of fit of the aerodynamic model to the actual measurements. The *Predict* function, however, is shown to be a much more severe criterion in this respect. A large increase of the *predict* function indicates that the larger models are inferior to more simple models in predicting the force or moment coefficient using a second, independent data set. Compared to the a priori models, the models as selected with the *predict* function are shown to contain only conditional variables.

For all aerodynamic force and moment coefficients, the selected candidate variables and corresponding improvements of the goodness of fit are shown in table 4-2. Here, the goodness of fit is expressed in terms of the multiple correlation coefficient R_ℓ and of $\sqrt{1 - R_\ell^2}$, expressed as a percentage.

With respect to goodness of fit, considerable differences exist particularly between models of aerodynamic force coefficients and models of

aerodynamic moment coefficients. Accurate models could be developed for C_X and C_Z. The fit of the models of C_n and in particular C_l, however, is rather poor. These results are of course not general, but rather depend on the aerodynamic characteristics of aircraft, on the nominal flight condition and on the flight test manoeuvres. A comprehensive presentation of experimental results related to this aerodynamic model development can be found in Blok and Mulder [178].

4.4 Conclusions

Several aspects of the regression technique have been described in this chapter. This technique is very efficient with respect to computing time and very convenient to apply when one wants to obtain the parameters of a given aerodynamic model. Moreover, it is also a very important tool for the determination of the structure of model.

In this chapter a number of statistical tests for the validity of the identification results were discussed. In addition, the use of a priori information in support of the model development was demonstrated. It is very important to stress, however, that the procedures that we describe here are certainly not 'black-box' procedures, which will automatically produce the right answers. The aerodynamic insight of the analyst is the best criterion for the validity of the results. In this we fully agree with the discussion by Maine and Iliff [1,2].

Linear Regression lends itself well for implementation in an interactive program package and quite a number of these packages have been developed. The essential features of such a package are complete freedom for the choice of candidate variables, complete freedom of selections within datasets and combinations of datasets and extensive facilities for inspecting the model residuals using a large variety of statistical tests and graphical presentations. In this way the analyst is able to apply his engineering judgement in the best possible way.

Like any other estimation method regression may give biased results when the statistical assumptions on which it is based are violated, see (4.1-2). In practice there is always measurement noise (or estimation errors) in the independent variables. In this case, the application of the *Total Least Squares* technique allows to take account of these errors in the independent variables, see Golub and Van Loan [230] and Huffel [231]. Initial applications of TLS have shown significant improvements over the standard regression method [219].

$$C_X = C_{X_0} + C_{X_{\Delta p_t}} \cdot \frac{\Delta p_t}{\frac{1}{2}\rho V^2} + C_{X_\alpha} \cdot \alpha + C_{X_{\alpha^2}} \cdot \alpha^2 + C_{X_q} \cdot \frac{q\bar{c}}{V} + C_{X_{\delta_e}} \cdot \delta_e$$

$$C_Z = C_{Z_0} + C_{Z_{\Delta p_t}} \cdot \frac{\Delta p_t}{\frac{1}{2}\rho V^2} + C_{Z_\alpha} \cdot \alpha + C_{Z_q} \cdot \frac{q\bar{c}}{V} + C_{Z_{\delta_e}} \cdot \delta_e$$

$$C_m = C_{m_0} + C_{m_{\Delta p_t}} \cdot \frac{\Delta p_t}{\frac{1}{2}\rho V^2} + C_{m_\alpha} \cdot \alpha + C_{m_{\alpha^2}} \cdot \alpha^2 + C_{m_q} \cdot \frac{q\bar{c}}{V} + C_{m_{\delta_e}} \cdot \delta_e$$

$$C_Y = C_{Y_0} + C_{Y_\beta} \cdot \beta + C_{Y_p} \cdot \frac{pb}{2V} + C_{Y_r} \cdot \frac{rb}{2V} + C_{Y_{\delta_a}} \cdot \delta_a + C_{Y_{\delta_r}} \cdot \delta_r$$

$$C_l = C_{l_0} + C_{l_\beta} \cdot \beta + C_{l_p} \cdot \frac{pb}{2V} + C_{l_r} \cdot \frac{rb}{2V} + C_{l_{\delta_a}} \cdot \delta_a + C_{l_{\delta_r}} \cdot \delta_r$$

$$C_n = C_{n_0} + C_{n_\beta} \cdot \beta + C_{n_p} \cdot \frac{pb}{2V} + C_{n_r} \cdot \frac{rb}{2V} + C_{n_{\delta_a}} \cdot \delta_a + C_{n_{\delta_r}} \cdot \delta_r$$

Table 4-1: *A priori longitudinal and lateral aerodynamic models.*

		R_λ	$\sqrt{1 - R_t^2}$ (%)	selected candidate variables
C_X		0.999415	3.41	
	1*	0.999533	3.05	rb/2V
	2	0.999552	2.99	$\delta_r \left(\Delta p_t / \frac{1}{2}\rho V^2\right)$
	3	0.999567	2.94	$\dot{\alpha}\bar{c}/V$
	4	0.999601	2.82	β^2
	5	0.999699	2.45	$\beta^2 \left(\Delta p_t / \frac{1}{2}\rho V^2\right)$
	6	0.999712	2.39	β
C_Z		0.996999	7.74	
	1	0.998327	5.78	α^2
	2*	0.998961	4.55	$\beta^2 \left(\Delta p_t / \frac{1}{2}\rho V^2\right)$
	3	0.999049	4.35	$\left(\Delta p_t / \frac{1}{2}\rho V^2\right)^2$
	4	0.999117	4.20	$\left(\Delta p_t / \frac{1}{2}\rho V^2\right)^3$
	5	0.999162	4.09	β^2
	6	0.999202	3.99	$\dot{\alpha}\bar{c}/V$
C_m		0.986309	16.49	
	1	0.991233	13.21	β^2
	2*	0.993302	11.55	rb/2V
	3	0.994284	10.67	β^3
	4	0.995078	9.90	β
	5	0.995479	9.49	$\beta^2 \left(\Delta p_t / \frac{1}{2}\rho V^2\right)$
	6	0.995857	9.09	$\delta_e \left(\Delta p_t / \frac{1}{2}\rho V^2\right)$

Table 4-2: *Statistically significant steps in the development of models of the aerodynamic force and moment coefficients. Model development is based on the combined data of longitudinal and lateral manoeuvres at three different nominal flight conditions at 6000 ft pressure altitude and TAS of 35, 45 and 55 m/s respectively. Asterix indicates the models as selected using the PREDICT function criterion of section 4.2.*

		R_λ	$\sqrt{1 - R_i^2}$ (%)	selected candidate variables
C_Y		0.996551	8.29	
	1	0.997119	7.58	$\dot{\beta}b/V$
	2*	0.997571	6.96	$\delta_r\alpha$
	3	0.997740	6.71	$q\bar{c}/V$
	4	0.997895	6.48	$\dot{\alpha}\bar{c}/V$
	5	0.997993	6.33	β^2
	6	0.998323	5.78	$\delta_e\beta^2$
C_l		0.954197	29.91	
	1	0.959872	28.04	α^3
	2*	0.964516	26.40	$\dot{\beta}b/V$
	3	0.967861	25.14	$\delta_a\alpha$
	4	0.969724	24.42	$\left(\Delta p_t/\frac{1}{2}\rho V^2\right)$
	5	0.972087	23.46	$\delta_r\beta^2$
	6	0.973925	22.68	$\beta\left(\Delta p_t/\frac{1}{2}\rho V^2\right)$
C_n		0.960266	27.90	
	1*	0.980841	19.48	$\left(\Delta p_t/\frac{1}{2}\rho V^2\right)^3$
	2	0.986839	16.17	$q\bar{c}/V$
	3	0.990024	14.08	β^3
	4	0.992129	12.52	$\delta_r\left(\Delta p_t/\frac{1}{2}\rho V^2\right)$
	5	0.992961	11.84	$\dot{\beta}b/V$
	6	0.993742	11.16	$\left(\Delta p_t/\frac{1}{2}\rho V^2\right)$

Table 4-2: *Continued.*

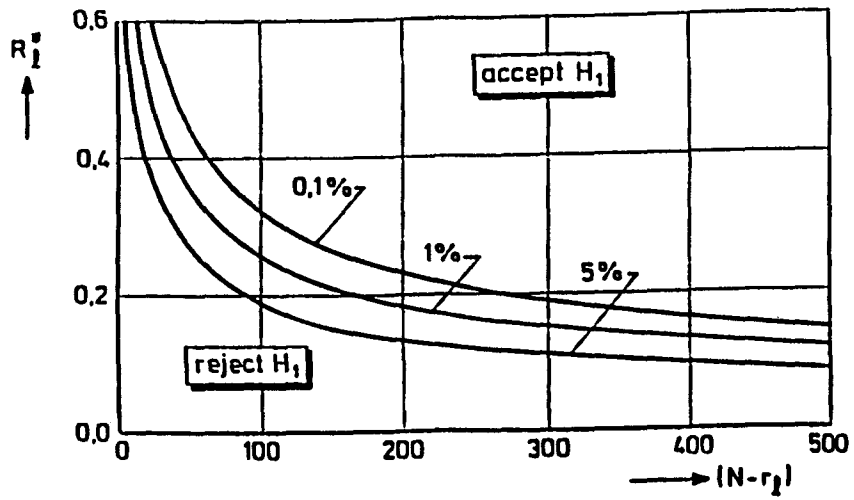

Figure 4-1: *F-test critical values of the partial correlation coefficient R_l^* for three levels of $\alpha=Pr\{H_1|H_o\}$.*

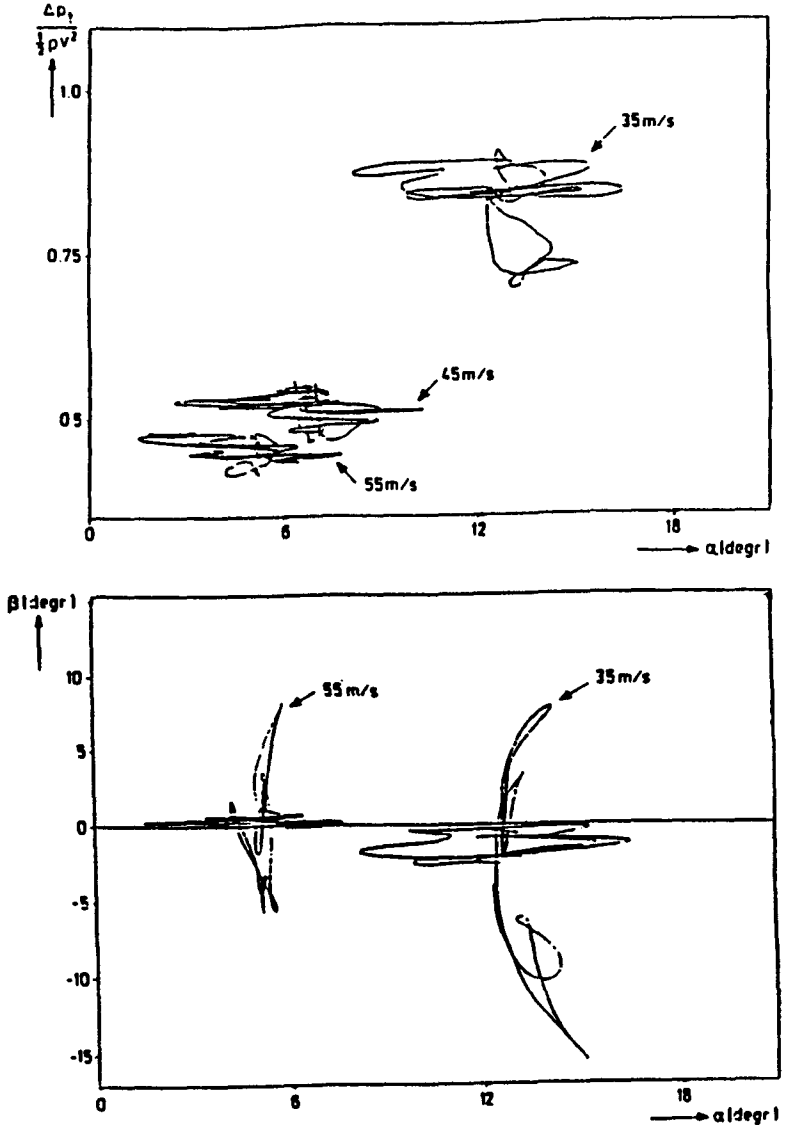

Figure 4-2: *Variations of $\Delta p_t/\frac{1}{2}\rho V^2$, α and β in three longitudinal and two lateral DUT manoeuvres at three different values of nominal TAS of 35, 45 and 55 m/s.*

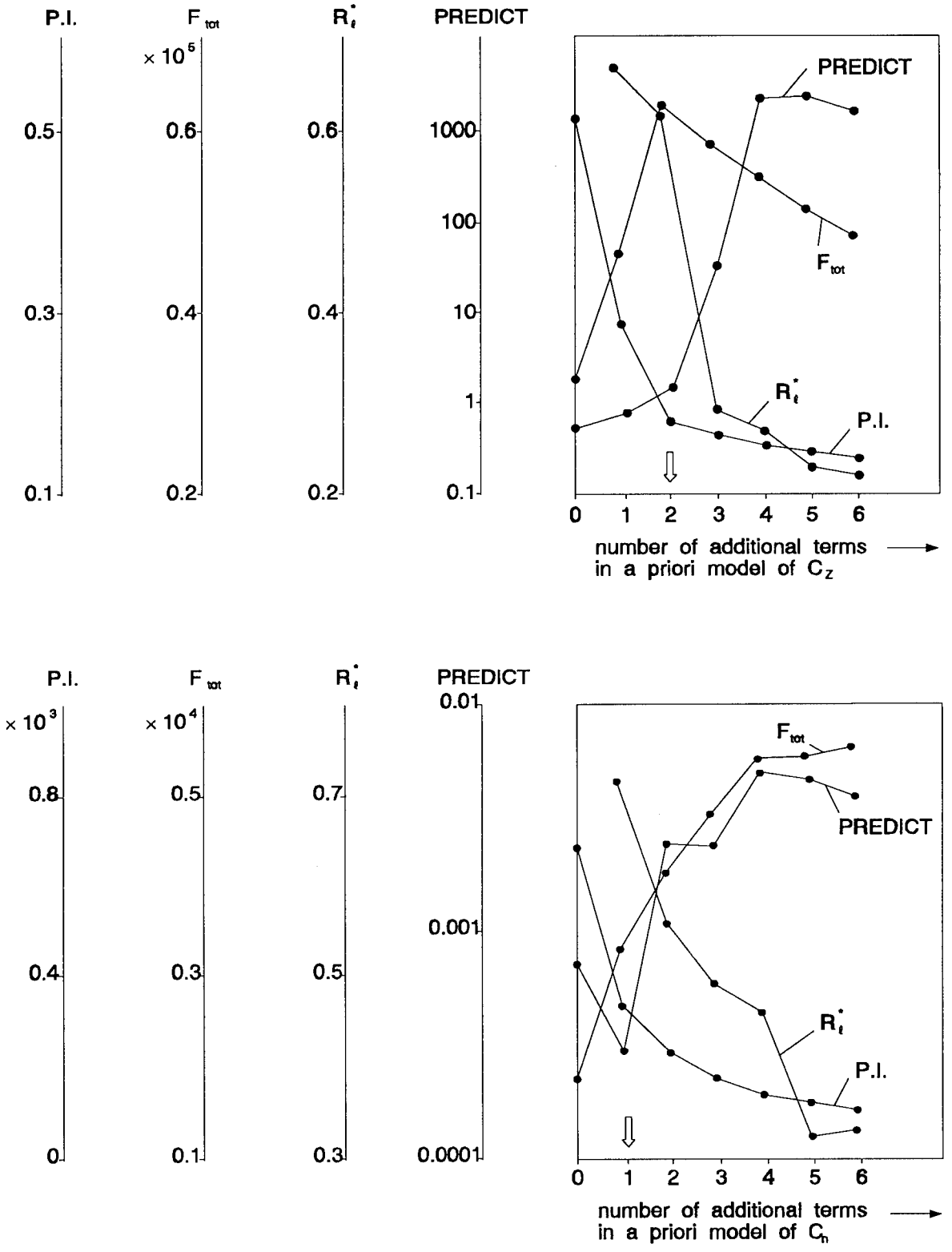

Figure 4-3: *Different criteria for model development for increasing number of additional terms in a priori aerodynamic models of C_Z and C_n. The open arrows indicate the selected number of additional terms based on the PREDICT function criterion.*

5 OPTIMAL INPUTS FOR AIRCRAFT PARAMETER ESTIMATION

In the estimation of aerodynamic parameters from flight tests the form of the flight test manoeuvre is vital for the accuracy of the parameter estimates. This naturally leads to the design of optimal input signals for flight test manoeuvres, which is the subject of the present chapter.

Several factors must be taken into account in designing input signals for flight test manoeuvres:

Model assumptions Input signal design must not result in violation of the assumptions underlying of the model description. In the case of linearized models the inputs should not cause too large a deviation from the nominal flight condition.

Flight test instrumentation The input signals must reflect the characteristics of the flight test transducers and data logging system such as dynamic range, measurement accuracy and sample rate.

Accuracies of parameter estimates The optimization of input signals should lead to maximum 'quality' of the data acquired during a flight test manoeuvre.

Length of individual flight test manoeuvres The flight test time should be kept as short as possible. This not only saves expensive flight testing time but also limits the volume of data storage and data processing.

Pilot acceptability The dynamic range and maximum amplitude of control input signals should be acceptable to the pilot. Only very 'simple' input signals are suitable for manual implementation. Input signals should, of course, never manoeuvre the aircraft outside of its flight envelope.

Aircraft structural constraints Input signals for flight test manoeuvres should not lead to larger than the design structural loads.

A fundamental problem in the design of input signals for system parameter estimation is that the design itself depends on the system parameters. Consequently, these parameters must be known before the actual flight tests are made. If they were known, however, then estimation would obviously no longer be necessary. This problem has been described as the *circularity problem.* Necessarily, the design of input signals must be based on a priori estimates of the actual system parameter values. The circularity problem can be addressed by calculating and implementing a sequence of 'optimal' input signals. Input signal design is then seen as an integral part of the identification procedure as shown in fig. 5-1. Starting from windtunnel experiments or other sources, one may develop an aerodynamic model structure and select a set of a priori parameter values. Together with the estimation objectives and experimental conditions, one has the basic presumptions for the design of input signals. Next actual identification results may be used to 'refine' the preliminary input signal design. Now, optimal input design and parameter identification can be used in an iterative manner until the desired objectives are met. Such an iterative procedure raises the interesting and yet unsolved question whether, and if so under which conditions, it will converge.

Historical background

In this section, we give a brief trace of the evolution of the theory of optimal input design. Starting with the work of Nahi et al., [159,160], the problem of deriving optimal input signals for the estimation of parameters in dynamical system models from response measurements has been studied intensively by several researchers. A detailed survey has been conducted by Goodwin and Payne [161] and Kalaba and Spingran [162]. In the field of dynamic flight testing, Gerlach [3] appears to be the first to explicitly recognize the influence of the form of input signals on the accuracy of estimated aerodynamic model derivatives. He proposed a qualitative method for the determination of 'optimal' frequencies in scalar input signals to linear second order systems [5].
The significance of the work of Nahi stems from the idea to use a norm of *Fisher's Information Matrix (M)* as a criterion for the optimization of input signals. The inverse of Fisher's information matrix yields a universal lower bound on parameter estimation accuracies, called the *Cramer Rao Lower Bound* (CRLB); see appendix A. The idea to

base the optimization of input signals on a norm of the information matrix results in input signals which have a general significance, in the sense of being independent of the type of estimation algorithm applied.

Important contributions to the theory and practice of the calculation of optimal aircraft input signals have been made subsequently by Mehra [164 to 166]. Based on the work of Kiefer and Wolfowitz [167], and Kiefer [168], Mehra proposes algorithms for the design of scalar and multi-dimensional input signals in the frequency domain as well as in the time domain.

The time domain optimization problem can be formulated in terms of a Nonlinear Control Problem with fixed end time [161 and 166]. These problems are notoriously difficult to solve [169]. A disadvantage of generating a solution in the time domain is that in practical applications constraints on the frequency contents of input signals may be important. A typical example are the constraints imposed by the finite bandwidths of anti-aliasing filters. It is not clear how such constraints can be taken account of in time domain optimizations.

As an alternative to the above formulation of a fixed-time control problem, one can specify the desired parameter accuracies and find those input signals which attain this goal in the shortest time. This time-optimal control problem has been studied by Chen [114] and more recently by Morelli [123]. The resulting input signals are of the bang-bang type. Chen is using combinations of Walsh functions, while Morelli adopts dynamic programming techniques to determine the optimal switching times. Morelli's technique was recently applied by Cobleigh [179] and the resulting input signals were applied by Noderer [147] for validation using actual flight test data from an X-31 drop model.

Optimization of input signals in the frequency domain is advocated by Mehra [165]. The resulting algorithms are very efficient with respect to computation time. Furthermore, the underlying optimization problem can be shown to be convex. In this context, convexity refers to the form of the object function or criterion for which the extreme must be located. Convexity is an attractive property, as it implies just one global extreme rather than multiple local extremes. The result of the optimization is in the form of line spectra consisting of a finite number of frequencies, see also [161].
Another approach in the frequency domain is by localizing 'identifiability' (in fact 'sensitivity') regions of individual parameters on the frequency axes of Bode diagrams. The diagrams indicate how 'identifiability' of different parameters depends on frequency and which frequency regions should thus be represented in the input signals. A procedure that optimized a sequence of step functions was developed by Koehler [20, 65]. The aim of the optimization was to find a signal with a shape as simple as possible and power distributed uniformly over a wide range of frequencies. This resulted in the now popular *3211 signal*, see also chapter 6.

A different form of broad band test signals which have been used in recent years are the 'frequency sweeps' as proposed by Tischler [139, 140]. Such signals are initiated by applying two sinusoidal cycles with a frequency corresponding to the lower end of the frequency range required. The frequency is then increased gradually while reducing the input signal amplitude. Next the input signal is returned to trim. The overall length of the test sequence is chosen ideally to allow good identification of the low frequency modes as well as to give a proper excitation of the vehicle over the frequency range of interest. These sweep signals were also applied by Sridhar and Wulff [232] in the evaluation of some of the lateral handling qualities of the BO-105 helicopter.

DUT Approaches

In this section we introduce two approaches developed at the Delft University of Technology (DUT) for the design of aircraft optimal input signals. Both approaches use a scalar norm of Fisher's information matrix as design criterion and exploit the advantages of parameter estimation via the two-step method, see chapter 4.
The first approach is based on the representation of input signals by means of finite sets of *orthonormal functions* in the time domain. This leads to a conceptually simple method in which the input signal design problem is converted into a nonlinear optimization problem. The method applies to linear as well as nonlinear systems. If

harmonic functions are used in the optimization there is a (loose) relation with the frequency domain. By excluding harmonics above a certain frequency it is possible to limit the frequency contents of the resulting input signals.

The second approach is a derivative of Mehra's method in the frequency domain [215, 216]. Its efficiency is enhanced by exploiting the two-step method for parameter estimation to reduce the information matrix to a block diagonal structure. *Convex analysis* is applied to minimize the number of harmonic signals in the input design. The optimization results in the optimal amplitude ratios and the frequencies of the harmonic signals selected by the algorithm.

Optimization criteria

Both DUT approaches use a scalar norm (J) of the information matrix M as the optimization criterion. Different norms can be used in the optimization, however, the following norms are frequently mentioned in the literature [158,161]:

tr M

Maximization of the trace of the information matrix indeed maximizes in a certain sense the amount of information present in the measured responses, but does not take any account of the condition of M. This means that the optimized input signals will not necessarily lead to acceptable parameter estimation accuracies, since the latter are related to the inverse of M, i.e. the Cramer Rao Lower Bound. In spite of this rather unfavourable characteristic, the criterion has been used by some authors mainly on account of computational efficiency of the resulting algorithms [159 and 163].

ln det M

It can be shown that the determinant of M is inversely proportional to the volume of the one-sigma ellipsoid of the Gaussian multi-dimensional probability density function of parameter estimation errors. Input signals which maximize ln det M are called *D-optimal* [161].

tr M^{-1}

The resulting input signals are called *A-optimal* [164], and minimize the sum of the variances of the parameter estimation errors, i.e. the diagonal elements of the Cramer Rao Lower Bound. It is possible to give priority to estimation errors of some parameters by multiplying M^{-1} with a weighting matrix and taking the trace of the matrix product.

λ_{max} of M^{-1}

Input signals are based on the minimization of the largest eigenvalue λ_{max} of M^{-1}. This cost function is related to the maximum radius of the uncertainty ellipsoid.

Fig. 5-2 shows the relationship between J and the one-sigma ellipsoid of the Gaussian probability density function of the estimates of a two-dimensional parameter vector $\underline{\theta}$. It can be seen that for strongly correlated parameter estimates, the maximization of tr M does not necessarily shrink the ellipsoid to a point.

Fisher's information matrix is not only influenced by the input signals, but also by the number of samples N, see appendix A. In order to eliminate this (trivial) effect on J, it is recommended to use $\bar{M}=M/N$ rather than M in the matrix norms defined above.

The last three cost functions require M to be of full rank. Only if M is of full rank it is possible to compute estimates of all parameters from the measured system responses to the applied input signals. In this case the parameters are called *identifiable*. It follows from appendix A that the condition of M is influenced by the form of the (multi-dimensional) input signal. If M's rank is not full, and cannot be improved by manipulating the form of the input signals then one or more of the parameters are *structurally unidentifiable*. In that case one should omit as many rows and columns (corresponding to the unidentifiable parameters) as needed to make M's rank full.

Constraints on input signals

In practice it will hardly ever be possible to apply input signals with maximum amplitudes corresponding to full deflections of control surfaces without exceeding the limits of the permissable flight envelope. Another restriction on the amplitude of input signals and responses is imposed by the calibrated measurement input ranges of the transducers in the measurement system. However, perhaps the most important

reason to restrict input signal amplitudes is to stay within that 'small' part of the flight envelope for which it may be assumed that the model structure as used for the optimization of the input signals is 'valid'. Since the present state of the art of input signal design is based on linearized models it follows immediately that only 'small' perturbations from a nominal flight condition are allowed.
If input signals of given form are scaled up each of the design criteria above will improve. The physical reason for this is that the signal to noise ratio improves with higher input signal amplitudes and so it is possible to arrive at better parameter estimates. So, also for the sake of a meaningful optimization of input signals (i.e. not leading to a trivial result of input signals with infinite amplitudes) the input signal amplitudes must be restricted.

While from the above it will be clear that constraints on input signal amplitudes are essential, a still open question is how these constraints must be imposed. Constraints can be imposed directly on the input signals themselves, but indirect constraints on one or more components of the state vector are feasible as well. Also, constraints can take the form of hard boundaries or may be specified in terms of input signal power or energy. The approach taken in the remainder of the present chapter is as follows:

- Hard constraints are not very relevant in input signal design for flight tests. The reason is that hard constraints either on input signals or state components are much less severe (except in the rather hypothetical case of a flight test manoeuvre planned on the very edge of the permissable flight envelope) than the constraints resulting from the use of a linearized system model.
- A power or energy constraint is applied to the components of the (multi-dimensional) input signal. The resulting optimized input signals can subsequently be scaled-up or down as a compromise between large signal to noise ratios (input signal scaled up) and small system model errors (input signal scaled down). Input signals for flight tests should be designed for optimal shape.

The total measurement interval time as well as the total number of discrete sample times play a major role in the attainable accuracies of the parameter estimates as expressed by the inverse of Fisher's information matrix. For optimization of input signals in the time domain, one may specify a fixed total interval time and sampling rate. As mentioned before sample rate as a design variable may be eliminated by using an *average Fisher information matrix* defined as $\bar{M}=M/N$. The same average information matrix is also used for the optimization of input signals in the frequency domain.

Organization of the chapter

chapter 5 is organized as follows. In section 5.1 the time domain approach for the calculation of optimal input signals composed of orthonormal functions is described. It is shown, that the optimal input signals may be derived from the solution of a nonlinear parameter optimization problem. Starting with the general case of nonlinear systems, it is shown that for the case of linear systems, the necessary calculations turns out to be remarkably simple and computationally efficient. In section 5.2, the method is applied to system and observation models which allow a decomposition of the parameter-state estimation problem as described in chapter 3 and 4.
The frequency domain approach is discussed in section 5.3 to 5.5. First, Fisher's information matrix is derived in the frequency domain, using the model for the decomposed parameter-state estimation problem. It is also shown that the information matrix can be represented as a simple convex combination of a limited number of point-input information matrices which each correspond to a single harmonic in the input design. Finally, the reconstruction of the optimal input signal is performed from the harmonic signals.

5.1 Optimization of Multi-dimensional Input Signals for Parameter Estimation of Nonlinear and Linear Systems

The present section describes in detail a method for the optimization of multi-dimensional input signals for parameter estimation of nonlinear and linear systems. The method is based on the representation of the components of multi-dimensional input signals by means of weighted sums of orthonormal functions [section 5.1.1]. In general, the numerical value of the criterion for optimality, i.e. a norm of

Fisher's information matrix or of the Cramer Rao Lower Bound, depends on the energy and form of the input signals. Therefore it is a function of the weighting factors of these orthonormal functions. This allows the formulation of the problem of input signal optimization in terms of a nonlinear parameter optimization problem, in which the parameters are the weighting factors. This is discussed in section 5.1.2. In section 5.1.3 it is shown that in the case of linear systems, it is possible to apply the concept of so called *elementary information matrices*. It is argued that this results in significant savings of computation time.

Initially, Powell's direct search method [170], was used to solve the nonlinear parameter optimization problems of section 5.1.2 and 5.1.3. The resulting algorithm was employed for the optimization of the Delft University of Technology (DUT) control input signals of the flight test program described in chapter 6. After completion of the flight test program, however, a new and faster version of the algorithm was developed in which the Newton-Raphson method was used. This version of the algorithm is described in section 5.1.4.

5.1.1 Representation of Multi-dimensional Input Signals

In the following, $\underline{u}(t)$ denotes an s-dimensional input signal with components $u_\ell(t)$, $\ell=1(1)s$:

$$\underline{u}(t) = \mathrm{col}\left(u_1(t),\ldots,u_\ell(t),\ldots,u_s(t)\right) . \qquad t \in [t_0,t_1] \tag{5.1-1}$$

The crux of the present method for the optimization of input signals lies in the introduction of certain constraints on form and energy of each of the components of the multi-dimensional input signal $\underline{u}$ in the time interval $[t_0,t_1]$. In section 5.1.2, it is shown how these constraints lead to the formulation of the parameter optimization problem mentioned above.

The constraints on the *form* are the consequence of an approximation of the components u_ℓ of $\underline{u}$ by means of a weighted sum of a finite number of p orthonormal functions $\psi_k(t)$, k=1(1)p, according to:

$$u_\ell(t) = \sum_{k=1}^{p} \beta_{k\ell}\, \psi_k(t) \tag{5.1-2}$$

where $\beta_{k\ell}$, k=1(1)p, denote a set of weighting factors. The functions $\psi_k(t)$ are assumed to be orthonormal on $[t_0,t_1]$, as defined by:

$$\int_{t_0}^{t_1} \psi_k(t)\, \psi_n(t)\, dt = \delta_{kn}$$

where δ_{kn} denotes the Kronecker delta. The shape of the orthonormal functions $\psi_k(t)$ has still to be defined in more detail later on.
The *energy* of the different components $u_\ell(t)$ of $\underline{u}(t)$ in the time interval $[t_0,t_1]$ is constrained to a set of fixed and a priori selected values. The energy E_ℓ of the component $u_\ell(t)$ in $[t_0,t_1]$ can be written as:

$$\begin{aligned} E_\ell &= \int_{t_0}^{t_1} u_\ell^2(t) = \int_{t_0}^{t_1} \left(\sum_{k=1}^{p} \beta_{k\ell}\, \psi_k(t) \right)^2 dt \\ &= \sum_{k=1}^{p} \sum_{n=1}^{p} \beta_{k\ell}\beta_{n\ell} \int_{t_0}^{t_1} \psi_k(t)\, \psi_n(t)\, dt \\ &= \sum_{k=1}^{p} (\beta_{k\ell})^2 \end{aligned} \tag{5.1-3}$$

Equation (5.1-3) is in fact, a particular form of Parseval's theorem [171]. It follows from here that for given energy E_ℓ in the time interval $[t_0,t_1]$, the component $u_\ell(t)$ can be represented by a point P_ℓ on a hypersphere with radius $R_\ell=\sqrt{E_\ell}$ in p-dimensional Euclidian space. The position of P_ℓ on the sphere can be expressed not only in cartesian or rectangular, but also in spherical coordinates. The rationale behind the introduction here of spherical coordinates will become clear in the next section 5.1.2. The relations between the rectangular coordinates $\beta_{k\ell}$ and the corresponding spherical coordinates $\phi_{j\ell}$ of P_ℓ can be written as:

$$\begin{aligned} \beta_{1\ell} &= R_\ell \cdot \sin\phi_{1\ell} , \\ \beta_{k\ell} &= R_\ell \cdot \prod_{j=1}^{k-1} \cos\phi_{j\ell} \sin\phi_{k\ell} , \\ \beta_{p\ell} &= R_\ell \cdot \prod_{j=1}^{p-1} \cos\phi_{j\ell} \end{aligned} \tag{5.1-4}$$

for k=2(1)(p-1), as depicted in fig. 5-3 for the case p=3.

It will be convenient to define the vectors:

$$\underline{\beta}_\ell = \mathrm{col}\left(\beta_{1\ell}, \beta_{2\ell}, \ldots, \beta_{p\ell}\right) ,$$

for ℓ=1(1)s in which p is the number of individual orthogonal functions in $u_\ell(t)$ and s denotes the dimension of $\underline{u}(t)$.

Next, the elements of all the vectors $\underline{\beta}_\ell$ are arranged in one column, in the form of a new vector $\underline{\beta}$ with elements $\underline{\beta}_\ell$ as:

$$\underline{\beta} = \begin{pmatrix} \underline{\beta}_1 \\ \vdots \\ \underline{\beta}_\ell \\ \vdots \\ \underline{\beta}_s \end{pmatrix} = \begin{pmatrix} \beta_1 \\ \vdots \\ \beta_i \\ \vdots \\ \beta_q \end{pmatrix} \qquad (5.1\text{-}5)$$

If q denotes the dimension of $\underline{\beta}$, then q=s·p.

Next, a set of q so called *elementary input signals* is introduced. An elementary input signal is an s-dimensional vector $\underline{e}_i(t)$ defined as follows:

$$\underline{e}_1(t) = \begin{pmatrix} \psi_1(t) \\ 0 \\ \vdots \\ \vdots \\ 0 \end{pmatrix} , \ldots , \underline{e}_p(t) = \begin{pmatrix} \psi_p(t) \\ 0 \\ \vdots \\ \vdots \\ 0 \end{pmatrix} , \ldots , \qquad (5.1\text{-}6)$$

$$\underline{e}_i = \begin{pmatrix} 0 \\ \vdots \\ 0 \\ \psi_k(t) \\ \vdots \\ 0 \end{pmatrix} , \ldots , \underline{e}_q(t) = \begin{pmatrix} 0 \\ \vdots \\ \vdots \\ \vdots \\ 0 \\ \psi_p(t) \end{pmatrix} .$$

where k=1(1)p.

The set of elementary input signals can be interpreted as the columns of a matrix D(t), as shown in fig. 5-4 for the case s=2 and p=4.

The input signal $\underline{u}(t)$ can now be written in the following compact form:

$$\underline{u}(t) = D(t)\cdot\underline{\beta} = \sum_{i=1}^{q} \beta_i \cdot \underline{e}_i(t) \qquad (5.1\text{-}7)$$

in which $\underline{\beta}$ denotes the vector of weighting factors as defined in equation (5.1-5).

In principle, any set of functions orthonormal on $[t_0,t_1]$ could be used in equation (5.1-2). If the set is 'complete' then any continuous function on $[t_0,t_1]$ can be approximated 'to any desired degree of accuracy' by increasing the total number p of orthonormal functions [171]. This means that for $p \rightarrow \infty$, optimized input signals of the form (5.1-2) will be independent of which class of orthonormal functions is used. In practice, for reasons discussed in the following sections, p is limited to finite and relatively small values. In that case, it must be expected that the form of the optimized input signals will show which set of orthonormal functions is used in equation (5.1-2). For example, in Swick [172] a set of orthonormal functions is described which consists of positive and negative steps to +1 and -1 respectively. Application of these so called Walsh functions, [fig. 5-5], would result in input signals consisting of a finite number of positive and negative steps of varying magnitudes. Input signals of this kind are considered to be less suitable for actual implementation in flight, see also section 6. However, for excitation of other types of systems, as for instance the pharmaco-kinetic system described in [173], such input signals would be very practical.

An attractive property of sinusoidal functions is that their energy is 'concentrated' around discrete frequencies. This property can be exploited to 'influence' the frequency contents of the optimized input signals by simply omitting functions outside a certain frequency range. The following two sets of sinusoidal functions were employed for the input signal optimizations as described in chapter 6:

set 1:

$$\psi_k(t) = \sqrt{\frac{2}{T}}\ \sin\omega_k t ,$$
$$\omega_k = k\cdot\omega_{o_1} , \quad \omega_{o_1} = \frac{2\pi}{T} , \qquad (5.1\text{-}8)$$

set 2:

$$\psi_k(t) = \sqrt{\frac{2}{T}}\ \sin\omega_k t ,$$
$$\omega_k = k\cdot\omega_{o_2} , \quad \omega_{o_2} = \frac{\pi}{T} , \qquad (5.1\text{-}9)$$

in which k=1(1)p, $t \in [t_0,t_1]$, and $T=t_1-t_0$, see figs. 5-6 and 5-7. It is noted that any input signal which is composed of set 1 or set 2 functions will be zero at the start and end times. This is another advantage of sine functions as there will be no discontinuities when input signals are superimposed on the steady state or trim deflections of control surfaces in the nominal flight condition.

The sine functions in both set 1 and set 2 are readily shown to be orthonormal over the time interval $[t_0,t_1]$. Set 1 consists of functions having k periods in $[t_0,t_1]$, set 2 consists of functions having k-half periods in $[t_0,t_1]$. Sets of only sine functions are not complete. It is possible to define a complete set of orthonormal functions by adding a constant and cosine functions to the sine functions of set 1. The resulting set of functions is indicated as set 3, see fig. 5-8:

set 3:

$$\begin{aligned} \psi_o(t) &= \frac{1}{T} , \\ \psi_{1_k}(t) &= \sqrt{\frac{2}{T}} \sin\omega_k t , \\ \psi_{2_k}(t) &= \sqrt{\frac{2}{T}} \cos\omega_k t , \\ \omega_k &= k\cdot\omega_{o_1} , \quad \omega_{o_1} = \frac{2\pi}{T} , \end{aligned} \tag{5.1-10}$$

in which again k=1(1)p, $t \in [t_0,t_1]$ and $T=t_1-t_0$.

In the present context, functions of set 3 are of theoretical interest only. Input signals based on these functions will lead to discontinuities and consequently, are not be suitable for actual implementation in flight.

As mentioned above, ω_k in equations (5.1-8), (5.1-9) and (5.1-10) is loosely related to the frequency contents of the particular function. As k becomes larger, the power of the corresponding sine or cosine function in a power spectral density plot is concentrated more closely around ω_k. This fact may be used by the designer to limit the frequency contents of input signals. In this way it is possible, for instance, to avoid measurement errors due to the finite bandwidth of the pre-sampling filters in the measurement system.

Another possibility is to design input signals such that undesirable characteristic modes of the dynamic system are not excited. A typical example of such characteristic modes are the high frequency structural modes of flexible aircraft.

5.1.2 Input Signal Optimization for Nonlinear System Parameter Estimation

In the present section it is shown that the design of multi-dimensional input signals for nonlinear system parameter estimation may be formulated in terms of a nonlinear parameter optimization problem. The nonlinear systems considered are of the following form:

$$\dot{\underline{x}}(t) = \underline{f}(\underline{\theta}, \underline{x}(t), \underline{u}(t)) \tag{5.1-11}$$

in which $\underline{x}(t)$ denotes an n-dimensional state vector, $\underline{u}(t)$ an s-dimensional input signal and $\underline{\theta}$ a vector of r system parameters for which it is assumed that a set of approximate a priori values is known. Furthermore, $\underline{f}$ denotes a real valued vector function of dimension n. Each of its components is assumed to be continuous, such that its partial derivatives with respect to $\underline{\theta}$, $\underline{x}(t)$ and $\underline{u}(t)$ exist. The system is observed at discrete instants of time $t_i \in [t_0,t_1]$, i=1(1)N, according to the following nonlinear observation model:

$$\underline{y}(i) = \underline{h}(\underline{\theta}, \underline{x}(i), \underline{u}(i)) \tag{5.1-12}$$

in which $\underline{y}(i)$ denotes an m-dimensional vector of observations at $t=t_i$. The usual assumption is made, that observation measurement errors are adequately represented by additive stationary Gaussian sequences of stochastic variables, which are assumed to have zero mean values and to be uncorrelated in time. However, measurement errors pertaining to the same instant of time are not assumed to be uncorrelated. This leads to the following measurement model:

$$\begin{aligned} \underline{y}_m(i) &= \underline{y}(i) + \underline{v}(i) , \\ E\{\underline{v}(i)\} &= \underline{0} , \\ E\{\underline{v}(i)\underline{v}^T(j)\} &= V_{vv}\cdot\delta_{ij} , \end{aligned} \tag{5.1-13}$$

for i,j=1(1)N.

The input signal $\underline{u}(t)$ is also sampled at discrete instants of time. The corresponding measurement

errors are assumed to be small enough to be negligible. This situation is considered to be quite representative for the case of dynamic flight tests, where control surface deflections can indeed be measured with high accuracy.

The system model (5.1-11) is restricted to be deterministic. In the present context, this implies that the actual measurements are made in a stable atmosphere, where turbulence is negligible. Furthermore, stochastic contributions to the aerodynamic forces and aerodynamic moments, as generated for instance in the (turbulent) boundary layer, are also neglected. In general these stochastic contributions are very small, except in those flight regimes where appreciable flow separation occurs.

With the assumptions made above, the solution of the system differential equations may, for given values of the initial state vector $\underline{x}_0=\underline{x}(t_0)$ and the parameter vector $\underline{\theta}$, be calculated according to:

$$\underline{x}(t) = \underline{x}_0 + \int_{t_0}^{t} \underline{f}(\underline{\theta}, \underline{x}(t), \underline{u}(t))\, dt \ . \qquad (5.1\text{-}14)$$

The maximum likelihood (ML) estimate of $\underline{\theta}$ corresponds to the global maximum of the logarithm of the likelihood function ln L of the observation measurements, see appendix A. For a given input signal time history $\underline{u}(t)$ in the time interval $[t_0,t_1]$, this likelihood function depends not only on the parameter vector $\underline{\theta}$, but also on $\underline{x}_0$ and on the elements of the covariance matrix of measurement errors V_{vv}. The dimensions of the parameter vector $\underline{\theta}$ and the initial vector $\underline{x}_0$ are r and n respectively. In the most general case, the total number of nonidentical elements in the symmetrical covariance matrix V_{vv} of observation measurement errors is ½m(m+1), if this matrix is assumed to be nondiagonal. In cases where $\underline{x}_0$ and V_{vv} are unknown, they must be estimated in addition to $\underline{\theta}$. The solution of the ML estimation problem then involves locating the global maximum in the r+n+½m(m+1)-dimensional space of $\underline{\theta}$, $\underline{x}_0$ and the upper triangular elements of V_{vv}. For convenience the elements of V_{vv}^{-1} rather than of V_{vv} are chosen as the unknowns to be estimated, see appendix A. The upper triangular elements of V_{vv}^{-1} can be arranged in a new parameter vector $\underline{\eta}$ of dimension ½m(m+1).

Next we compute the covariance matrix of parameter estimation errors. First we gather all parameters in $\underline{\theta}$, $\underline{x}_0$ and $\underline{\eta}$ in one augmented parameter vector $\underline{\theta}_a$ of dimension r+n+½m(m+1):

$$\underline{\theta}_a = \begin{pmatrix} \underline{\theta} \\ \cdots \\ \underline{x}_0 \\ \cdots \\ \underline{\eta} \end{pmatrix} .$$

In correspondence with this partitioning, it is now possible to partition the 'augmented' covariance matrix $V_{\theta_a\theta_a}$ of the estimated parameters, $\underline{\hat{\theta}}_a$, in the following manner:

$$V_{\theta_a\theta_a} = \begin{bmatrix} V_{\theta\theta} & \vdots & V_{\theta x_0} & \vdots & V_{\theta\eta} \\ \cdots & \cdot\vdots\cdot & \cdots & \cdot\vdots\cdot & \cdots \\ V_{x_0\theta} & \vdots & V_{x_0x_0} & \vdots & V_{x_0\eta} \\ \cdots & \cdot\vdots\cdot & \cdots & \cdot\vdots\cdot & \cdots \\ V_{\eta\theta} & \vdots & V_{\eta x_0} & \vdots & V_{\eta\eta} \end{bmatrix} . \qquad (5.1\text{-}15)$$

The important role of Fisher's information matrix in ML estimation theory stems from the fact that its inverse, $C_{\theta_a\theta_a}$, called the Cramer-Rao lower bound (CRLB), constitutes an asymptotic limit for $V_{\theta_a\theta_a}$ as N goes to infinity [53]:

$$\lim_{N \to \infty} V_{\theta_a\theta_a} = M_{\theta_a\theta_a}^{-1} = C_{\theta_a\theta_a}$$

The information matrix $M_{\theta_a\theta_a}$ is a positive, semi-definite and symmetrical matrix which can be partitioned as:

$$M_{\theta_a\theta_a} = \begin{bmatrix} M_{\theta\theta} & \vdots & M_{\theta x_0} & \vdots & M_{\theta\eta} \\ \cdots & \cdot\vdots\cdot & \cdots & \cdot\vdots\cdot & \cdots \\ M_{x_0\theta} & \vdots & M_{x_0x_0} & \vdots & M_{x_0\eta} \\ \cdots & \cdot\vdots\cdot & \cdots & \cdot\vdots\cdot & \cdots \\ M_{\eta\theta} & \vdots & M_{\eta x_0} & \vdots & M_{\eta\eta} \end{bmatrix} .$$

According to appendix A the blocks $M_{\theta\eta}$, $M_{\eta\theta}$, $M_{x_0\eta}$ and $M_{\eta x_0}$ are empty:

$$M_{\theta_a\theta_a} = \begin{bmatrix} M_{\theta\theta} & \vdots & M_{\theta x_0} & \vdots & O \\ \cdots & \cdot\vdots\cdot & \cdots & \cdot\vdots\cdot & \cdots \\ M_{x_0\theta} & \vdots & M_{x_0x_0} & \vdots & O \\ \cdots & \cdot\vdots\cdot & \cdots & \cdot\vdots\cdot & \cdots \\ O & \vdots & O & \vdots & M_{\eta\eta} \end{bmatrix} . \qquad (5.1\text{-}16)$$

Now, $C_{\theta_a\theta_a}$ the CRLB, can be written as:

$$C_{\theta_a\theta_a} = \begin{bmatrix} \begin{bmatrix} M_{\theta\theta} & \vdots & M_{\theta x_0} \\ \cdots & \cdot\vdots\cdot & \cdots \\ M_{x_0\theta} & \vdots & M_{x_0x_0} \end{bmatrix}^{-1} & \begin{matrix} O \\ \cdots \\ O \end{matrix} \\ \begin{matrix} O & \vdots & O \end{matrix} & M_{\eta\eta}^{-1} \end{bmatrix} .$$

From (A.2-8) and (5.1-15) it follows that:

$$\lim_{N\to\infty} \begin{bmatrix} V_{\theta\theta} & \vdots & V_{\theta x_0} \\ \cdots & \cdot\vdots\cdot & \cdots \\ V_{x_0\theta} & \vdots & V_{x_0x_0} \end{bmatrix} = \begin{bmatrix} M_{\theta\theta} & \vdots & M_{\theta x_0} \\ \cdots & \cdot\vdots\cdot & \cdots \\ M_{x_0\theta} & \vdots & M_{x_0x_0} \end{bmatrix}^{-1} ,$$

$$\lim_{N\to\infty} V_{\eta\eta} = M_{\eta\eta}^{-1} ,$$

$$\lim_{N\to\infty} V_{\theta\eta} = \lim_{N\to\infty} V_{\eta\theta} = O ,$$

$$\lim_{N\to\infty} V_{x_0\eta} = \lim_{N\to\infty} V_{\eta x_0} = O .$$

The upperdiagonal block of $M_{\theta_a\theta_a}$ in equation (5.1-16) represents the combined information matrix on the parameter vector $\underline{\theta}$ and the vector of initial conditions $\underline{x}_0$. For convenience this matrix is written below as:

$$M = \begin{bmatrix} M_{\theta\theta} & \vdots & M_{\theta x_0} \\ \cdots & \cdot\vdots\cdot & \cdots \\ M_{x_0\theta} & \vdots & M_{x_0x_0} \end{bmatrix} . \qquad (5.1\text{-}17)$$

With (5.1-17), it is now possible to write $M_{\theta_a\theta_a}$ in (5.1-16) and $C_{\theta_a\theta_a}$ as follows:

$$M_{\theta_a\theta_a} = \begin{bmatrix} M & \vdots & O \\ \cdots & \cdot\vdots\cdot & \cdots \\ O & \vdots & M_{\eta\eta} \end{bmatrix} \qquad (5.1\text{-}18)$$

$$C_{\theta_a\theta_a} = \begin{bmatrix} M^{-1} & \vdots & O \\ \cdots & \cdot\vdots\cdot & \cdots \\ O & \vdots & M_{\eta\eta}^{-1} \end{bmatrix} \qquad (5.1\text{-}19)$$

Three matrix norms for the optimization of input signals, as defined earlier, may now be applied to equations (5.1-18) and (5.1-19). The resulting criteria can be written as follows:

a) $J = \mathrm{tr} M_{\theta_a\theta_a} = \mathrm{tr} M + \mathrm{tr} M_{\eta\eta}$

b) $J = \ln\det M_{\theta_a\theta_a} = \ln(\det M \cdot \det M_{\eta\eta})$
$= \ln\det M + \ln\det M_{\eta\eta}$

c) $J = \mathrm{tr} M_{\theta_a\theta_a}^{-1} = \mathrm{tr} M^{-1} + \mathrm{tr} M_{\eta\eta}^{-1}$

It is shown in appendix A that the elements of M depend on $\underline{u}(t)$, $t\in[t_0,t_1]$. The elements of $M_{\eta\eta}$, however, are shown to be fully independent of $\underline{u}(t)$. If we omit the terms containing $M_{\eta\eta}$ the following simplified criteria result:

a) $J = \mathrm{tr} M$,

b) $J = \ln\det M$,

c) $J = \mathrm{tr} M^{-1}$.

J may now be written as a nonlinear scalar function of q=s·p weighting factors $\beta_{k\ell}$:

$$J = J(\underline{\beta}) = J\left(\underline{\beta}_1,\ldots,\underline{\beta}_\ell,\ldots,\underline{\beta}_s\right) , \qquad (5.1\text{-}20)$$

where:

$$\underline{\beta}_\ell = \mathrm{col}\left(\beta_{1\ell},\beta_{2\ell},\ldots,\beta_{p\ell}\right) .$$

According to section 5.1.1, the components of the s-dimensional input signal with prescribed energies E_ℓ, ℓ=1(1)s, can also be represented as s points P_ℓ on hyperspheres in a p-dimensional space with radii $r_\ell=\sqrt{E_\ell}$. Let $\underline{\phi}_\ell$ denote the vector of spherical coordinates of one of these points P_ℓ, as defined in (5.1-4) and fig. 5-3, then J in (5.1-20) can be written in an alternate form with a smaller number, viz. s(p-1), of spherical coordinates as arguments:

$$J = J\left(\underline{\phi}_1,\ldots,\underline{\phi}_\ell,\ldots,\underline{\phi}_s\right) . \qquad (5.1\text{-}21)$$

where

$$\underline{\phi}_\ell = \mathrm{col}\left(\phi_{1\ell},\phi_{2\ell},\ldots,\phi_{p-1,\ell}\right) ,$$

With (5.1-20) or (5.1-21) it is possible to formulate the input signal design problem in terms of a parameter optimization problem. The correspondence between (5.1-20) and (5.1-21) is that J in both expressions depends on a finite number of arguments or parameters. There is, however, an important difference when applying (5.1-20) and (5.1-21). Equation (5.1-20) needs an additional set of constraints on input signal

energies in order to obtain a meaningful optimization problem. However, optimization of J in (5.1-21) directly leads to optimal input signal components $u_\ell(t)$ of prescribed energy E_ℓ. Therefore, optimization of (5.1-21) rather than (5.1-20) allows us to solve an unconstrained optimization problem, which is much easier to solve than an optimization problem with constraints.

In principle, a variety of algorithms may be applied to solve such optimization problems [174]. If partial derivatives of J with respect to its arguments $\underline{\phi}_1,...,\underline{\phi}_s$, are not available, it may be appropriate to apply one of the direct search types of optimization methods, which depend only on the feasibility to calculate the value of the function J for given values of the arguments in (5.1-21), e.g. Powell's algorithm [170].

It is noted here, that each evaluation of the function J in (5.1-21), requires the numerical solution of the system differential equations in (5.1-11), and the solution of a set of sensitivity differential equations for the calculation of the information matrix. Therefore, the optimization of input signals as described above, must be expected to be rather time consuming. In the next section, it is shown that in the case of linear system and observation models, the repeated solution of system and sensitivity equations for every function evaluation can be avoided.

5.1.3 Input Signal Optimization for Linear System Parameter Estimation

The method, described in the previous section 5.1.2 for the calculation of optimal input signals for nonlinear system parameter estimation, is now applied to the more restricted case of linear system parameter estimation. The systems considered are of the following form:

$$\dot{\underline{x}}(t) = F(\underline{\theta})\underline{x}(t) + G(\underline{\theta})\underline{u}(t) , \qquad (5.1\text{-}22)$$

in which as before $\underline{x}$ denotes an n-dimensional state vector, $\underline{u}$ an s-dimensional input signal and $\underline{\theta}$ a vector of the r parameters which are to be estimated. $F(\underline{\theta})$ and $G(\underline{\theta})$ denote constant matrices of appropriate dimensions. At N discrete instants of time $t_i \in [t_0,t_1]$, i=1(1)N, the system is observed according to the following model:

$$\begin{aligned} \underline{y}(i) &= H(\underline{\theta})\underline{x}(i) + J(\underline{\theta})\underline{u}(i) , \\ \underline{y}_m(i) &= \underline{y}(i) + \underline{v}(i) . \end{aligned} \qquad (5.1\text{-}23)$$

in which $\underline{y}$ denotes an m-dimensional observation vector, $H(\underline{\theta})$ and $J(\underline{\theta})$ denote constant matrices of appropriate dimensions, and $\underline{y}_m$ denotes the measurement of $\underline{y}$. The measurement noise $\underline{v}(i)$ is assumed to be zero mean, uncorrelated in time and Gaussian as in equation (5.1-13). It is assumed again, that $\underline{u}(t)$ is known exactly and that equation (5.1-22) is deterministic, i.e. the system (5.1-22) is not subjected to unmeasurable stochastic inputs.

The performance criterion for input signals is again a scalar norm J of M, the joint information matrix of $\underline{\theta}$ and $\underline{x}_0$:

$$M = \begin{bmatrix} M_{\theta\theta} & \vdots & M_{\theta x_0} \\ \cdots\cdots & \cdot\vdots\cdot & \cdots\cdots \\ M_{x_0\theta} & \vdots & M_{x_0x_0} \end{bmatrix} . \qquad (5.1\text{-}24)$$

The general expression for M, as derived for the case of nonlinear systems, is still valid in the present case of linear systems [29]. In this expression, M is described in terms of sensitivity matrices S(t). The elements of these sensitivity matrices are partial derivatives, representing the sensitivity of the components of the observation vector $\underline{y}$ with respect to the components of the parameter vector $\underline{\theta}$ and the vector of initial conditions $\underline{x}_0$. The information matrix M for observation measurements at discrete instants of time t_i can be written as:

$$M = \sum_{i=1}^{N} S^T(i) \cdot V_{vv}^{-1} \cdot S(i) , \qquad (5.1\text{-}25)$$

in which the index i refers to the discrete time instant t_i and V_{vv} represents the not necessarily diagonal covariance matrix of the vector $\underline{v}(i)$ of observation measurement errors. The matrix S(i) in equation (5.1-25) represents the sensitivity matrix S at the discrete sampling time t_i. The sensitivity matrix S(t) can be partitioned as follows:

$$S(t) = \begin{bmatrix} S_\theta(t) & S_{x_0}(t) \end{bmatrix} \qquad (5.1\text{-}26)$$

The partial derivatives of the components $\underline{y}$ with respect to the components of r are contained in the matrix $S_\theta(t)$, while the partial derivatives of the components of $\underline{y}$ with respect to the components of $\underline{x}_0$ are contained in the matrix $S_\theta(t)$.

First the matrix $S_\theta(t)$ is partitioned in terms of column vectors as follows:

$$S_\theta(t) = \left[\underline{y}_{\theta_1}(t) \quad \underline{y}_{\theta_2}(t) \quad \cdots \quad \underline{y}_{\theta_r}(t)\right],$$

where the j-th column vector $\underline{y}_{\theta_i}(t)$ is defined as $\partial\underline{y}/\partial\theta_j$.
Next, the partial derivatives of the matrices of the system and observation model in equations (5.1-22) and (5.1-23) respectively, with respect to the component θ_j of $\underline{\theta}$, are defined as:

$$F_{\theta_j}(\underline{\theta}) = \frac{\partial F(\underline{\theta})}{\partial\theta_j}, \qquad G_{\theta_j}(\underline{\theta}) = \frac{\partial G(\underline{\theta})}{\partial\theta_j},$$

$$H_{\theta_j}(\underline{\theta}) = \frac{\partial H(\underline{\theta})}{\partial\theta_j}, \qquad J_{\theta_j}(\underline{\theta}) = \frac{\partial J(\underline{\theta})}{\partial\theta_j},$$

where j=1(1)r.
It is to be noted that these matrix partial derivatives are constant for a given parameter vector $\underline{\theta}$, i.e. independent of the state vector $\underline{x}(t)$ and the input signal $\underline{u}(t)$.
In a similar way, the partial derivatives of the state vector $\underline{x}$ with respect to the components θ_j of $\underline{\theta}$ are defined as:

$$\underline{x}_{\theta_j}(t) = \frac{\partial\underline{x}(t)}{\partial\theta_j}.$$

These vectors of partial derivatives vary as a function of time depending on $\underline{x}_0$ and $\underline{u}$. This follows directly from the particular form of the sensitivity differential equations used to calculate these vectors of partial derivatives [53].
The sensitivity equations are readily derived from equation (5.1-22) by partially differentiating both sides of this equation with respect to θ_j, and subsequently changing the order of the differentiation with respect to θ_j and t, for which it must be assumed that $\underline{x}$ is analytic [171]. The resulting sensitivity equations of $\underline{x}_\theta$ are constant, linear and of the following form:

$$\dot{\underline{x}}_{\theta_j}(t) = F(\underline{\theta})\underline{x}_{\theta_j}(t) + F_{\theta_j}(\underline{\theta})\underline{x}(t) + G_{\theta_j}(\underline{\theta})\underline{u}(t), \tag{5.1-27}$$

with initial conditions:

$$\underline{x}_{\theta_j}(t_0) = \underline{0},$$

where j=1(1)r.

The vectors of partial derivatives $\underline{y}_{\theta_j}$ are calculated with the following relation, resulting from partial differentiation of both sides of equation (5.1-23) with respect to θ_j:

$$\underline{y}_{\theta_j}(i) = H(\underline{\theta})\underline{x}_{\theta_j}(i) + H_{\theta_j}(\underline{\theta})\underline{x}(i) + J_{\theta_j}(\underline{\theta})\underline{u}(i), \tag{5.1-28}$$

where j=1(1)r, and the index i refers to the discrete sample times $t_i \in [t_0, t_1]$.

The second matrix of partial derivatives in S(t) is $S_{x_0}(t)$. In a similar way to $S_\theta(t)$ above, $S_{x_0}(t)$ may also be partitioned in terms of column vectors according to:

$$S_{x_0}(t) = \left[\underline{y}_{x_{0_1}}(t) \quad \underline{y}_{x_{0_2}}(t) \quad \cdots \quad \underline{y}_{x_{0_n}}(t)\right]$$

Next, analogous to $\underline{x}_{\theta_j}$ above, the partial derivatives of the state vector $\underline{x}$ with respect to the components x_{0_j} of the initial state $\underline{x}_0$, j=1(1)n, are defined as:

$$\underline{x}_{x_{0_j}}(t) = \frac{\partial\underline{x}(t)}{\partial x_{0_j}}.$$

The vectors of partial derivatives $\underline{x}_{x_{0_j}}$ may also be calculated with a set of sensitivity differential equations, in a similar way as the vectors $\underline{x}_{\theta_j}$ above. These sensitivity equations are derived by partially differentiating both sides of equation (5.1-22) with respect to x_{0_j}, and subsequently changing the order of differentiation with respect to x_{0_j} and with respect to time of the term in the left hand side. The resulting sensitivity equations of $\underline{x}_{x_{0_j}}$ are of the following form [46]:

$$\dot{\underline{x}}_{x_{0_j}}(t) = F(\underline{\theta})\underline{x}_{x_{0_j}}(t) \tag{5.1-29}$$

with initial conditions:

$$\underline{x}_{\underline{x}_0}(t_0) = I,$$

where j=1(1)n.
It is noted that these sensitivity equations are constant and linear similar to the sensitivity equations in (5.1-27).
Finally, partial differentiation of both sides of equation (5.1-23) with respect to x_{0_j} results in the following relation for the vectors of partial derivatives $\underline{y}_{x_{0_j}}$:

$$\underline{y}_{x_{0_j}}(i) = H(\underline{\theta})\underline{x}_{x_{0_j}}(i) \tag{5.1-30}$$

where j=1(1)n, and the index i refers again to the discrete sample times $t_i \in [t_0, t_1]$.

By solving the sensitivity differential equations in (5.1-27) and (5.1-29), and subsequently applying the relations (5.1-28) and (5.1-30), it is now possible to compute the vectors of partial derivatives in the matrices $S_\theta(i)$ and $S_{x_0}(i)$, i=1(1)N. Subsequently, these matrices are used to compose the sensitivity matrices S(i) according to equation (5.1-26). Finally, the information matrix M of $\underline{\theta}$ and $\underline{x}_0$ is computed with equation (5.1-25).

It is noted that the solution of the system differential equations (5.1-22) is needed for the solution of the sensitivity differential equations (5.1-27) in which $\underline{x}$ appears as a forcing function.

In a manner, completely analogous to the nonlinear case discussed in section 5.1.2, we may now formulate the problem of optimizing input signals $u_\ell(t)$, ℓ=1(1)s of given energy E_ℓ in $[t_0,t_1]$ in terms of an unconstrained nonlinear parameter optimization problem. The problem is to calculate the global extreme of the criterion J with respect to its arguments, the elements of the vectors of spherical coordinates,

$$J = J\left(\underline{\Phi}_1,\ldots,\underline{\Phi}_\ell,\ldots,\underline{\Phi}_s\right) .$$

As mentioned before, application of direct search methods will be time consuming since every function evaluation requires the solution of the system and sensitivity differential equation, (5.1-22), (5.1-27) and (5.1-29). In the present case of linear system models, however, the repeated integration of differential equations for every function evaluation can be avoided. To this end a set of so called *elementary information matrices* is calculated instead. Each of these matrices corresponds to particular elementary input signals defined by equation (5.1-6).

Now it is shown that M can be determined directly from these elementary information matrices. As discussed above, the information matrix M is computed from the sensitivity matrix S, which is composed of the sensitivity matrices S_θ and S_{x_0} for the parameter vector $\underline{\theta}$ and the initial condition $\underline{x}_0$ respectively. The sensitivity matrices $S_\theta(i)$ at the discrete sample times $t_i \in [t_0,t_1]$ are derived from the solution of the system differential equations (5.1-22) and the sensitivity differential equations (5.1-27). The solution of these differential equations is the response to a given initial condition $\underline{x}_0$ and given input signal $\underline{u}(t)$, $t\in[t_0,t_1]$. It is readily ascertained that the relations (5.1-22) and (5.1-27) represent a set of nonhomogeneous linear ordinary differential equations. This means that the solution of these differential equations is in fact a superposition of the response of the homogeneous equations to the initial condition $\underline{x}_0$, and the response of the nonhomogeneous equations to the forcing function $\underline{u}$ with zero initial condition.

According to equation (5.1-7), the forcing function or input signal $\underline{u}$ is composed of linear combinations of elementary input signals $\underline{e}_i$:

$$\underline{u}(t) = \sum_{i=1}^{q} \beta_i \cdot \underline{e}_i(t) .$$

Due to the linearity of the nonhomogeneous differential equations (5.1-22) and (5.1-27), the response to $\underline{u}$ is in fact identical to a superposition of elementary responses to elementary input signals $\underline{e}_i$. This allows the total sensitivity matrix $S_\theta(t)$ to be written as follows:

$$S_\theta(t) = \sum_{i=1}^{q} \beta_i \cdot S_\theta(t,i) , \qquad (5.1\text{-}31)$$

in which index i refers to the elementary input signal $\underline{e}_i$. The matrices $S_\theta(t,i)$ are, for obvious reasons, called here *elementary sensitivity matrices*. Turning now to the sensitivity matrix S(t) in equation (5.1-26) it should be remarked that $\underline{x}_0$, although assumed zero in the manoeuvre optimization process, has still to be estimated from the actual flight test data. Keeping this in mind, S(t) may be written as:

$$S(t) = \left[\sum_{i=1}^{q} \beta_i \cdot S_\theta(t,i) \;\vdots\; S_{x_0}(t)\right] . \qquad (5.1\text{-}32)$$

This expression for the sensitivity matrix may be substituted in Equation (5.1-25) for the information matrix M of the parameter vector $\underline{\theta}$ and the vector of initial conditions $\underline{x}_0$.

The result is that the information matrix M can be expressed as:

$$M = \begin{bmatrix} \sum_{i=1}^{q}\sum_{j=1}^{q} \beta_i\beta_j \cdot M_{\theta\theta}(i,j) & \vdots & \sum_{i=1}^{q} \beta_i \cdot M_{\theta x_0}(i) \\ \cdots\cdots\cdots\cdots & \cdot\vdots\cdot & \cdots\cdots\cdots \\ \sum_{i=1}^{q} \beta_i \cdot M_{x_0\theta}(i) & \vdots & M_{x_0x_0} \end{bmatrix} , \tag{5.1-33}$$

where the following so called *elementary information matrices* are introduced:

$$\begin{aligned} M_{\theta\theta}(i,j) &= \sum_{k=1}^{N} S_\theta^T(k,i) \cdot V_{vv}^{-1} \cdot S_\theta(k,j) , \\ M_{\theta x_0}(i) &= \sum_{k=1}^{N} S_\theta^T(k,i) \cdot V_{vv}^{-1} \cdot S_{x_0}(k) , \\ M_{x_0\theta}(i) &= \sum_{k=1}^{N} S_{x_0}^T(k) \cdot V_{vv}^{-1} \cdot S_\theta(k,i) , \end{aligned} \tag{5.1-34}$$

and where:

$$M_{x_0x_0} = \sum_{k=1}^{N} S_{x_0}^T(k) \cdot V_{vv}^{-1} \cdot S_{x_0}(k) . \tag{5.1-35}$$

It is noted that the elementary information matrices introduced in equation (5.1-34) are not information matrices in the sense of Fisher because, in general, they are not symmetrical. It follows from equation (5.1-34) that:

$$M_{\theta\theta}(i,j) = M_{\theta\theta}^T(i,j) , \tag{5.1-36}$$

and:

$$M_{\theta x_0}(i) = M_{x_0\theta}^T(i) . \tag{5.1-37}$$

For the computation of the elementary information matrices in equation (5.1-34), the input signal $\underline{u}$, that is the values of the parameters β_i in equation (5.1-7), may be yet unknown. This means that, these elementary information matrices may be computed prior to the actual optimization of the object function given by the criterion in (5.1-21). It should be noted that the asymmetrical relations (5.1-36) and (5.1-37) may be employed to reduce the total number of different elementary information matrices to be computed.
The information matrix M in relation (5.1-33) can be calculated from these elementary information matrices for any set of values of the parameters β_i, that is any input signal $\underline{u}$ of the form (5.1-7). Accordingly, the elementary information matrices are computed only once for a given set of elementary input signals $\underline{e}_i$.
In cases where direct search methods are applied for the optimization of the object function, it is not uncommon that the function has to be evaluated in a very large number of points in the space of its arguments. In those cases, the calculation of M with relation (5.1-33) instead from relation (5.1-25), will result in a considerable reduction of computation of time needed for the optimization of J.

5.1.4 Application of the Method of Newton and Raphson

Experience gained in the course of the work with Powell's direct search method [170], showed that convergence became progressively slower as the total number of spherical coordinates in equation (5.1-21) increased. This limited the number of arguments for practical purposes to approximately 20.
A very attractive characteristic of Newton-Raphson methods, [174], is that the sequence of steps to a local extreme may be given a simple geometrical interpretation. Furthermore, the original method may readily be modified in order to assure convergence in cases of large numbers of arguments [130 and 173].
The slightly disappointing performance of Powell's direct search method and the attractive properties of Newton-Raphson methods led to the application of these latter methods to the present problem of input signal optimization.

For application of Newton-Raphson methods it is convenient to introduce a new vector $\underline{\Phi}$ of spherical coordinates which contains all vectors $\underline{\phi}_\ell$, ℓ=1(1)s, in (5.1-21), s denoting again the dimension of the input signal $\underline{u}$. As explained earlier in section 5.1.2, each vector $\underline{\phi}_\ell$ is of the same dimension (p-1). This means that the new vector $\underline{\Phi}$ is of dimension s·(p-1). $\underline{\Phi}$ can be defined similarly to $\underline{\beta}$, as:

$$\underline{\Phi} = \begin{pmatrix} \underline{\phi}_1 \\ \vdots \\ \underline{\phi}_\ell \\ \vdots \\ \underline{\phi}_s \end{pmatrix} \tag{5.1-38}$$

Starting from a given approximation $\underline{\phi}(i)$ of $\underline{\phi}_{stat}$ at which J attains a stationary and therefore extreme value, the Newton-Raphson method of calculating a closer approximation $\underline{\phi}(i+1)$ is:

$$\underline{\phi}(i+1) = \underline{\phi}(i) - \left[\frac{\partial^2 J}{\partial \underline{\phi}\ \partial \underline{\phi}^T}\right]^{-1} \cdot \frac{\partial J}{\partial \underline{\phi}}, \qquad (5.1\text{-}39)$$

assuming, that the Hessian matrix $\partial^2 J/(\partial\underline{\phi}\partial\underline{\phi}^T)$ is either positive or negative definite.
The Newton-Raphson method requires calculation of the first and second order partial derivatives of J, with respect to its arguments, the elements of $\underline{\phi}$. It is possible to derive analytical expressions for these derivatives in terms of the elementary information matrices $M_{\theta\theta}(i,j)$, $M_{\theta x_0}(i)$ and $M_{x_0\theta}(i)$. This leads to significant savings in computing time, as the elementary information matrices are calculated only once for a given set of elementary input signals.
The Newton-Raphson method itself is discussed in more detail by Schmidt [174]. The original method was modified, in order to assure convergence in cases where the Hessian matrix was ill-conditioned [173].

The Newton-Raphson method was applied to the optimization of rudder and aileron input signals for the aircraft and flight conditions in chapter 6. Present experience is that the algorithm quickly converges even in cases with up to 62 arguments (s=2, p=32) [29].

5.2 Effect of Decomposition of System Parameter-State Estimation Problems

The subject of section 5.1 was the optimization of input signals for nonlinear and linear deterministic systems with respect to different scalar norms of Fisher's information matrix M. According to equation (5.1-17), the information matrix could be partitioned as:

$$M = \begin{bmatrix} M_{\theta\theta} & \vdots & M_{\theta x_0} \\ \cdots & \cdot\vdots\cdot & \cdots \\ M_{x_0\theta} & \vdots & M_{x_0 x_0} \end{bmatrix},$$

in which the subscripts θ and $\underline{x}_0$ refer to the r-dimensional parameter vector $\underline{\theta}$ and the n-dimensional vector $\underline{x}_0$ of initial conditions respectively. The particular form of M reflects the fact that the parameter vector $\underline{\theta}$, as well as the initial state vector $\underline{x}_0$, are to be estimated simultaneously from given sets of observation measurements of the response of the system to a given input signal $\underline{u}$ and initial condition $\underline{x}_0$. Therefore, it would perhaps be appropriate to call M as defined in equation (5.1-17), the *joint information matrix* of $\underline{\theta}$ and $\underline{x}_0$. Correspondingly, the estimates $\hat{\underline{\theta}}$ and $\hat{\underline{x}}_0$ arise as the solution of what is called a *joint parameter-state estimation problem.*

In the present section, a particular class of deterministic, linear system and observation models is described, which allows decomposition of the joint parameter-state estimation problem into two other estimation problems i.e. a state reconstruction problem and a parameter estimation problem. These two estimation problems are independent in the sense that the joint information matrix has the following form:

$$M = \begin{bmatrix} M_{\theta\theta} & \vdots & O \\ \cdots & \cdot\vdots\cdot & \cdots \\ O & \vdots & M_{x_0 x_0} \end{bmatrix}. \qquad (5.2\text{-}1)$$

This class of system- and observation models allows application of the *two-step method* for dynamic flight test data analysis as discussed in chapter 4. If the parameter-state estimation problem can be decomposed, it is possible to compute the elementary information matrices as defined in section 5.1.3 much more efficiently.

It can be seen that in correspondence with the results of section 5.1.2, the class of deterministic, linear system and observation models considered here, the parameters to be estimated are absent in the system matrices F and G [equation (5.1-22)] but present only in the matrices H and J of the observation model [equation (5.1-23)]. Interestingly, these parameters appear only in some part of the total number of rows of these observation matrices. This permits the separation of the elements of the observation vector $\underline{y}$ into two different groups, as elements of the vectors $\underline{y}_1$ and $\underline{y}_2$. The elements of $\underline{y}_1$ correspond to the rows in H and J containing no parameters to be estimated, while the elements of $\underline{y}_2$ correspond to the rows of matrices H and J which contain one or more of those parameters. The corresponding system and

observation models may now be written as:

$$\begin{aligned} \dot{\underline{x}}(t) &= F\underline{x}(t) + G\underline{u}(t) , \\ \underline{y}_1(i) &= H_1\underline{x}(i) + J_1\underline{u}(i) , \\ \underline{y}_2(i) &= H_2(\underline{\theta})\underline{x}(i) + J_2(\underline{\theta})\underline{u}(i) . \end{aligned} \tag{5.2-2}$$

in which the index i refers to discrete instants of time $t_i \in [t_0,t_1]$, i=1(1)N, $\underline{x}$ again denotes the n-dimensional state vector and $\underline{u}$ the s-dimensional input signal. $\underline{y}_1$ and $\underline{y}_2$ denote the components of the observation vector $\underline{y}$ of dimension m_1 and m_2 respectively. The separation of the elements of $\underline{y}$ into two groups corresponds, of course, to the following partitioning of the original observation matrices H and J in as:

$$H(\underline{\theta}) = \begin{bmatrix} H_1 \\ \cdots\cdots \\ H_2(\underline{\theta}) \end{bmatrix} , \tag{5.2-3}$$

$$J(\underline{\theta}) = \begin{bmatrix} J_1 \\ \cdots\cdots \\ J_2(\underline{\theta}) \end{bmatrix} .$$

It is assumed that the components $\underline{y}_1$ and $\underline{y}_2$ of the observation vector $\underline{y}$, are corrupted by additive measurement errors according to:

$$\begin{aligned} \underline{y}_{1_m}(i) &= \underline{y}_1(i) + \underline{v}_1(i) , \\ \underline{y}_{2_m}(i) &= \underline{y}_2(i) + \underline{v}_2(i) , \end{aligned} \tag{5.2-4}$$

where $\underline{v}_1(i)$ and $\underline{v}_2(i)$ are components of an m-dimensional vector $\underline{v}(i)$ with dimensions m_1 and m_2. These measurement errors are represented by stationary Gaussian sequences of stochastic variables with zero mean and uncorrelated in time. In addition, it is also assumed that the elements of $\underline{v}_1(i)$ are not correlated with the elements of $\underline{v}_2(i)$. The above assumptions correspond to:

$$E\{\underline{v}(i)\} = E\left\{\begin{pmatrix} \underline{v}_1(i) \\ \cdots\cdots \\ \underline{v}_2(i) \end{pmatrix}\right\} = \underline{0} ,$$

$$E\{\underline{v}(i)\underline{v}^T(j)\} = E\left\{\begin{bmatrix} \underline{v}_1(i)\underline{v}_1^T(j) & \vdots & \underline{v}_1(i)\underline{v}_2^T(j) \\ \cdots\cdots & \cdot\vdots\cdot & \cdots\cdots \\ \underline{v}_2(i)\underline{v}_1^T(j) & \vdots & \underline{v}_2(i)\underline{v}_2^T(j) \end{bmatrix}\right\}$$

$$= \begin{bmatrix} V_{v_1v_1} & \vdots & O \\ \cdots\cdots & \cdot\vdots\cdot & \cdots\cdots \\ O & \vdots & V_{v_2v_2} \end{bmatrix} \cdot \delta_{ij} = V_{vv} \cdot \delta_{ij} \tag{5.2-5}$$

for i,j=1(1)N.

Now we compute the joint information matrix M in equation (5.2-1) for the system and observation models in equations (5.2-2) and (5.2-4) respectively and the measurement statistics in (5.2-5) as:

$$M = \sum_{i=1}^{N} S^T(i) \cdot V_{vv}^{-1} \cdot S(i) ,$$

where the sensitivity matrix S(t) can be partitioned as:

$$S(t) = \left[S_\theta(t) \quad S_{x_0}(t)\right] .$$

Each of the sensitivity matrices $S_\theta(t)$ and $S_{x_0}(t)$ can be partitioned next according to the partitioning of $\underline{y}(t)$ in $\underline{y}_1(t)$ and $\underline{y}_2(t)$:

$$S(t) = \begin{bmatrix} S_{\theta_1}(t) & \vdots & S_{x_{0_1}}(t) \\ \cdots\cdots & \cdot\vdots\cdot & \cdots\cdots \\ S_{\theta_2}(t) & \vdots & S_{x_{0_2}}(t) \end{bmatrix} . \tag{5.2-6}$$

Finally, the matrices $S_{\theta_1}(t)$ and $S_{\theta_2}(t)$ may be partitioned into column vectors for each of the elements θ_j of the parameter vector $\underline{\theta}$. In similar way, the matrices $S_{x_{o_1}}(t)$ and $S_{x_{o_2}}(t)$ may be partitioned in column vectors for each of the elements x_{0_j} of the initial state vector $\underline{x}_0$. The constituting column vectors of partial derivatives obey the following relations which are readily seen to be equivalent to relations in (5.1-28) and (5.1-30):

$$\begin{aligned} \underline{y}_{1_{\theta_j}}(i) &= H_1\underline{x}_{\theta_j}(i) + H_{1_{\theta_j}}\underline{x}(i) + J_{1_{\theta_j}}\underline{u}(i) , \\ \underline{y}_{2_{\theta_j}}(i) &= H_2(\underline{\theta})\underline{x}_{\theta_j}(i) + H_{2_{\theta_j}}(\underline{\theta})\underline{x}(i) + J_{2_{\theta_j}}(\underline{\theta})\underline{u}(i), \end{aligned} \tag{5.2-7}$$

$$\underline{y}_{1_{x_{0_j}}}(i) = H_1 \underline{x}_{x_{0_j}}(i) ,$$
$$\underline{y}_{2_{x_{0_j}}}(i) = H_2(\underline{\theta})\underline{x}_{x_{0_j}}(i) . \qquad (5.2\text{-}8)$$

The matrices H_1 and J_1 do not contain any elements of the parameter vector $\underline{\theta}$. This means that the partial derivatives of H_1 and J_1 with respect to θ_j are zero:

$$H_{1_{\theta_j}} = O , \quad J_{1_{\theta_j}} = O ,$$

which simplifies the first of two relations in (5.2-7) to:

$$\underline{y}_{1_{\theta_j}}(i) = H_1 \underline{x}_{\theta_j}(i) . \qquad (5.2\text{-}9)$$

The partial derivatives of the state vector $\underline{x}$ with respect to θ_j obey the sensitivity differential equation (5.1-27) derived in section 5.1.3 for the case of linear system models. In the present case, the partial derivatives of F and G with respect to θ_j are equal to zero:

$$F_{\theta_j} = O , \quad G_{\theta_j} = O . \qquad (5.2\text{-}10)$$

Now the simplified sensitivity equations are:

$$\dot{\underline{x}}_{\theta_j}(t) = F\underline{x}_{\theta_j}(t) , \qquad (5.2\text{-}11)$$

with initial conditions:

$$\underline{x}_{\theta_j}(t_0) = \underline{0} ,$$

for j=1(1)r.

It can be seen that these simplified sensitivity equations are homogeneous, as the two forcing terms containing the state vector $\underline{x}$ and the input signal $\underline{u}$ have disappeared. For the given set of initial conditions the solution of these sensitivity equations is readily seen to be:

$$\underline{x}_{\theta_j}(t) = \underline{0} , \qquad (5.2\text{-}12)$$

for $t \geq t_0$ and j=1(1)r.

Substitution of equation (5.2-9) and (5.2-12) in (5.2-7) results in the following simplified expression for the partial derivatives of $\underline{y}_1(i)$ and $\underline{y}_2(i)$ with respect to θ_j:

$$\underline{y}_{1_{\theta_j}}(i) = \underline{0} ,$$
$$\underline{y}_{2_{\theta_j}}(i) = H_{2_{\theta_j}}(\underline{\theta})\underline{x}(i) + J_{2_{\theta_j}}(\underline{\theta})\underline{u}(i) . \qquad (5.2\text{-}13)$$

It is not possible, to simplify the relations in (5.2-8) for the partial derivatives of $\underline{y}_1(i)$ and $\underline{y}_2(i)$ with respect to the elements x_{0_j} of the initial state vector $\underline{x}_0$. Substituting $F(\underline{\theta})=F$, the sensitivity differential equations (5.1-29) as derived in section 5.1.3 can be written as:

$$\dot{\underline{x}}_{x_{0_j}}(t) = F\underline{x}_{x_{0_j}}(t) , \qquad (5.2\text{-}14)$$

with initial conditions:

$$\underline{x}_{\underline{x}_0}(t_0) = I ,$$

for j=1(1)n.

It may be concluded from the above that, for the present class of system and observation models, the calculation of the sensitivity matrices S(i) as defined in (5.2-6) is significantly simplified. This is due to the fact, that the sensitivity matrix $S_{\theta_1}(i)$ is equal to zero and that for the calculation of the sensitivity matrix $S_{\theta_2}(i)$ it is no longer necessary to solve the corresponding sets of sensitivity differential equations (5.1-27).

It is possible, however, to simplify the calculation of the joint information matrix M in (5.1-17) still further. This next simplification exploits the decomposition of the joint parameter-state estimation problem into independent state and parameter estimation problems. The feasibility of such a decomposition arises when the system model and the first part of the observation model presented in equation (5.2-2), viz:

$$\dot{\underline{x}}(t) = F\underline{x}(t) + G\underline{u}(t) ,$$
$$\underline{y}_1(i) = H_1\underline{x}(i) + J_1\underline{u}(i) .$$

result in a reconstructible state vector [70]. This implies that the following information matrix:

$$M_{x_0x_0} = \sum_{i=1}^{N} S_{x_{0_1}}{}^T(i) \cdot V_{v_1v_1}^{-1} \cdot S_{x_{0_1}}(i) , \qquad (5.2\text{-}15)$$

is of full rank n, and that all components of $\underline{x}_0$ can be estimated from the set of N observation measurements $\underline{y}_{1_m}(i)$. Neglecting the information

contained in the observation measurements $\underline{y}_2(i)$ concerning the initial state vector $\underline{x}_0$ is equivalent to substituting:

$$S_{x_{0_2}}(i) = O \tag{5.2-16}$$

in the partitioned sensitivity matrix S(i), as defined in (5.2-6). If in addition,

$$S_{\theta_1}(i) = O \tag{5.2-17}$$

is substituted in (5.2-6), the result is:

$$S(i) = \begin{bmatrix} O & \vdots & S_{x_{0_1}}(i) \\ \cdots & \cdot\vdots\cdot & \cdots \\ S_{\theta_2}(i) & \vdots & O \end{bmatrix} . \tag{5.2-18}$$

Using relations (5.2-18) and (5.2-5) in (5.1-25) leads to the following form for the joint matrix M:

$$M = \begin{bmatrix} M_{\theta\theta} & \vdots & O \\ \cdots & \cdot\vdots\cdot & \cdots \\ O & \vdots & M_{x_0x_0} \end{bmatrix} \tag{5.2-19}$$

where:

$$\begin{aligned} M_{\theta\theta} &= \sum_{i=1}^{N} S_{\theta_2}^T(i) \cdot V_{v_2v_2}^{-1} \cdot S_{\theta_2}(i) \\ M_{x_0x_0} &= \sum_{i=1}^{N} S_{x_{0_1}}^T(i) \cdot V_{v_1v_1}^{-1} \cdot S_{x_{0_1}}(i) \end{aligned} \tag{5.2-20}$$

When the three criteria J for the optimization of input signals are applied to M, they can be written as:

a) $J = \mathrm{tr}M = \mathrm{tr}M_{\theta\theta} + \mathrm{tr}M_{x_0x_0}$,

b) $J = \ln\det M = \ln\det M_{\theta\theta} + \ln\det M_{x_0x_0}$,

c) $J = \mathrm{tr}M^{-1} = \mathrm{tr}M_{\theta\theta} + \mathrm{tr}M_{x_0x_0}^{-1}$.

The matrix $M_{x_0x_0}$ cannot be influenced by form or energy of the system input signals [29]. This means that in the expressions for the three criteria above, the terms containing $M_{x_0x_0}$ are constant. Consequently, the optimization of input signals may be based on one of the following simplified criteria:

a) $J = \mathrm{tr}M_{\theta\theta}$,

b) $J = \ln\det M_{\theta\theta}$,

c) $J = \mathrm{tr}M_{\theta\theta}^{-1}$.

It may be concluded that for the present class of system and observation models, the optimization of input signals requires computation of only one of the matrices in the partitioned joint information matrix M in (5.1-17), i.e. $M_{\theta\theta}$, the information matrix for the parameter vector $\underline{\theta}$.

Analogous to section 5.1.3, the information matrix $M_{\theta\theta}$ above can be computed from a set of elementary information matrices $M_{\theta\theta}(i,j)$. According to (5.1-33), $M_{\theta\theta}$ can be written as:

$$M_{\theta\theta} = \sum_{i=1}^{q} \sum_{j=1}^{q} \beta_i\beta_j \cdot M_{\theta\theta}(i,j) \tag{5.2-21}$$

in which β_i denotes again a weighting factor in the s-dimensional input signal $\underline{u}$ and q=s·p, p denoting the selected number of orthonormal functions in (5.1-7). The general form of the elementary information matrix $M_{\theta\theta}(i,j)$ is given by:

$$M_{\theta\theta}(i,j) = \sum_{k=1}^{N} S_\theta^T(k,i) \cdot V_{vv}^{-1} \cdot S_\theta(k,j) , \tag{5.2-22}$$

where the index k refers to the discrete sample time $t_k \in [t_0,t_1]$, and $S_\theta(k,i)$ denotes an elementary sensitivity matrix for the elementary input signal $\underline{e}_i$. $S_\theta(k,i)$ is the result of the response of the system to this elementary input signal $\underline{e}_i$, starting from the initial condition $\underline{x}_0=\underline{0}$ at time t_0.
The elementary information matrices may be written as:

$$M_{\theta\theta}(i,j) = \sum_{k=1}^{N} S_{\theta_2}^T(k,i) \cdot V_{v_2v_2}^{-1} \cdot S_{\theta_2}(k,j) . \tag{5.2-23}$$

where the sensitivity matrices $S_{\theta_2}(k,i)$ are independent of the solutions of sensitivity differential equations, just as $S_{\theta_2}(k)$. The only difference is in the input signal and the initial condition, i.e. $\underline{e}_i$ and $\underline{x}_0=\underline{0}$ for $S_{\theta_2}(k,i)$ rather than $\underline{u}$ and an arbitrary $\underline{x}_0$ for $S_\theta(k)$. No sensitivity differential equations need to be solved when computing the elementary information matrices $M_{\theta\theta}(i,j)$ in equation (5.2-23). This leads to considerable savings in computing time.

The results of the present section were applied to the optimization of the longitudinal and lateral control input signals for the dynamic flight test manoeuvres as described in chapter 6.

In section 5.1.3 the optimization of input signals is

based on scalar norms of the information matrix M in (5.1-33). In the present section it was shown that for the system and observation models given in equation (5.2-2), simplified criteria can be used based on the information matrix $M_{\theta\theta}$ given in equation (5.2-21).

5.3 Input Signal Optimization for Linear Systems in Frequency Domain

The present section describes a method for the optimization in the frequency domain of multi-dimensional input signals for parameter estimation of linear systems [215,216]. The method was initially developed by Mehra [164,165] and is also discussed by Goodwin and Payne [161]. It can be shown that in the frequency domain each Fisher information matrix is an element of a convex set of *point-input information matrices* which encloses all realizable input power constrained information matrices. With this property, the optimal information matrix and the optimal input signal can be expressed as a linear combination of point-input information matrices and harmonic input signals respectively. The efficiency of the method is enhanced by taking account of the application of the two-step method for parameter estimation, see chapter 4. This leads to a reduction of the minimum number of harmonic signals in the optimized input signal. Convex analysis is used later on to prove the global optimality of the input design.

5.3.1 Fisher's Information Matrix in the Frequency Domain

In the present section, Fisher's information matrix is derived for the class of linear system- and observation models as defined in section 5.2, which allows decomposition of the joint parameter-state estimation problem. For input optimization it is sufficient to consider only the following system and observation model:

$$\begin{aligned} \dot{\underline{x}}(t) &= F(\underline{\theta})\,\underline{x}(t) + G(\underline{\theta})\,\underline{u}(t) \\ \underline{y}_2(t) &= H_2(\underline{\theta})\,\underline{x}(t) + J_2(\underline{\theta})\,\underline{u}(t) \\ \underline{y}_{m_2}(i) &= \underline{y}_2(i) + \underline{v}_2(i) \end{aligned} \qquad (5.3\text{-}1)$$

$i = 1(1)N$

where $\underline{x}(t)$ denotes the n-dimensional state vector and $\underline{u}(t)$ the s-dimensional input signal of either the longitudinal or the lateral-directional linearized equations of motion, see chapter 2. The m_2-dimensional observation vector $\underline{y}_2(t)$ belongs to the second part of the observation model which contains all parameters to be estimated. These parameters are collected in the r-dimensional parameter vector $\underline{\theta}$. The observations of $\underline{y}_1$ belonging to the first part of the observation model are only used in the state estimation problem. These latter observations do not contribute to the information matrix of $\underline{\theta}$ if state estimation errors are small enough to be negligible. Additive measurement and/or model errors are assumed with a Gaussian distribution:

$$\begin{aligned} E\{\underline{v}_2(i)\} &= \underline{0} \\ E\{\underline{v}_2(i)\underline{v}_2^T(j)\} &= V_{v_2v_2}\cdot\delta_{ij} \\ &= \mathrm{diag}(\sigma_1^2,\ldots,\sigma_{m_2}^2)\cdot\delta_{ij} \end{aligned} \qquad (5.3\text{-}2)$$

The average information matrix* per sample $\bar{M}=M/N$ may now be written as, see also (5.2-20):

$$\begin{aligned} \bar{M} = \frac{1}{N} M &= \frac{1}{N}\sum_{i=1}^{N} \frac{\partial \underline{y}_2^T(i)}{\partial \underline{\theta}}\, V_{v_2v_2}^{-1}\, \frac{\partial \underline{y}_2(i)}{\partial \underline{\theta}^T} \\ &= \frac{1}{N}\sum_{i=1}^{N} S_{\theta_2}^T(i)\cdot V_{v_2v_2}^{-1}\cdot S_{\theta_2}(i) \end{aligned} \qquad (5.3\text{-}3)$$

For what follows it will be convenient to write (5.3-3) in continuous, rather than in discrete time. The resulting expression for $\bar{M}$ is:

$$\begin{aligned} \bar{M} &= \frac{1}{T}\int_{t=0}^{T} \frac{\partial \underline{y}_2^T(t)}{\partial \underline{\theta}}\, V_{v_2v_2}^{-1}\, \frac{\partial \underline{y}_2(t)}{\partial \underline{\theta}^T}\, dt \\ &= \frac{1}{T}\int_{t=0}^{T} S_{\theta_2}^T(t)\cdot V_{v_2v_2}^{-1}\cdot S_{\theta_2}(t)\, dt \end{aligned} \qquad (5.3\text{-}4)$$

The frequency domain representation of $\bar{M}$ is obtained by applying Parseval's theorem:

$$\begin{aligned} \bar{M} &= \frac{1}{T}\frac{1}{2\pi}\int_{\omega=-\infty}^{+\infty} \frac{\partial \underline{Y}_2^T(\omega)}{\partial \underline{\theta}}\, V_{v_2v_2}^{-1}\, \frac{\partial \underline{Y}_2(-\omega)}{\partial \underline{\theta}^T}\, d\omega \\ &= \frac{1}{T}\frac{1}{2\pi}\int_{\omega=-\infty}^{+\infty} S_{\theta_2}^T(\omega)\cdot V_{v_2v_2}^{-1}\cdot S_{\theta_2}(-\omega)\, d\omega \end{aligned} \qquad (5.3\text{-}5)$$

---

* The matrix M denotes the information matrix $M_{\theta\theta}$ for the parameter vector $\underline{\theta}$ in the remaining.

In the frequency domain $\underline{Y}_2(\omega)$ can be obtained from Fourier transforming the system equations (5.3-1):

$$\begin{aligned}\underline{Y}_2(\omega) &= H_2(\underline{\theta})\underline{X}(\omega) + J_2(\underline{\theta})\underline{U}(\omega) \\ &= \left[H_2(\underline{\theta})T(\omega,\underline{\theta}) + J_2(\underline{\theta})\right]\underline{U}(\omega)\end{aligned} \tag{5.3-6}$$

where:

$$T(\omega,\underline{\theta}) = \left[j\omega I - F(\underline{\theta})\right]^{-1} G(\underline{\theta}) \tag{5.3-7}$$

The columns of the sensitivity matrix $S_{\theta_2}(\omega)$ follow from partial differentiation of $\underline{Y}_2(\omega)$ with respect to individual elements of $\underline{\theta}$:

$$\frac{\partial \underline{Y}_2(\omega)}{\partial \theta_k} = \left[\frac{\partial H_2(\underline{\theta})}{\partial \theta_k} T(\omega,\underline{\theta}) + H_2(\underline{\theta})\frac{\partial T(\omega,\underline{\theta})}{\partial \theta_k} + \frac{\partial J_2(\underline{\theta})}{\partial \theta_k}\right]\underline{U}(\omega) \tag{5.3-8}$$

The above expressions implicitly assume a steady state response of the system, so the system should be stable and the observation time interval T large enough for the effect of transients to be negligible. From (5.3-7) it follows that the frequency response matrix $T(\omega,\underline{\theta})$ depends on the parameter vector $\underline{\theta}$. In the two-step method, however, the state is reconstructed in the first step using a kinematical model, see chapter 3, while the second step in which the parameters are estimated has no influence on the first step. In the present context this means that the dependence of $T(\omega,\underline{\theta})$ on the parameter vector $\underline{\theta}$ should be disregarded. This is expressed in what follows by writing $T(\omega)$ rather than $T(\omega,\underline{\theta})$. Substituting $\partial T(\omega,\underline{\theta})/\partial\theta_k = O$ in (5.3-8) results in:

$$\frac{\partial \underline{Y}_2(\omega)}{\partial \theta_k} = \left[\frac{\partial H_2(\underline{\theta})}{\partial \theta_k} T(\omega) + \frac{\partial J_2(\underline{\theta})}{\partial \theta_k}\right]\underline{U}(\omega) \tag{5.3-9}$$

Each of the elements of the matrices $H_2(\underline{\theta})$ and $J_2(\underline{\theta})$ corresponds to one of the stability and control derivatives in the parameter vector $\underline{\theta}$. If no derivatives would be excluded from $\underline{\theta}$ (i.e. $\underline{\theta}$ contains $m_2(n+s)$ derivatives) then by substituting the partial derivatives of the matrices $H_2(\underline{\theta})$ and $J_2(\underline{\theta})$ into equation (5.3-9) it is readily seen that the senstivity matrix $S_{\theta_2}(\omega)$ can be written as:

$$S_{\theta_2}(\omega) = \begin{bmatrix} \underline{U}^T(\omega)T^T(\omega) & & \underline{U}^T(\omega) & & O \\ & \ddots & & \ddots & \\ O & & \underline{U}^T(\omega)T^T(\omega) & & \underline{U}(\omega) \end{bmatrix} \tag{5.3-10}$$

Noting that $V_{v_2v_2}$ is a diagonal matrix, one can easily verify by substituting (5.3-10) in (5.3-5) that the average information matrix takes a block diagonal structure:

$$\bar{M} = \begin{bmatrix} \bar{M}_1 & & O \\ & \ddots & \\ O & & \bar{M}_{m_2} \end{bmatrix} \tag{5.3-11}$$

Each individual block in (5.3-11) can be written as:

$$\bar{M}_j = \frac{1}{\sigma_j^2}\frac{1}{2\pi}\int_{\omega=-\infty}^{+\infty} \hat{M}(\omega)\ \mathrm{tr}\{S_{uu}(\omega)\}\ d\omega \tag{5.3-12}$$

$j = 1(1)m_2$

where:

$$\begin{aligned}\hat{M}(\omega) &= \mathrm{Re}\left\{\begin{bmatrix} T(\omega) \\ \cdots \\ I \end{bmatrix} \hat{S}_{uu}^T(\omega)\left[T^H(\omega) \ \vdots\ I\right]\right\} \\ \hat{S}_{uu}(\omega) &= \frac{1}{\mathrm{tr}\{S_{uu}(\omega)\}} S_{uu}(\omega) \\ S_{uu}(\omega) &= \frac{1}{T}\underline{U}(-\omega)\underline{U}^T(\omega)\end{aligned} \tag{5.3-13}$$

and the subscript ^{H} denotes the conjugate transpose. If the parameters in each output equation are with respect to the same state variables and inputs, then the blocks $\bar{M}_j$ in (5.3-11) are identical except for a scalar factor $1/\sigma_j^2$. Otherwise, each block $\bar{M}_j$ can be derived from the matrix $\hat{M}(\omega)$ by omitting rows and columns form $\hat{M}(\omega)$ corresponding to the excluded derivatives in the j-th output equation.

$\hat{M}(\omega)$ in (5.3-12) may be expressed as a function of numerator and denominator polynomials in the frequency response matrix $T(\omega)$ and the power spectral density matrix $S_{uu}(\omega)$ of the input signal $\underline{u}(t)$. By representing each element of the frequency response matrix $[T(\omega)]_{k\ell}$ as a rational function with varying polynomials $n^{(k\ell)}(\omega)$ in the numerator and a common polynomial $d(\omega)$ in the denominator according to:

$$[T(\omega)]_{k\ell} = \frac{n^{(k\ell)}(\omega)}{d(\omega)} = \frac{b_0^{(k\ell)} + b_1^{(k\ell)} j\omega + \ldots + b_{n-1}^{(k\ell)} (j\omega)^{n-1}}{a_0 + a_1 j\omega + \ldots + a_{n-1}(j\omega)^{n-1} + (j\omega)^n} \qquad (5.3\text{-}14)$$

$k=1(1)n$, $\ell=1(1)s$

one obtains:

$$\hat{M}(\omega) = \frac{1}{|d(\omega)|^2} \mathrm{Re}\{N(\omega)\, \hat{S}_{uu}^{T}(\omega)\, N^{H}(\omega)\} \qquad (5.3\text{-}15)$$

where:

$$N(\omega) = \begin{bmatrix} n^{(11)}(\omega) & \ldots & n^{(1s)}(\omega) \\ \vdots & & \vdots \\ n^{(n1)}(\omega) & \ldots & n^{(ns)}(\omega) \\ d(\omega) & & O \\ & \ddots & \\ O & & d(\omega) \end{bmatrix} \qquad (5.3\text{-}16)$$

5.3.2 Representation of the Information Matrix in Information Space

The average information matrix as defined in (5.3-11) may be represented by an *information vector* $\underline{\psi}$ with components ψ_i in an *information space* $\mathcal{R}_{\bar{M}}$ spanned by basis vectors $\underline{e}_i$:

$$\underline{\psi} = \sum_{i=1}^{d} \psi_i \cdot \underline{e}_i \qquad (5.3\text{-}17)$$

The vector representation of $\bar{M}$ is intelligently chosen so that the dimension of $\mathcal{R}_{\bar{M}}$ is as small as possible. As shown in the previous section $\bar{M}$ may completely be reconstructed via the block matrices $\bar{M}_j$ where each block is derived from the matrix $\hat{M}(\omega)$. The information vector is therefore compiled from the independent elements of $\hat{M}(\omega)$. It follows from equation (5.3-15) that $\hat{M}(\omega)$ is a symmetric (n+s)×(n+s) matrix. This means that $\underline{\psi}$ may be composed of just the $d=\frac{1}{2}(n+s)(n+s+1)$ upper triangular elements in $\hat{M}(\omega)$:

$$\underline{\psi} = \frac{1}{2\pi} \int_{\omega=-\infty}^{+\infty} \hat{\underline{\psi}}(\omega)\, \mathrm{tr}\{S_{uu}(\omega)\}\, d\omega$$

$$\hat{\underline{\psi}}(\omega) = \mathrm{col}\left([\hat{M}(\omega)]_{11} , [\hat{M}(\omega)]_{12} , \ldots , [\hat{M}(\omega)]_{(n+s)(n+s)} \right) \qquad (5.3\text{-}18)$$

where $\bar{M}_j$ follows from:

$$\bar{M}_j = \frac{1}{\sigma_j^2} \begin{bmatrix} \psi_1 & \psi_2 & \ldots & \psi_{n+s} \\ \psi_2 & \psi_{n+s+1} & \vdots & \\ \vdots & & & \\ \psi_{n+s} & \ldots & & \psi_{\frac{1}{2}(n+s)(n+s+1)} \end{bmatrix} \qquad (5.3\text{-}19)$$

Power constraints on input signals may be written in the frequency domain as:

$$P_u = \frac{1}{2\pi} \int_{\omega=-\infty}^{+\infty} \mathrm{tr}\{S_{uu}(\omega)\}\, d\omega \qquad (5.3\text{-}20)$$

The geometric interpretation of a power constraint is a (d-1)-dimensional hyperplane in the d-dimensional information space $\mathcal{R}_{\bar{M}}$. Consider the lower s diagonal elements of $\hat{M}(\omega)$, i.e. the elements $[\hat{M}(\omega)]_{kk}$, $k=(n+1)(1)(n+s)$. By substituting (5.3-15) in (5.3-18) it is readily shown that the sum of the corresponding components of $\underline{\psi}$ is equal to P_u:

$$\begin{aligned} \sum_{i=1}^{s} \psi_{d+1-\frac{1}{2}i(i+1)} &= \\ &= \sum_{i=1}^{s} \frac{1}{2\pi} \int_{\omega=-\infty}^{+\infty} \psi_{d+1-\frac{1}{2}i(i+1)}(\omega)\, \mathrm{tr}\{S_{uu}(\omega)\}\, d\omega \\ &= \frac{1}{2\pi} \int_{\omega=-\infty}^{+\infty} \sum_{k=n+1}^{n+s} [\hat{M}(\omega)]_{kk}\, \mathrm{tr}\{S_{uu}(\omega)\}\, d\omega \\ &= \frac{1}{2\pi} \int_{\omega=-\infty}^{+\infty} \mathrm{tr}\{\hat{S}_{uu}^{T}(\omega)\}\, \mathrm{tr}\{S_{uu}(\omega)\}\, d\omega = P_u \end{aligned} \qquad (5.3\text{-}21)$$

Now, $\bar{M}$ may be represented in terms of (d-1) basisvectors $\underline{e}_i$ and $(\underline{e}_i - \underline{e}_d)$ in the hyperplane which is positioned by the vector $P_u \cdot \underline{e}_d$:

$$\underline{\Psi} = P_u \cdot \underline{e}_d + \sum_{\substack{i=1 \\ i \notin I}}^{d-1} \psi_i \cdot \underline{e}_i + \sum_{\substack{i=1 \\ i \in I}}^{d-1} \psi_i \cdot (\underline{e}_i - \underline{e}_d)$$

$$I = \{ i \mid i = d+1-\tfrac{1}{2}j(j+1) \ , \ j = 1(1)s \} \qquad (5.3\text{-}22)$$

5.4 Calculation of Optimal Input Signals using Convex Analysis

The criterion for optimal input signals is a scalar norm J of the average information matrix $\bar{M}$. From section 5.3 above it follows that J becomes a vector function in the (d-1)-dimensional hyperplane of $\mathcal{R}_{\mathcal{M}}$. The optimal input signal $\underline{u}^o(t)$ consists of a finite number of harmonics and will produce the optimal average information matrix $\bar{M}^o$.

5.4.1 Application of Convex Analysis

The actual optimization is performed by applying convex analysis. If one defines the set $\mathcal{M}$ of all average information matrices corresponding to power constrained input designs, then $\mathcal{M}$ is a convex set. Convexity means that for two elements belonging to a set, any element on the line segment between those elements also belongs to the set. The property of convexity thus implies that any information matrix in $\mathcal{M}$, including the optimal information matrix $\bar{M}^o$, can be obtained from other information matrices in $\mathcal{M}$. We will use this property by composing the input signal $\underline{u}(t)$ of elementary signals $\underline{u}^{(k)}(t)$ in such a way that the information matrix $\bar{M}$ from $\underline{u}(t)$ is a convex combination of information matrices $\bar{M}^{(k)}$ from $\underline{u}^{(k)}(t)$. $\bar{M}$ or its representation as information vector $\underline{\Psi}$ can thus be written as:

$$\begin{aligned} \bar{M} &= \sum_k \alpha^{(k)} \, \bar{M}^{(k)} \\ \underline{\Psi} &= \sum_k \alpha^{(k)} \, \underline{\Psi}^{(k)} \\ 1 &= \sum_k \alpha^{(k)} \qquad , \alpha^{(k)} > 0 \end{aligned} \qquad (5.4\text{-}1)$$

A necessary condition for this composition is that the power spectral density matrix $S_{uu}(\omega)$ is a convex combination of the power spectral density matrices $S_{uu}^{(k)}(\omega)$ of $\underline{u}^{(k)}(t)$:

$$\begin{aligned} S_{uu}(\omega) &= \sum_k \alpha^{(k)} \, S_{uu}^{(k)}(\omega) \\ 1 &= \sum_k \alpha^{(k)} \qquad , \alpha^{(k)} > 0 \end{aligned} \qquad (5.4\text{-}2)$$

The above equation automatically implies that the elementary input signals $\underline{u}^{(k)}(t)$ also have power P_u, just as the input signal $\underline{u}(t)$ itself.
The maximum number of matrices $\bar{M}^{(k)}$ to realize any $\bar{M}$ in $\mathcal{M}$ follows from the dimension of the smallest linear variety in which $\mathcal{M}$ may be situated. As stated by the theorem of Carathéodory, see Rockafellar [221], the required number is at most that dimension plus one. Locating the set $\mathcal{M}$ in a (d-1)-dimensional hyperplane of the information space $\mathcal{R}_{\mathcal{M}}$, the number of required elementary signals $\underline{u}^{(k)}(t)$ in the input signal becomes d, i.e. the dimension of $\mathcal{R}_{\mathcal{M}}$.

5.4.2 Harmonic Input Signals

Now that the information matrix $\bar{M}$ is obtained in terms of information matrices $\bar{M}^{(k)}$ from the signals $\underline{u}^{(k)}(t)$, the problem is to find $\underline{u}^{(k)}(t)$. In principle, the signals $\underline{u}^{(k)}(t)$ should make the whole set $\mathcal{M}$ *realizable* so that the matrices $\bar{M}^{(k)}$ constitute the convex hull of $\mathcal{M}$. The set $\mathcal{M}$ is specified by all information vectors $\underline{\Psi}$ which satisfy the integral equation (5.3-18) and the power constraint (5.3-20):

$$\begin{aligned} \underline{\Psi} &= \frac{1}{2\pi} \int_{\omega=-\infty}^{+\infty} \hat{\underline{\Psi}}(\omega) \, \mathrm{tr}\{S_{uu}(\omega)\} \, d\omega \\ P_u &= \frac{1}{2\pi} \int_{\omega=-\infty}^{+\infty} \mathrm{tr}\{S_{uu}(\omega)\} \, d\omega \end{aligned} \qquad (5.4\text{-}3)$$

It can be shown that the whole convex set $\mathcal{M}$ is realizable by the choice of single harmonics with power P_u for the elementary signals $\underline{u}^{(k)}(t)$. These single harmonics have a power spectral density matrix $S_{uu}^{(k)}(\omega)$ whose trace is a Dirac pulse with magnitude πP_u at their frequencies $\omega=\omega_k$. The information matrices $\bar{M}^{(k)}$ become *point-input information matrices* and they are represented by the information vectors $P_u \underline{\Psi}(\omega_k)$. The s-dimensional elementary input signal $\underline{u}^{(k)}(t)$ is now defined by:

$$\underline{u}^{(k)}(t) = \mathrm{col}\left(u_{k1}(t),\ldots,u_{ks}(t)\right)$$

$$u_{kp}(t) = \begin{cases} \mu_{kp}\sin(\omega_k t+\varphi_{kp}) & , \omega_k \neq 0 \\ \tfrac{1}{2}\mu_{kp}\sqrt{2} & , \omega_k = 0 \end{cases} \qquad (5.4\text{-}4)$$

$$p=1(1)s \ , \ t\in[0,T] \ , \ \omega_k T/2\pi \in \mathbb{N}, \ \sum_{p=1}^{s}\mu_{kp}^2 = 2P_u$$

where μ_{kp} and φ_{kp} are the amplitude and the phase of the p-th component of $\underline{u}^{(k)}(t)$. The power specral denstiy matrix of $\underline{u}^{(k)}(t)$ is given as:

$$S_{uu}^{(k)}(\omega) = S_k^{T}\delta(\omega+\omega_k) + S_k\delta(\omega-\omega_k)$$

$$[S_k]_{pq} = \frac{\pi}{2}\mu_{kp}\mu_{kq}\times \qquad (5.4\text{-}5)$$

$$\left(\cos(\varphi_{kp}-\varphi_{kq}) - j\sin(\varphi_{kp}-\varphi_{kq})\right)$$

If the harmonics are combined into the input signal $\underline{u}(t)$, then the resulting input signal $\underline{u}(t)$ is given by:

$$\underline{u}(t) = \sum_{k=1}^{d}\sqrt{\alpha^{(k)}}\ \underline{u}^{(k)}(t) \qquad (5.4\text{-}6)$$

The average information matrix can be derived from (5.4-1) via substitution of the above $S_{uu}(\omega)$ in equation (5.3-12) for $\bar{M}_j$ and subsequently in (5.3-11) for $\bar{M}$ and in (5.3-18) for $\underline{\psi}$. For input signals formulated in the above way, the average information matrix and information vector become:

$$\bar{M} = P_u\sum_{k=1}^{d}\alpha^{(k)}\begin{bmatrix} \frac{1}{\sigma_1^2}\hat{M}(\omega_k) & & O \\ & \ddots & \\ O & & \frac{1}{\sigma_{m_2}^2}\hat{M}(\omega_k) \end{bmatrix}$$

$$\underline{\psi} = P_u\sum_{k=1}^{d}\alpha^{(k)}\,\hat{\underline{\psi}}(\omega_k) \qquad (5.4\text{-}7)$$

$$1 = \sum_{k=1}^{d}\alpha^{(k)} \quad , \alpha^{(k)} > 0$$

5.4.3 Global Optimality of Input Design

The global optimality of the optimal average information matrix $\bar{M}^o$ is examined by verifying whether the gradient of the optimization criterion J along a line segment in $\mathcal{M}$ starting from $\bar{M}^o$ in any direction is positive anywhere. If there is another (local) minimum for J, then there must exist a line segment from $\bar{M}^o$ which has negative gradients.

Consider an arbitrary information matrix $\bar{M}^*$ in $\mathcal{M}$. The complete line segment between $\bar{M}^o$ and $\bar{M}^*$ lies in $\mathcal{M}$ due to the convexity of $\mathcal{M}$. Any information matrix $\bar{M}$ on the line segment is given by:

$$\bar{M} = (1-\alpha)\bar{M}^o + \alpha\bar{M}^* \quad , 0\le\alpha\le 1 \qquad (5.4\text{-}8)$$

The gradient of J along the line segment is given by:

$$\frac{\partial J}{\partial\alpha} = \mathrm{tr}\left\{\frac{\partial J}{\partial\bar{M}}\frac{\partial\bar{M}}{\partial\alpha}\right\} = -\mathrm{tr}\left\{\frac{\partial J}{\partial\bar{M}}\left[\bar{M}^o-\bar{M}^*\right]\right\} \qquad (5.4\text{-}9)$$

The matrix $\partial J/\partial\bar{M}$ can be obtained from differentiating the optimization criteria as defined earlier with respect to $\bar{M}$. With $\bar{M}$ being a non-negative symmetric matrix, it follows that $\partial J/\partial\bar{M}$ is a non-positive symmetric matrix and thus has non-positive real eigenvalues. Let now D represent the diagonal matrix with eigenvalues μ of $\partial J/\partial\bar{M}$, and let P denote the unitary matrix with the corresponding orthonormal eigenvectors $\underline{p}$ as columns. Then the gradient satisfies:

$$\begin{aligned}\frac{\partial J}{\partial\alpha} &= -\mathrm{tr}\{PDP^H\left[\bar{M}^o-\bar{M}^*\right]\} \\ &= -\sum_{k=1}^{r}\mu_k\,[P^H\left[\bar{M}^o-\bar{M}^*\right]P]_{kk} \\ &\ge -\mu_{max}\ \mathrm{tr}\{P^H\left[\bar{M}^o-\bar{M}^*\right]P\} \\ &= -\mu_{max}\ \mathrm{tr}\{\bar{M}^o-\bar{M}^*\}\end{aligned} \qquad (5.4\text{-}10)$$

The above expression comprises the complete line segment, including $\bar{M}^o$. Since $\bar{M}^o$ is the optimal information matrix, the gradient for $\bar{M}=\bar{M}^o$ is non-negative. This implies that $\mathrm{tr}\{\bar{M}^o-\bar{M}^*\}$ is non-negative, so that $\partial J/\partial\alpha$ is non-negative along the complete line segment. Therefore, for all line segments in $\mathcal{M}$ starting from $\bar{M}^o$, the gradients are non-negative anywhere and $\bar{M}^o$ is the only minimum and thus the global minimum.

5.5 Optimization of Harmonic Input Signals

The optimization of the input signal corresponds to the search of the optimal coefficients $\alpha^{(k)}$ and the power spectral density matrices $S_{uu}^{(k)}(\omega)$ of the

elementary signals $\underline{u}^{(k)}(t)$. By restricting the $\underline{u}^{(k)}(t)$ to single harmonics with power P_u, the variables to be optimized are the frequencies ω_k in $\underline{u}^{(k)}(t)$, and the amplitudes μ_{kp} and phase shifts φ_{kp}, p=1(1)s, between the components of $\underline{u}^{(k)}(t)$. For single-input designs, μ_{k1} follows directly from P_u while φ_{k1} is cancelled out by the Fourier transformation. It is possible to specify additional constraints on the frequencies of the harmonics, for instance by choosing allowable discrete frequencies or a frequency range in the input design.

5.5.1 Application of the Gradient Method

As algorithm for the optimization, the gradient method is most attractive due to the formulation of $\bar{M}$ as convex combination. The optimization of each harmonic input signal corresponds to the search of the minimal gradient of the optimization criterion J. This leads to the frequency ω_k and the power spectral density matrix $S_{uu}^{(k)}(\omega)$ of an additional elementary signal. The matrix $S_{uu}^{(k)}(\omega)$ is later on converted to the amplitudes μ_{kp} and phases φ_{kp} for the signal components.
For finding the minimal gradient from the present iteration point, let the average information matrix $\bar{M}$ be positioned on a 'line segment' between the present iterated $\bar{M}^*$ and the point-input information matrix $\bar{M}^{(k)}$. Because of the convexity, $\bar{M}$ always belongs to the set of information matrices $\mathcal{M}$. The gradient for the criterion function J for $\bar{M}^*$ along the line segment

$$\bar{M} = (1-\alpha^{(k)})\,\bar{M}^* + \alpha^{(k)}\,\bar{M}^{(k)} \tag{5.5-1}$$

is given by:

$$\begin{aligned}\frac{\partial J(\bar{M}^*)}{\partial \alpha^{(k)}} &= \frac{\partial J(\bar{M})}{\partial \alpha^{(k)}}\bigg|_{\alpha^{(k)}=0} \\ &= \mathrm{tr}\{\frac{\partial J(\bar{M})}{\partial \bar{M}}\,\frac{\partial \bar{M}}{\partial \alpha^{(k)}}\}\bigg|_{\alpha^{(k)}=0} \\ &= -\mathrm{tr}\{\frac{\partial J(\bar{M}^*)}{\partial \bar{M}}\,[\bar{M}^*-\bar{M}^{(k)}]\}\end{aligned} \tag{5.5-2}$$

Because of the application of the two-step method, the matrices $\bar{M}^*$ and $\bar{M}^o$ have a block diagonal structure, see equation (5.3-11). With this property, the above equation can be rewritten as:

$$\begin{aligned}\frac{\partial J(\bar{M}^*)}{\partial \alpha^{(k)}} = &-\sum_{j=1}^{m_2}\mathrm{tr}\{\frac{\partial J(\bar{M}^*)}{\partial \bar{M}_j}\,\bar{M}_j^*\} + \\ &+\sum_{j=1}^{m_2}\mathrm{tr}\{\frac{\partial J(\bar{M}^*)}{\partial \bar{M}_j}\,\bar{M}_j^{(k)}\}\end{aligned} \tag{5.5-3}$$

where $\partial J/\partial \bar{M}_j$, j=1(1)$m_2$, are the block matrices on the diagonal of the matrix derivative $\partial J/\partial \bar{M}$. The first term on the right hand side is a constant which is determined by the present iteration point. The second term is influenced by the additional harmonic input signal and it has to be minimized. The matrix multiplications of $\partial J/\partial \bar{M}_j$ and $\bar{M}_j$ are now expressed as a function of the power spectral density matrix $S_{uu}^{(k)}(\omega)$ by subsequently using the equations (5.3-12) for $\bar{M}_j$ and (5.3-15) for $\bar{M}(\omega)$. This leads to:

$$\begin{aligned}&\mathrm{tr}\{\frac{\partial J(\bar{M}^*)}{\partial \bar{M}_j}\,\bar{M}_j^{(k)}\} = \\ &= \frac{1}{\sigma_j^2}\,\frac{1}{2\pi}\int_{\omega=-\infty}^{+\infty}\mathrm{tr}\{\frac{\partial J(\bar{M}^*)}{\partial \bar{M}_j}\times \\ &\quad \frac{1}{|d(\omega)|^2}\,\mathrm{Re}\{N(\omega)\,\hat{S}_{uu}^{(k)\,T}(\omega)\,N^H(\omega)\}\}\times \\ &\quad \mathrm{tr}\{S_{uu}^{(k)}(\omega)\}\,d\omega \\ &= \frac{1}{2\pi}\int_{\omega=-\infty}^{+\infty}\mathrm{Re}\;\mathrm{tr}\{Q_j(\omega)\,\hat{S}_{uu}^{(k)\,T}(\omega)\}\times \\ &\quad \mathrm{tr}\{S_{uu}^{(k)}(\omega)\}\,d\omega\end{aligned} \tag{5.5-4}$$

where:

$$Q_j(\omega) = \frac{1}{\sigma_j^2}\,\frac{1}{|d(\omega)|^2}\,N^H(\omega)\,\frac{\partial J(\bar{M}^*)}{\partial \bar{M}_j}\,N(\omega) \tag{5.5-5}$$

The matrix $Q_j(\omega)$ is a hermitian matrix which follows from the symmetric property of $\partial J/\partial \bar{M}$ and the properties of the polynomials in $N(\omega)$, see equation (5.3-16).
Now, the minimal gradient can be found by substituting the functions for the power spectral density matrices of the harmonic signals. With the hermitian property of $Q_j(\omega)$ one gets with equation (5.4-5):

$$\mathrm{tr}\{\frac{\partial J(\bar{M}^*)}{\partial \bar{M}_j}\,\bar{M}_j^{(k)}\} = \frac{1}{\pi}\,\mathrm{Re}\,\mathrm{tr}\{Q_j(\omega_k)\hat{S}_k^T\}\,\mathrm{tr}\{S_k\}$$

$$\mathrm{tr}\{\frac{\partial J(\bar{M}^*)}{\partial \bar{M}}\,\bar{M}^{(k)}\} = \frac{1}{\pi}\,\mathrm{Re}\,\mathrm{tr}\{Q(\omega_k)\hat{S}_k^T\}\,\mathrm{tr}\{S_k\}$$

$$Q(\omega) = \sum_{j=1}^{m_2} Q_j(\omega) \qquad (5.5\text{-}6)$$

Since the matrices $Q(\omega)$ and S_k are hermitian, their eigenvalues are real. Furthermore, S_k is non-negative definite. Let now $D(\omega)$ represent the diagonal matrix with eigenvalues $\mu(\omega)$ of $Q(\omega)$, and let $P(\omega)$ denote the unitary matrix with the corresponding orthonormal eigenvectors $\underline{p}(\omega)$ as columns. Then:

$$\begin{aligned}\mathrm{tr}\{\frac{\partial J(\bar{M}^*)}{\partial \bar{M}}\,\bar{M}^{(k)}\} &= \\ &= \frac{1}{\pi}\,\mathrm{Re}\,\mathrm{tr}\{P(\omega_k)D(\omega_k)P^H(\omega_k)\,\hat{S}_k^T\}\,\mathrm{tr}\{S_k\} \\ &= \frac{1}{\pi}\sum_{\ell=1}^{s}\mu_\ell(\omega_k)\,[P^H(\omega_k)\,\hat{S}_k^T\,P(\omega_k)]_{\ell\ell}\,\mathrm{tr}\{S_k\} \\ &\geq \frac{1}{\pi}\,\mu_{\min}(\omega_k)\,\mathrm{tr}\{S_k\} = \mu_{\min}(\omega_k)\,P_u\end{aligned} \qquad (5.5\text{-}7)$$

The equality occurs for $S_k^T = \pi P_u\,\underline{p}_{\min}(\omega_k)\underline{p}_{\min}^H(\omega_k)$, where $\underline{p}_{\min}(\omega_k)$ is the normalized eigenvector associated with the minimal eigenvalue $\mu_{\min}(\omega_k)$ of $Q(\omega_k)$. This eigenvector is directly related to a harmonic signal as can be seen from (5.4-5):

$$\begin{aligned}S_k^T &= \pi P_u\,\underline{p}_{\min}(\omega_k)\,\underline{p}_{\min}^H(\omega_k) \\ \underline{p}_{\min}(\omega_k) &= \sqrt{\frac{1}{2P_u}}\,\mathrm{col}\left(\mu_{k1}e^{j\varphi_{k1}},\ldots,\mu_{ks}e^{j\varphi_{ks}}\right)\end{aligned} \qquad (5.5\text{-}8)$$

It is to be noted that the above specified eigenvalues and eigenvectors are functions of frequency. One therefore needs to search for those frequencies ω_k which result in matrices $Q(\omega_k)$ for which the smallest eigenvalue $\mu_{\min}(\omega_k)$ is minimal for all frequencies. This search is conducted by a standard one-dimensional search method.

5.5.2 Combination of Harmonic Input Signals

To determine the optimal ratio between an input signal $\underline{u}^*(t)$ resulting from the optimization in section 5.5.1 above and an additional harmonic input signal $\underline{u}^{(k)}(t)$, a standard one-dimensional search method is again applied. Along the line segment between $\bar{M}^*$ and $\bar{M}^{(k)}$ this leads to a coefficient $\alpha^{(k)}$ for which the optimization criterion is minimal. This coefficient can now be applied for the new iterated input signal, see equations (5.4-6). If $\underline{u}^{(k)}(t)$ comprises a new frequency, then its power spectral density matrix $S_{uu}^{(k)}(\omega)$ can directly be joined with the other power spectral density matrices in $S_{uu}^*(\omega)$. As they also consist of Dirac pulses. This leads to:

$$\begin{aligned}S_{uu}(\omega) &= (1-\alpha^{(k)})S_{uu}^*(\omega) + \alpha^{(k)}S_{uu}^{(k)}(\omega) \\ &= (1-\alpha^{(k)})\sum_{\ell=1}^{k-1}\alpha^{*(\ell)}S_{uu}^{*(\ell)}(\omega) + \alpha^{(k)}S_{uu}(\omega) \\ &= \sum_{\ell=1}^{k}\alpha^{(\ell)}S_{uu}^{(\ell)}(\omega)\end{aligned}$$

$$\begin{aligned}\underline{u}(t) &= \sqrt{1-\alpha^{(k)}}\;\underline{u}^*(t) + \sqrt{\alpha^{(k)}}\;\underline{u}^{(k)}(t) \\ &= \sum_{\ell=1}^{k}\sqrt{\alpha^{(\ell)}}\;\underline{u}^{(\ell)}(t)\end{aligned} \qquad (5.5\text{-}9)$$

where:

$$\begin{aligned}\alpha^{(\ell)} &= (1-\alpha^{(k)})\alpha^{*(\ell)} \quad , S_{uu}^{(\ell)}(\omega) = S_{uu}^{*(\ell)}(\omega) \quad , \ell \neq k \\ \alpha^{(\ell)} &= \alpha^{(k)} \quad , S_{uu}^{(\ell)}(\omega) = S_{uu}^{(k)}(\omega) \quad , \ell = k\end{aligned} \qquad (5.5\text{-}10)$$

If the frequency in the addtional $\underline{u}^{(k)}(t)$ is already present in $\underline{u}^*(t)$, say in $\underline{u}^{(j)}(t)$, then $\underline{u}^{(k)}(t)$ and $S_{uu}^{(k)}(\omega)$ have to be linked with $\underline{u}^{(j)}(t)$ and $S_{uu}^{(j)}(\omega)$ respectively. This now leads to:

$$\begin{aligned}S_{uu}(\omega) &= (1-\alpha^{(k)})S_{uu}^*(\omega) + \alpha^{(k)}S_{uu}^{(k)}(\omega) \\ &= (1-\alpha^{(k)})\sum_{\ell=1}^{k-1}\alpha^{*(\ell)}S_{uu}^{*(\ell)}(\omega) + \alpha^{(k)}S_{uu}(\omega) \\ &= \sum_{\ell=1}^{k-1}\alpha^{(\ell)}S_{uu}^{(\ell)}(\omega)\end{aligned} \qquad (5.5\text{-}11)$$

where:

$$\alpha^{(\ell)} = (1-\alpha^{(k)})\alpha^{*(\ell)} \quad , \; S_{uu}^{(\ell)}(\omega) = S_{uu}^{*(\ell)}(\omega) \quad , \; \ell \neq j$$

$$\alpha^{(j)} S_{uu}^{(j)}(\omega) = (1-\alpha^{(k)})\alpha^{*(j)} S_{uu}^{*(j)}(\omega) + \\ + \alpha^{(k)} S_{uu}^{(k)}(\omega) \quad , \; \ell = j \tag{5.5-12}$$

The coefficient $\alpha^{(j)}$ and harmonic signal $\underline{u}^{(j)}(t)$ can be found by representing the power spectral density matrices of the harmonics as a multiplication of normalized vectors, see equation (5.5-8). In this way one obtains:

$$\alpha^{(j)} S_{uu}^{(j)\,T}(\omega) = \alpha^{(j)} \pi P_u \cdot \underline{p}^{(j)}(\omega_j) \underline{p}^{(j)\,H}(\omega_j) \\ = (1-\alpha^{(k)})\alpha^{*(j)} S_{uu}^{*(j)\,T}(\omega) + \alpha^{(k)} S_{uu}^{(k)\,T}(\omega) \tag{5.5-13}$$

$$\alpha^{(j)} \pi P_u \cdot \underline{p}^{(j)}(\omega_j) = \left[(1-\alpha^{(k)})\alpha^{*(j)} S_{uu}^{*(j)\,T}(\omega) + \right. \\ \left. + \alpha_{(k)} S_{uu}^{(k)\,T} \right] \underline{p}^{(j)}(\omega_j)$$

Hence, the addtional harmonic input signal is included in an already existing harmonic input signal which is modified by solving an eigenvalue problem. The eigenvalue results in the modified coefficient $\alpha^{(j)}$ and the eigenvector is used for the determination of $S_{uu}^{(j)}(\omega)$ and $\underline{u}^{(j)}(t)$ according to equation (5.5-8).

5.5.3 Elimination of Superfluous Harmonic Input Signal

Each iteration step is concluded with a check if one harmonic input signal can be expressed in terms of other harmonic input signals so that it may be eliminated. With the above procedure, the input signal is extended with an addtional harmonic resulting in an additional point-input information matrix $M^{(k)}$ with vector representation $\underline{\psi}^{(k)}$. After a number of iteration steps, the number of harmonic signals may become larger than the dimension of the hyperplane of $\mathcal{R}_{\mathcal{M}}$ in which the average information matrices are situated. This means that the vectors $\underline{\psi}^{(k)}$ become dependent and that one vector can be expressed as a linear combination of the other vectors. The procedure results in:

$$\underline{u}(t) = \sum_{k=1}^{p} \sqrt{\alpha^{(k)}} \; \underline{u}^{(k)}(t) = \sum_{\substack{k=1 \\ k \neq j}}^{p} \sqrt{\alpha^{\#(k)}} \; \underline{u}^{(k)}(t)$$

$$\alpha^{\#(k)} = \alpha^{(k)} - \frac{\mu_k}{\mu_j}\alpha^{(j)} \quad , \; \frac{\alpha^{(j)}}{|\mu_j|} \leq \frac{\alpha^{(k)}}{|\mu_k|} \tag{5.5-14}$$

$$\sum_{k=1}^{p-1} \mu_k (\underline{\psi}^{(p)} - \underline{\psi}^{(k)}) = \underline{0} \quad , \; p \leq d$$

The upper bound on $p \leq d$ is specified by the dimension d of the information space $\mathcal{R}_{\mathcal{M}}$. At this stage, one can see how a reduction of d, established by applying the two-step method in combination with convex analysis, leads to a reduction of the number of elementary input signals.

5.6 Conclusions

In this section we have explained that input design is essential for accurate estimation of parameters. A brief survey of different approaches available has been given. We have described in more detail two approaches developed at the Delft University of Technology. In the time domain approach, we have shown that multi-dimensional input signals for parameter estimation of nonlinear and linear dynamical systems can be represented in terms of sets of orthonormal functions or *elementary signals*. Input signals described in this way may be optimized with respect to one of several optimization criteria based on Fisher's information matrix, by solving a nonlinear optimization problem. Linear dynamical systems allow a more efficient computation of the information matrix if a set of *elementary information matrices* is computed and stored beforehand. A special class of linear systems was introduced allowing a decomposition of the joint parameter-state estimation problem. For this class of systems, the elementary information matrices take a remarkably simple form.

In the frequency domain approach, we have shown that convex analysis leads to computational efficiency in the design of input signals, in particular for the case of parameter-state estimation problems which allow decomposition. We have also shown that such estimation problems lead to more simple input signals consisting of a fewer number of harmonic signals.

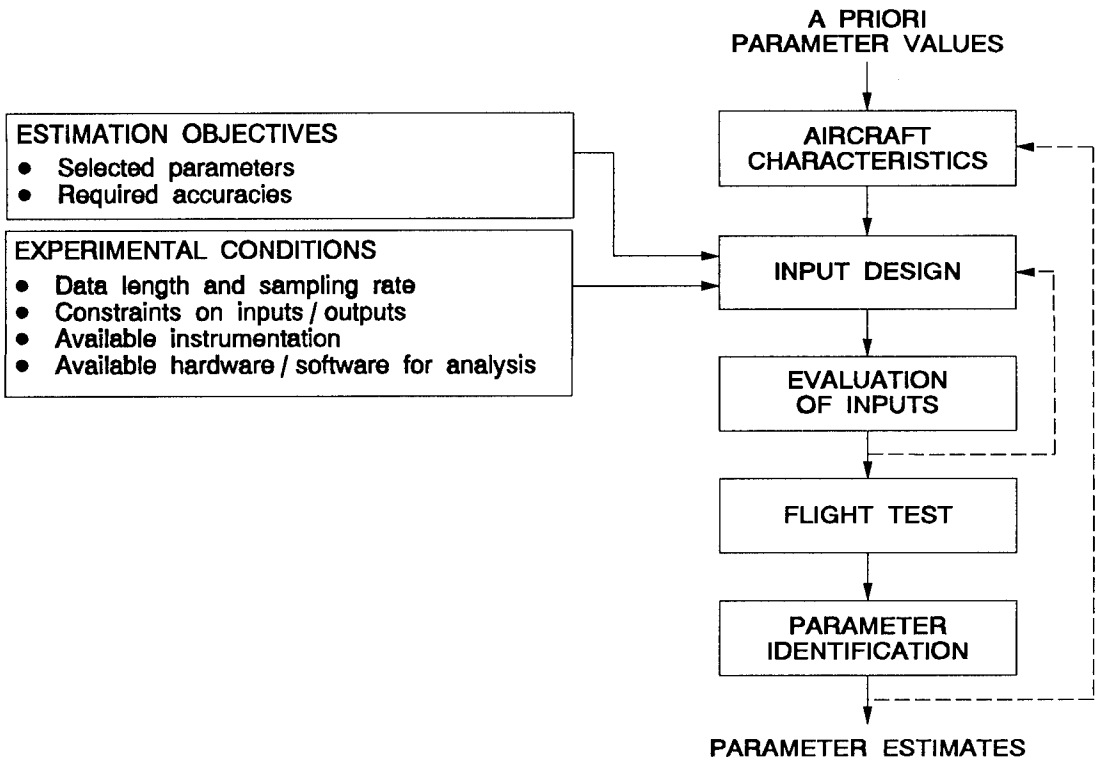

Figure 5-1: *Optimal input design within identification procedure.*

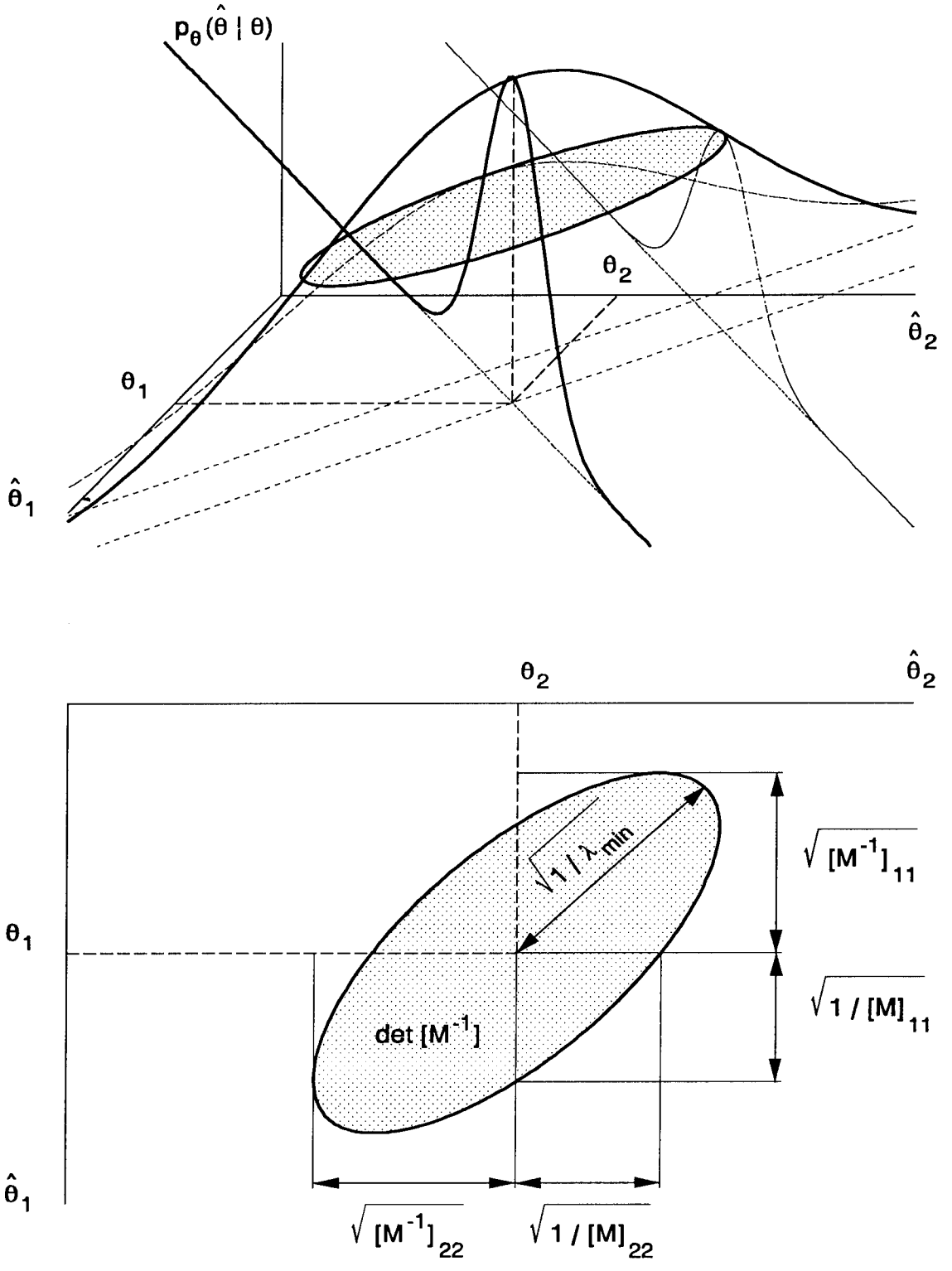

Figure 5-2: *Probability density function and uncertainty ellipsoid for a two-dimensional gaussian distribution of the paramter estimates.*

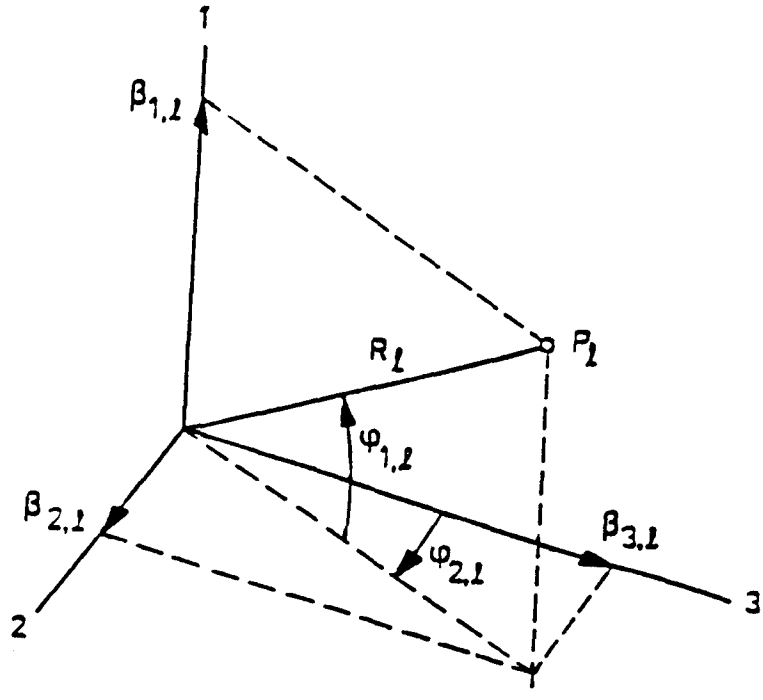

Figure 5-3: *Rectangular and spherical coordinates of P_λ in p-dimensional Euclidian space representing u_λ with energy $E_\lambda=R_l^2$ in $[t_0 t_1]$.*

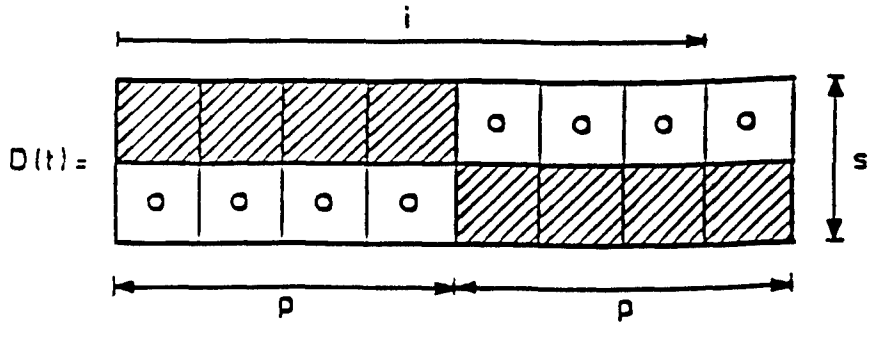

Figure 5-4: *Definition of matrix D(t) of a two-dimensional input signal (s=2) consisting of four orthonormal functions (p=4). Shaded areas denote nonzero elements; i refers to a particular column of D(t), i.e. the elementary input signal $\underline{e}_i(t)$.*

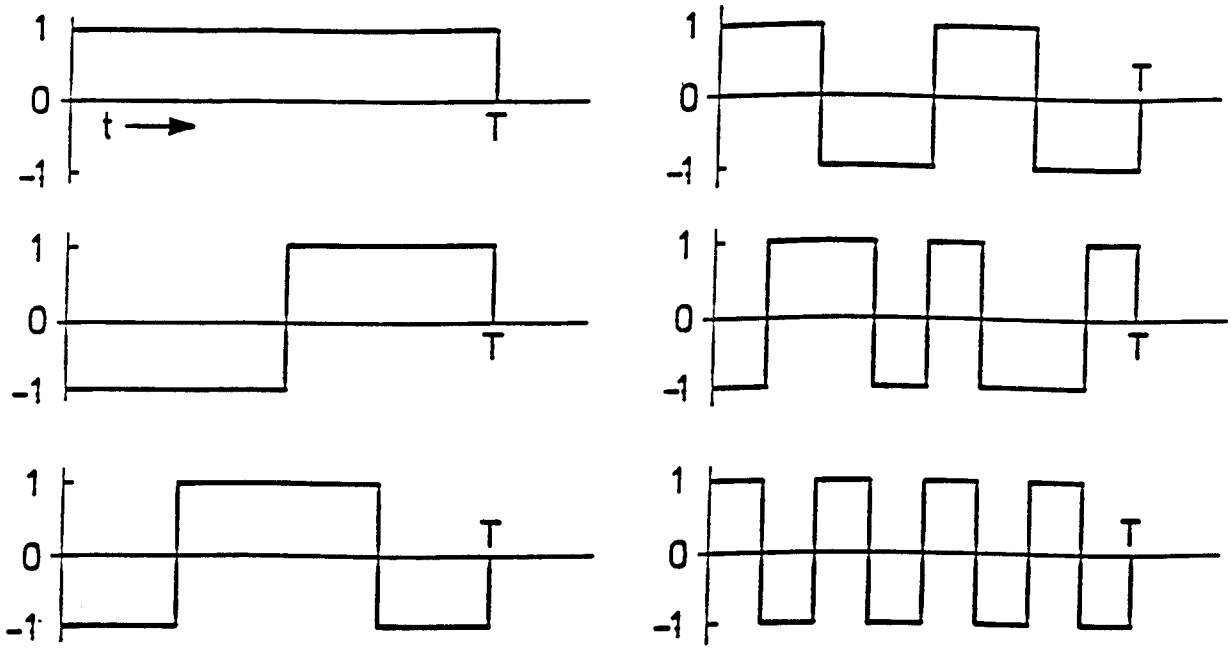

Figure 5-5: *Example of orthonormal Walsh functions in the time interval [0,T].*

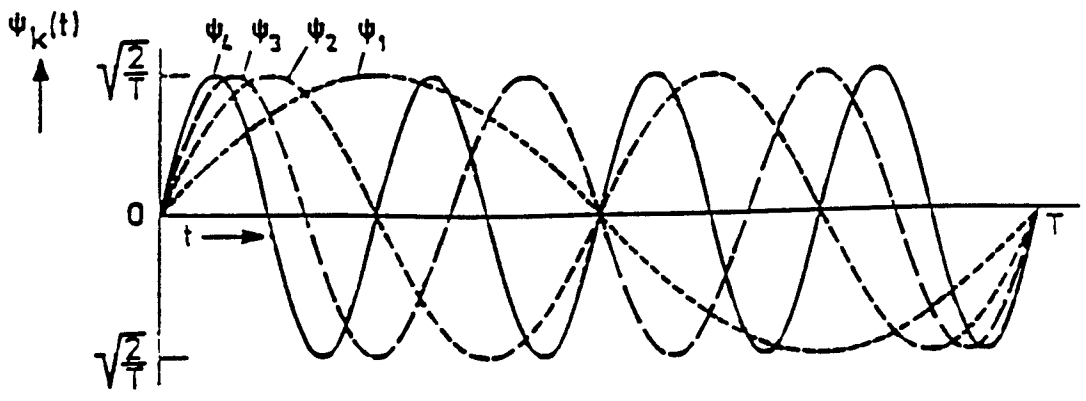

Figure 5-6: *Orthonormal functions of set 1, Eq. (5.1-8), in the time interval [0,T].*

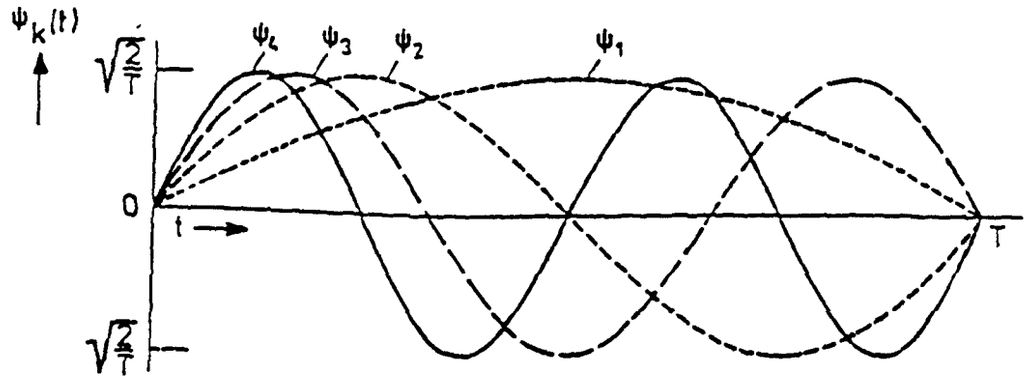

Figure 5-7: *Orthonormal functions of set 2, Eq. (5.1-9), in the time interval [0,T].*

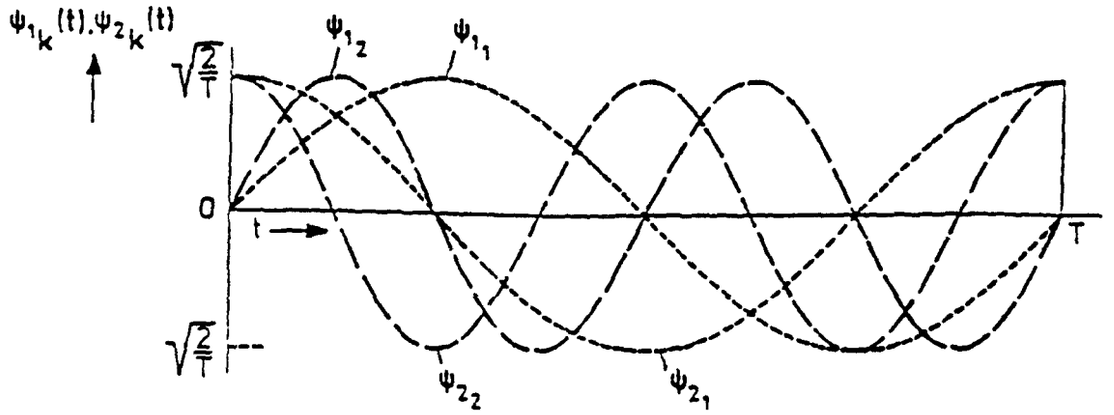

Figure 5-8: *Orthonormal functions of set 3, Eq. (5.1-10), in the time interval [0,T].*

6 DESIGN AND EVALUATION OF OPTIMAL INPUT SIGNALS

In earlier chapters, we have discussed the theoretical aspects of Flight Path Reconstruction, Aerodynamic Model Identification and Optimal Input Design. In this chapter we lay emphasis on:

- Optimization of Longitudinal and Lateral Input signals.
- Evaluation of different types of input signals with respect to parameter estimation accuracy.

We discuss *DUT* approaches in the time and frequency domain.

The *DUT* approach in the time domain considers the results of the flight test program with the De Havilland DHC-2 Beaver experimental aircraft. We focus our attention on the design of longitudinal and lateral input signals using the theory developed in section 5.1. We also briefly describe other well-known signals for the purpose of comparison. The main basis for the comparison of results from flight tests will be centred around the sample covariance matrices of estimated parameters corresponding to the different types of longitudinal and lateral input signals.

The *DUT* approach in the frequency domain considers the results of simulated experiments only. The optimal input signals are obtained by the method developed in section 5.3 to 5.5. The results are presented for a case study of designing elevator control input for estimating short period parameters of the C-8 Buffalo aircraft. The performance evaluation of the derived optimal signal is done against the results of Mehra [165]. Some results are also presented for designing simultaneous optimal rudder and aileron inputs. In this case the Beaver example is chosen for the purpose of comparison with well-known *Doublet* and *3211* signals. The basis for the comparisons in both the case studies are in terms of standard deviations of the parameter estimates. Additionally, some useful quantities of interest like norms of Fisher's information matrix and aircraft response to the optimal signals are presented.

6.1 Input Design in Time Domain

For the design of the longitudinal and lateral *DUT* input signals, use was made of the method developed in section 5.1 and in particular, the version for linear system and observation models as described in section 5.1.3 based on the concept of elementary information matrices. As discussed earlier, the two step method was applied to the analysis of the actual flight measurements. This means that the reconstruction of the state is separated from, and independent of the estimation of the aerodynamic model parameters. According to section 5.2, this leads to significant savings in the computation time for the elementary information matrices. The actual optimization of the input signals was initially performed by applying Powell's algorithm and later by a more powerful Newton-Raphson algorithm.

The input designs depend on a priori values of the parameters. These values were determined from results of earlier measurements in strictly longitudinal dynamic flight test manoeuvres [4]. The a priori values of the lateral stability and control derivatives were obtained from the results of wind tunnel experiments, see fig. 2-1. The derivatives with respect to pb/2V and rb/2V were determined from measurements in stationary horizontal turns. The derivatives with respect to $\dot{\beta}$b/V were set equal to zero. For a condition of nominally steady rectilinear flight at a TAS of 45 m/s and altitude of 6000 ft, the resulting set of values has been listed in table 6-1. The flight tests reported here were the result of a cooperation of three organisations namely DLR Braunschweig, Delft TU and NLR Amsterdam.
The comparison of the performance of the different types of input signals, was agreed to be based on the traces of the covariance matrices of the estimated parameters. The corresponding criterion for the optimization of the input signals is:

$$J = \mathrm{tr} M^{-1}$$

in which M denotes the information matrix.
The longitudinal manoeuvres were assumed to be flown via the elevator control only, while the lateral manoeuvres were assumed to be flown via

both the aileron and rudder controls simultaneously.

6.1.1 Design of *DUT* Longitudinal Input Signals

The longitudinal input signals were designed to minimize the trace of the covariance matrix of the estimated longitudinal stability and control derivatives in the linear equations of motion. In the body-fixed reference frame F_B, these linear derivatives are, see (2.2-4):

$$\begin{aligned} &C_{X_u}\ ,\ C_{X_\alpha}\ ,\ C_{X_q}\ ,\ C_{X_{\dot\alpha}}\ ,\ C_{X_{\delta_e}}\ ,\\ &C_{Z_u}\ ,\ C_{Z_\alpha}\ ,\ C_{Z_q}\ ,\ C_{Z_{\dot\alpha}}\ ,\ C_{Z_{\delta_e}}\ ,\\ &C_{m_u}\ ,\ C_{m_\alpha}\ ,\ C_{m_q}\ ,\ C_{m_{\dot\alpha}}\ ,\ C_{m_{\delta_e}}\ . \end{aligned} \qquad (6.1\text{-}1)$$

The dimension of the information matrix corresponding to these 15 derivatives is 15×15. In section 4.1 it is shown, that in the case of nominally horizontal flight, which is considered in the present section, this information matrix is never of full rank due to the presence of the derivatives with respect to $\dot{\alpha}\bar{c}/V_0$. These derivatives could be eliminated by rewriting the linearized equations of motion in an appropriate form. With respect to the information matrix this means that the corresponding rows and columns must be omitted. The resulting reduced information matrix is of dimension 12×12 and is, in general, of full rank.
The dimension of the information matrix was further reduced, on the basis of the sufficiently wide separation of the two characteristic longitudinal motions. The weakly damped low frequency motion or phugoid had a period of approximately 25 seconds. The period of the heavily damped short period motion was approximately 1.7 seconds. The wide separation between the two characteristic motions allowed the omission of the rows and columns in the information matrix of the derivatives with respect to airspeed. An explanation for this is that airspeed variations are significant only in the phugoid. The input signal optimizations in the present section were based on the idea to combine the information matrices obtained in relatively short dynamic manoeuvres, at different values of the nominal airspeed. These latter, short manoeuvres may then be optimized with respect to estimation accuracies of only those stability and control derivatives which are strongly related to the short period characteristic motion. As a consequence, the estimation accuracies of the derivatives with respect to airspeed should not be taken into account in the design of such short dynamic manoeuvres. Eliminating the corresponding rows and columns in the information matrix, all longitudinal dynamic manoeuvres were 'assigned' a relatively short time interval of 10 seconds which should be long enough for a proper excitation of the short period characteristic motion having a characteristic period of only 1.7 seconds. It should be quite feasible to combine the information matrices of manoeuvres at different airspeeds. In practice, however, it would introduce additional data management problems. In addition, differences in centre of gravity locations during the various manoeuvres must be carefully corrected for. In order to avoid such complications, it was decided to base the comparison of the longitudinal input signals on single longitudinal manoeuvres, at nominally constant airspeeds. The corresponding results are presented in section 6.2. As a consequence, all longitudinal manoeuvres should be expected to be sub optimal compared to longer manoeuvres, optimized for the estimation of all longitudinal stability and control derivatives, including those with respect to airspeed.
Finally, the derivatives C_{X_q} and $C_{X_{\delta e}}$, were considered of minor importance only. They also were not taken into account in the design of the longitudinal manoeuvre. This was accomplished by eliminating again the corresponding rows and columns in the information matrix. It is noted that this may have produced another contribution to the sub optimality of the longitudinal input signals, as in the actual analysis of the flight tests these two derivatives were found to be of some importance for a proper model fit.
The remaining information matrix is of dimension 7×7. The corresponding 7 stability derivatives are:

$$\begin{aligned} &C_{X_\alpha}\ ,\\ &C_{Z_\alpha}\ ,\ C_{Z_q}\ ,\ C_{Z_{\delta_e}}\ ,\\ &C_{m_\alpha}\ ,\ C_{m_q}\ ,\ C_{m_{\delta_e}}\ . \end{aligned} \qquad (6.1\text{-}2)$$

According to section 5.1, multi-dimensional input signals are represented in terms of finite series of orthonormal functions. They are written as:

$$u_\ell(t) = \sum_{k=1}^{p} \beta_{k\ell} \cdot \psi_k(t) \qquad (6.1\text{-}3)$$

in which ℓ refers to the ℓ-th component of the s-dimensional input signal $\underline{u}(t)$ and $\psi_k(t)$ is a member of a set of p orthonormal functions in the interval $[t_0,t_1]$. Different kinds of orthonormal functions were discussed in section 5.1. The performance index J depends on the coefficients $\beta_{k\ell}$. Input signal optimization is equivalent to minimization of J with respect to the coefficients $\beta_{k\ell}$, see section 5.1.

In the present section, ℓ=1 since only elevator inputs are considered. The length of the input signal was selected to be $T=t_1-t_0=10$ sec. For this value of T, the elevator input signals may now be optimized for different values of p and different sets of orthonormal functions $\psi_k(t)$. Two different sets of orthonormal functions were used. They were indicated as set 1 and set 2 in section 5.1.1. Both sets of functions consist of sine functions of the form:

$$\psi_k(t) = \sin\omega_k t \ ,$$

in which k=1(1)p and t belonging to the interval $[t_0,t_1]$, see equations (5.1-8) and (5.1-9) and figs. 5-6 and 5-7. The frequencies ω_k of the first set of functions correspond to those in a Fourier series:

$$\omega_k = k \frac{2\pi}{T} \ .$$

In the second set of functions the frequencies are chosen to be:

$$\omega_k = k \frac{\pi}{T} \ .$$

The functions of both set 1 and set 2 are orthogonal in the interval $[t_0, t_1]$, as can easily be shown; see also section 5.1.1.

Fig. 6-1 shows the relative performance index and the relative standard deviations of the estimated parameters of optimal input signals consisting of varying numbers p of set 1 or set 2 orthonormal functions. The relative performance index J_{rel} is defined as:

$$J_{rel} = \frac{J}{J_n} \ ,$$

in which J_n denotes the performance index of an optimized input signal consisting of 2 orthonormal functions of set 1. In a similar way, the relative standard deviation σ_{rel} of an estimated parameter is defined as:

$$\sigma_{rel} = \frac{\sigma}{\sigma_n} \ ,$$

in which σ_n denotes the standard deviation of an estimated parameter resulting from the implementation of an input signal consisting of 2 orthonormal functions of set 1.

The relative performance index and the relative standard deviations appear to depend strongly on input signal 'bandwidth' $f_p=\omega_p/2\pi$, where f_p denotes the highest frequency of any of the orthonormal sine functions in set 1 or set 2. In particular as long as f_p is below the short period characteristic frequency J_{rel} decreases markedly with increasing f_p. Fig. 6-1(a) shows that J_{rel} decreases monotonically with increasing values of p. This holds true for input signals consisting of set 1 functions as well as for input signals consisting of set 2 functions. Figs. 6-1(b) and (c) show that the relative standard deviations of the estimated derivatives with respect to α depend in a quite different way on p. The standard deviation of $\hat{C}_{X_\alpha}$ increases with increasing values of p, while the standard deviations of $\hat{C}_{Z_\alpha}$ and $\hat{C}_{m_\alpha}$ decrease with increasing values of p only for f_p below the characteristic frequency of the short period oscillation. The standard deviations of $\hat{C}_{Z_q}$, $\hat{C}_{m_q}$, $\hat{C}_{Z_{\delta e}}$ and $\hat{C}_{m_{\delta e}}$ in fig. 6-1(a) behave similarly to J_{rel} in fig. 6-1(a), i.e. a monotonic decrease with increasing values of p.

Furthermore, for a given value of f_p, input signals consisting of functions of set 2 prove to be superior to input signals of functions of set 1 with respect to the performance index as well as with respect to each of the standard deviations of the estimated parameters.

Results for p>20 are not shown since for these high values of p the convergence of Powell's algorithm was very slow.

Plots as shown in fig. 6-1 allow a deliberate selection of the number and type of orthogonal functions from which to compose the input signal. For the actual flight tests the input signals were prerecorded on an FM tape recorder connected to the electro-hydraulic control system. These input signals had to be generated, therefore, in real time on a digital computer. The software was designed

such that three input signals, for the aileron, elevator and rudder channel respectively were simultaneously generated. In the case of a longitudinal manoeuvre, the coefficients $\beta_{k\ell}$ of the aileron and rudder input signals were set equal to zero and conversely, in the case of a lateral manoeuvre the coefficients $\beta_{k\ell}$ of the elevator input signal were set equal to zero. The input signal values were calculated at a rate of 20 times per second. The maximum number of sine functions which could be calculated simultaneously in real time turned out to be equal to 24. Therefore each of the 3 input signals could maximally consist of only 8 sin functions.
Fig. 6-1 indicates that the potential improvement of input signal performance resulting from selecting f_p in excess of about 0.8 Hz is only marginal. This corresponds to 8 functions in set 1 or 16 functions in set 2. Considering the limitation on p mentioned above, the best input signal for implementation in the present flight tests can be seen to consist of 8 functions of set 1.

From the viewpoint of safety and economy, it is essential in the design of input signals for dynamic flight tests to take into account the aircraft's terminal flight condition at $t=t_f$. It should not be 'too far' from the original, nominal flight condition. The deviation of the terminal from the nominal flight condition can explicitly be taken account by adding a penalty function to the performance index, according to:

$$J_p = J + \underline{x}^T(t_f)\cdot W\cdot\underline{x}(t_f) \ , \qquad (6.1\text{-}4)$$

in which $\underline{x}(t_f)$ denotes the linearized state vector at time $t=t_f$ and W denotes a positive semi-definite weighting matrix. It is understood that $\underline{x}(t_0)=\underline{0}$. Minimization of J_p rather than of J leads in general to a different input signal and therefore to a higher value of J. The input signals calculated in fig. 6-1 turned out to result in rather large deviations from the nominal flight condition. The input signal selected for implementation in the flight tests was, therefore, slightly adapted, by adding a penalty function as in equation (6.1-4). It was found that at the cost of a relatively minor increase of J, in the order of 15%, the terminal flight condition at $t=t_f$ could be moved closely to the original, nominal flight condition.

The resulting input signal as actually measured in flight, is shown in fig. 6-3(e).

6.1.2 Design of *DUT* Lateral Input Signals

The design of the *DUT* lateral input signals was also based on linear equations of motion and minimization of the trace of the covariance matrix of the estimates of the lateral stability and control derivatives. In the body-fixed reference frame F_B these derivatives are, according to (2.2-9):

$$\begin{aligned} &C_{Y_\beta}\ ,\ C_{Y_p}\ ,\ C_{Y_r}\ ,\ C_{Y_{\dot\beta}}\ ,\ C_{Y_{\delta_a}}\ ,\ C_{Y_{\delta_r}}\ , \\ &C_{l_\beta}\ ,\ C_{l_p}\ ,\ C_{l_r}\ ,\ C_{l_{\dot\beta}}\ ,\ C_{l_{\delta_a}}\ ,\ C_{l_{\delta_r}}\ , \\ &C_{n_\beta}\ ,\ C_{n_p}\ ,\ C_{n_r}\ ,\ C_{n_{\dot\beta}}\ ,\ C_{n_{\delta_a}}\ ,\ C_{n_{\delta_r}}\ . \end{aligned} \qquad (6.1\text{-}5)$$

The dimension of the corresponding information matrix is 18×18.

Before the actual flight tests were performed, the stability derivatives with respect to $\dot\beta b/V$ were expected to be of minor importance only. These derivatives were therefore not taken into account in the input signal optimization. This was accomplished by omitting the corresponding rows and columns in the information matrix, reducing its dimension to 15×15.
The lateral motions are dominated by the Dutch roll periodic motion and the roll aperiodic motion. The Dutch roll motion had a period of approximately 5 seconds. The time constant of the roll motion was approximately 1.4 seconds. As a consequence, the length of the lateral input signal was chosen to be 16 seconds which is about 3 times the period of the Dutch roll characteristic motion. Such fairly long input signals compared to the period of the Dutch roll motion were considered to guarantee a proper excitation of the dominant characteristic lateral motions.

Fig. 6-2 presents the results of the optimization of the lateral input signals. Two sets of orthogonal functions as mentioned in the previous section were used to calculate the optimal performance index and corresponding square roots of the diagonal elements of the covariance matrix for increasing values of p.
Analogous to the longitudinal case, Powell's algorithm was found to converge more slowly if p was larger. This prevented in fact the optimization

of input signals consisting of more than 10 orthogonal functions per input signal component. All curves of fig. 6-2 clearly suggest that an additional increase of p and therefore higher 'bandwidth' f_p would probably have resulted in slightly better input signals.
As mentioned earlier, in the practical implementation, each input signal component could consist of maximally 8 functions of set 1 or set 2. Given this restriction on p, the best practical input signals consisted of the maximum number of 8 functions of set 1.
The resulting optimized input signals were slightly adapted again, by adding a penalty function to the original performance index J, as in (6.1-4). The adapted input signals were found to result in a terminal flight condition at $t=t_f$ which was very close to the original, nominal flight condition at the cost of only a negligible increase of J.

The resulting aileron and rudder input signals, as actually measured in flight, are shown in fig. 6-3(e).

6.1.3 *Doublet, 3211, Mehra* and *Schulz* Input Signals

The *Doublet, 3211, Mehra* and *Schulz* longitudinal and lateral input signals are shown in fig. 6-3. The rationale behind these signals is given below. For a more detailed description,the reader is referred to reference [20].

Doublet
The *Doublet* input signals are of the 'bang-bang' type, switching between plus or minus the signal amplitude Δa. For a signal length of $2\Delta t$, the instant to switch from $+\Delta a$ to $-\Delta a$ is at time $t=\Delta t$. This type of input signal has been, and probably still is, widely used for excitation of aircraft longitudinal and lateral characteristic motions. In the present case, different t-values were used for the elevator, aileron and rudder input signals. These Δt-values were selected to result in a proper excitation of the short period, roll and Dutch roll characteristic motions respectively.
As mentioned before, all 5 types of elevator input signals as well as all 5 types of aileron and rudder input signals were scaled to have the same energy in the longitudinal and lateral time intervals of 10 and 16 seconds respectively. Since Δt is rather small, this would in the case of *Doublet* signals have resulted in rather large amplitudes. It was decided, therefore, to implement the *Doublet* signals twice during each observation time interval. Actually measured time histories are shown in fig. 6-3(a).

3211
The *3211* input signal is also of the 'bang-bang' type. Let the signal length be $7\Delta t$. The switching times are then at $t=3\Delta t$, $t=5\Delta t$ and $t=6\Delta t$. The signal can be optimized with respect to parameter estimation accuracies by searching for the best value of Δt. Marchand [180] has shown that a deliberate choice of Δt can be made through qualitative considerations in the frequency domain. In order to avoid too large amplitudes, the 3211 signals were also implemented twice during each observation time interval. Actually measured time histories are shown in fig. 6-3(b).

Mehra
Mehra and Gupta [164] propose the use of frequency domain techniques for the design of input signals, see also chapter 5. The result of an optimization in the frequency domain is a line spectrum which is subsequently approximated by a set of weighted sine functions in a finite observation time interval. Since the more general algorithm for multidimensional input signals was not available when the flight test program started, the aileron and rudder input signals had to be calculated separately, i.e. as in the case of scalar input signals. The resulting signals were nevertheless implemented simultaneously in each lateral manoeuvre. Furthermore, the criterion used for the design of the *Mehra* input signals was the determinant of the information matrix, rather than the trace of the covariance matrix. Actually measured time histories are shown in fig. 6-3(c).

Schulz
Schulz [163] formulates the problem of designing an input signal as an optimal control problem in the time domain. In order to simplify the calculations, the criterion used is the trace of the information matrix, see chapter 5. In the lateral case, the aileron and rudder signals were calculated separately, as one-dimensional input signals. Analogous to the lateral *Mehra* input signals, they were nevertheless implemented simultaneously in

each lateral manoeuvre. Actually measured time histories are shown in fig. 6-3(d).

All longitudinal and lateral input signals were low-pass filtered, before being recorded on tape for use with the electro-hydraulic control system. The filter used consisted of two identical second-order filter with undamped natural frequencies of 19 rad/s (corresponding to approximately 3 Hz) and damping ratios of 0.691. The filtering caused some significant distortions, in particular of the block type *Doublet* and *3211* input signals, see fig. 6-3. The distortion of the input signals of the *Mehra, Schulz* and *DUT* type proved to be negligible.

Even after filtering, significant differences remained in the frequency contents of the different types of input signals. This is illustrated by the power spectral densities of the elevator input signals of the longitudinal and the aileron and rudder input signals of the lateral manoeuvres in fig. 6.4. It follows that only the *Doublet* and *3211* input signals contain a significant amount of power above 1 Hz. A considerable difference in bandwidth appears to exist between these two input signal types. Compared to the *Doublet* signals, the *3211* signals contain much higher frequencies.
Compared to the two block type input signals, the remaining input signals may be classified as low-frequency-type input signals. Of these input signals, the *Schulz* input signals appear to contain the lowest frequencies.

6.2 Performance Evaluation of Longitudinal and Lateral Input Signals

In the present section a comparison is made of the performance of the different types of longitudinal and lateral input signals. The calculation of sample statistics of the estimated parameters is discussed in section 6.2.1. The actual comparison of input signal performance is made in section 6.2.2.

6.2.1 Sample Statistics of the Estimated Parameters

One set of computer programs was used for the calculation of all longitudinal and lateral parameter estimates from the 47 flight test manoeuvres at the nominal steady rectilinear flight condition of 45 m/s TAS and 6000 ft SA. The programs were implementations of the algorithms described in section 3.3 and 4.3. However, rather than applying the model development procedure of section 4.3, fixed and a priori specified longitudinal and lateral aerodynamic models had to be used for the estimation of the aerodynamic derivatives. The reason for this was that different flight test manoeuvres usually led to the selection of slightly different sets of candidate variables. This prevents the calculation of sample statistics of the estimated parameters.
The specified longitudinal and lateral aerodynamic models are shown in table 4-1. It is noticed that, in accordance with the identifiability analysis in section 4.1.1, the variable $\dot{\alpha}\bar{c}/V$ is not present in the model. On the other hand, a nonlinear variable α^2 in the models of C_X and C_m was found to be indispensable for an acceptable model fit. This is in agreement with the nonlinearity of the C_X-α and C_m-α relationships as manifested in the wind tunnel results of fig. 2-1. Inclusion, however, of derivatives with respect to α^2 affects the estimation accuracies of the derivatives with respect to α. The estimated derivatives with respect to α and α^2 were, therefore, 'combined' into one 'linearized derivative' according to:

$$\begin{aligned} \tilde{\hat{C}}_{X_\alpha} &= \hat{C}_{X_\alpha} + 2\cdot\bar{\alpha}\cdot\hat{C}_{X_{\alpha^2}} \\ \tilde{\hat{C}}_{X_\alpha} &= \hat{C}_{m_\alpha} + 2\cdot\bar{\alpha}\cdot\hat{C}_{m_{\alpha^2}} \end{aligned} \qquad (6.2\text{-}1)$$

in which $\bar{\alpha}$ denoted the mean value of α during the flight test manoeuvre.
The estimates were obtained by the two step method and subsequently used to calculate sample standard deviations.
One set of derivatives relating to the C_Z- and C_l-equations are plotted in fig. 6-5. In figs. 6-6 and 6-7 the sample standard deviations of the *Doublet, 3211, Mehra* and *Schulz* manoeuvres are plotted, relative to the standard deviations of the *DUT* manoeuvres in order to expose more clearly the existing differences. For comparison, the same is done with respect to the theoretical standard deviations, as derived from the theoretical covariance matrix $V(\hat{\underline{a}}_1)$:

$$V(\hat{\underline{a}}_1^*) = V_e \left[X_1^T \cdot X_1\right]^{-1} .$$

6.2.2 Comparison of Input Signal Performance

The results of fig. 6-5 allow a comparison of the different manoeuvre types with respect to sample means and sample standard deviations of estimated aerodynamic derivatives.

The large differences between corresponding sample means, show that most of the estimated aerodynamic derivatives are strongly biased. Furthermore, biases prove to depend on manoeuvre type. The expected value of an estimated parameter in simplified models is given by equation (4.2-22):

$$E(\hat{\underline{a}}_1^*) = \underline{a}_1 + C \cdot \underline{a}_2$$

where

$$C = \left[X_1^T \cdot X_1\right]^{-1} X_1^T X_2 \qquad (6.2\text{-}2)$$

The phenomenon of estimation bias in regression analysis is often connected with the existence of additive measurement errors in the independent variables [182]. In the present work, the independent variables are either measured directly or derived from a flight path reconstruction and thus corrupted with measurement or reconstruction errors respectively. These errors, however, are much too small to be held responsible for the observed differences between samples means. A more plausible model for the observed estimation biases is given in section 4.2.2. Aerodynamic models, as defined in table 4-1 comprising a limited number of independent variables, will only approximate the underlying much more complex aerodynamic mechanisms. These models are therefore always simplified versions of hypothetical 'perfect models'.

Following chapter 2, aerodynamic models are represented here as Taylor series expansions of a given set of variables and their first and higher order time derivatives. Simplified models contain finite subsets of these variables. The simplified models used in the present section are linear with the exception of α^2 terms in the models of C_X and C_m; see section 4.2. The variables in X_2 include, therefore, nonlinear products of the variables in X. This means, that those elements in C which are related to these nonlinear products will depend on the magnitude of the deviations from the nominal flight condition. A measure for these deviations, as occurring in the course of a flight test manoeuvre, is the root mean square deviation:

$$d = \sqrt{tr\left[\tilde{\underline{X}}_1^T \cdot \tilde{X}_1\right] / \underline{N}} \ , \qquad (6.2\text{-}3)$$

in which $\tilde{X}_1 = X_1 - \underline{X}_1$. In the present flight test program it was found that different types of input signals resulted in different values of d. This is clearly shown in table 6-2. It follows, that in particular the longitudinal and lateral *Schulz* input signals produce large values of d. This is not surprising, as these input signals were designed to maximize the trace of the information matrix, see section 6.1.3. It is noted that *3211* manoeuvres on the other hand, result in rather small values of d.

Fig. 6-5 shows striking differences between sample standard deviations of the estimated parameters of different types of input signals. This holds true for the longitudinal as well as the lateral input signals. Since the present work is focused on the design of *DUT* input signals, the sample standard deviations of the *3211, Doublet, Mehra* and *Schulz* input signals were expressed in terms of the corresponding sample standard deviations of the *DUT* input signals in figs. 6-6 and 6-7, see also section 6.2.1.

In tables 6-3 and 6-4 the observed differences of sample standard deviations were tested for statistical significance. The results indicate that, even for a fairly high value of $\alpha = Pr\{H_1|H_0\} = 5\%$, relatively few statistically significant differences exist. This is a direct consequence of the fact that the sample sizes are relatively small. Even less statistically significant differences would have resulted, if the actually observed differences in sample standard deviations were identical to the differences as predicted by theory in figs. 6-6 and 6-7. These predicted statistically significant differences are also shown in tables 6-3 and 6-4.

The sample standard deviations of the *3211, Doublet, Mehra* and *Schulz* manoeuvres relative to the corresponding *DUT* values were subsequently tested for statistically significant deviations from the corresponding theoretical results, see again tables 6-3 and 6-4. The tests show that statistically significant deviations from theory do indeed exist. It is noted that, with only one exception, all these deviations resulting from *Doublet, Mehra* and *Schulz* manoeuvres are positive, i.e. the relative

sample standard deviations are larger than predicted by theory. On the other hand, also with only one exception, all statistically significant deviations resulting from the 3211 manoeuvres turn out to be negative.

The results for the experimental and theoretical sample relative standard deviations can be explained as follows. The theoretical covariance matrix $V(\underline{\hat{a}}_1^*)$ for biased estimates in simplified models is based on the assumption that C in (6.2-2) is deterministic. For the calculation of a sample variance matrix of $\underline{\hat{a}}_1^*$, C must, therefore, be constant. From (6.2-2) it follows that C depends on the form of the flight test manoeuvre, i.e. the time histories of the independent variables in X_1 and X_2. The use of an electro-hydraulic control system for the implementation of pre-recorded input signals, as in the present work, results in highly reproducible flight test manoeuvres. Yet, two flight test manoeuvres of the same type will never be exactly identical, due to for instance small deviations from the initial nominal flight condition, differences in aircraft weight and centre of gravity location and non-reproducible components in the control system outputs. Furthermore, during the execution of the longitudinal manoeuvres, the pilot would manually add small lateral control inputs to keep the wings level. During the lateral manoeuvres the pilot would add small longitudinal control inputs, in order to prevent too large pitch and airspeed variations. These additional control inputs generated by the pilot were non-reproducible and turned out to be largest in the case of the Schulz manoeuvres, while virtually nonexistent in the case of the 3211 manoeuvres.
It follows from equation (6.2-2), that differences between longitudinal or lateral manoeuvres of the same type will result in C being not exactly constant. The matrix rather depends on the particular realization of the manoeuvre. Different biases may, therefore, be expected to exist in the estimated parameters $\underline{\hat{a}}_1^*$, as calculated from a set of realizations of a particular type of flight test manoeuvre. The effect of this is an increase of sample variance.
The root mean square deviations d in table 6-2 are loosely connected to the magnitude of the parameter bias in simplified models. There exists a marked difference in this respect between for instance *3211* and other manoeuvres. Furthermore, it follows from the above, that due to the smaller pilot implemented control inputs, *3211* manoeuvres can, compared again to the other manoeuvres types, be reproduced more accurately.

The above reasoning may now serve to explain, although rather tentatively the results of the statistical tests in tables 6-3 and 6-4. For example, the negative deviations of relative sample standard deviations of the *3211* manoeuvres may be attributed to the parameter biases being smaller and the flight test manoeuvre reproducibility being higher than the *DUT* manoeuvres.

For a comparison of only the input signal performance, in terms of variances of parameter estimates, perhaps a clearer picture results if the parasitic effects of parameter bias and manoeuvre reproducibility are ignored. This would indeed indicate that the comparison should be based on the theoretical, rather than on the sample relative standard deviations. These theoretical standard deviations, in relative rather than in absolute form, were presented in figs. 6-6 and 6-7.

The relative theoretical standard deviations of the estimated longitudinal parameters are shown in fig. 6-6. Perhaps the most remarkable result is the relatively poor performance of Schulz manoeuvres, in particular with respect to the $q\bar{c}/V$ and δ_e derivatives. The differences between the remaining types of input signals seem to be less marked in the sense of one type of input signal being markedly superior to the others. This does not imply, however, that variations in parameter estimation accuracies would exist. The theoretical standard deviation of, for example, the δ_e derivatives of the *Doublet* manoeuvres prove to be more than 135% of the corresponding results of the *DUT* manoeuvres, while the theoretical standard deviations of $\Delta p_t/\frac{1}{2}\rho V^2$ derivatives of the *3211* manoeuvres are found to be less than 70% of the corresponding results of *DUT* manoeuvres.

The relative theoretical standard deviations of the estimated lateral parameters are shown in fig. 6-7. Remarkable is again the poor performance of the *Schulz* manoeuvres. Also the *Mehra* manoeuvres can, however, for all derivatives be seen to result in relatively large standard deviations. Only small differences prove to exist between the standard

deviations of the remaining *Doublet*, *3211* and *DUT* manoeuvres, although the *Doublet* manoeuvre is seen to be slightly superior.

In the comparison made above, the *Schulz* manoeuvres shown were optimized with respect to the trace of Fisher's information matrix. The relatively poor performance of these manoeuvres indicates that this criterion does not guarantee good performance in terms of standard deviations of the estimated parameters.
In the longitudinal case, the performance of the *Mehra* manoeuvres is of approximately the same level as the performance of *DUT* manoeuvres, although both manoeuvres types were optimized with respect to different criteria, see section 6.1.1 and section 6.1.4. However, as mentioned above, in the lateral case the performance of the *Mehra* input manoeuvres is considerably lower. Since the longitudinal *Mehra* input signal performed quite well, the cause of the relatively low performance in the lateral case is thought to be the separate optimization of the aileron and rudder input signals. Compared to the corresponding *DUT* input signals, this resulted in a relatively low frequency aileron signal for proper excitation of the Dutch roll characteristic motion. Simultaneous optimization would probably have 'assigned' excitation of the Dutch roll motion to the rudder control, which is in this respect much more efficient. The multidimensional version of *Mehra's* algorithm might, therefore, be expected to result in improved input signals, see [165].
The differences with respect to theoretical standard deviations between the remaining types of input signals, i.e. the *Doublet*, *3211* and *DUT* signals appear to be less pronounced although significant differences exist for individual derivatives.
The *Doublet* and *3211* manoeuvres appear to result in relatively high estimation accuracies of the control derivatives with respect to δ_a and δ_r in the lateral case. In the longitudinal case, the *3211* signal results in a higher estimation accuracy of the control derivative with respect to δ_e compared to the *DUT* signal. The *Doublet* signal, however, results in a lower estimation accuracy. In fig. 6-4 it may be seen that estimation accuracies of control derivatives in general appear to depend on the bandwidth of the input signal, in the sense that a higher bandwidth results in a higher estimation accuracy. This beneficial effect of higher frequencies on the estimation accuracies of control derivatives is also evident in figs. 6-1 and 6-2. In the lateral case, the *Doublet* manoeuvre results in slightly higher estimation accuracies of all derivatives compared to the *DUT* manoeuvre. The *3211* manoeuvre results in higher estimation accuracies of the control derivatives, but in lower estimation accuracies of the derivatives with respect to the side slip angle β and the (dimensionless) rotation rates p and r. In the longitudinal case, it is the *3211* manoeuvre which results in the higher estimation accuracies compared to the *DUT* manoeuvre. The *Doublet* manoeuvre results in higher estimation accuracies of the derivatives with respect to $\Delta p_t/\frac{1}{2}\rho V^2$ and angle of attack α, but in lower estimation accuracies of the derivatives with respect to the (dimensionless) rotation rate q and the control angle δ_e.

6.3 Input Design in Frequency Domain

This section illustrates the results of the input design technique in the frequency domain described in section 5.3 to 5.5. The input design for the estimation of parameters in the model of the short period mode of the C-8 Buffalo aircraft is discussed in section 6.3.1. Section 6.3.2 presents the simulation results for the designed input signal. Input signals of Mehra discussed in Gupta and Hall [158], Chen [114] and Morelli [123] are also briefly discussed. Section 6.3.3 illustrates the design technique for the estimation of the parameters in the lateral model of the DHC-2 Beaver aircraft. In section 6.3.4, the evaluation of the results of the designed aileron and rudder inputs is discussed.

6.3.1 Design of Longitudinal Input Signal

The input design for the estimation of the short period mode parameters is previously investigated by Mehra, Chen and Morelli. The applied model is given by Gupta and Hall [158]:

$$\begin{bmatrix}\dot{\alpha}\\ \dot{q}\end{bmatrix} = \begin{bmatrix}Z_\alpha & 1\\ M_\alpha & M_q\end{bmatrix}\begin{bmatrix}\alpha\\ q\end{bmatrix} + \begin{bmatrix}Z_{\delta_e}\\ M_{\delta_e}\end{bmatrix}\delta_e \qquad (6.3\text{-}1)$$

$$\begin{bmatrix}y_1\\ y_2\end{bmatrix} = \begin{bmatrix}\alpha\\ q\end{bmatrix} = \begin{bmatrix}1 & 0\\ 0 & 1\end{bmatrix}\begin{bmatrix}\alpha\\ q\end{bmatrix}$$

where α is angle of attack, q is pitch rate and δ_e is elevator deflection. The parameters are specified in table 6-5. The output signals consist of α and q which are measured at a sampling rate of 25 Hz. The measurement errors are zero mean and uncorrelated. Their standard deviations are given in table 6-6.

With respect to the application of the two-step method, the system is replaced by

$$\begin{bmatrix}\dot{\alpha}\\ \dot{q}\end{bmatrix} = \begin{bmatrix}Z_\alpha & 1\\ M_\alpha & M_q\end{bmatrix}\begin{bmatrix}\alpha\\ q\end{bmatrix} + \begin{bmatrix}Z_{\delta_e}\\ M_{\delta_e}\end{bmatrix}\delta_e \qquad (6.3\text{-}2)$$

$$\begin{bmatrix}y_1\\ y_2\end{bmatrix} = \begin{bmatrix}\dot{\alpha}\\ \dot{q}\end{bmatrix} = \begin{bmatrix}Z_\alpha & 1\\ M_\alpha & M_q\end{bmatrix}\begin{bmatrix}\alpha\\ q\end{bmatrix} + \begin{bmatrix}Z_{\delta_e}\\ M_{\delta_e}\end{bmatrix}\delta_e$$

where the parameters in the differential equations are not treated as parameters any more. The differential equations are only used for generating the state trajectory. The standard deviations of the 'measured' time derivatives can be constructed via five-point Taylor polynomials of α and q. The values are also listed in table 6-6.

The replaced model is only used for the optimization of the input signals. For the evaluation of the optimal input signal and for uniform comparison with other optimization techniques, the derived input signal is submitted to the original system.

The optimal elevator control is derived via a search of the optimal information matrix $\underline{M}^\circ$ in the convex set $\mathcal{M}$ of information matrices $\underline{M}$ with power constrained inputs. As explained in section 5.3, $\underline{M}$ has a block diagonal structure structure where each matrix block is constructed from the matrix $\hat{M}(\omega)$. Via the independent elements of $\hat{M}(\omega)$, $\underline{M}$ can be represented by the information vector $\underline{\psi}$ in the information space $\mathcal{R}_{\mathcal{M}}$. The number of independent elements can be restricted to (n+1) for single input systems, see [216], where n is the number of independent state variables. The elements of $\hat{M}(\omega)$ are hereto expanded as a power series of $\omega^{2(i-1)}/|d(\omega)|^2$, $i=1(1)(n+1)$. The term $\omega^{2n}/|d(\omega)|^2$, however, only appears in the bottom diagonal element of $M(\omega)$ which is equal to unity by the imposed power constraint; see equation (5.3-21). This now puts the set $\mathcal{M}$ in a n-dimensional linear variety $\mathcal{R}_{\mathcal{M}}$. As the system (6.3-2) has only one input and two state variables, $\mathcal{M}$ can be situated in a two-dimensional plane. $\underline{M}$ can thus be represented by the information vector $\underline{\psi}$ with two independent components ψ_1 and ψ_2 and the scalar norms J, defined earlier as optimization criteria, become two-dimensional vector functions. The two- and three-dimensional views of the matrix norms are shown in fig. 6-8 and fig. 6-9. In fig. 6-8, the contours represent constant values of the norms, while the depths in fig. 6-9 correspond to the values of the norms.

The location $\underline{\psi}^\circ$ of $\underline{M}^\circ$, i.e. the location with minimal value of the norm, can be seen in these figures. The different norms locate $\underline{M}^\circ$ more or less in the same position. This may lead to the conclusion that one may expect similar performances for the input designs optimized to different criteria.

The elevator control is optimized for the criterion $J=\text{tr}\,\underline{M}^{-1}$ as used by other investigators. Let the elevator control be composed of harmonic signals whose power is set to $P_u=16.667\ \text{deg}^2$ for the purpose of comparison. The frequencies of the sine functions are set to specified values $\omega\in[0, 1.5, 4.5]$ rad/s and they are optimized within the range 0 to 4.5 rad/s. The first iterations of the optimization process with optimizing frequencies are shown in fig. 6-10.

The average information matrix is represented in a two-dimensional plane in the information space $\mathcal{R}_{\mathcal{M}}$ as described above. The point-information matrices $\underline{M}^{(k)}$ are first calculated from the harmonic signals $\underline{u}^{(k)}(t)$ of which the input signal $\underline{u}(t)$ is composed. It follows from equations (5.3-18) and (5.4-5) that the set of $\underline{M}^{(k)}$, represented by $\underline{\psi}^{(k)}$ in $\mathcal{R}_{\mathcal{M}}$, is a curve depicted by the dash-dot arc in fig. 6-10. This curve determines the convex hull of $\mathcal{M}$. Each point on the curve corresponds to a single frequency in the input signal. By composing $\underline{u}(t)$ from $\underline{u}^{(k)}(t)$ the information matrix $\underline{M}$ becomes a

convex combination of $\bar{M}^{(k)}$ for power constrained input designs. In vector representation, the information vector $\underline{\psi}$ is situated in a polyhedron where the vertices are specified by $\underline{\psi}^{(k)}$. By connecting all vertices one may find the sufficient $\underline{\psi}^{(k)}$ to attain $\underline{\psi}$. The sufficient number of harmonics is three, since the set $\mathcal{M}$ lies in a two-dimenional plane.

The initial harmonics $\underline{u}^{(k)}(t)$ are chosen so that the evaluated information matrix is nonsingular. At each iteration, the minimal gradient of J with respect to the power ratio of any harmonic signal is searched. This results in a direction indicated by the dashed line in fig. 6-10. The crossing of this line with the curve for $\underline{\psi}^{(k)}$ now represents a new harmonic in the input signal. If the frequencies are fixed, then the resulting harmonic is one of the specified harmonic signals. If the frequencies are optimized, the resulting harmonic is an additive harmonic signal. The amplitude of the new harmonic is calculated by a direct search of the minimal value of J along the direction of the minimal gradient. The location of the minimal value represents the power ration between the previous iterated input signal and the new harmonic. It can be seen that after some iterations, this leads to superfluous usage of harmonic signals. Therefore, by applying Caratheodory's theorem, the new iterated input signal can still be represented by three harmonic signals, dispensing one of the harmonics when the new information matrix is found. The iterations are continued until the gradient becomes larger than -0.1%, indicating a flat surface and small changes in estimation errors for successive input designs, or until the shift of $\underline{\psi}$ becomes smaller than 0.1%, indicating a small change only in $\bar{M}$ and a small contribution of new harmonics in the input design.

The schematic sketch of the optimal harmonic signals for the optimal elevator control is shown in fig. 6-11 for both specified and optimized frequencies. One can see that the frequencies do not differ much for both cases and result in close approximations for the location of the optimal information matrix. The derived optimal signals, however, are not unique. Several other combinations of harmonic signals are possible. For the present case, even an optimal signal consisting of only two harmonic signals is possible. This is caused by allowing an arbitrary choice of input frequencies. It also follows from the figure that for a limited frequency range, which corresponds to a restricted segment of the hull, the optimal $\bar{M}^{\circ}$ may not be attainable. Furthermore, in order to keep the highest input frequency limited, the input signal must be allowed to have very low frequencies.

The time history of the *DUT* elevator inputs with fixed and optimized frequencies are shown in fig. 6-12 for a time length of T=6 sec, together with their power spectral densities. The corresponding frequencies, amplitudes and powers of the elementary signals are presented in table 6-7.

The optimal input with optimized frequencies does not differ much from the input with specified frequencies. Both input signals contain one high frequency, and two low frequencies. One frequency is close to the natural frequency of the short period mode (ω_0=1.32 rad/sec). This is logical since around this frequency the input is generally amplified most, which results in higher signal/noise ratios for the outputs. The other two frequencies make the regression equations from which the parameters can be identified in the frequency domain less dependent on each other, see Gerlach [3].

The optimal input time histories according to fig. 6-12 are not unique because of the phase shifts in the elementary signals. These phase shifts do not follow from the synthesis in the frequency domain. In order to avoid disturbancies at $t=t_0$, the phases are set to zero.

6.3.2 Evaluation of Longitudinal Input Signal

For the evaluation of the *DUT* signal, the original system (6.3-1) is driven with the *DUT* elevator input for specified frequencies. The generated angle of attack and pitch response are given in fig. 6-13. The original system is also driven with the *DUT* signal to evaluate the average Fisher's information matrix $\bar{M}$ for each of the scalar norms J mentioned earlier. The average information matrix $\bar{M}=M/N$ is computed as a function of the measuring time interval T with a constant sampling interval set to Δt=0.04 sec. The resulting criteria J are plotted in fig. 6-14.

It can be seen that around T=4 sec, the criteria $J=\text{tr } \bar{M}^{-1}$, $J=-\ln \det \bar{M}$ and $J=1/(\text{eig } \bar{M})_{min}$ become stable. This means that larger measuring time intervals yield little or no gain in accuracy.

The present short period mode is also investigated by Mehra, presented in Gupta and Hall [158], Chen [114] and Morelli [123]. These optimal inputs are shown in fig. 6-15.

The optimal elevator input derived by Mehra in the time domain technique started from a doublet input. The applied optimization criterion is $J=\text{tr}\,M^{-1}$ at a measuring time interval T=6 sec. Maintaining the same energy over the measuring time interval, the doublet input is optimized by adding new elementary signals which are eigen functions of a matrix function of Fisher's information matrix.

The optimal elevator input derived by Mehra in the frequency domain technique started from a signal with two frequencies with equal power. The signal is now optimized for the criterion $J=\text{tr}\,\bar{M}^{-1}$. The optimization technique is equal to the present technique but with the parameters occurring in the differential equations, the model in equation (6.3-1), and without reducing the number of elementary signals. The input signal has a total of eight frequencies in the input spectrum.

The optimal elevator input by Chen is a member of an orthogonal set of Walsh functions with full positive and negative amplitude. From functions with different block lengths, the function which results in the shortest time to achieve all specified parameter standard deviations is regarded as optimal. The optimal input signal thus depends on the goals for the parameter accuracies.

The optimal elevator input by Morelli also minimizes the measuring time interval to attain specified parameter standard deviations. The input may also be optimized for a apecified measuring time interval by setting the desired parameter standard deviations to zero. The input consists of a sequence of zero and full positive and negative amplitudes where the block lengths are optimized via dynamic programming techniques. This entails that for regular time instants the input signal is continued with an amplitude resulting in the lowest optimization criterion at the next time instant.

The *DUT* optimized input signal is compared with the optimal input signals from the Mehra techniques which are based on the same conditions. The elevator inputs have input power constraint $P_u=16.667\ \text{deg}^2$ and they are submitted to the original system (6.3-1) with same noise characteristics (table 6-6), sampling rate (25 Hz) and measuring time interval (6 sec). The signal performance is evaluated via the criterion $J=\text{tr}\,\bar{M}^{-1}$ and the parameter standard deviations σ_θ. The results are presented in table 6-8 and fig. 6-16. It can be seen that the *DUT* input signals perform well.

6.3.3 Design of Lateral Input Signal

The input design for the estimation of the lateral control and stability derivatives is based on the same model and flight conditions as in section 6.1.3 for the time domain approach. The applied model is obtained by merging the kinematic lateral flight path model (2.1-16) and the lateral aerodynamic model (2.2-9):

$$\begin{bmatrix} \dot{\tilde{\beta}} \\ \dot{\tilde{\psi}} \\ \dot{\tilde{\varphi}} \\ \dot{\tilde{p}} \\ \dot{\tilde{r}} \end{bmatrix} = \begin{bmatrix} y_\beta & 0 & y_\varphi & y_p & y_r & 0 \\ 0 & 0 & 0 & 0 & \dfrac{1}{\cos\gamma_0} & 0 \\ 0 & 0 & 0 & 1 & \tan\gamma_0 & 0 \\ l_\beta & 0 & l_\varphi & l_p & l_r & 0 \\ n_\beta & 0 & n_\varphi & n_p & n_r & 0 \end{bmatrix} \begin{bmatrix} \tilde{\beta} \\ \tilde{\psi} \\ \tilde{\varphi} \\ \tilde{p} \\ \tilde{r} \end{bmatrix} + \begin{bmatrix} y_{\delta_a} & y_{\delta_r} \\ 0 & 0 \\ 0 & 0 \\ l_{\delta_a} & l_{\delta_r} \\ n_{\delta_a} & n_{\delta_r} \end{bmatrix} \begin{bmatrix} \tilde{\delta}_a \\ \tilde{\delta}_r \end{bmatrix}$$

$$\begin{bmatrix} y_1 \\ y_2 \\ y_3 \end{bmatrix} = \begin{bmatrix} \tilde{C}_Y \\ \tilde{C}_l \\ \tilde{C}_n \end{bmatrix} = \left[C_{Y,l,n}\right] \cdot \begin{bmatrix} \tilde{\beta} \\ \tilde{p}\,b/2V_0 \\ \tilde{r}\,b/2V_0 \\ \dot{\tilde{\beta}}\,b/V_0 \\ \tilde{\delta}_a \\ \tilde{\delta}_r \end{bmatrix} \qquad (6.3\text{-}3)$$

where:

$$\left[C_{Y,l,n}\right] = \begin{bmatrix} C_{Y_\beta} & C_{Y_p} & C_{Y_r} & C_{Y_{\dot\beta}} & C_{Y_{\delta_a}} & C_{Y_{\delta_r}} \\ C_{l_\beta} & C_{l_p} & C_{l_r} & C_{l_{\dot\beta}} & C_{l_{\delta_a}} & C_{l_{\delta_r}} \\ C_{n_\beta} & C_{n_p} & C_{n_r} & C_{n_{\dot\beta}} & C_{n_{\delta_a}} & C_{n_{\delta_r}} \end{bmatrix} \qquad (6.3\text{-}4)$$

and where the matrix elements $y_\beta,\ldots,n_{\delta_r}$ are functions of the control and stability derivatives. The element functions are listed in table 6-9 and the derivatives are listed in table 6-1. It should be noted that $y_\beta,\ldots,n_{\delta_r}$ are regarded as independent of the parameters since the state estimation is decoupled from the parameter estimation.

The aileron input δ_a and rudder input δ_r are

simultaneously optimized for the estimation of the following parameters:

$$C_{Y_\beta}, C_{Y_p}, C_{Y_r}, C_{Y_{\delta_a}}, C_{Y_{\delta_r}},$$
$$C_{l_\beta}, C_{l_p}, C_{l_r}, C_{l_{\delta_a}}, C_{l_{\delta_r}}, \qquad (6.3\text{-}5)$$
$$C_{n_\beta}, C_{n_p}, C_{n_r}, C_{n_{\delta_a}}, C_{n_{\delta_r}}.$$

The output signals consist of the specific lateral force and moment coefficients which are computed from acceleration and body rotation measurements at a sampling rate of 10 Hz. The errors are zero mean and uncorrelated with standard deviations listed in table 6-10. These standard deviations are derived from the standard deviations of the measured specific lateral force and constructed via five point Taylor polynomials of the roll and yaw rates. The output signals become mutually uncorrelated by approximating the product of inertia $I_{zx}=0$, see equation (4.1-15). The criterion for the optimization is specified as $J=\text{tr}\,\bar{M}^{-1}$.

The optimal aileron and rudder inputs are again derived via a search for the optimal information matrix $\bar{M}^\circ$. Because of the zero values of derivatives with respect to $\dot{\beta}$ and by approximating the product of inertia $I_{zx}=0$, the information matrix $\bar{M}$ has a block diagonal structure where all blocks are identical except for a scalar factor $1/\sigma_j^2$, j=1(1)3. The input design can therefore be restricted to one block corresponding to the derivatives in one output equation. The five state variables in equation (6.3-3) can be reduced to the four independent state variables $\tilde{\beta}$, $\tilde{\varphi}$, $\tilde{p}$ and $\tilde{r}$. With two input signals $\tilde{\delta}_a$ and $\tilde{\delta}_r$, $\bar{M}$ can be situated in a 20-dimensional plane $\mathcal{R}_M$ where $\bar{M}$ is represented by the vector $\underline{\psi}$. The number of sufficient harmonic signals is thus at most twenty-one. However, the optimal inputs may generally be approximated by fewer harmonic input signals.

The aileron and rudder inputs are optimized for a total power $P_u=18.75\ \text{deg}^2$ as in section 6.1.3. The inputs consist of harmonic signals whose frequencies are set to specified values and are optimized as well. The frequency range of the sine functions is restricted from $2\frac{2\pi}{16}$ to $9\frac{2\pi}{16}$ rad/s. The initial signal has frequencies at the specified values $\omega=k\frac{2\pi}{16}$ rad/s, k=2(1)9, where the aileron power is uniformly distributed over the four upper frequencies and the rudder power over the four lower frequencies. This choice was made because the low frequency Dutch roll is most efficiently initiated by a rudder input, while the highly damped aperiodic roll is best initiated by an aileron input.

The optimal inputs are again derived via the gradient method. At each iteration, the input signal is either added with a harmonic incorporating a new frequency, or the amplitudes and phases of the harmonics at the existing frequencies are modified. The derived aileron and rudder inputs with specified and optimized frequencies are shown in fig. 6-17 by their time histories and power spectral densities. The corresponding frequencies, amplitudes and powers of the harmonic signals for both cases are presented in table 6-11.

It can be seen that the power is almost entirely concentrated at the highest frequency for the aileron input. Furthermore, the rudder input remains concentrated at the low frequencies around the natural frequency of the Dutch roll motion ($\omega_0=1.22$ rad/s). If the frequencies are optimized, the rudder input gets additional frequencies around this natural frequency. It can be seen from the phase shifts that only the harmonics with frequencies around the natural frequency of the Dutch roll and at the highest frequency are modified.

6.3.4 Evaluation of Lateral Input Signal

The evaluation of the *DUT* input signal is carried out for the aileron and rudder inputs with specified frequencies. The generated state variables are shown in fig. 6-18. It can be seen that the yaw angle ψ has a strong deviation from the nominal condition. The deviations of the other variables remain limited. Furthermore, the roll rate strictly follows the aileron input, where the other output and state variables contain lower frequencies from the rudder input.

The average Fisher's information matrix and its norms are also calculated for the *DUT* inputs. The norms J of the matrix $\bar{M}=M/N$ are shown in fig. 6-19 as a function of the measuring time interval T with a sampling rate $\Delta t=0.1$ sec. The norms become stable around T=7.5 sec. This is about one and half the period of the Dutch roll motion.

The performance of the *DUT* input signals is compared with *Doublet* and *3211* inputs. These

latter two heuristic input signals are described in section 6.1.4. For the purpose of comparison all inputs have the same total power P_u=18.75 deg^2 and they are submitted to the original system. The comparison is made via the criterion J=tr $\bar{M}^{-1}$ and via the standard deviations σ_θ of the parameter estimates. The results are presented in fig. 6-20 and table 6-12.
The comparison of the different input signals sow contrasting values for J and σ_θ. The *DUT* aileron and rudder inputs perform relatively better than *3211* inputs.

6.4 Conclusions

When we look at the theoretical results for the performance of input signals optimized in the time domain, there are no large differences between the results of the different types of input signals (except for *Schulz*). Certainly improvements of 20-50% in the parameter standard deviations hardly seem to be worth the trouble of optimal input design.

It is even more surprising that in the case of the actual flight tests a simple heuristic input signal such as a *Doublet* or a *3211* can perform as well as and sometimes even better than one of the optimal signals.

For the *DUT* input design in the frequency domain, the estimation results of the short period and lateral stability and control derivatives gave a good comparison with other input signals.

Representing the optimal information matrix via a vector in the information space can be used to evaluate the mutual performance of different input designs and design criteria. If the locations are very close to each other one may expect equal accuracies of the parameter estimates. The input designs from different optimization criteria yields almost similar locations for the information vector and provided equivalent input designs and performances.

It must be kept in mind, however, that these conclusions hold for the simple aerodynamic model used in the examples and they may not be true for a more complicated model. In any case, if the aircraft to be tested is as simple as the one presented here, one can feel reassured by the knowledge that it is difficult to do better than a multi-step input with a well-chosen step length. This has the added advantage that these inputs are easy to fly manually.

On the other hand the aircraft to be tested may be more complicated, for example it may have some (combination of) parameters in its model description which are nearly unidentifiable, but which are nevertheless required for a certain application. For the Beaver example the $\dot{\alpha}$-derivatives are a case in point, because one may not be content to remove those parameters from the model and in that way introduce an error may become noticeable in certain flight manoeuvres. In this case it is certainly worthwhile to apply one of the described optimal input signal design methods and find an input signal that allows the identification of all parameters.

The optimal input signals have the advantage that their frequency contents are much lower than the multi-step signals and do not contain 'superfluous' frequency components. This can be of great importance, e.g. to avoid structural modes being excited by the input signal or to avoid the influence of the frequency-dependence on the aerodynamic model. The aerodynamic model description in terms of Taylor polynomials, as used in this volume, is really only a low-frequency approximation of the (infinite-dimensional) physical system. Exciting the aircraft with higher frequencies will therefore yield different parameter estimates in the approximate model than exciting the aircraft with lower frequencies. This effect is responsible for some of the systematic differences shown in the previous section. Ideally one should identify the aircraft model using the same input signal frequency content as in the application for which it will be used, i.e. with a low frequency content for a commercial training simulator or with high frequency content for an air-combat simulator.

Some of the practical advantages of using higher frequencies can also be achieved with the optimal input signals by specifying a higher frequency content, for instance by using a weighting function in the criterion which emphasizes the 'higher-frequency' parameters (e.g. the control derivatives) or by choosing higher frequency elementary signal

components (sinus or square wave) which can be done quite easily using the *DUT* methods.

Even if we intend to apply multi-step input signals, e.g. because the signals have to be flown manually, the amplitude, duration and relative phase of the multi-step input signals can be inspired by the optimal design. The analysis will also show how much you may be losing in theory by applying a multi-step input signal. Furthermore, the extra effort spent on optimal input design yields important extra information for the planning of the flight tests, such as safe input amplitudes, minimum required manoeuvre times, etc.

Finally, it must be said that the instrumentation and the algorithms to accomplish the parameter identification task have now advanced to the point where the choice of optimal control inputs may be the only and ultimate limiting factor in the attainable accuracy of these stability and control parameters.

$C_{X_{0_S}}$	=	0	$C_{Z_{0_S}}$	=	-0.9019			
$C_{X_{u_S}}$	=	-0.2019	$C_{Z_{u_S}}$	=	-1.7203	$C_{m_{u_S}}$	=	0.0413
$C_{X_{\alpha_S}}$	=	0.3715	$C_{Z_{\alpha_S}}$	=	-5.817	$C_{m_{\alpha_S}}$	=	-1.5466
$C_{X_{q_S}}$	=	-0.5316	$C_{Z_{q_S}}$	=	-3.8131	$C_{m_{q_S}}$	=	-18
$C_{X_{\delta_{eS}}}$	=	-0.0795	$C_{Z_{\delta_{eS}}}$	=	-0.5705	$C_{m_{\delta_{eS}}}$	=	-2.19
$C_{Y_{\beta_S}}$	=	-0.684	$C_{l_{\beta_S}}$	=	-0.0759	$C_{n_{\beta_S}}$	=	0.0419
$C_{Y_{p_S}}$	=	0	$C_{l_{\beta_S}}$	=	-0.6312	$C_{n_{\beta_S}}$	=	0.0496
$C_{Y_{r_S}}$	=	-0.145	$C_{l_{\beta_S}}$	=	0.0842	$C_{n_{\beta_S}}$	=	-0.0693
$C_{Y_{\dot{\beta}_S}}$	=	0	$C_{l_{\beta_S}}$	=	0	$C_{n_{\dot{\beta}_S}}$	=	0
$C_{Y_{\delta_{aS}}}$	=	0	$C_{l_{\dot{\beta}_S}}$	=	-0.115	$C_{n_{\delta_{aS}}}$	=	0.008
$C_{Y_{\delta_{rS}}}$	=	0.061	$C_{l_{\delta_{aS}}}$	=	-0.0026	$C_{n_{\delta_{rS}}}$	=	-0.0622
V_0	=	45 m/s	μ_c	=	58.656	K_X	=	0.1058
α_0	=	0.1385 rad	μ_b	=	6.365	K_Y	=	1.0832
ρ_0	=	1.024 $kg.m^3$				K_Z	=	0.1438
m_0	=	2215 kg				K_{XZ}	=	-0.0021

Table 6-1: *Nominal flight condition and a priori values of longintudinal and lateral stability and control derivatives as used for the design of longitudinal and lateral input signals.*

	$d = \sqrt{tr\left[\tilde{X}_1^T \cdot \tilde{X}_1\right] / N}$	
	longitudinal	**lateral**
DOUBLET	0.0605	0.1115
3211	0.0497	0.0728
MEHRA	0.0569	0.1169
SCHULZ	0.0620	0.1488
DUT	0.0578	0.1070

Table 6-2: *Root mean square deviation d from a nominal rectilinear flight condition, at 45 m/s TAS and 6000 ft, during different types of longitudinal and lateral flight test maneouvres.*

	theoretical and sample standard deviations with respect to DUT manoevres				relative sample standard deviations with respect to theoretical results			
	DOUBLET / DUT	3211 / DUT	MEHRA / DUT	SCHULZ / DUT	DOUBLET / theory	3211 / theory	MEHRA / theory	SCHULZ / theory
C_{X_0}				↑				↑
$C_{X_{\Delta p_t}}$				↑				↑
$\tilde{C}_{X_\alpha}$	↑			↑	↑		↑	↑
C_{X_q}				* ↑				
$C_{X_{\delta_e}}$				* ↑				
C_{Z_0}	↑				↑			
$C_{Z_{\Delta p_t}}$	↑				↑			
C_{Z_α}		↓				↓		
C_{Z_q}		↓		* ↑		↓		
$C_{Z_{\delta_e}}$		↓		* ↑		↓		
C_{m_0}	↑		↑	↑	↑		↑	↑
$C_{m_{\Delta p_t}}$	↑		↑	↑	↑		↑	↑
$\tilde{C}_{m_\alpha}$								
C_{m_q}				* ↑				
$C_{m_{\delta_e}}$				*				
	↑ (↓) Sample variance significantly higher (lower) than obtained from DUT manoeuvres * Theory predicts a significant difference from DUT manoeuvres				↑ (↓) Relative (with respect to DUT) sample standard deriviation significantly higher (lower) than corresponding theoretical value			

Table 6-3: *Statistically significant differences of theoretical and sample standard deviations between different manoeuvres, and of relative sample standard deviations between experimental and theoretical results for estimated longitudinal aerodynamic derivatives.*

	theoretical and sample standard deviations with respect to DUT manoeuvres				relative sample standard deviations with respect to theoretical results			
	DOUBLET / DUT	3211 / DUT	MEHRA / DUT	SCHULZ / DUT	DOUBLET / theory	3211 / theory	MEHRA / theory	SCHULZ / theory
C_{Y_0}				↑	↑	↑		
C_{Y_β}			↑	* ↑				
C_{Y_p}			↑	* ↑			↑	
C_{Y_r}								
$C_{Y_{\delta_a}}$		↓	↑	* ↑		↓		
$C_{Y_{\delta_r}}$		↓		* ↑		↓		
C_{l_0}								↑
C_{l_β}			↑	* ↑				
C_{l_p}			↑	* ↑	↑			
C_{l_r}								
$C_{l_{\delta_a}}$			↑	* ↑		↓		
$C_{l_{\delta_r}}$		↓		*				
C_{n_0}								
C_{n_β}				*				
C_{n_p}				* ↑				
C_{n_r}			↑				↑	
$C_{n_{\delta_a}}$				* ↑				
$C_{n_{\delta_r}}$				* ↑				
	↑ (↓) Sample variance significantly higher (lower) than obtained from DUT manoeuvres * Theory predicts a significant difference from DUT manoeuvres				↑ (↓) Relative (with respect to DUT) sample standard deriviation significantly higher (lower) than corresponding theoretical value			

Table 6-4: *Statistically significant differences of theoretical and sample standard deviations between different manoeuvres, and of relative sample standard deviations between experimental and theoretical results for estimated lateral aerodynamic derivatives.*

parameter	parameter value	parameter	parameter value
Z_α	-0.737 1/sec	M_α	-0.562 $1/sec^2$
		M_q	-1.588 1/sec
Z_{δ_e}	0.005 1/sec	M_{δ_e}	-1.660 $1/sec^2$
V = 41.2 m/sec h = Sea Level			

Table 6-5: *Parameter values and flight condition for short period mode of C-8 Buffalo aircraft.*

output signal	original model		modified model for two-step method	
	signal	σ_y	signal	σ_y
y_1	α	1.00 deg	$\dot{\alpha}$	23.75 deg/sec
y_2	q	0.70 deg	$\dot{q}$	16.62 deg/sec^2

Table 6-6: *Standard deviations of measurement errors for short period mode models of C-8 Buffalo aircraft.*

	freq. (rad/s)	power ratio	power (deg^2)	ampl. (deg)
1	0	0.278	4.626	2.151
2	1.5	0.438	7.296	3.820
3	4.5	0.285	4.745	3.081
optimal $\underline{\Psi}^o$:		ψ_1=0.128 ψ_2=0.092		

DUT signals with fixed frequencies

	freq. (rad/s)	power ratio	power (deg^2)	ampl. (deg)
1	0.000	0.296	4.928	2.220
2	1.674	0.479	7.989	3.997
3	4.500	0.225	3.750	2.739
optimal $\underline{\Psi}^o$:		ψ_1=0.128 ψ_2=0.093		

DUT signals with optimized frequencies

Table 6-7: *Optimal elevator input with harmonic input signals for short period mode parameters of C-8 Buffalo aircraft.*

Parameter	Parameter value	Parameter standard deviations σ_θ		
		Mehra	Mehra	DUT signals specified ω_k
		time domain	freq. domain	freq. domain
M_q	-1.588	0.1130	0.1400	0.1292
M_α	-0.562	0.0676	0.0819	0.0696
Z_α	-0.737	0.0561	0.0704	0.0596
M_{δ_e}	-1.660	0.0672	0.0801	0.0748
Z_{δ_e}	0.005	0.0400	0.0409	0.0400
J=tr $\bar{M}^{-1}$		3.986	5.949	4.874
Max. amplitude (deg)		9.47	7.68	7.33

Table 6-8: *Comparison of Cramer-Rao lower bounds for T=6 sec (N=151) for optimal elevator inputs with design criterion J=tr $\bar{M}^{-1}$ via different optimization techniques for short period mode parameters of C-8 Buffalo aircraft.*

$y_\beta = \frac{V_0}{b}\frac{C_{Y_\beta}}{2\mu_b - C_{Y_{\dot\beta}}}$	$\ell_\beta = \frac{V_0^2}{b^2}\frac{1}{2\mu_b}\left\{\frac{K_Z^2 C_{\ell_\beta} + K_{XZ} C_{n_\beta}}{K_X^2 K_Z^2 - K_{XZ}^2} + \frac{C_{Y_\beta}}{2\mu_b - C_{Y_{\dot\beta}}}\frac{K_Z^2 C_{\ell_{\dot\beta}} + K_{XZ} C_{n_{\dot\beta}}}{K_X^2 K_Z^2 - K_{XZ}^2}\right\}$	$n_\beta = \frac{V_0^2}{b^2}\frac{1}{2\mu_b}\left\{\frac{K_{XZ} C_{\ell_\beta} + K_X^2 C_{n_\beta}}{K_X^2 K_Z^2 - K_{XZ}^2} + \frac{C_{Y_\beta}}{2\mu_b - C_{Y_{\dot\beta}}}\frac{K_{XZ} C_{\ell_{\dot\beta}} + K_X^2 C_{n_{\dot\beta}}}{K_X^2 K_Z^2 - K_{XZ}^2}\right\}$
$y_\varphi = -\frac{V_0}{b}\frac{C_{Z_0}}{2\mu_b - C_{Y_{\dot\beta}}}$	$\ell_\varphi = -\frac{V_0^2}{b^2}\frac{1}{2\mu_b}\frac{C_{Z_0}}{2\mu_b - C_{Y_{\dot\beta}}}\frac{K_Z^2 C_{\ell_{\dot\beta}} + K_{XZ} C_{n_{\dot\beta}}}{K_X^2 K_Z^2 - K_{XZ}^2}$	$n_\varphi = -\frac{V_0^2}{b^2}\frac{1}{2\mu_b}\frac{C_{Z_0}}{2\mu_b - C_{Y_{\dot\beta}}}\frac{K_{XZ} C_{\ell_{\dot\beta}} + K_X^2 C_{n_{\dot\beta}}}{K_X^2 K_Z^2 - K_{XZ}^2}$
$y_p = \frac{1}{2}\frac{C_{Y_p}}{2\mu_b - C_{Y_{\dot\beta}}}$	$\ell_p = \frac{V_0}{b}\frac{1}{4\mu_b}\left\{\frac{K_Z^2 C_{\ell_p} + K_{XZ} C_{n_p}}{K_X^2 K_Z^2 - K_{XZ}^2} + \frac{C_{Y_p}}{2\mu_b - C_{Y_{\dot\beta}}}\frac{K_Z^2 C_{\ell_{\dot\beta}} + K_{XZ} C_{n_{\dot\beta}}}{K_X^2 K_Z^2 - K_{XZ}^2}\right\}$	$n_p = \frac{V_0}{b}\frac{1}{4\mu_b}\left\{\frac{K_{XZ} C_{\ell_p} + K_X^2 C_{n_p}}{K_X^2 K_Z^2 - K_{XZ}^2} + \frac{C_{Y_p}}{2\mu_b - C_{Y_{\dot\beta}}}\frac{K_{XZ} C_{\ell_{\dot\beta}} + K_X^2 C_{n_{\dot\beta}}}{K_X^2 K_Z^2 - K_{XZ}^2}\right\}$
$y_r = -\frac{1}{2}\frac{4\mu_b - C_{Y_r}}{2\mu_b - C_{Y_{\dot\beta}}}$	$\ell_r = \frac{V_0}{b}\frac{1}{4\mu_b}\left\{\frac{K_Z^2 C_{\ell_r} + K_{XZ} C_{n_r}}{K_X^2 K_Z^2 - K_{XZ}^2} - \frac{4\mu_b - C_{Y_r}}{2\mu_b - C_{Y_{\dot\beta}}}\frac{K_Z^2 C_{\ell_{\dot\beta}} + K_{XZ} C_{n_{\dot\beta}}}{K_X^2 K_Z^2 - K_{XZ}^2}\right\}$	$n_r = \frac{V_0}{b}\frac{1}{4\mu_b}\left\{\frac{K_{XZ} C_{\ell_r} + K_X^2 C_{n_r}}{K_X^2 K_Z^2 - K_{XZ}^2} - \frac{4\mu_b - C_{Y_r}}{2\mu_b - C_{Y_{\dot\beta}}}\frac{K_{XZ} C_{\ell_{\dot\beta}} + K_X^2 C_{n_{\dot\beta}}}{K_X^2 K_Z^2 - K_{XZ}^2}\right\}$
$y_{\delta_a} = \frac{V_0}{b}\frac{C_{Y_{\delta_a}}}{2\mu_b - C_{Y_{\dot\beta}}}$	$\ell_{\delta_a} = \frac{V_0^2}{b^2}\frac{1}{2\mu_b}\left\{\frac{K_Z^2 C_{\ell_{\delta_a}} + K_{XZ} C_{n_{\delta_a}}}{K_X^2 K_Z^2 - K_{XZ}^2} + \frac{C_{Y_{\delta_a}}}{2\mu_b - C_{Y_{\dot\beta}}}\frac{K_Z^2 C_{\ell_{\dot\beta}} + K_{XZ} C_{n_{\dot\beta}}}{K_X^2 K_Z^2 - K_{XZ}^2}\right\}$	$n_{\delta_a} = \frac{V_0^2}{b^2}\frac{1}{2\mu_b}\left\{\frac{K_{XZ} C_{\ell_{\delta_a}} + K_X^2 C_{n_{\delta_a}}}{K_X^2 K_Z^2 - K_{XZ}^2} + \frac{C_{Y_{\delta_a}}}{2\mu_b - C_{Y_{\dot\beta}}}\frac{K_{XZ} C_{\ell_{\dot\beta}} + K_X^2 C_{n_{\dot\beta}}}{K_X^2 K_Z^2 - K_{XZ}^2}\right\}$
$y_{\delta_r} = \frac{V_0}{b}\frac{C_{Y_{\delta_r}}}{2\mu_b - C_{Y_{\dot\beta}}}$	$\ell_{\delta_r} = \frac{V_0^2}{b^2}\frac{1}{2\mu_b}\left\{\frac{K_Z^2 C_{\ell_{\delta_r}} + K_{XZ} C_{n_{\delta_r}}}{K_X^2 K_Z^2 - K_{XZ}^2} + \frac{C_{Y_{\delta_r}}}{2\mu_b - C_{Y_{\dot\beta}}}\frac{K_Z^2 C_{\ell_{\dot\beta}} + K_{XZ} C_{n_{\dot\beta}}}{K_X^2 K_Z^2 - K_{XZ}^2}\right\}$	$n_{\delta_r} = \frac{V_0^2}{b^2}\frac{1}{2\mu_b}\left\{\frac{K_{XZ} C_{\ell_{\delta_r}} + K_X^2 C_{n_{\delta_r}}}{K_X^2 K_Z^2 - K_{XZ}^2} + \frac{C_{Y_{\delta_r}}}{2\mu_b - C_{Y_{\dot\beta}}}\frac{K_{XZ} C_{\ell_{\dot\beta}} + K_X^2 C_{n_{\dot\beta}}}{K_X^2 K_Z^2 - K_{XZ}^2}\right\}$

Table 6-9: *Matrix elements in the linearized aircraft system model for the lateral motion.*

output signal	measured signal		applied signal	
	signal	σ_y	signal	σ_y
y_1	$\tilde{A}_y$	0.0014 m/sec^2	$\tilde{C}_y$	$1.288\ 10^{-4}$
y_2	$\tilde{p}$	0.0032 deg/sec^2	$\tilde{C}_\ell$	$7.993\ 10^{-6}$
y_3	$\tilde{r}$	0.0032 deg/sec^2	$\tilde{C}_n$	$1.477\ 10^{-5}$

output signal	measured signals		applied signals	
	signals	$\sqrt{\sigma_{y_k}\ \sigma_{y_\ell}}$	signals	$\sqrt{\sigma_{y_k}\ \sigma_{y_\ell}}$
y_1 - y_2			$\tilde{C}_\ell$ - $\tilde{C}_n$	$3.412\ 10^{-11}$

Table 6-10: *Standard deviations and non-zero correlations of measurement errors for lateral mode model of DHC-2 Beaver aircraft.*

	freq. (rad/s)	power ratio	aileron input			rudder input		
			power (deg^2)	ampl. (deg)	phase (rad)	power (deg^2)	ampl. (deg)	phase (rad)
2	0.785	0.048	0	0	0	0.896	1.339	0
3	1.178	0.052	0.966	1.390	0	0.000	0.008	0.070
4	1.571	0.064	1.201	1.550	0	0.000	0.016	-1.125
5	1.964	0.048	0	0	0	0.896	1.339	0
6	2.356	0.024	0.448	0.946	0	0	0	0
7	2.749	0.024	0.448	0.946	0	0	0	0
8	3.142	0.024	0.448	0.946	0	0	0	0
9	3.534	0.717	13.435	5.184	0	0.013	0.159	0.195

DUT signals with specified frequencies

	freq. (rad/s)	power ratio	aileron input			rudder input		
			power (deg^2)	ampl. (deg)	phase (rad)	power (deg^2)	ampl. (deg)	phase (rad)
2	0.785	0.048	0	0	0	0.899	1.341	0
3	1.178	0.048	0	0	0	0.899	1.341	0
	1.341	0.016	0.008	0.127	-2.569	0.285	0.754	0.000
	1.492	0.001	0.000	0.022	-2.001	0.011	0.146	0.000
4	1.571	0.048	0	0	0	0.899	1.341	0
5	1.964	0.048	0	0	0	0.899	1.341	0
6	2.356	0.024	0.449	0.948	0	0	0	0
7	2.749	0.024	0.449	0.948	0	0	0	0
8	3.142	0.024	0.449	0.948	0	0	0	0
9	3.534	0.710	13.489	5.194	0	0.013	0.162	0.195

DUT signals with optimized frequencies

Table 6-11: *Optimal aileron and rudder inputs with harmonic input signals for lateral mode parameters of DHC-2 Beaver aircraft.*

Parameter	Parameter value	Parameter standard deviation $\sigma_\theta \times 10^4$		
		doublet	3211	DUT signals fixed ω_k
C_{Y_β}	-0.684	3.42	3.26	3.40
C_{Y_p}	0	24.82	22.32	18.36
C_{Y_r}	-0.145	42.14	26.89	24.58
$C_{Y_{\dot\beta}}$	0	18.38	12.89	13.44
$C_{Y_{\delta a}}$	0	3.86	2.89	2.99
$C_{Y_{\delta r}}$	0.061	2.08	1.89	5.29
C_{ℓ_β}	-0.0759	0.22	0.21	0.21
C_{ℓ_p}	-0.6312	1.57	1.41	1.16
C_{ℓ_r}	5.0842	2.66	1.70	1.55
$C_{\ell_{\dot\beta}}$	0	1.16	0.81	0.85
$C_{\ell_{\delta a}}$	-0.115	0.24	0.18	0.19
$C_{\ell_{\delta r}}$	-0.0026	0.13	0.12	0.33
C_{n_β}	0.0419	0.39	0.38	0.39
C_{n_p}	0.0496	2.86	2.57	2.12
C_{n_r}	-0.0693	4.86	3.10	2.83
$C_{n_{\dot\beta}}$	0	2.12	1.49	1.55
$C_{n_{\delta a}}$	0.008	0.44	0.33	0.34
$C_{n_{\delta r}}$	-0.0622	0.24	0.22	0.61
$J=tr\ \bar{M}^{-1}$		$4.521\ 10^{-3}$	$2.309\ 10^{-3}$	$1.917\ 10^{-3}$
Max. amplitude (deg)	aileron	5.77 -5.77	5.77 -5.77	9.70 -9.70
	rudder	3.20 -7.20	3.77 -7.77	0.45 -4.45

Table 6-12: *Comparison of Cramer-Rao lower bounds for T=16 sec (N=161) for heuristic and optimal aileron and rudder inputs with design criteria $J=tr\ \bar{M}^{-1}$ for lateral mode parameters of DHC-2 Beaver aircraft.*

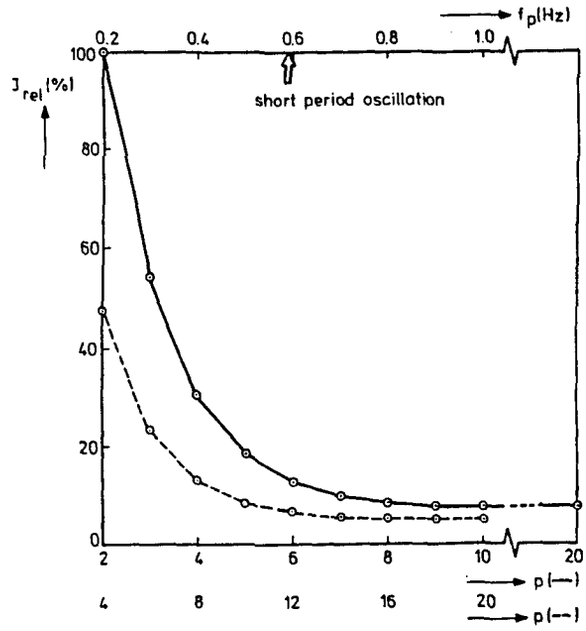

(a) *The relative performance index as a function of p*

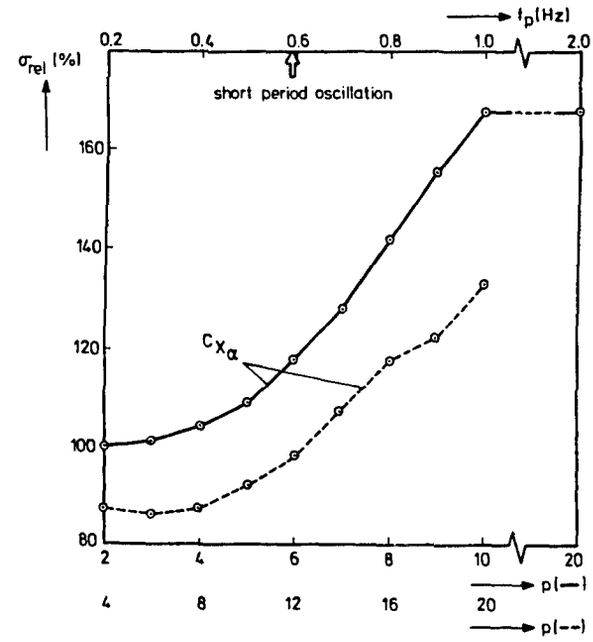

(b) *The relative standard deviation of $\hat{C}_{X_\alpha}$ as a function of p*

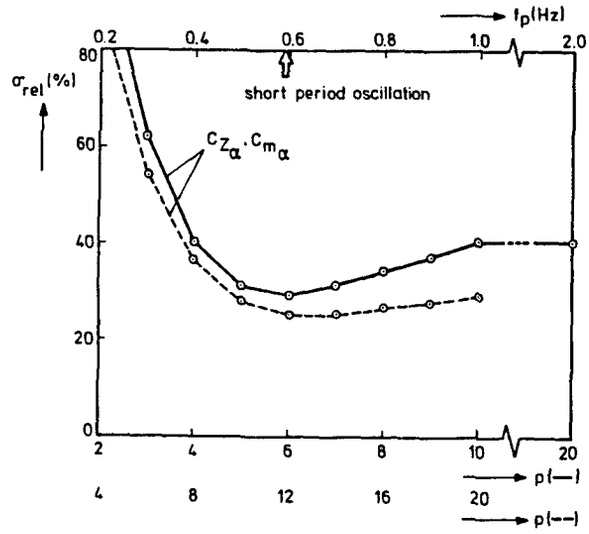

(c) *The relative standard deviation of $\hat{C}_{Z_\alpha}$ and $\hat{C}_{m_\alpha}$ as a function of p*

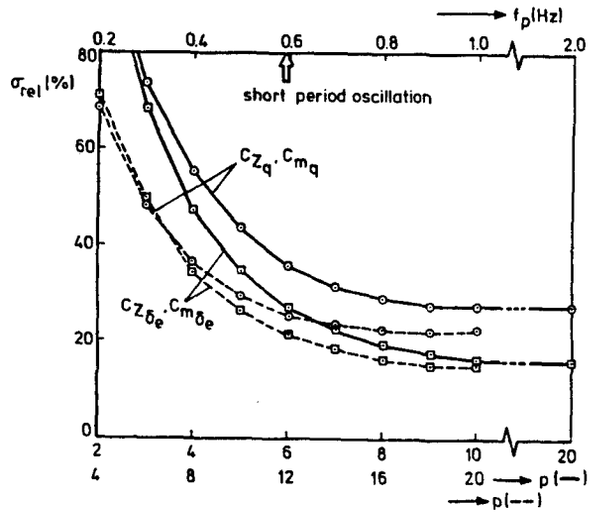

(d) *The relative standard deviation of $\hat{C}_{Z_q}$, $\hat{C}_{m_q}$, $\hat{C}_{Z_{\delta_e}}$ and $\hat{C}_{m_{\delta_e}}$ as a function of p*

Figure 6-1: *The relative performance index J_{rel} and relative standard deviations σ_{rel} of the estimated longitudinal parameters as a function of the total number of orthonormal functions p in set 1 (——) and set 2 (- -).*

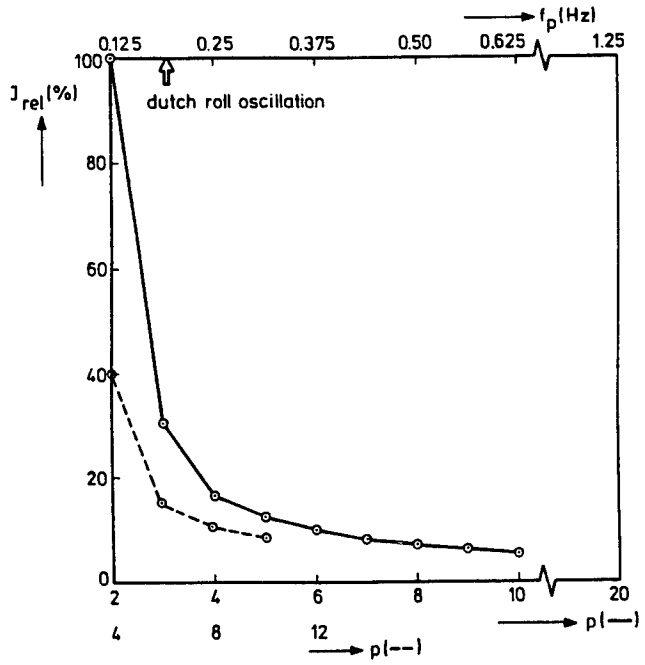

(a) *The relative performance index as a function of p*

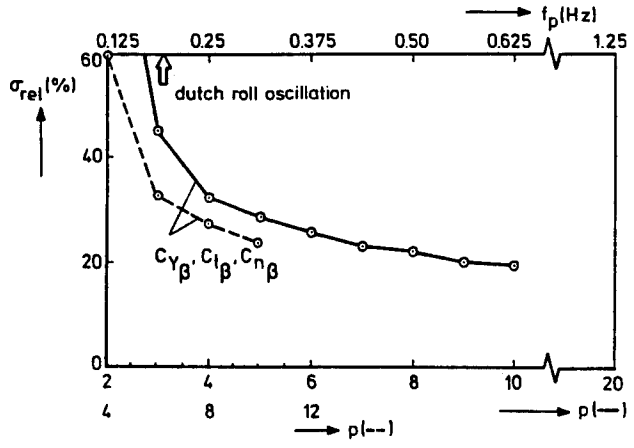

(b) *The relative standard deviation of* $\hat{C}_{Y_\beta}$, $\hat{C}_{l_\beta}$ *and* $\hat{C}_{n_\beta}$ *as a function of p*

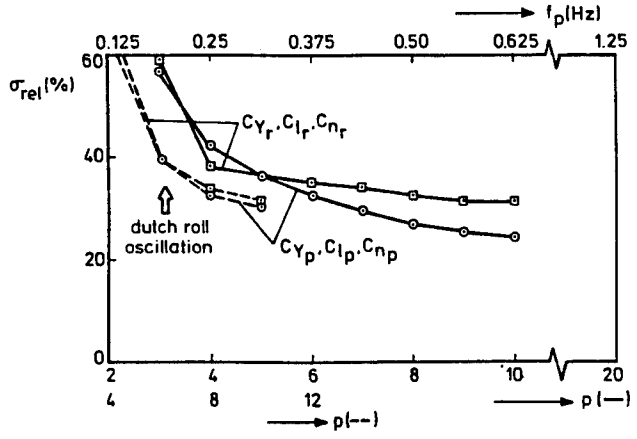

(c) *The relative standard deviation of* $\hat{C}_{Y_r}$, $\hat{C}_{l_r}$, $\hat{C}_{n_r}$, $\hat{C}_{Y_p}$, $\hat{C}_{l_p}$ *and* $\hat{C}_{n_p}$ *as function of p*

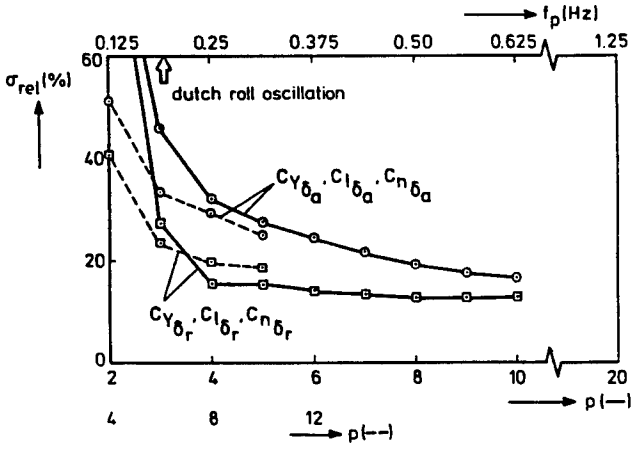

(d) *The relative standard deviation of* $\hat{C}_{Y_{\delta_a}}$, $\hat{C}_{l_{\delta_a}}$, $\hat{C}_{n_{\delta_a}}$, $\hat{C}_{Y_{\delta_r}}$, $\hat{C}_{l_{\delta_r}}$ *and* $\hat{C}_{n_{\delta_r}}$ *as a function of p*

Figure 6-2: *The relative performance index* J_{rel} *and relative standard deviations* σ_{rel} *of the estimated longitudinal parameters as a function of the total number of orthonormal functions p in set 1 (—) and set 2 (- -).*

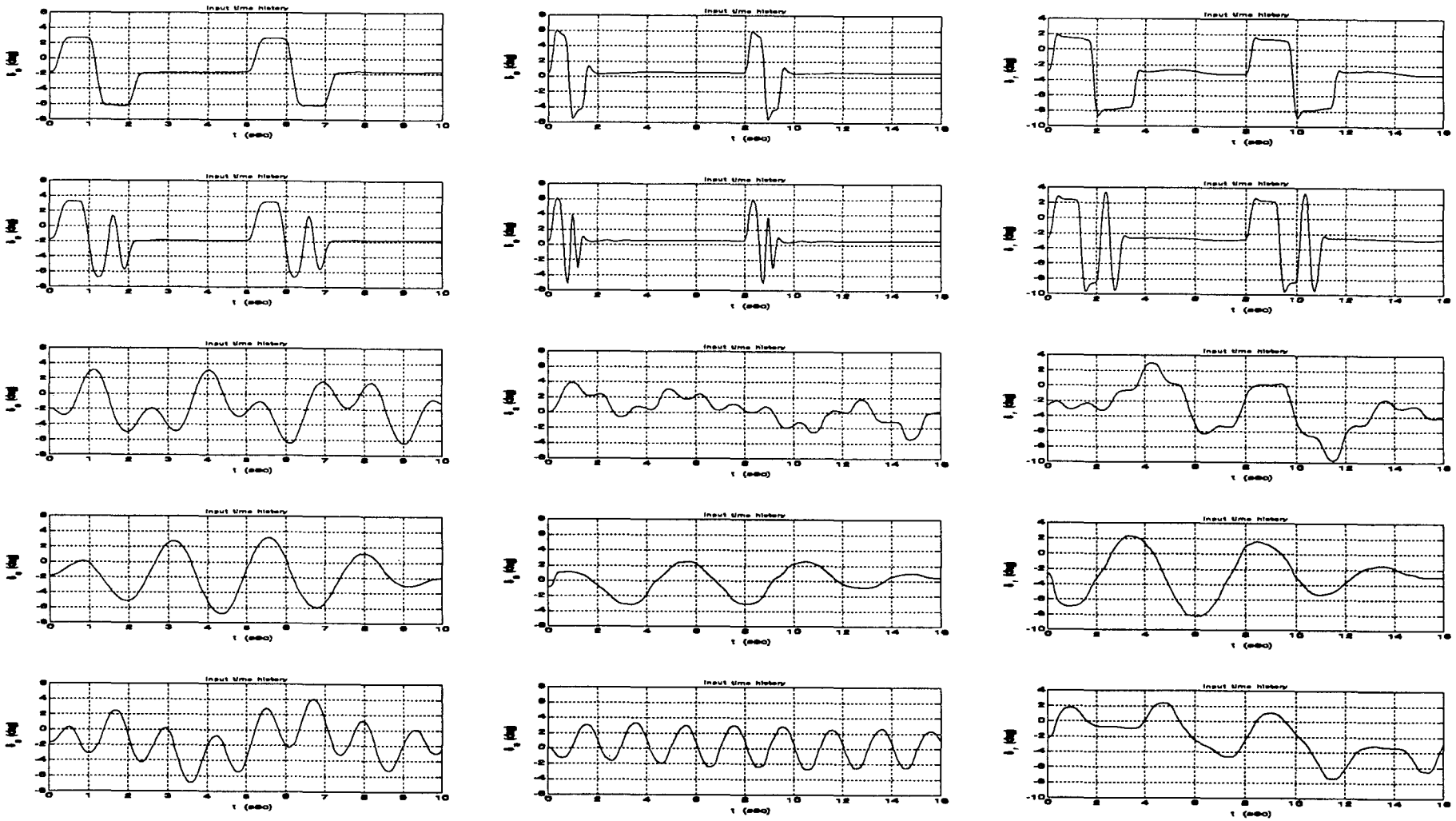

elevator input *aileron input* *rudder input*

Figure 6-3: *Input signals of 5 different types as recorded in flight; rows successively correspond to doublet, 3211, Mehra, Schulz and DUT signals.*

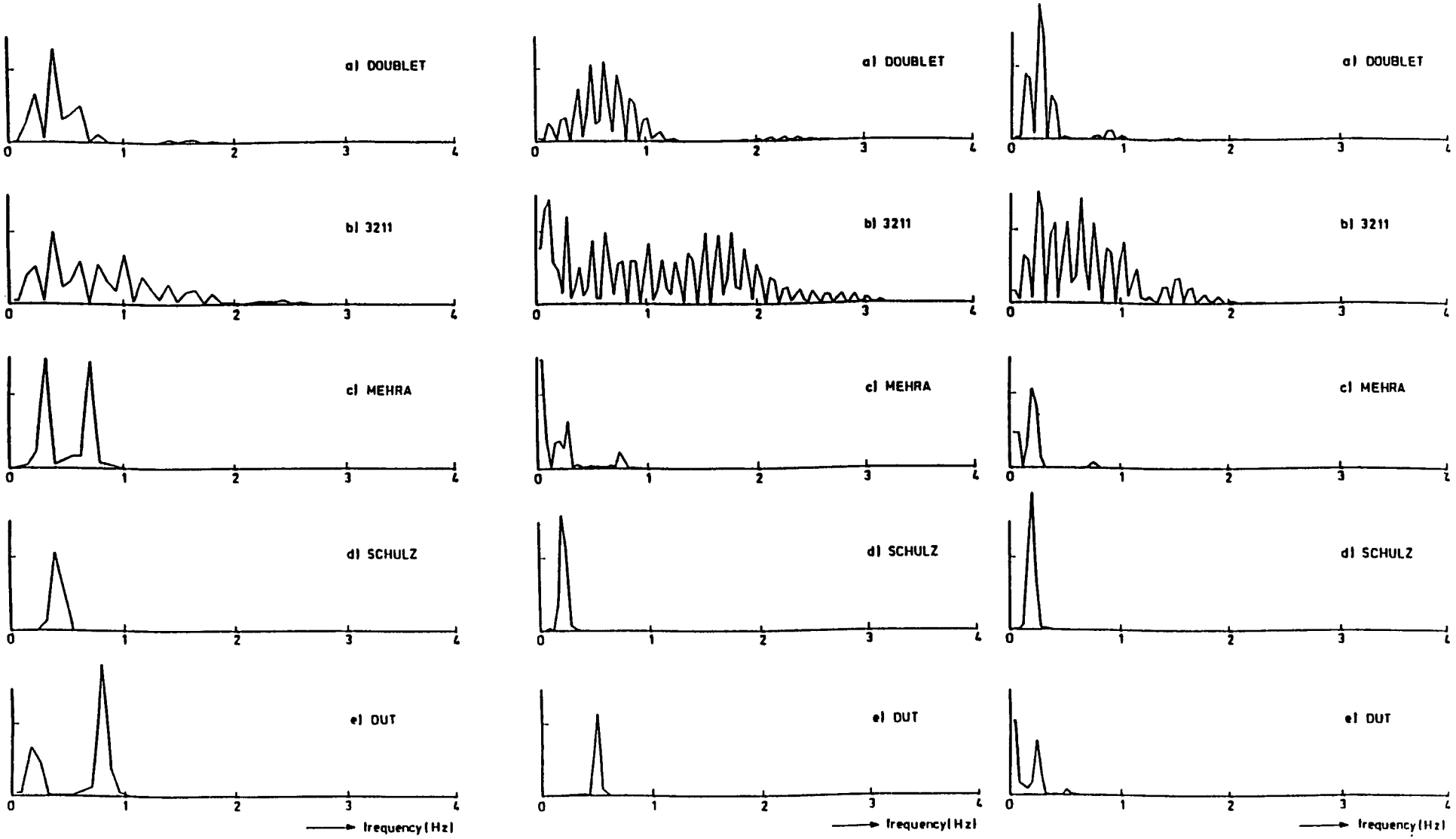

Figure 6-4: *Power spectral densities on linear scales as determined from measurements in longitudinal and lateral manoeuvres.*

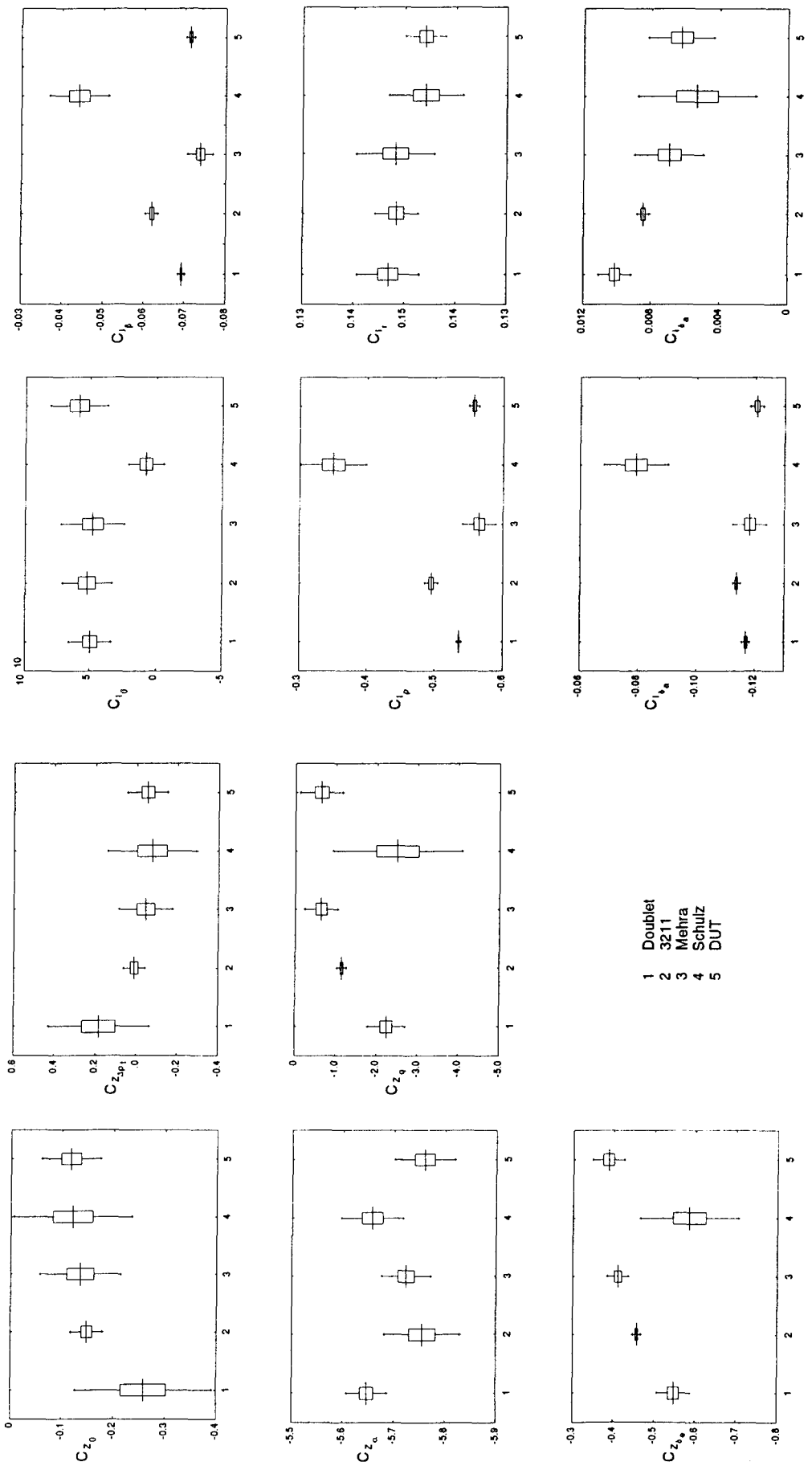

Figure 6-5: *Sample means, standard derivations of sample means (indicated by blocks) and standard deviations of estimated C_Z- and C_l-derivatives of five different types of flight test manoeuvres.*

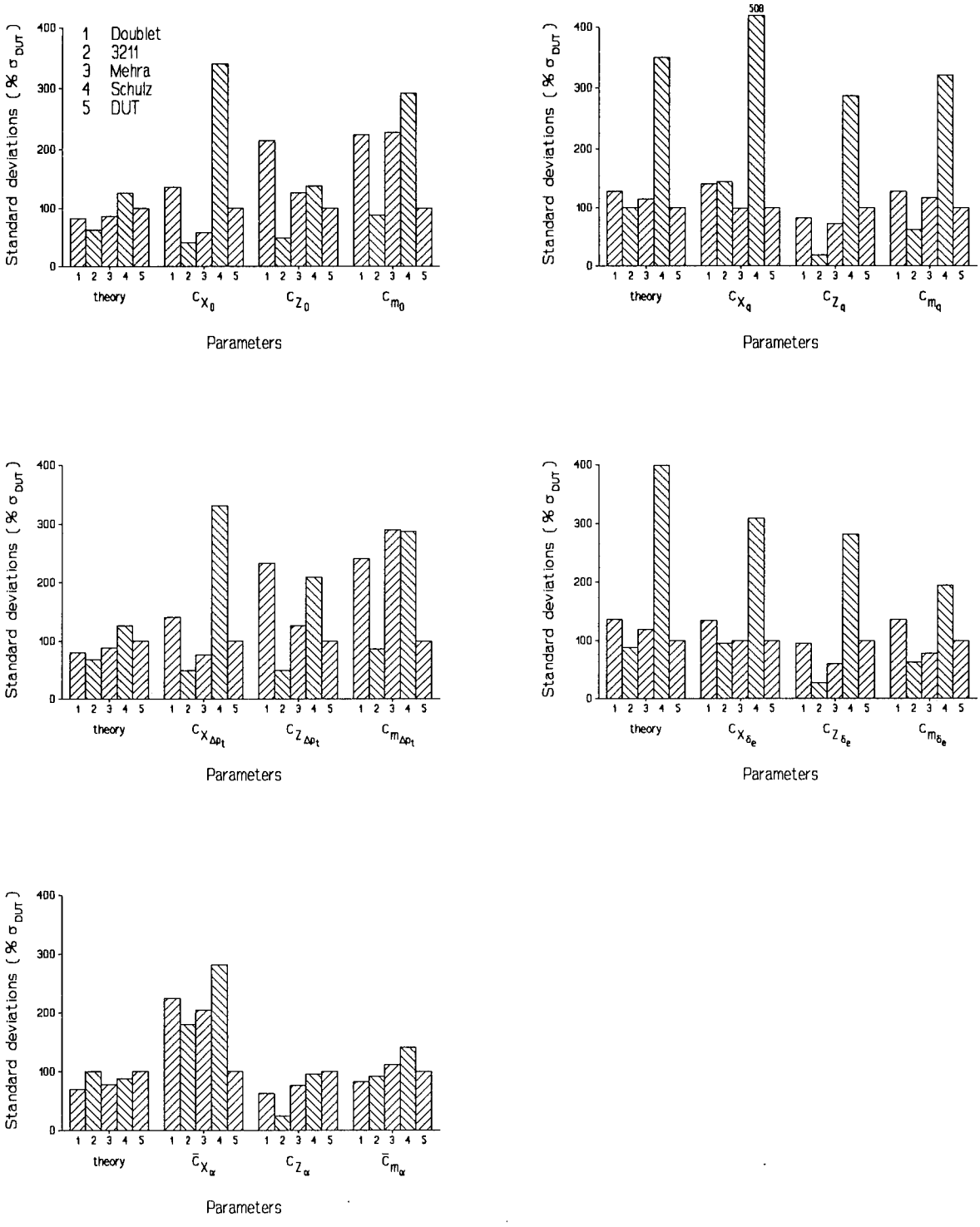

Figure 6-6: *Relative (with respect to corresponding results from DUT manoeuvres) theoretical and sample standard deviations of estimated longitudinal aerodynamic derivatives of 5 different types of longitudinal dynamic flight test manoeuvres; sample results are shown immediately above each aerodynamic derivative, corresponding theoretical results are presented as the left most group of bars.*

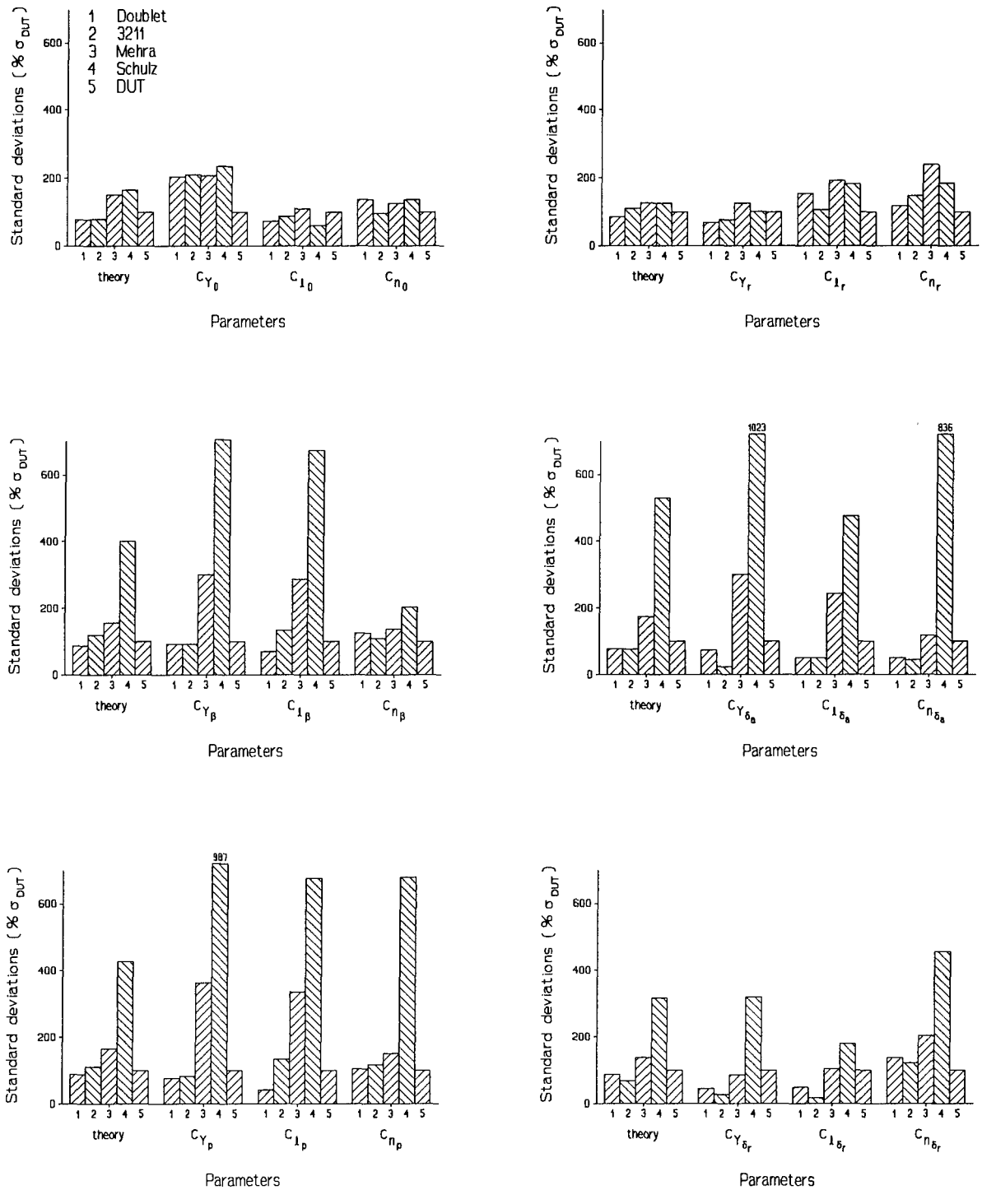

Figure 6-7: *Relative (with respect to corresponding results from DUT manoeuvres) theoretical and sample standard deviations of estimated lateral aerodynamic derivatives of 5 different types of lateral dynamic flight test manoeuvres; sample results are shown immediately above each aerodynamic derivative, corresponding theoretical results are presented as the left most group of bars.*

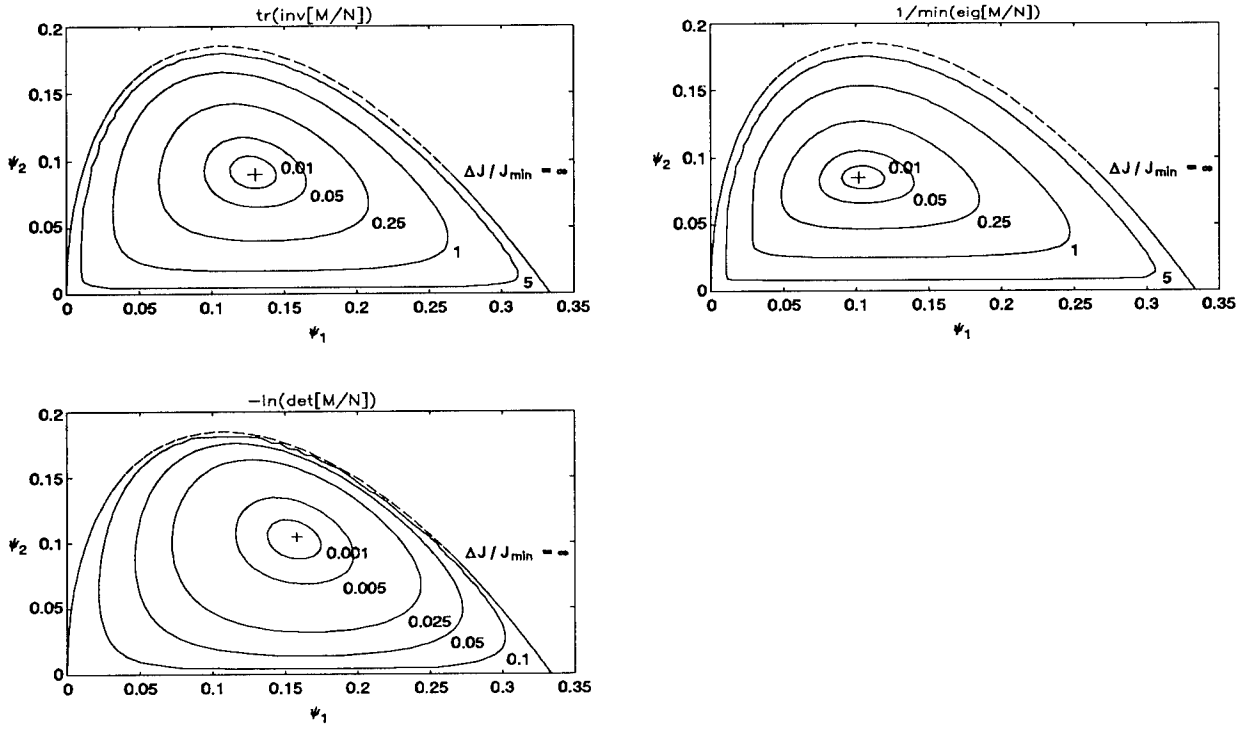

Figure 6-8: *2D view of attainable optimization criteria.*

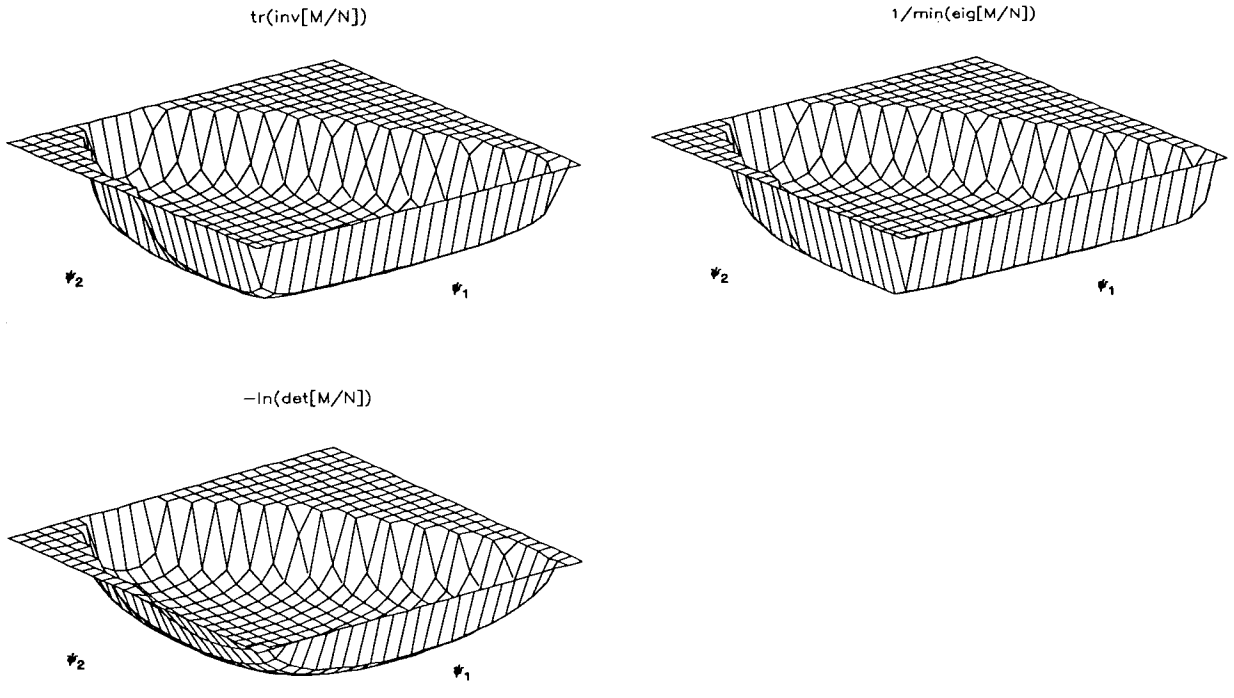

Figure 6-9: *3D view of attainable optimization criteria.*

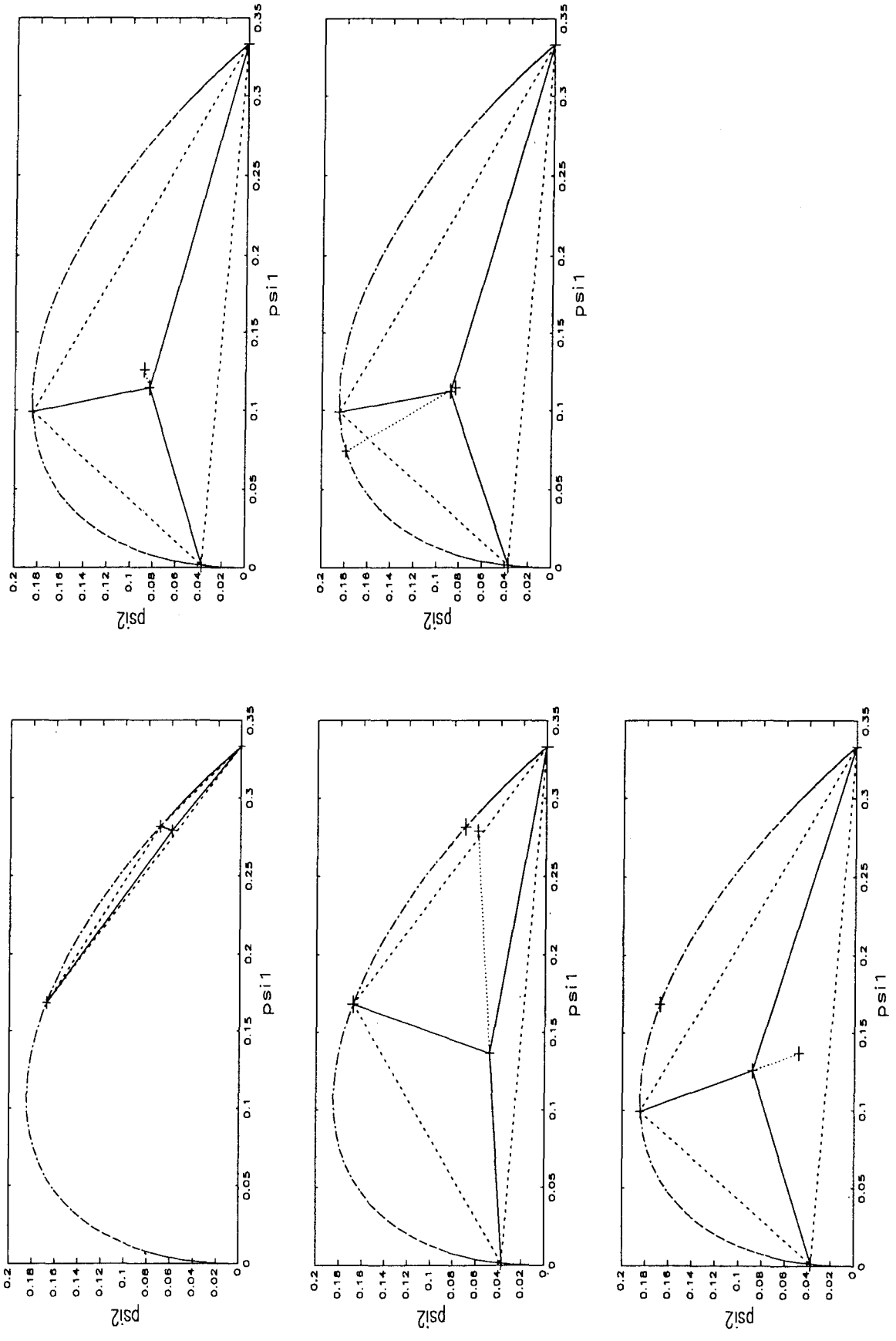

Figure 6-10: *First iteration steps in the computation of optimal input signal.*

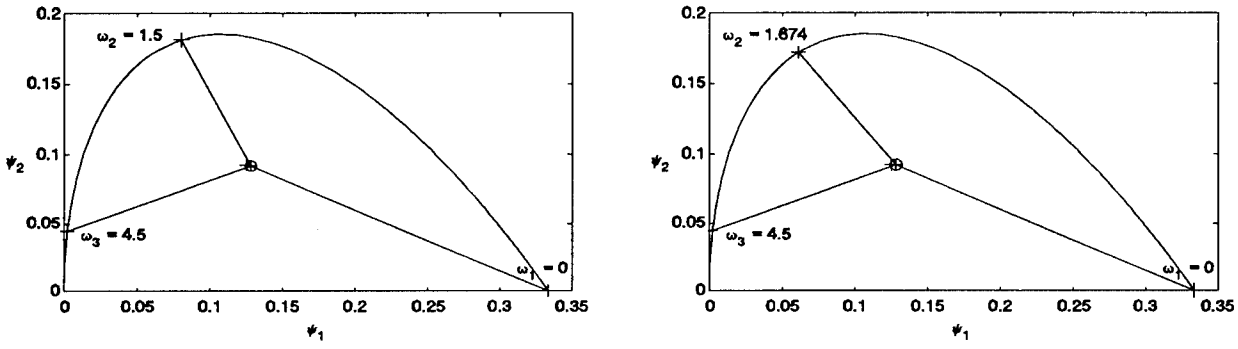

specified frequencies *optimized frequencies*

Figure 6-11: *Reconstruction of optimal information matrix from elementary signals (⊕) and as a function of* $\underline{\psi}$ *(+) for elevator input for criterion* $J=tr\ M^{-1}$.

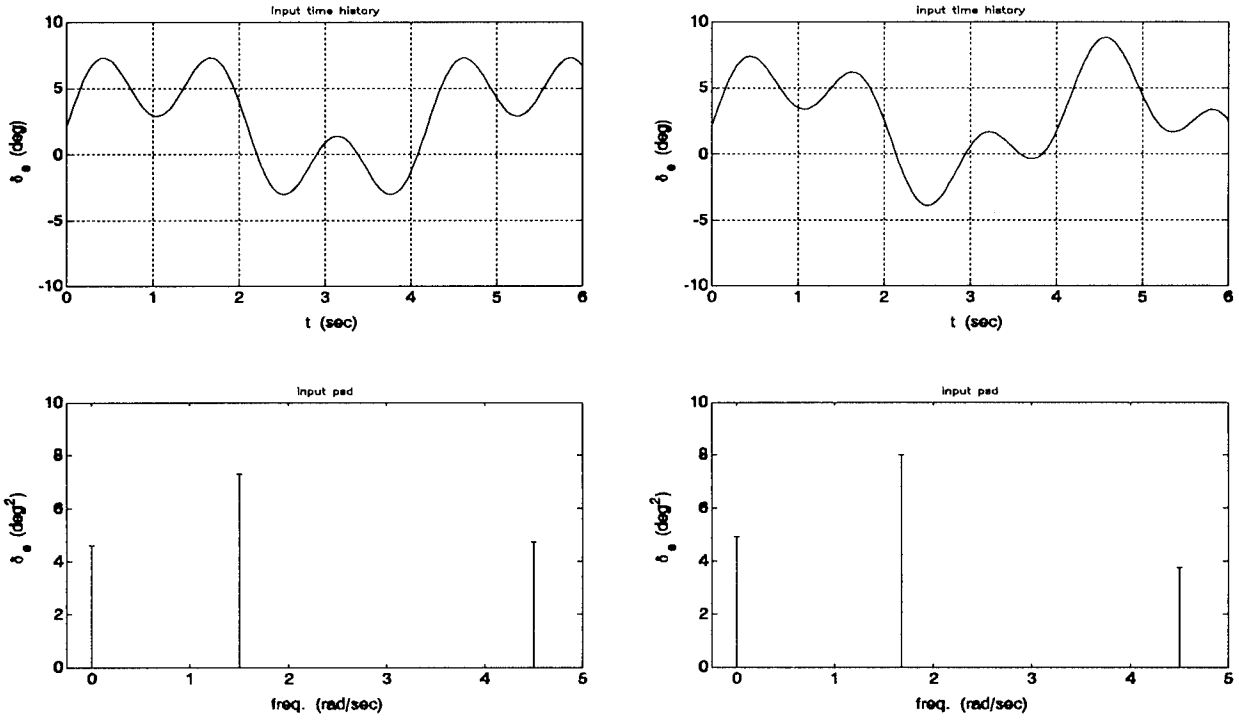

specified frequencies *optimized frequencies*

Figure 6-12: *Time history and normalized power spectral density of DUT elevator input with specified and optimized frequencies for criterion* $J=tr\ M^{-1}$.

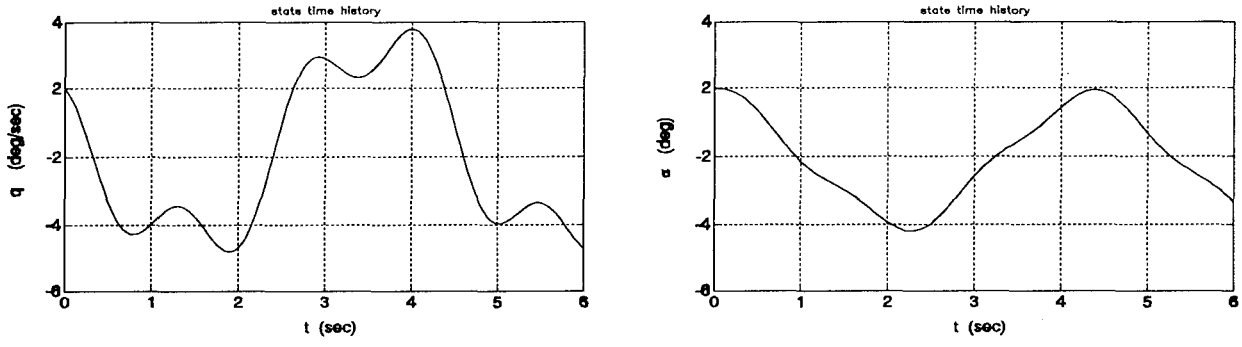

Figure 6-13: *Time history of angle of attack and pitch response from DUT elevator input with specified frequencies.*

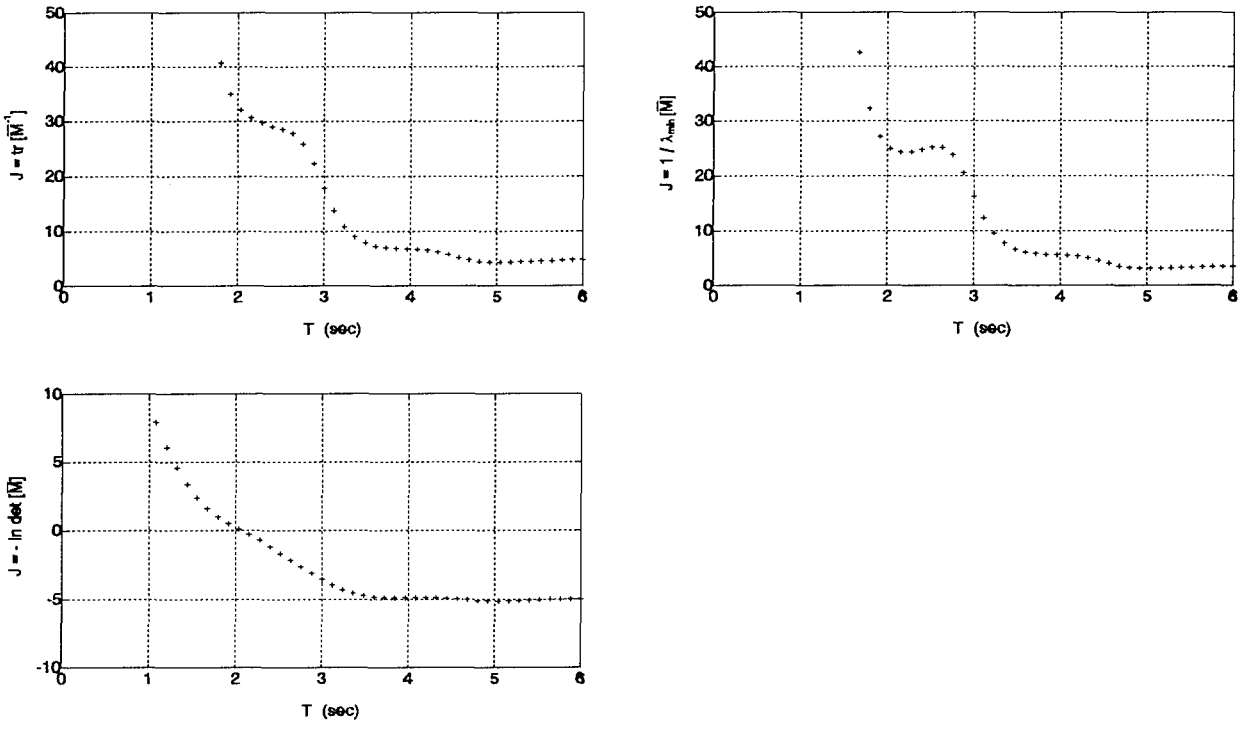

Figure 6-14: *Optimization criteria as function of measuring time interval (Δt=0.04 sec).*

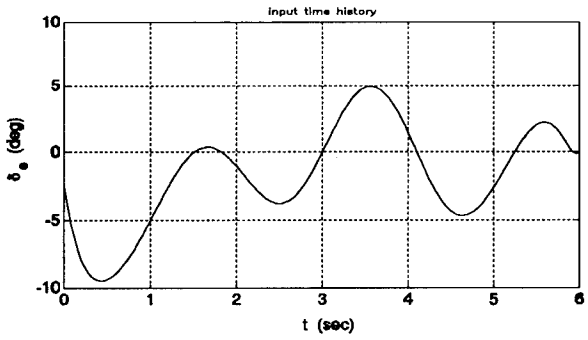

elevator input by Mehra from time domain technique

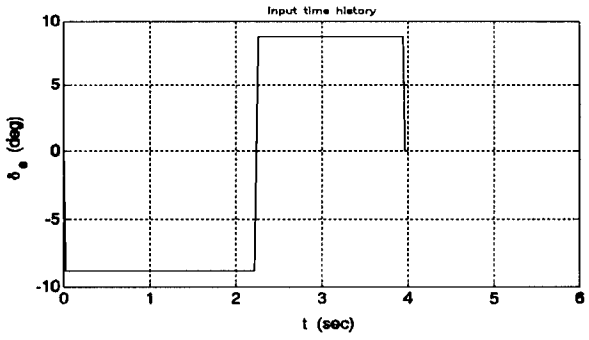

elevator input by Chen

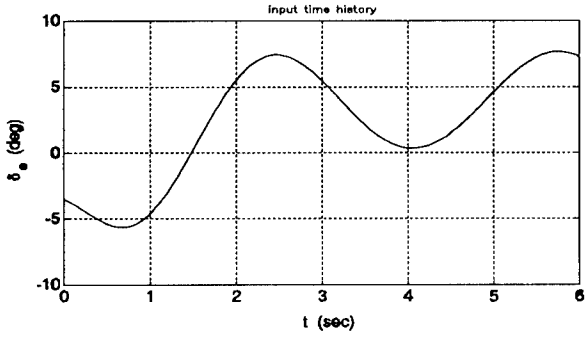

elevator input by Mehra from frequency domain technique

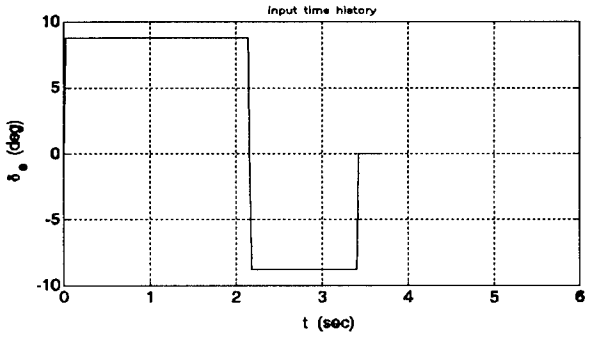

elevator input by Morelli

Figure 6-15: *Optimal elevator inputs from different optimization techniques.*

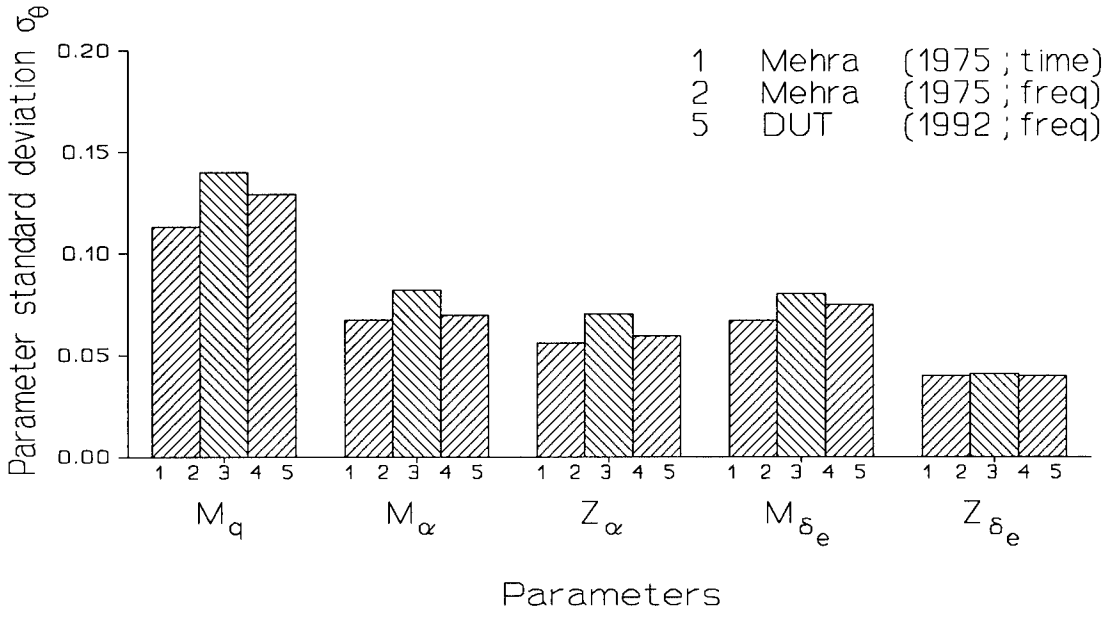

Figure 6-16: *Comparison of Cramer-Rao Lower Bounds.*

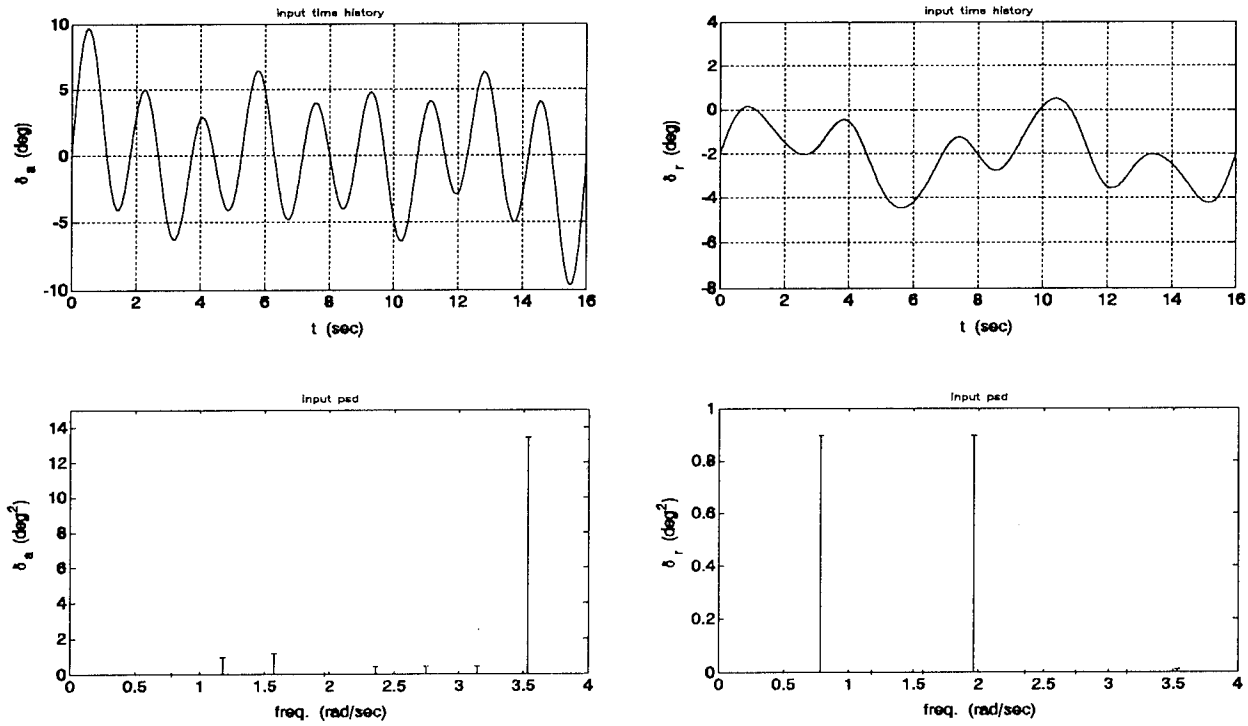

specified frequencies

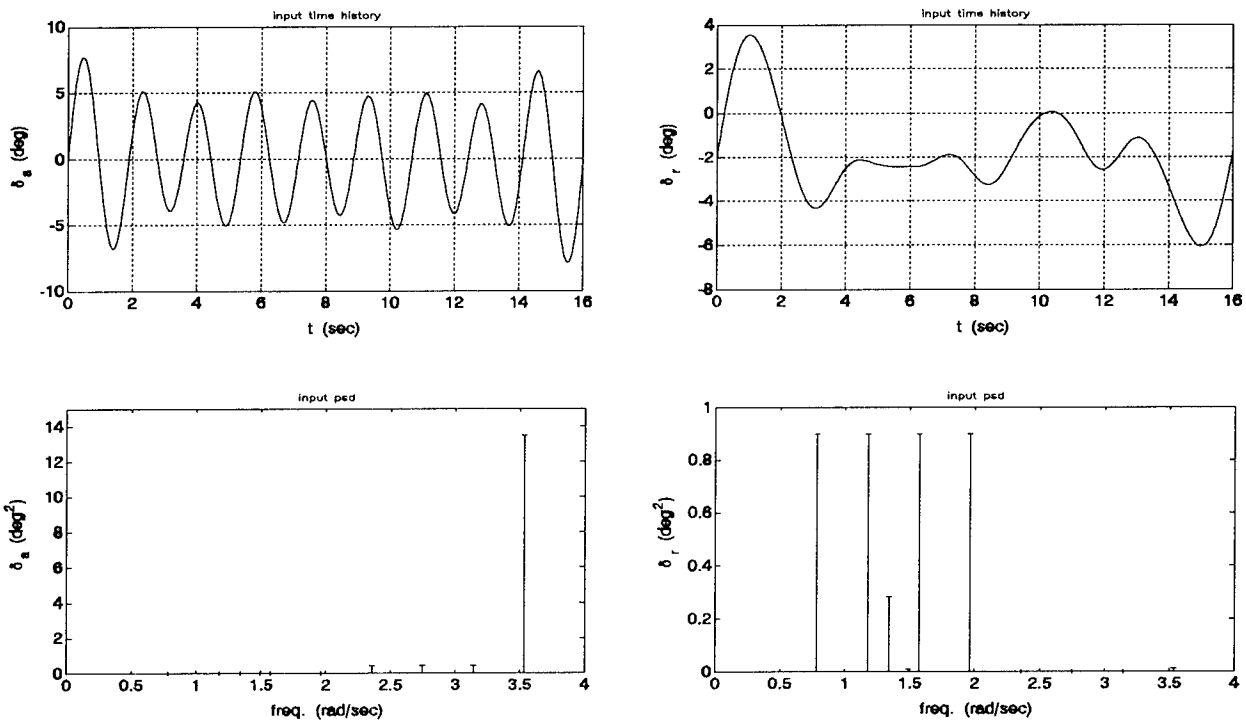

optimized frequencies

Figure 6-17: *Time histories and normalized power spectral densities of DUT aileron and rudder inputs with specified frequencies for criterion* $J=tr\ \bar{M}^{-1}$.

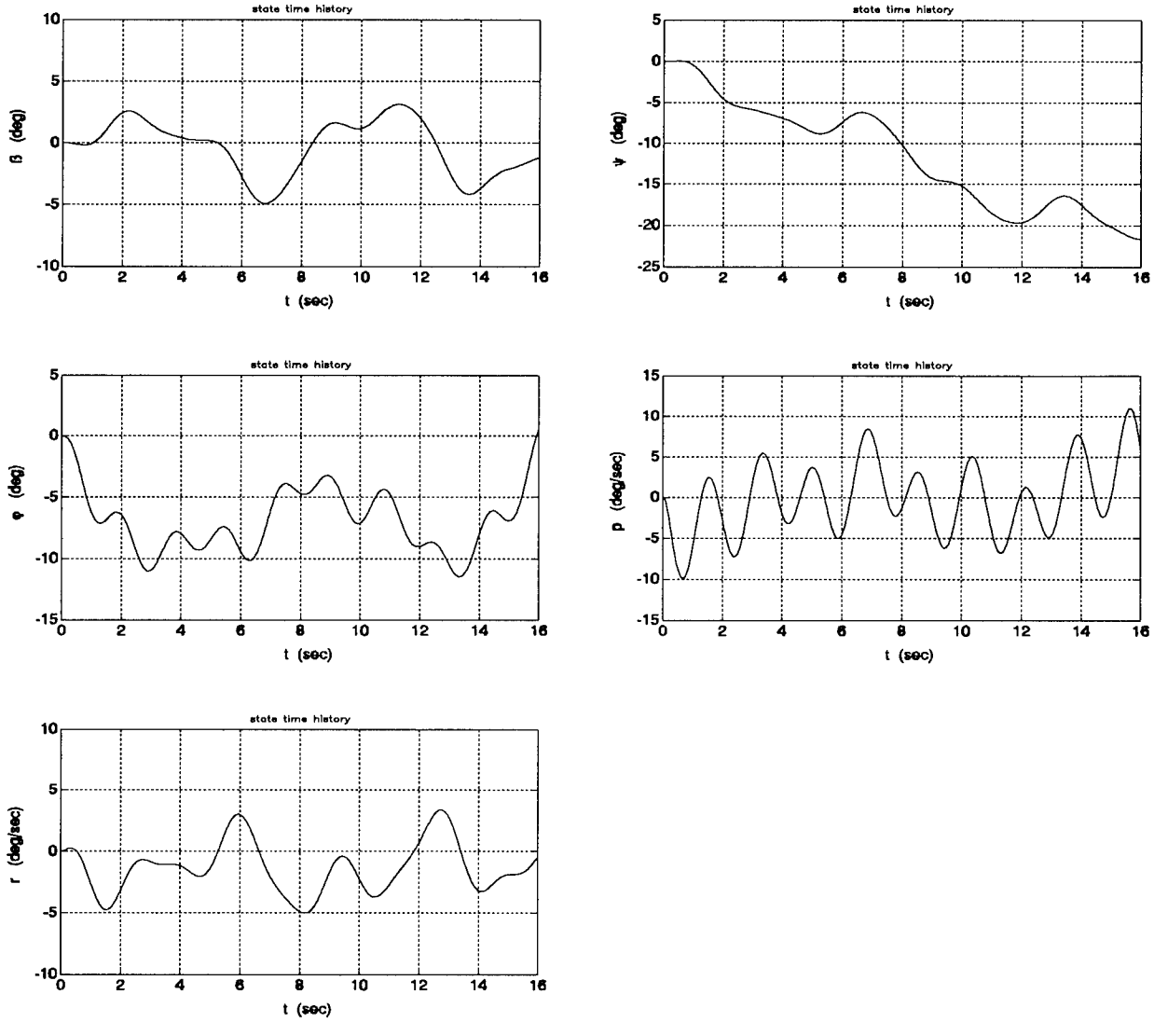

Figure 6-18: *Time histories of state variables from DUT aileron and rudder inputs with specified frequencies.*

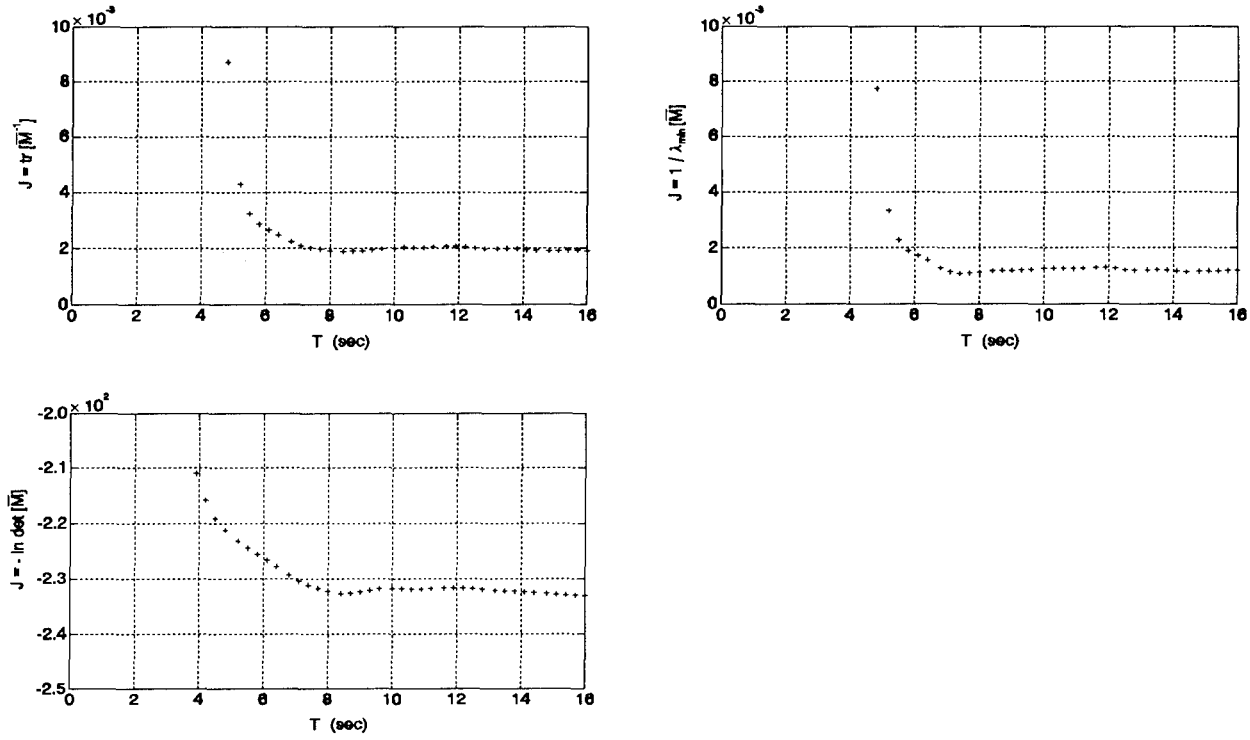

Figure 6-19: *Optimization criteria as function of measuring time interval (Δt=0.1 sec).*

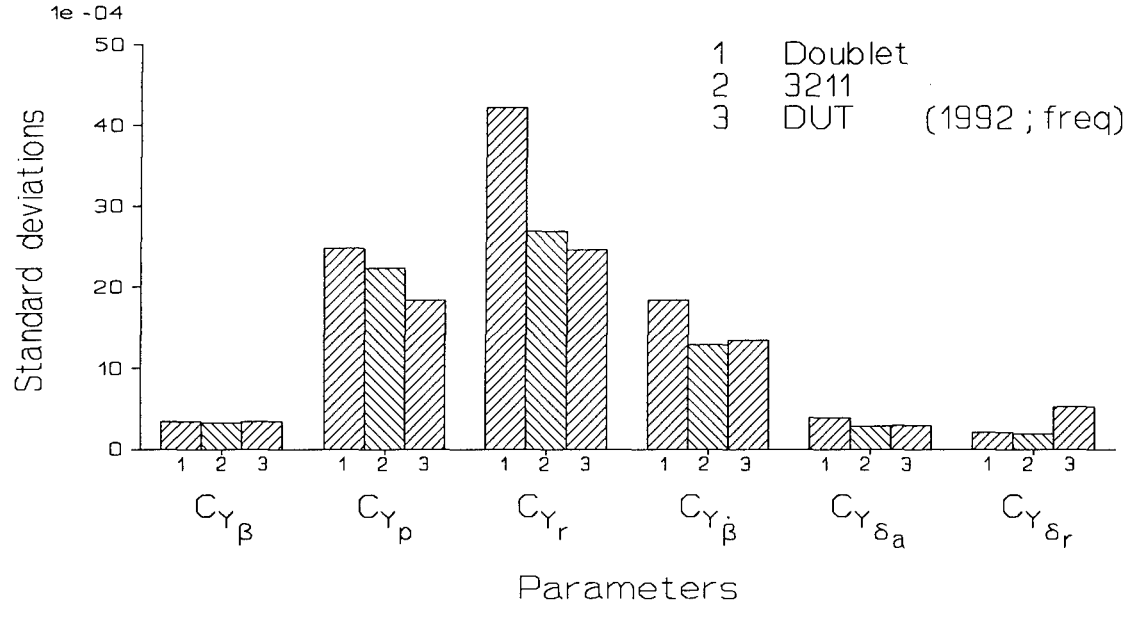

Figure 6-20: *Comparison of Cramer-Rao Lower Bounds.*

7 PRACTICAL ASPECTS OF FLIGHT TESTS

In this chapter the instrumentation, flight test design and execution, the data processing and the data quality evaluation are discussed. All of these topics are present in all flight tests, but parameter identification tests add special requirements.
In addition the software development will be briefly described, because this is an area that can be very expensive both during development and during use, especially when the software fails to perform according to specifications.

7.1 Flight Test Instrumentation

For the purpose of parameter identification flight tests, the inertial transducers, the pressure transducers and the angular position transducers are the most important. Other transducers such as temperature and outputs from navigation systems will also be discussed. Some aspects of signal conditioning will be covered. Finally the characterization of measurement channel will be described.

7.1.1 Inertial Transducers

As discussed in chapter 3 the accurate measurement of specific forces and angular rates is very important for an accurate flight path reconstruction, because these measurements form the components of the input vector to the system model describing the aircraft's flight path. In particular it is important that the bias, scale factor and alignment do not change. For instance a bias variation over the range of operational conditions should be in the order of 0.001 m/s^2 for the specific forces and 0.001 deg/s for the angular rates. This level of accuracy leads to the use of 'inertial grade' transducers. It is possible to build an inertial sensor package of this accuracy from components, as described by van Woerkom [16] or Breeman [22]. However, it may be preferable to buy an existing inertial sensor package of the shelf. Such packages are produced for missile guidance and often include gyroscope drive electronics, signal conditioning and accurate A/D converters.

Another possibility is the use of a commercially available Inertial Navigation System (INS) or Inertial Reference System (IRS). The term INS usually refers to a system with transducers mounted on a stabilized gimballed platform, while the term IRS always refers to a system with transducers rigidly mounted to the case. In civil aircraft these systems are likely to be already available onboard. Although these systems are more expensive than separate transducers or a simple inertial sensor package, their superior accuracy, stability and reliability imply that they are much cheaper to operate, because calibrations or repairs will be very infrequent.

On the other hand, a gimballed platform INS is not very suitable for parameter identification flight tests, because there are no body referenced specific forces or angular rates directly available. In addition the resolution of the attitude angles is usually poor and the accuracy is further degraded by the internal shock mounting that is used to protect the sensitive transducers.

A strap down IRS is much better in this respect. All IRS's built today use laser gyroscopes. The advantage of the laser gyroscope is the excellent stability of bias, scale factor and alignment and the inherently small time delays. The main disadvantage is the amount of noise in the outputs, which is caused by the need for dithering to prevent lock-in (see Aronowitz [224]). In commercially available IRS's the signal outputs are heavily filtered, which leads to signal distortion and time delay. Furthermore the lack of adequate anti-aliasing filtering combined with low sampling rate lead to problems with aliasing, especially in a high-vibration environment, in practice the sampling rates used in commercial IRS's are about 50 Hz. Most of the above-mentioned problems can be eliminated by having the manufacturer modify the IRS specifically for flight test. NLR has operated modified IRS's successfully during the last eight years for a number of flight test applications.

The mounting of inertial transducers requires special care. The sensors should be accurately aligned with respect to the aircraft body axes or, equivalently, the misalignments should be measured very accurately. This also means that the mounting of the sensors in the box as well as the

mounting of the box to the airframe should be very rigid and stable.

7.1.2 Pressure Transducers

As discussed in chapter 3 the accurate measurement of static and dynamic pressure is very important for an accurate flight path reconstruction, because these measurements form the primary components of the observation vector of the system model describing the flight path.

The required absolute accuracy is about 20 Pa, but a differential accuracy of better than 5 Pa is very desirable. This last number translates to about 0.5 m accuracy in the change in altitude, which is the important quantity for the reconstruction of altitude variations. Any errors here will affect the reconstructed state trajectory directly.

This level of accuracy is obtainable by modern high quality pressure transducers, but only if the temperature of the transducer is either kept constant or measured and accounted for in the calibration. The approach of keeping the transducer at a constant temperature was applied in the system described in section 7.1.5 below. Modern air data computers (ADC) normally measure the transducer temperature and account for it in an internal calibration procedure and in this way can be about as accurate as temperature-stabilized transducers, however, without the operational difficulties associated with temperature stabilization. This makes ADC's attractive as flight test transducers and NLR has applied these transducers successfully for flight test application for a number of years.
Time delays in the pressure measurements are mainly due to the pressure tubing connecting the sensing port to the transducer. The small internal volume of modern pressure transducers has helped to reduce this effect, but it still pays to keep the length of the pressure tubes as small as possible by placing the transducers near the sensing ports.

The effect of time delays in the pressure measurements on the flight path reconstruction is generally not very large, although they show up very clearly in the residuals. It is in any case a good idea to measure the time delays on the ground [208 and 214] and correct the flight data for the time delays. It must be kept in mind that the delays are dependent on the pressure in the tubing, so that the ground measurement has to be performed for several static pressure levels.

7.1.3 Angular Position Transducers

Angular position transducers are needed to measure the air flow angles and the control surface deflections. For the air flow angle transducer (α and β) an accuracy of about 0.02 deg is required. The stability of the alignment of the air flow vanes with respect to the body axes is more important than the absolute accuracy, because the angle of attack and angle of sideslip resulting from the flight path reconstruction can be used to obtain an accurate calibration of the air flow vanes [208 and 213]. Ideally, this calibration will take into account the upwash and sidewash effects discussed in chapter 2, as well as the effect of structural deformation of the boom or the aircraft. It is important to check the alignment of the vanes with the aircraft on a regular basis, before each flight if possible. For the control surface deflections the accuracy requirements are somewhat less, about 0.02 degree. In this case the correct mounting of the deflection transducer to the airframe is very important, because the structure of the aircraft as well as the control surface will deform significantly under loading. A good design of the mounting will minimize this effect [207]. In any case the deflection of the aerodynamic surface itself must be measured and not the pilot stick deflection or the cable displacement.

The time delay of the control surface deflection measurements is very important for aerodynamic model identification, see Iliff [2]. Especially the rate derivatives are very sensitive to this delay. The time delay between the deflection measurements and the inertial measurements can be checked directly by mounting an accelerometer to a control surface and moving the controls at different frequencies. If the same data acquisition chain is used as for the flight tests, this test can readily exhibit the delay of the deflection measurements relative to the inertial measurements to an accuracy of about 1 ms.

7.1.4 Signal Conditioning Characterization

As described in chapter 3, state reconstruction can be used to obtain accurate reconstructed variables using the redundancy present in the measurement data set. In order to apply this technique it is necessary to formulate a precise and complete characterization of the measurement system. In the past a characterization of a measurand could consist of accuracy and bandwidth of the sensor. Nowadays most measurands are the result of a complex sequence of processing steps in the flight hardware. In this subsection a general framework is proposed for specifying the characteristics of measurands. This general framework can then be filled in for each of the measurands used for state reconstruction. We will begin by introducing the following definitions:

Definitions

Translation The desired physical quantity often cannot be sensed directly but must first be translated to the transducer. Examples are the pitot probe and the pressure tubing for air data and the mechanical gearing for rotary position.

Transducer The translated physical quantity is transformed into a secondary physical quantity (the transducer output) which can be measured more easy or more accurately. Nowadays the secondary physical quantity is usually a voltage, a current or an impedance change.

Signal conditioning The transducer output is not directly suitable for conversion, because the signal level is not compatible with the A/D converter or because the frequency content would cause aliasing errors. Consequently the transducer output must be bias shifted, amplified and filtered.

A/D converter After signal conditioning the signal is converted to a digital code. There are two common conversion techniques: successive approximation converters yield a number which directly represents the signal amplitude at the sampling instant and integrating converters, which yield a number representing the analog integral of the signal over the last sampling interval.

Digital processing The digitized transducer signals are in many cases not the desired results. Therefore, modern sensor systems contain digital processing. In simple cases this involves calibrations, corrections and digital filtering, but it can also involve a complex calculation based on a number of different transducer signals.

Data transmission The processed digital data must be finally transferred to the user equipment, in the present case the flight control computer. This involves formatting the data and transmitting the data over a digital data bus.

The proposed framework is just a subset of the characteristics that come into play in the selection of transducers. Only the characteristics that are judged relevant for the application must be included. In figure 7-1 the general structure for a measurement channel is shown. It consists of translation, transducer, analog signal conditioning, analog to digital conversion, digital processing and data transmission. For each of these elements characteristics can be specified. Taken all together these specifications determine the overall response of the measurement channel.

A complicating factor is that in modern measurement systems the output measurand often depends on more than one sensor. In the simple case the output of one sensor is corrected for a sensitivity for another physical quantity, e.g a pressure sensor is corrected for temperature. In this case only the remaining sensitivity after compensation is relevant. More complicated is the case where the measurand is derived from a number of sensors, e.g. groundspeed from body accelerations and gyroscopes. This can be treated by defining the transfer characteristics from each sensor to each measurand separately.

For simplicity the characteristics of the translation of the physical quantity to the sensor input might be included in the transducer characteristics. Examples are the pneumatic tubing between the sensing hole and the pressure sensor and the shock mounting of an inertial sensor. A list of characteristics is:

1. Translation
   (a) Transfer function
   (b) Time delay

2. Transducer
   (a) Range
   (b) Bias
   (c) Scale factor
   (d) Resolution (sensitivity)
   (e) Sensitivity to temperature, off-axis signals
   (f) Hysteresis
   (g) Transfer function H(ω)
   (h) Time delay
   (i) Electrical noise spectrum

3. Analog signal conditioning
   (a) Range
   (b) Bias
   (c) Scale factor
   (d) Transfer function H(ω)
   (e) Time delay
   (f) Electrical noise spectrum

4. Analog to Digital conversion
   (a) Range
   (b) Accuracy
   (c) Resolution
   (d) Sample rate
   (e) Sample instant jitter
   (f) Digital noise spectrum

5. Digital processing
   (a) Amplitude limitation
   (b) Digital transfer function H(z)
   (c) Time delay
   (d) Round-off
   (e) Numerical noise spectrum

6. Data transmission
   (a) Truncation
   (b) Transmission rate
   (c) Transmission delays
   (d) Transmission delay jitter

To reduce the amount of work, characteristics that are judged less important can be left blank. For example, the analog signal conditioning may have a negligible bias compared to the sensor. In other cases it may be impossible to tell whether the error must be attributed to the sensor or to the signal conditioning. This is also true for sensors which form part of a feedback loop.

In the above list time delays are listed separately from the transfer functions. This implies that the transfer functions are defined to have no fixed delay components. An alternative is to list the complete transfer function and to incorporate the delays in factors like $e^{-j\omega t}$ or z in the transfer functions.

The next step in this activity is the drawing up of a list of physical quantities of measurand transfer characteristics that could be of interest to the project. Subsequently this list can be filled in with information obtained from vendor brochures, by questioning vendors or by direct measurements in the laboratory or in flight.

7.1.5 Example of Flight Test Measurement System

The general arrangement of the flight test instrumentation system as used in the flight test programs with the DHC-2 Beaver aircraft is shown in figure 7-2. A detailed description of the predecessor of this flight test measurement system is given in Van Woerkom [16]. The present system like its predecessor was designed and built by the Faculty of Aerospace Engineering of the TU Delft.

The transducers of the instrumentation system are listed in table 7-1. The first set of these transducers, mounted in the so-called Inertial Measurement Unit (IMU) are shown in figure 7-3. Three accelerometers were positioned such that their axes of sensitivity were mutually perpendicular inside a temperature-controlled box. The effect of temperature on the characteristics of these accelerometers was eliminated by maintaining a fixed temperature inside the box during instrumentation calibrations as well as in flight. Three rate gyros were mounted outside on the box. Their axes of sensitivity were mutually perpendicular as well.

The second set of transducers, used to measure various total and static pressures, consisted of one absolute and four differential pressure transducers which were also positioned in a temperature controlled box for the same reasons as stated as above. This can be seen in figure 7.4.

This box contained in addition a vacuum bottle with which the reference static pressure at the start of a flight test manoeuvre could be sampled. It further contained a heater and fan, a set of two-way valves and the necessary electronics. More details are given in Van Woerkom [205].
All transducer outputs were converted and scaled to a range from 0 to 10,000 mV dc. Next,these outputs were filtered by identical 4th order low-pass anti-aliasing filters. Each filter consisted of two identical second order filters with undamped natural frequencies of 19 rad/s and damping ratios of 0.691. These damping ratios were selected so as to obtain an approximately constant gain and linear phase characteristics in the region of low frequencies. The only effect on the low frequency components of the transducer outputs was, therefore a common time delay. This in turn led to considerable simplifications of the computations required for 'elementary data processing' [176]. The resolution of the analog to digital converter was equal to 1 mV or 0.01% of full scale. Each channel of the system was scanned at a rate of 10 times per second. The multiplexer comprised 40 channels and the system was capable of digitizing and recording 400 samples per second. The number of transducers in the instrumentation system (26) was smaller than the number of multiplexer channels (40). The excess channels were used to sample the accelerometers, rate gyro's and elevator, aileron and rudder deflection transducers at the double rate of 20 samples per second.

The instrumentation system was repeatedly calibrated before, during and after the flight test program. These repeated calibrations made it possible to monitor variations of instrumentation and transducer characteristics with time, in the course of the flight test program. The calibrations comprised the complete measurement channels, from the transducers up to the outputs of the analog to digital converter, rather than just the individual components in each channel, because it was thought that the results of calibrations of complete channels would be the most representative for the actual in-flight performance of the measurement system. Some typical calibration results are shown in figure 7-5. Especially the calibration of the pressure transducers show bias changes with time.

Electro-hydraulic control system
A diagram of the electro-hydraulic control system which was used to generate the optimal input signals is shown in figure 7-6. The system included three electro-hydraulic actuators for control of the ailerons, rudder and elevator respectively. The actuators were coupled via pilot controllable electro-magnetic couplings and safety shear pins to the existing manual control system. Hydraulic power was generated by an auxiliary hydraulic pump which was fitted to the engine. In order to eliminate the possibility of hydraulic fluid spillage in flight, the system was designed to have no open connections with the outside air. Therefore it was not possible to use an open reservoir for hydraulic fluid storage and a so-called compensator was used, this is in essence a cylinder and piston providing a variable volume. Together with an accumulator, filters and hydraulic valves, the compensator was mounted in a hydraulic power pack installed in the back of the Beaver passenger cabin. The electro-hydraulic control system was operated by the pilot via an overhead control panel. The actuator servo valves could be commanded by means of a three-axes side stick controller, by three trim wheels or by input signals recorded on a multi-channel FM tape recorder.

7.2 Ground Preparations

Before the actual flight tests a number of activities have to be performed on the ground. The instrumentation system must be calibrated and it must be installed and aligned with the aircraft axes and finally the aircraft's weight, center of gravity and moments of inertia must be determined.

7.2.1 Calibrations

Analysis of the calibrations consisted of fitting polynomials of degree appropriate to the calibration data, using regression analysis. For each channel, this appropriate degree of the polynomial for an *adequate* fit to the calibration data was determined in a rather qualitative way, based on the root mean square of the residuals. These rms-values are subsequently taken as a measure of the accuracy of the channels of the measurement system.

An impression of the accuracy, as defined above, of some of the transducers (channels) of the

instrumentation system can be deduced from figures 7-5(a) through (d). These figures show the residuals resulting from fitting one polynomial to several sets of calibration data resulted from calibrations made at different calender dates. Figure 7-5(a) shows the residuals of four tilting table calibrations of the longitudinal accelerometer instrumentation channel. The relative rms-values (rms divided by the calibrated input range) of these particular residuals amounted to 0.0023%, which is equivalent to 0.00046 m/s^2. Still lower relative rms-values, when the polynomials were fitted to each of the calibration data sets individually. This clearly indicated a change of characteristics from the first calibration to the next calibration. Figure 7-5(a) shows that it is in particular the constant part of the channel outputs which appears to vary with time. This is quite typical characteristic of inertial transducers like accelerometers and rate gyros. This is the basis for the inclusion of corresponding zero shifts as unknown parameters in the flight path reconstruction problem.
The residuals of five calibrations of the roll rate gyro channel are shown in figure 7-5(d). The rms-value was 0.0035 deg/s. Also in these calibrations, a variation of the constant part of the channel output over successive calibrations appeared to exist. When polynomials were fitted to individual calibrations, rms-values of approximately 0.0020 deg/s resulted. The instrumentation system used high quality differential-pressure transducers. In terms of relative rms-value of calibration residuals, they proved to be of the same level of accuracy as the high quality accelerometers and rate gyro's discussed above. This is illustrated by figure 7-5(c), showing the residuals of two calibrations of the Δp_1 differential pressure channel. The rms-value of the residuals was 0.6 N/m^2.
Figure 7-5 (d) shows the residuals of four calibrations of p_{st}, the absolute pressure channel. The rms-value of the residuals was 81 N/m^2. This relatively high rms-value was obviously caused by deterministic differences between successive calibrations, due to variations with time of the transducer input-output relationship. Figure 7-5(d) clearly demonstrates the advantage of multiple calibrations in the course of a flight test program. It was possible to fit a calibration polynomial to each of the calibrations individually and to determine for each flight the probably best polynomial by interpolation in time. Examples of calibration results of other types of transducers, such as control surface angle, air flow angle, temperature and engine rotation rate transducers are presented by Kranenburg [176].

7.2.2 Measurement of Moments and Products of Inertia

The total aerodynamic moments acting on the aircraft cannot be measured directly in flight. They must be determined indirectly from the equations of motion. For the case of a rigid aircraft, this leads to a set of relations for L, M and N as given in chapter 2. These relations hold for a symmetrical aircraft for which the products of inertia I_{xy} and I_{yz} are equal to zero. It follows, that the angular accelerations and angular velocities must be measured and that the moments of inertia I_x, I_y and I_z as well as the product of inertia I_{xz} must be known. This motivated the design of a rig for the experimental determination of aircraft moments and product of inertia, shown in figure 7-7. A detailed description of the rig has been given by Kranenburg [175] and De Jong [223].
Depending on the configuration of the rig, the aircraft could be oscillated about either the longitudinal, lateral or vertical axis. In the case of oscillations about the longitudinal and lateral axes the aircraft mass center was below the axis of rotation, while for oscillations about the vertical axes the aircraft was suspended as a bifilar pendulum. All these oscillations are readily recognized as being inherently stable. This eliminated the need for the application of external stabilizing springs. The rig was carefully designed such that mechanical friction would be as small as possible. This was obtained, among other things, by the application of high precision knife-edge bearings. The damping of the roll, pitch and yaw oscillations about the longitudinal, lateral and vertical axis respectively proved to be very low. Evidence for the low damping of these oscillations is provided by table 7-2, showing typical values of period and damping of the roll, pitch and yaw oscillations respectively.

The virtual absence of mechanical friction was thought to be essential for accurate moment of inertia measurements, for the following reasons. In the first place, weakly damped oscillations allow ample opportunity to accurately determine period

and damping. In the second place, the absence of mechanical friction and in particular Coulomb friction, will permit the use of linear equations of motion for oscillations with sufficiently small amplitudes.

The moments and products of inertia can be very easily calculated from the observed oscillation periods, but this can also be formulated in terms of a system parameter estimation problem. At first sight, this might seem to lead to unnecessary complications, because the application of e.g. maximum likelihood estimation as discussed in Appendix A implies solving a nonlinear minimization problem. There arise new possibilities, however, when the rig configuration is designed to allow more complex oscillations for instance involving translations as well as rotations about different axes.

7.3 Flight Test Design and Execution

The design and execution of parameter identification flight tests require careful planning and organization. This process has to begin with a definition of the goals of the flight test program. These goals can be specified as to the different topics to be covered (e.g. aerodynamics, engine, flight control), to the desired coverage of the flight envelope and to the desired confidence level of the results. Next a detailed flight test plan can be written, flight test cards can be drawn up and the flight test program can be executed.

7.3.1 Flight Envelope

As far as the number of topics and the coverage of the flight envelope are concerned, parameter identification in general places no special requirements other than those of other type of flight tests. Special care is required, however, at the boundaries of the flight envelope. For instance during dynamic manoeuvres at low speeds the stall boundary may easily be crossed. It is also necessary to take into account that the dynamic stall boundary usually is at a different angle of attack than the static stall boundary. Also at high flight speeds the Mach buffet boundary is usually very close to the steady-state flight condition. One result may be that undesired effects are introduced into the parameter identification due to the unmodelled effect of stall. An even worse result may be that the pilot loses control of the aircraft.

The total number of recordings is determined by the requirements of parameter identification on the one hand and by budgetary constraints on the other hand. In the end a compromise between these two factors has to be found.

7.3.2 Experimental Design

The identification of a complete aerodynamic model often requires more information than is present in any single manoeuvre. This can be solved by combining recordings of different manoeuvre types during the data processing (multi-manoeuvre analysis). The intended use of combined recordings has to be taken into account during the flight planning. Although it is possible to correct for the differences in e.g. centre of gravity or moments of inertias between recordings, these variations may still introduce a degree of uncertainty into the analysis. The best approach may be to execute all manoeuvres which are going to be combined as closely paced in time as possible. This does, however, have the operational disadvantage of forcing the pilot to execute all the different manoeuvres types in sequence, which is more difficult than executing all recordings of one manoeuvre type before starting the next.

The results from parameter identification will always show a certain scatter due to a number of effects, such as atmospheric disturbances and instrumentation errors. The confidence in the identification results can be improved markedly by repeating individual manoeuvres or sequences of manoeuvres. This allows us to obtain experimental standard deviations of parameter estimates which may be a much more reliable indication of the accuracy of these estimates than theoretical standard deviations as resulting from the Cramer-Rao lower bound or the covariance matrix from regression analysis, see also [2]. The number of repetitions can be limited to two or three in most cases, but it is necessary to use at least five repetitions for a few reference conditions and configurations. The conclusions from the larger number of repetitions can then be extrapolated to the other cases. A minimum number of repetitions for all other cases will ensure that no unique

effects will be missed, as for example the crossing of a stall boundary which will show up as an increase the scatter of the parameter estimates. The results of parameter identification can also show variations from flight to flight or even between the beginning and the end of the same flight. This can be caused by a number of factors such as:

- the accuracy of the calculated centre of gravity position, mass or moments of inertia,
- changes in the instrumentation (calibration shifts, instrument exchange),
- changes in the weather conditions at different altitudes or on different days.

It is very important to schedule extra repeat recordings of a chosen reference configuration and condition to evaluate these factors. These repeat recordings should preferably be distributed over the flights in a quasi-random fashion.

The task of the pilot can be lightened by utilizing a Stability Augmentation System (SAS) if present. The SAS can be used to stabilize those axes which are not excited during the flight tests. One has to be very careful, however, that the SAS does not contribute an effective input signal to the excited axes, because this may introduce correlated inputs into the system. The result of correlated inputs is a significant decrease in identifiability.

7.3.3 Test Plan

The total test plan should be approved by the analysts, the pilots, the flight test engineer and the flight instrumentation engineer. Subsequently the test plan has to be divided in parts which can be executed in one flight. Careful planning can save flying time by finding the best sequence of manoeuvres. These savings are often negated by the demands of experimental design, however, because this may require either a more random sequencing of recordings or the execution of related tests in a prescribed sequence.

Each of the separate tests should be summarized on a flight test card. This card should contain all necessary information to execute the test, but nothing more. It should at least define initial conditions, aircraft configuration and input signal. For manual test inputs a simplified graph may be very helpful. The flight test card could also list hints, warnings, desired final conditions or possible excursion limits. It can be very useful to have alternate flight test cards on hand, for example in the case that the weather or air traffic control precludes the execution of the original flight plan.

The execution of the flight test plan requires the full attention of a flight test engineer. He has to select the items to be covered during a particular flight, prepare flight test cards, brief the pilots, conduct the tests during flight and finally document all the relevant parameters, such as weight, c.g., fuel load, etc. All observations made by the pilot or by the other members of the crew should be recorded, possibly on audio tape.

7.4 Flight Test Data Processing

The flight test data processing involves more than just the implementation of the algorithms presented in the earlier chapters. It involves transcription of flight tapes, data storage and data management, calibration, processing, analysis and presentation. All of these steps are not unique to the processing of parameter identification flight tests and normally will already be available in your organization, but the use for parameter identification imposes special requirements with respect to data management, accuracy and time correlation. This may necessitate a significant effort to upgrade the existing system or the bold decision to develop a new system from scratch. In the following subsections the special requirements for parameter identification will be discussed for each of the data processing steps.

7.4.1 Data Management

Large amounts of data are gathered during parameter identification flight tests in a variety of conditions and configurations. The subsequent processing of the data involves a large number of steps. The data management requirements are therefore twofold:

The administration of the original measured recordings This should describe of the purpose and the execution of a recording, together with the aircraft configuration (flap angle, gear position, engine setting) the flight condition (altitude, airspeed). In addition all the reference data needed for the data processing should be included, such as aircraft weight and centre of gravity position,

instrumentation settings, etc. The importance of this administration lies e.g. in the possibility to select recordings which contain information which pertain to a specific condition and use these recordings in a combined (multi-manoeuvre) analysis.

The administration of intermediate and final results
This should describe the precise meaning of each calculated variable, such as the program which created the variable, the date and time of the calculation and the unique identification of the data sets on which the calculation depended. In particular the ability to identify the source of a final result is essential. This allows e.g. the reinterpretation of final results in the light of later changes in data processing parameters or in model structure used for parameter identification.

7.4.2 Accuracy

Parameter identification and in particular the Two-Step method places special demands on these processing steps in terms of accuracy. As mentioned earlier it may be necessary to perform special calibrations before and after a flight test program. In addition it may be necessary to use more sophisticated calibration procedures, e.g. to incorporate additional terms in the calibration formulae. The precise correction for instrument sensitivities also demands extra attention. Examples are the correction of accelerometers for off-axis sensitivity or the correction of air data for Pressure Error Correction.

7.4.3 Time Correlation

A time correlation accuracy in the order of 1 millisecond is essential for PI. Numerical experiments have shown that a shift of a 10 ms in dynamic measurands may give errors of 50% in some parameter estimates. In an ideal data acquisition system all measurands are recorded by the same measurement chain. In actual practice the measurands are derived from different systems with different sample rates, filter characteristics and internal delays. Very often a special synchronization signal (e.g. a Time Code) is recorded by all channels, so that it can be used to restore the synchronization. The actual restoration may require very difficult software algorithms.

Very often it is necessary to filter and re sample the data to reduce high-frequency noise in the data. The use of nonrecursive filter techniques (see Oppenheim and Schafer [225] or Rabiner and Gold [226]) will ensure that no additional time delays are introduced. Another aspect is that some calculations in the processing are actually filter operations (e.g. interpolation, differentiation or integration). Again it is necessary to use formulations that do not introduce a phase distortion. An example is calculating the numerical derivative of a signal where the use of a central difference formula will ensure zero time shift.

7.4.4 Presentation

A good presentation is very important for the easy interpretation of intermediate as well as final results. Although tables have their place for precise documentation, especially graphical presentation can give enhanced insight, e.g. to highlight trends in the data. Flexible interactive plotting procedures are needed here allowing for different plot styles (e.g. X-Y, T-Y, bar charts, box- and-whisker plots), line styles and plot symbols. Special care is needed to label the data clearly and unambiguously and to identify the plots with date and time. Easy change of scaling is also required.

7.5 Flight Test Data Quality Evaluation

The quality of the measurement data is defined here as the degree of absence of all factors that would detract from its usability for the intended purpose. It is obvious that this quality will directly determine the accuracy of the parameter identification results. Therefore it is of utmost importance to ensure the data quality before any attempt at identification is made. In principle the best time to perform data quality checks is in dedicated tests before or during the actual flight tests: in the instrumentation laboratory, on the flight line and during instrumentation check-out flights. Accurate determination of each individual error effect can also be done best in a dedicated test. These tests are ideally performed with a computer on-line in the aircraft to reduce the loss of time and the cost of flight tests with inaccurate measurements.

The evaluation of the data quality from existing

flight test data, as sometimes the case, is generally much more difficult. But it is still very important to do this evaluation for the following reasons:

1. A particular measurement channel may deteriorate or fail during the course of a flight test program.

2. A specific error effect may only be present during actual flight tests, such as static pressure distortions in dynamic flight conditions. These effects can only be determined from the flight tests.

Another good reason is the fact that the evaluation of the data quality also gives a good feel for the data contents. It gives a first indication of the actual accuracy of the measurements and it can clear up misunderstandings in the definition of measured variables (e.g. sign conventions). Apart from complete failure, which is often (but not always!) easy to spot there are a number of errors that can occur during all stages of the measurement channel as described in section 7.1.4.
Some examples are:

Sensing The transducer may not sense the desired quantity directly, for example a static pressure may be distorted by the flow around the aircraft.

Transducer These could be changes in bias or scale factor, sensitivity to temperature, vibration or electromagnetic radiation.

Data acquisition system These could be changes in the analog components, such as amplifiers, pre-sample filters and A/D converters, or bit errors in the recording chain (dropouts) or time shifts and other phase errors.

Because of the large number of possible error sources, an intimate knowledge with the characteristics of the instrumentation system is absolutely necessary for successful correction of data errors.

7.5.1 Data Inspection

Visual inspection of data plots is an important first step in the evaluation of data quality. The measurements can be scrutinized for obvious errors such as wrong signs, excessive measurement noise, data dropouts, spikes and missing (or even exchanged!) data channels.
In addition frequency domain techniques can be very useful for data quality evaluation. Examples are:

1. Time shift of a signal can be determined by examining the slope of the phase response of the signal with respect to a reference. This method is very sensitive, but it is most useful in ground checks as it may be difficult to find a suitable reference measurement in flight. Time domain modelling can also be used to determine time shift.

2. Initial checks of compatibility between variables may be quickly performed in the frequency domain. For instance it can be verified that q/θ has a 1/s frequency response characteristic. Sign errors are also easily detected by inspecting the phase response.

3. Coherence functions can be used to ensure that both input and output signals have low noise contents and are well correlated with each other.

4. The noise spectrum can give an indication of the correct functioning of a transducer (channel). Excessive noise (perhaps in part of the frequency spectrum) can give an indication of malfunction in sensing, transducer or data acquisition. For example discrete frequencies in a gyroscope signal could indicate a bearing failure, noise spikes could be a vibration problem or faulty wiring or connectors. Noise analysis also gives vital information for the design of data processing filters, which remove the measurement noise and allow the sampling rate to be reduced.

This may also be a good place to warn for the effect of pre-sample filtering. If a failing transducer has high-frequency noise or sudden steps in its output, the pre-sample filters will transform the signals in smooth signals, thus masking the problem. In normal operation pre-sample filters are essential to prevent aliasing errors, but it may be a good idea to record the unfiltered signals as an instrumentation test. Another important point is the

negative effect of phase errors in the analogue filters on the parameter identification. Some authors even recommend dispensing with anti-aliasing filters altogether. If recording techniques permit it, it is therefore recommended to use the highest possible sampling rates (and pre-sample filter bandwidth) and to reduce the sample rate in the analysis by linear-phase digital filtering in the ground processing. This has the added advantage of allowing a more considered choice of sampling rate in the data analysis.

7.5.2 Compatibility Checking

Any redundancy in the measured variables can be exploited to verify the data quality. There are a large number of techniques in use for the purpose of data quality evaluation.

A simple example is the measurement of a single variable by two different transducers. If the transducers are of the same type, then the outputs of the two measurement channels can be directly compared to find discrepancies in sensing, transducer or data acquisition. If the two transducers use a different measurement principle, then the comparison is not so straightforward. However, the characteristic errors will be different. If these differences are taken into account properly, comparison of the two transducers can still yield important information.

In practice it is rare that two redundant transducers are used, but it is not uncommon to have a standard aircraft instrument as well as a flight test instrumentation sensor. In this case it is strongly recommended to record the aircraft instrument output as well. The disadvantage is not so much the extra data channel to be wired in the aircraft, but rather the extra effort needed to calibrate and evaluate the aircraft instrument, which is necessary to allow its use for data quality checks.

Partially redundant measurements can also be used in a complementary filter approach, thus making the best use of all available information. Such a filter can be designed using the Kalman filter approach. For example, rate gyro data can be used for the low frequency range and angular accelerometer data can be used for the higher frequency range. However, it is very important that undesirable error characteristics of one of the transducers, such as hysteresis, nonlinearities or spurious responses, do not destroy the quality of the overall result.

A special case of compatibility checking is Kinematic Compatibility checking. Here the kinematic relationships that exist between the different measured variables are used. The procedure can be applied in many forms: from the simple comparison between two signals to the complete six-degree-of-freedom flight path reconstruction described in chapter 3. The procedure is also called Kinematic Consistency checking or Flight Path Reconstruction. The chosen name reflects whether the procedure is seen as an independent check or as an integral part of the processing.

The set of equations describing the six-degree-of-freedom kinematic equations were given in chapter 2. In practice these equations are extended with terms describing the navigation over a spherical and rotating earth.

In principle any measurement which depends on the state vector defined in chapter 3 can appear in the observation equation, for example air speed or doppler velocity, pressure or radio altitude, angle of attack or angle of sideslip, latitude and longitude from Inertial Navigation Systems, VOR/DME or the Global Positioning System. The error in the measurements, whether in the input or in the observation vector, can be modelled as bias (λ), scale factor error (k), time shift (τ) and white, Gaussian random noise (n), see for instance Blackwell and Feik [236]. If this random noise is not white it may be necessary to augment the state vector with a model of the noise characteristics.

With modern inertial sensors the measurement errors are very small. As a consequence the variations in the wind components during a recording become the dominant error source. This makes it possible as well as desirable to estimate these wind variations. The estimation of the absolute wind components requires the presence of absolute position or velocity references of reasonable accuracy, e.g. from an INS, VOR/DME or GPS. However, it should be noted that in general only the variations in the wind speed components are of interest for flight mechanics,

because constant wind components only affect the error in the absolute velocities in earth-fixed coordinates. This means that absolute position references are not strictly required, although they can be of great use.

One simple way of modelling the wind variations that works very well in practice describes the wind variation as a linear trend in time and as proportional to altitude. A more sophisticated description may use a Markov model (see 3.1.4), but the parameters in such a wind model will depend on the weather conditions. The estimation of wind components is an example of the use of estimation procedures to reconstruct an unmeasured state component. Another practical example is the estimation of the angle of attack in the case that no direct measurement is available or the direct measurement is unusable.

It is in general not possible to identify the large number of parameters in the described error models, because the basic observability and identifiability theory is applicable here. If too many error components are included the standard deviations of the estimates increase rapidly and the correlation coefficients approach one. The degree of correlation is also dependent on the type of and shape of the manoeuvre, so it is feasible to perform specially designed manoeuvres for the purpose of identifying the error components, but these manoeuvres will not necessarily be optimal for parameter identification. It may be more fruitful to combine several different manoeuvres in a multi-manoeuvre analysis and then estimate an error model which is valid for all the recordings (see section 7.5.3).

As mentioned above, a simple example of compatibility checking is the comparison of a rate gyroscope and an attitude gyroscope. The rate signal can be integrated and compared with the attitude signal. Error models for each of the two types of gyroscopes can be defined, e.g. bias and time shift for the rate gyroscope and linear drift and time shift for the attitude gyroscope. The difference between the signals can then be attributed to various errors sources and the parameters of the error model can be estimated using parameter identification.

Even this simple example already points out a common problem, i.e. the bias of the rate gyroscope has exactly the same effect as the linear drift of the attitude gyroscope and the same is true for time shifts. This means that the errors in the different measurements must have different characteristics in order to be useful for compatibility checking. If it could be assumed that the attitude gyroscope has negligible drift and the rate gyroscope has a negligible (or perhaps known) time shift, then rate gyro bias and the time shift of the attitude gyro can be put in the error model and values for these parameters can be found. But in general these assumptions are difficult to make and need the advice of the instrumentation department.

The bias in the rate gyro will always have the same effect, a linear increase of the error with time. But a scale factor error, e.g. in the attitude measurement, will only be noticeable if larger excursions are present. Even in the case of large excursions, the estimate of bias and scale factor may be highly correlated, e.g. when the attitude angle happens to increases linearly with time. This demonstrates the dependence of identifiability on the manoeuvre shape.

7.5.3 Use of Error Corrections

After all error corrections have been determined as far as possible, the question remains what to do with this information. There are two extreme philosophies:

The identified error components are put in an error model, which is added to the aerodynamic model. The parameter identification procedure is then performed on the combined model, using the original measured variables as observations.

Finally the instrumentation department should always be asked to verify the estimated instrument errors. It may turn out that an error which seems to have been successfully modelled in one way, should be actually attributed to an entirely different error source which happens to have the same effect.

When a large number of manoeuvres are conducted in a particular flight and in one flight condition, the error model identified for each of the

manoeuvres should ideally be the same. This makes good physical sense since the calibration of the instrumentation will change very little during one particular flight. Failure of a sensor or other instrumentation components during the flight would, of course, be an exception.

This suggests that when a sufficient number of recordings is available, mean values of the biases and scale factors should be used as corrections for the whole flight. Simple statistical analysis can be performed to establish if the sample is large enough so that statistically significant values can be determined. If only some of the estimated error components are significant, it may be necessary to reduce the size of the error model until only significant parameters remain.

7.5.4 Final Remarks

It can be concluded that data quality evaluation is a necessary step in the process leading to successful parameter identification. However, the final test of the validity of this procedure lies in the quality of the parameter identification results.

7.6 Computer Software Development

The cost of developing complex software systems has increased enormously in the last decades. Moreover, the resulting programs often are full of errors and perform miserably. This is the reason that the discipline of Software Engineering has generated a tremendous interest. Every few years completely new approaches are proposed, become popular and are in turn replaced by newer ideas. Nevertheless a consensus on general principles seems to have arrived, the so-called Structured Analysis [183] and Structured Design [184] approaches.

This approach states that the software development process should be divided in a number of strictly separated stages. In each stage only a limited number of concerns are addressed:

User requirements In this stage the user requirements are spelt out in detail. The most important point here is that this specification should be complete, all relevant details should be included.

System analysis Based on the detailed specification the user requirements are analyzed and brought into a structured form. The use of Computer Aided Software Engineering (CASE) tools can be of benefit here. This stage concentrates on what is needed.

Technical design On the basis of the previous analysis, the program is designed. This stage concentrates on how the problem is solved.

Implementation On the basis of the technical design the computer program is written.

Testing Using the test data sets defined during the earlier stages, the program is tested. This stage should benefit the most from the structured development approach.

In our opinion the separation between these stages is a helpful way to keep the development process organized and to prevent mixing solutions into the problem analysis. However, we think that this seperation cannot and should not be rigidly enforced. For instance, if the person writing the user requirements is already considering possible design solutions, this may prevent the drafting of requirements, which are impossible to meet. But then the suggested solutions should not be mixed with the requirements, but confined to a final section with recommendations.

A disadvantage of the structured techniques is that they are based on generating multitudes of abstract charts, which are very hard to understand for anybody but the analysts themselves. The newer Object-Oriented Analysis and Design techniques [237,238] promise to be much better in this respect, among others because they concentrate more useful information into fewer charts.

In principle flight data processing software has no special distinguishing characteristics with respect to software engineering. Most programs run non real-time and in a strict input-processing-output sequence. This is even true for interactive programs where the user interaction is mostly limited to the overall control over complete software modules. However, for Real-Time software implemented in onboard computers the story is completely different. Here the possibilities for testing under

realistic circumstances is limited and structured approaches, in particular those developed for real-time use [185], should be of benefit.

The development of processing software for parameter identification demands a considerable effort. It may be wiser to buy software off the shelf. Unfortunately not too much is available. What is available may not run on the available computer system. Conversion of software from one computer to another can also be a major effort depending on the differences between the computers. The latter situation is mitigated somewhat by the general trend towards the use of graphics work stations running UNIX. Another trend is the use of X-windows for user interface and graphics and the use of graphics standards such as PHIGS.

Even under UNIX not all problems are solved, the data management systems, graphical libraries and user interfaces may vary considerably among systems. There is also some software developed by institutes and universities, such as MMLE3 or pEst/GetData/THPlot (NASA), MANS (RAE) and FTDA (TUD). One should also look seriously at commercially available software, because this software may be better supported.
In the end it may be cost effective to first select software purely on the basis of requirements and financial possibilities and then to buy the requisite hardware to match this software.

7.7 Conclusions

In this chapter several practical aspects of flight testing were discussed with special emphasis on the requirements for parameter identification. The flight test instrumentation was discussed and the need for a detailed knowledge of each measurement channel was shown. The ground preparations involving the transducer calibrations and the determination of the moments of inertia were discussed. The flight test design and execution are very important to the success of a flight test program. Several aspects of the flight test data processing were discussed such as data management and graphical presentation, while accuracy and time correlation were emphasized. The evaluation of the quality of the flight test data is a necessary step to gain confidence in the results derived from this data. Finally the systematic development of the data processing software is important to insure reliable results.

Channel Number		Measured Variable	Transducer Type	calibrated transducer input range (unit)	sample rate (Hz)
1	A_x	specific force along X-axis	Donner 4810	-10 → 10 (m/s^2)	20
2	A_y	specific force along Y-axis	Donner 4310	-5 → 5 (m/s^2)	20
3	A_z	specific force along Z-axis	Donner 4310/Sundstrand Q-Flex	0 → 20 (m/s^2)	20
4	p	roll rate	Honeywell GG87B	-20 → 20 (°/s)	20
5	q	pitch rate	Honeywell GG87B	-20 → 20 (°/s)	20
6	r	yaw rate	Honeywell GG87B	-20 → 20 (°/s)	20
7	ψ	yaw angle	Sperry Tarsyn	0 → 360 (°)	20
8	n	engine speed	General Electric	500 → 2400 (rpm)	10
9	T_t	total temperature	Rosemount 102	-30 → 30 (°C)	10
10	δ_e	elevator angle	CIC linear potentiometer	-28 → 23 (°)	20
11	δ_{a_l}	port aileron angle	CIC linear potentiometer	-17 → 33 (°)	20
12	δ_{a_r}	starboard aileron flap angle	CIC linear potentiometer	-17 → 33 (°)	20
13	δ_r	rudder angle	CIC linear potentiometer	-25 → 25 (°)	20
14	δ_{f_l}	port wing flap angle	CIC linear potentiometer	0 → 58 (°)	10
15	δ_{f_r}	starboard wing flap angle	CIC linear potentiometer	0 → 58 (°)	10
16	δ_{t_e}	elevator trim angle	Bourns linear potentiometer	-18 → 26 (°)	10
17	δ_{t_r}	rudder trim angle	Bourns linear potentiometer	-18 → 18 (°)	10
18	α_v	α-vane angle	DUT	-10 → 30 (°)	10
19	β_v	β-vane angle	NLR	-30 → 30 (°)	10
20	Δp_t	increase in total pressure behind propeller disc	MKS Baratron 145	0 → 30 (mbar)	10
21	Δp_1	variation in static pressure	MKS Baratron 145	-30 → 30 (mbar)	10
22	q_c	impact pressure	MKS Baratron 145	0 → 30 (mbar)	10
23	p_z	engine manifold pressure	MKS Baratron 145	500 → 1300 (mbar)	10
24	p_{st}	static pressure	MKS Baratron 145	500 → 1050 (mbar)	10
25	DME	Distance Measuring Equipment	King 705A	0 → 90 (N-Mile)	10
26	T_{carb}	carburator temperature	aircraft instrument	-30 → 30 (°C)	10

Table 7-1: *List of measured variables and corresponding transducers.*

Type of oscillation	P (sec)	ς	$T_{1/2}$ (sec)	$C_{1/2}$
about longitudinal axis	3.92	0.0083	52	13
about lateral axis	4.19	0.0040	116	28
about vertical axis	7.51	0.0040	207	28

Table 7-2: *Typical values of period (P), damping ratio (ς), and time and number of periods to damp to one half of the initial amplitude ($T_{1/2}$ and $C_{1/2}$) of the three different types of oscillation of the 'Beaver' DHC-2 experimental aircraft in the rig for the measurement of aircraft moments and products of inertia.*

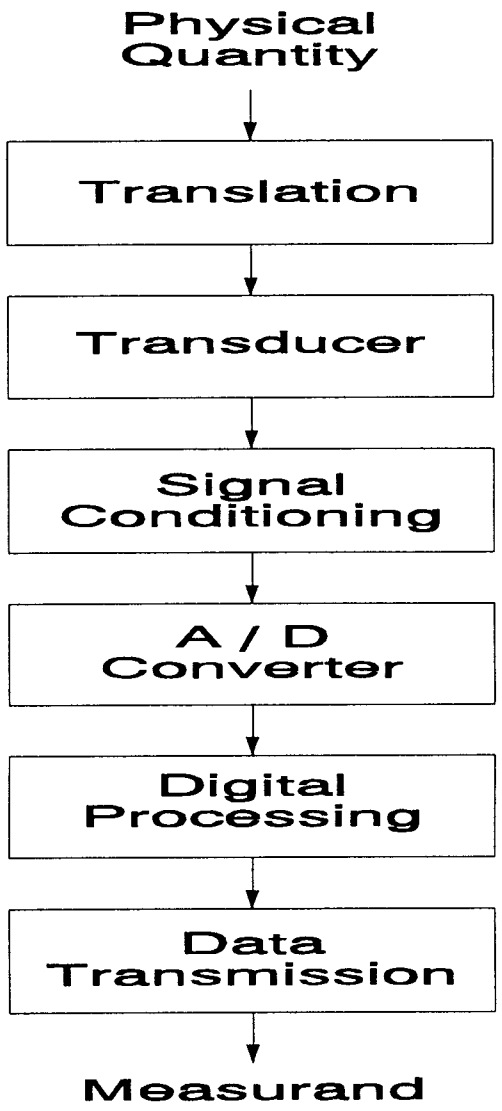

Figure 7-1: *General block diagram of measurement channel.*

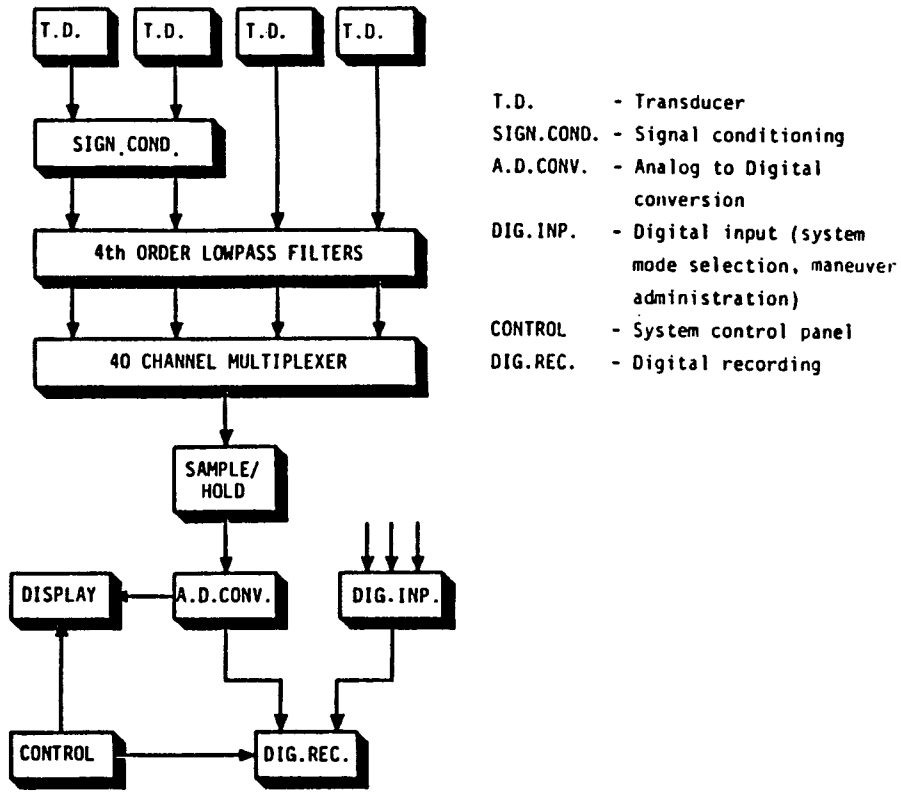

Figure 7-2: *General scheme of flight test measurement system.*

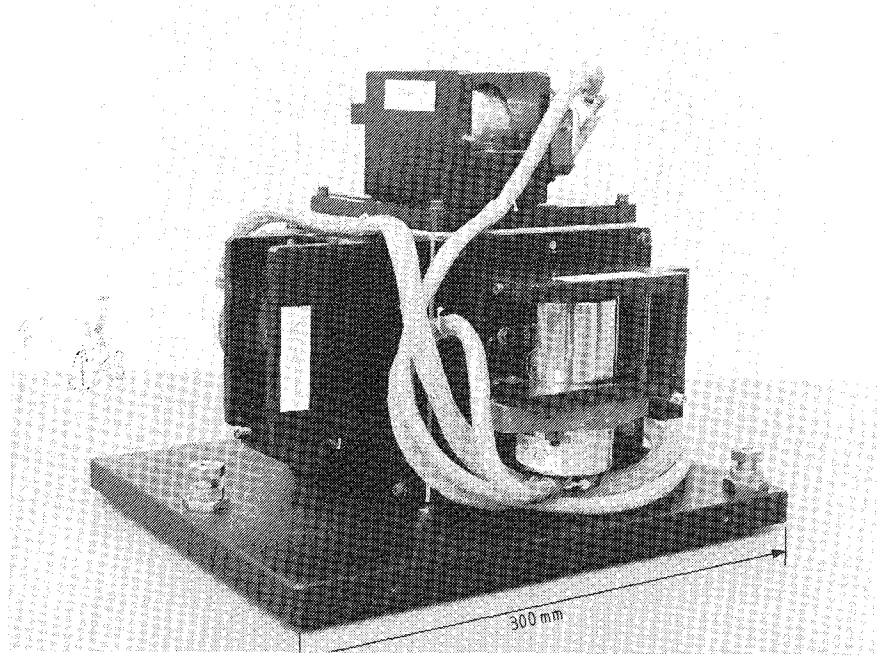

Figure 7-3: *Inertial measurement system consisting of three accelerometers and three rate gyros.*

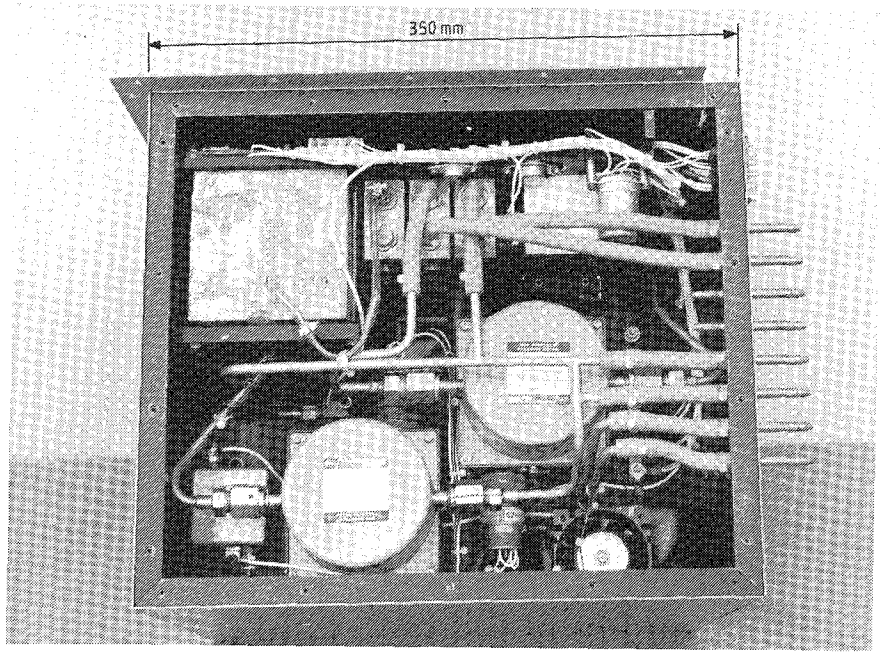

Figure 7-4: *Temperature controlled box containing one absolute and four differential pressure transducers.*

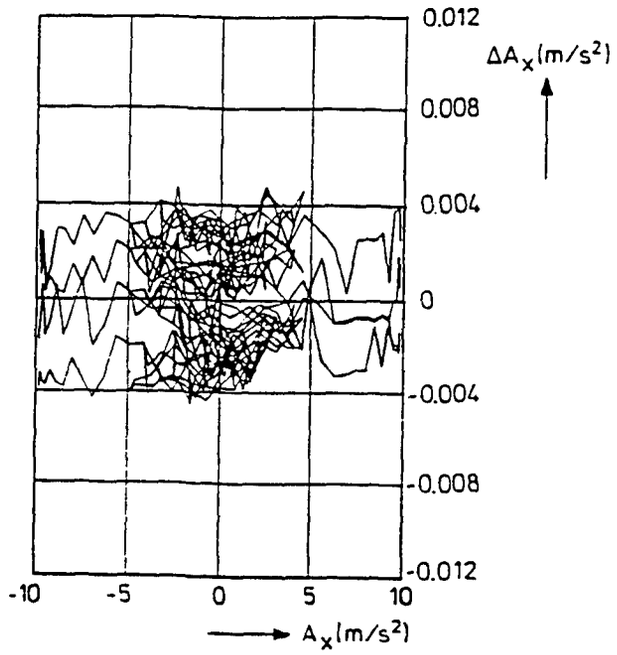

(a) *Longitudinal accelerometer channel (transducer type: Donner 4810)*

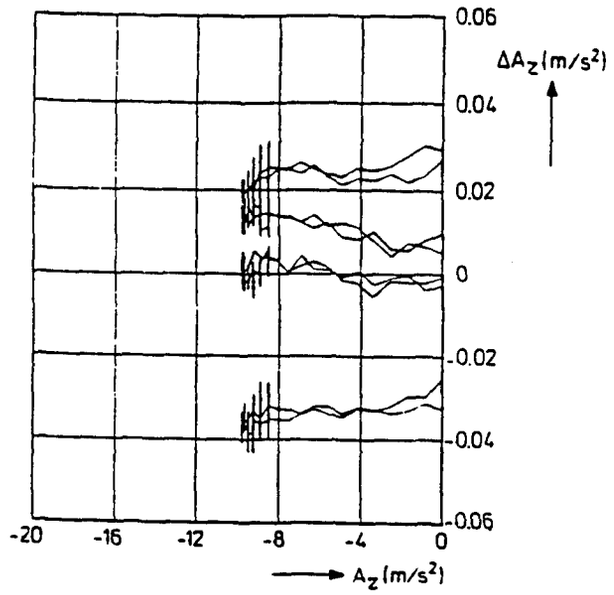

(b) *Vertical accelerometer channel (transducer type: 4310)*

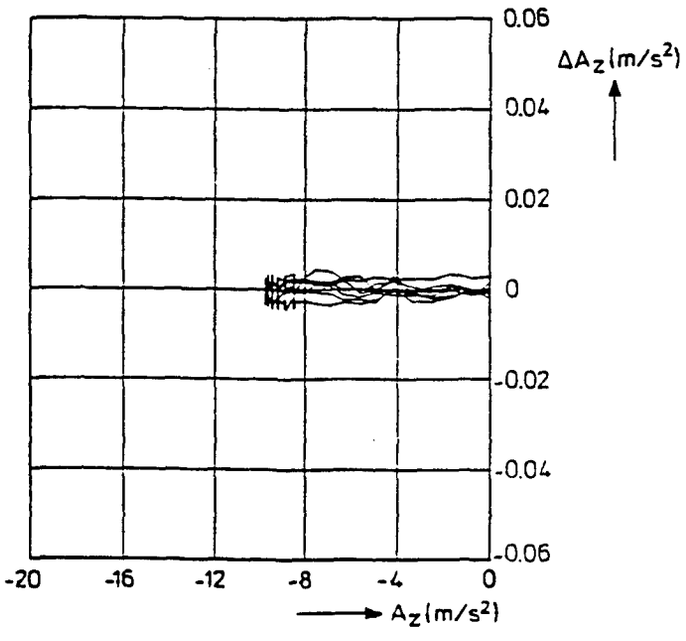

(c) *Vertical accelerometer channel (transducer type: sundstrand Q-Flex)*

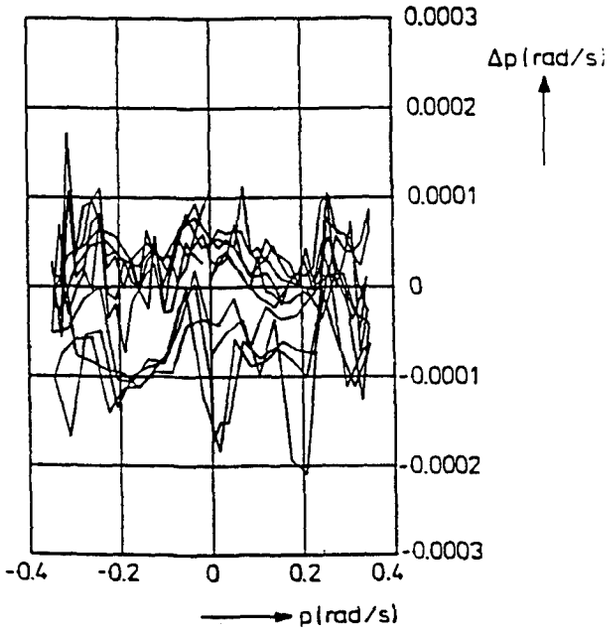

(d) *Roll rate gyro channel (transducer type: Honeywell GG87B)*

Figure 7-5: *Calibration residuals of the measurement channels of the instrumentation system.*

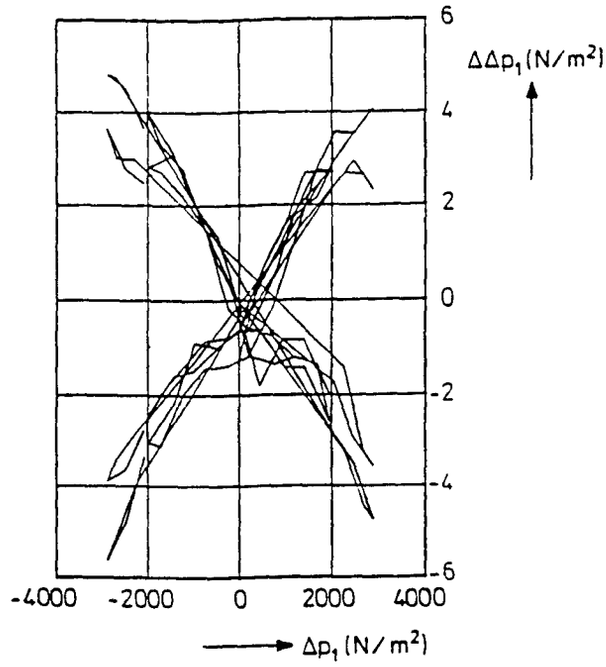

(e) *Differential pressure channel (transsducer type: MKS Baratron 145)*

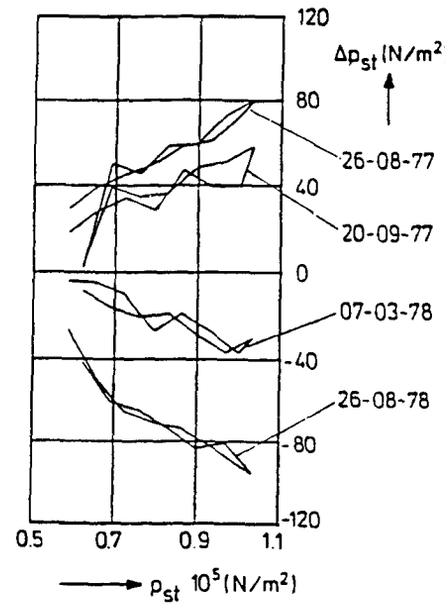

(f) *Absolute pressure channel (transsducer type: MKS Baratron 145)*

Figure 7-5: *Continued.*

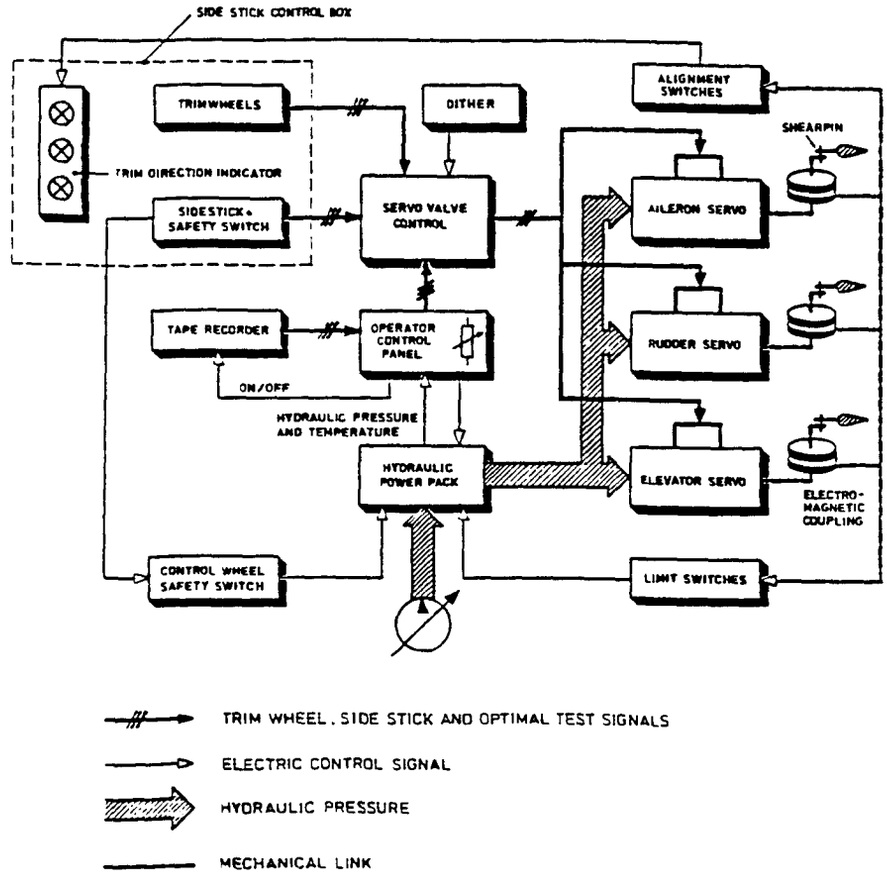

Figure 7-6: *Functional diagram of the electro-hydraulic control system.*

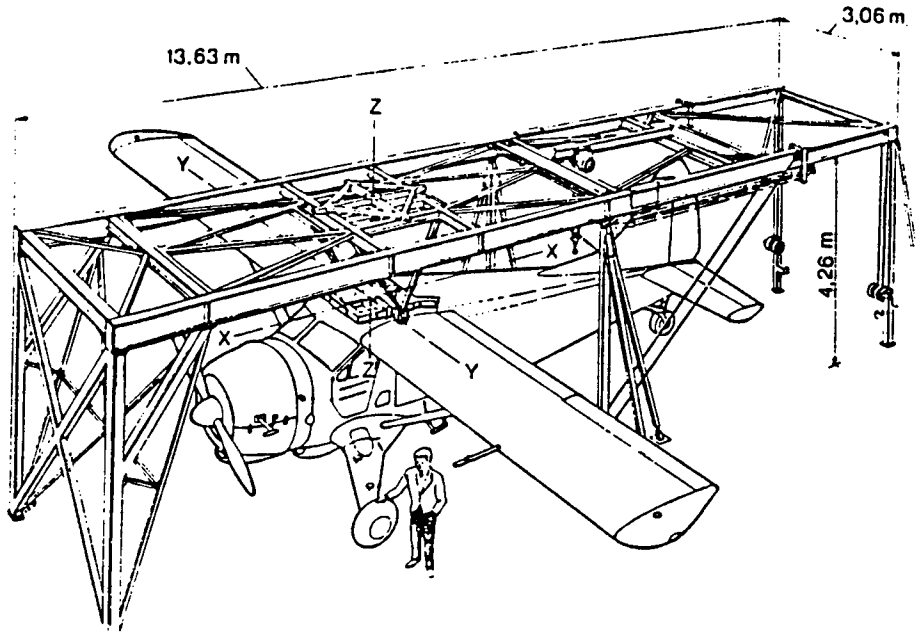

Figure 7-7: *Rig for the measurement of aircraft moments and products of inertia.*

8 CONCLUDING REMARKS

This volume is brought out as a sequel to the two earlier volumes already published in the AGARD Flight Test Technique Series, volume 2 on *'Identification of Dynamic Systems'* and volume 3 on *'Identification of Dynamic Systems - Applications to Aircraft Part - 1: The output error approach'* both written by R.E. Maine and K.W. Iliff. The present part 2 of volume 3 has examined in some detail the practical application of the *Two Step Method* for estimating aircraft aerodynamic model parameters from flight test data and has discussed in some detail the practical aspects of control input design for estimation of stability and control derivatives. Two different DUT approaches for control input optimization were presented.

The identification of aerodynamic models from measurements of dynamic flight test manoeuvres requires the solution of a sequence of nonlinear state-parameter estimation problems in which a set of aerodynamic model structures is tested with respect to model fit and parameter identifiability. If accurate measurements are made of specific aerodynamic forces (outputs of accelerometers) and angular rates, the parameter-state estimation problem may then be decomposed into two parts i.e. a state reconstruction problem, called flight path reconstruction and a parameter estimation problem which is linear-in-the-parameters.

It was noted that since the system and observation models of the flight path reconstruction problem are known in much detail, it is not necessary to evaluate different model structures, and the flight path reconstruction problem needs only to be solved once for each flight test manoeuvre. This means that the identification of aerodynamic models is considerably simplified because linear in the parameter estimation problems are much easier to solve than nonlinear state-parameter estimation problems.

In the linear case the flight path reconstruction problem (a nonlinear state estimation problem if based on nonlinear equations of motion) separates into two independent linear state estimation problems of the longitudinal and lateral components of the state vector respectively. The linearity of these estimation problems can be exploited in a reconstructibility analysis. The results of such an analysis may be used to compare different observation model configurations with respect to the dimension and character of the reconstructible subspace of the state space.

Nonlinear system and observation models are used for actual flight path reconstructions of the dynamic flight test manoeuvres executed in the course of a flight test program. Well-known extended Kalman filtering and smoothing algorithms can be successfully applied. The selection of the variables to be reconstructed as components of an augmented state vector was made using the results of the linear reconstructibility analysis for the chosen observation configuration.

After the flight path reconstruction, it has been shown that the aerodynamic model identification can be formulated in terms of a linear least squares problem. This permits the application of powerful numerical techniques for the calculation of parameter estimates. The resulting algorithms turn out to be very computer time efficient, which paves the way for the development of an interactive identification computer program. Combined with extensive computer graphics facilities, this program allows the analyst to rapidly evaluate alternative model structures on a few selected measurements. Also the possibility exists to combine measurement data from several different flight test manoeuvres for the purpose of aerodynamic model identification.

Analogous to the reconstructibility analysis of the flight path reconstruction problem we have discussed that it is possible to analyze the identifiability of the stability and control derivatives, i.e. the parameters in the linearized aerodynamic models. We have shown that not all longitudinal stability and control derivatives were identifiable if the nominal flight condition was straight horizontal flight. On the other hand, all lateral stability and control derivatives were shown to be identifiable if the flight test manoeuvre is executed such that independent roll angle excursions occur.

Since the parameter estimation problem of the second step of the analysis was linear-in-the-parameters it is possible to develop aerodynamic models stepwise via residual analysis. In each step the best of a set of candidate model extensions was selected. The problem was to decide how many model extensions should be included in the model. To this end a new criterion was proposed based on the theoretical accuracy of a predicted model output and its actual deviations from a second independent set of measurements.

We have then turned our attention to a most important aspect of flight test technique namely, the optimal input design. We have discussed that the accuracy of aerodynamic model parameters estimated from measurements of dynamic flight test manoeuvres depends, among other things, on the control input signals, i.e. the shape of the control input time histories. This means that different control input signals result in different parameter estimation accuracies. In order to express the theoretical performance of control input signals with respect to parameter estimation accuracy several performance indices can be based on the theoretical covariance matrix of parameter estimation errors (the Cramer-Rao Lower Bound). It follows that control input signals may be optimized with respect to each one of these performance indices.

Two new techniques were presented with which such optimizations may be carried out. The first technique is based on the representation of multi-dimensional control input signals in terms of a finite number of orthonormal functions. The second technique is based on the application of convex analysis in frequency domain for the optimization of input signals. We have shown that when energy constraints were imposed on the control inputs, constrained optimization problems which are generally difficult to solve can be transformed into an unconstrained optimization problem. This makes the optimization problem easier to solve.
Next we have pointed out that the optimization of control input signals is meaningful only if theoretical performance indices are adequate predictions of corresponding actual or sample performance indices. While theoretical performance indices are based on the CRLB, actual performance indices must be judged on sample covariance matrices.
In order to determine sample covariance matrices of parameter estimation errors corresponding to particular types of control input signals, an automatic (open loop) flight control system was installed in the De Havilland DHC-2 Beaver aircraft to allow precise repetition of control input signal in a series of (almost) identical manoeuvres. As an important result from the described flight test program it was observed that in relative, rather than in absolute terms, theoretical performance indices were adequate predictions of sample performance indices. This result is the experimental foundation for the application of control input signal optimization techniques.

In the present part 2 of volume 3 of the AGARD Flight Test Techmiques Series we have also discussed in some depth, the aspects of instrumentation, flight test design and execution, the data processing and data quality evaluation which are all very important, and which will be present in all flight test programs for aircraft parameter identification irrespective of which methods are to be used for the identification of the aerodynamic model parameters.

REFERENCES

1. R.E. Maine, K.W. Iliff, 'AGARD Flight Test Technique Series' on 'Identification of Dynamic Systems', AGARD AG-300, Vol. 2, January 1985.

2. R.E. Maine, K.W. Iliff, 'AGARD Flight Test Technique Series' on 'Identification of Dynamic Systems - Applications to Aircraft, Part 1: The output error approach', AGARD AG-300, Vol. 3 Part 1, December 1986.

3. O.H. Gerlach, 'Analyse van een mogelijke methode voor het meten van prestaties en stabiliteits- en besturingseigenschappen van een vliegtuig in niet stationaire, symmetrische vluchten (Analysis of a possible method for the measurement of performance and stability and control characteristics in non-steady symmetrical flight)', Report VTH-117, Delft University of Technology, Department of Aerospace Engineering, November 1964.

4. O.H. Gerlach, 'Determination of performance and stability parameters from non-steady flight test manoeuvres', SAE Paper 700236, National business aircraft meeting, Wichita, Kansas, 1970.

5. O.H. Gerlach, 'Determination of stability derivatives and performance characteristics from non-steady flight test manoeuvres', AGARD CP-85, Toulouse, 1971. Also as Report VTH-163, Delft University of Technology, Department of Aerospace Engineering, 1971.

6. H.L. Jonkers, 'Application of the Kalman filter to flight path reconstruction from flight test data including estimation of instrumental bias error corrections', Report VTH-162, Delft University of Technology, Department of Aerospace Engineering, February 1976.

7. H.L. Jonkers, J.A. Mulder, 'Accuracy limits in nonsteady flight testing', ICAS Paper No. 76-46, The tenth congress of the International council of the aeronautical sciences, Ottawa, October 1976.

8. H.L. Jonkers, J.A. Mulder, 'New developments and accuracy limits in aircraft flight testing', AIAA Paper 76-897, AIAA Aircraft System and Technology meeting, Dallas, Texas, September 1976.

9. J.A. Mulder, 'Aircraft performance measurements in non-steady flights', 3rd IFAC Symposium on 'Identification and System Parameter Estimation', The Hague, June 1973.

10. J.A. Mulder, 'Estimation of the aircraft state in non-steady flight', AGARD CP-172 on 'Methods for Aircraft State and Parameter Identification', Hampton, Virginia, November 1974.

11. J.A. Mulder, 'Estimation of thrust and drag in non-steady flight', 4th IFAC Symposium on 'Identification and System Parameter Estimation', Tbilisi, September 1976.

12. J.A. Mulder, J.M. van Sliedregt, 'Estimation of drag and thrust of jet propelled aircraft by non-steady flight test maneuvers', Memorandum M-255, Delft University of Technology, Department of Aerospace Engineering, December 1976.

13. J.A. Mulder, H.L. Jonkers, J.J. Horsten, J.H. Breeman, J.L. Simons, 'Analysis of aircraft performance, stability and control measurements, Part I - Theoretical aspects, Part II - Technical aspects and results', AGARD LS-104 on 'Parameter Identification', Delft, London, November 1979.

14. J.A. Mulder, J.G. den Hollander, H. Binkhorst, 'Aerodynamic model identification from dynamic flight test data and wind tunnel experiments', AGARD CP-339 on 'Ground/Flight Test Techniques and Correlation', Cesme, October 1982. Also as Report LR-361, Delft University of Technology, Department of Aerospace Engineering, Delft, The Netherlands, October 1982.

15. J.A. Mulder, R.J.A.W. Hosman, 'The application of high accuracy instrumentation techniques to aircraft flight testing', Shell Aviation News, No. 425, 1974.

16. K. van Woerkom, 'Design and evaluation of an instrumentation system for measurements in non-steady symmetrical flight conditions with the Hawker Hunter MK VII', Report LR-308, Delft University of Technology, Department of Aerospace Engineering, 1981.

17. K. van Woerkom, 'Instrumentation requirements and pre-sample filter design for measurements during non steady manoeuvres with the Hawker Hunter MK VII, PH-NLH' in 'Essays on stability and control', Report LR-600, edited by M. Baarspul and J.A. Mulder, Delft University of Technology, Department of Aerospace Engineering, 1989.

18. H.C. Garretson, 'Beaver Aircraft Parameter Identification - Technical Preparations and Preliminary Results', Mitteilung 78-01, DFVLR Institut für Flugmechanik, Braunschweig, Germany, July 1978.

19. E. Plaetschke, J.A. Mulder, J.H. Breeman, 'Results of Beaver aircraft parameter identification', FB 83-10, DFVLR Institut für Flugmechanik, Braunschweig, Germany, 1983.

20. E. Plaetschke, G. Schulz, 'Practical input signal design', AGARD LS-104 on 'Parameter Identification', Delft, London, November 1979.

21. J.H. Breeman, L.J.J. Erkelens, A.M.H. Nieuwpoort, 'Determination of performance and stability characteristics from dynamic manoeuvres with a transport aircraft using parameter identification', AGARD FMP Symposium on 'Flight Test Techniques', Lisbon, 1984.

22. J.H. Breeman, J.L. Simons, 'Evaluation of a method to extract performance data from dynamic manoeuvres for a jet transport aircraft', 11th ICAS Congress, Lisbon, 1978.

23. J.A. Mulder, M. Baarspul, J.H. Breeman, A.M.H. Nieuwpoort, 'Determination of the mathematical model for the new Dutch Government civil aviation flying school flight simulator', Society of Flight Test Engineers, 18th Annual symposium, Amsterdam, September 1987. Also as Memorandum M-578, Delft University of Technology, Department of Aerospace Enginereering, July 1987.

24. M. Laban, J.A. Mulder, 'Online identification of aircraft aerodynamic model parameters', 9th IFAC/IFORS Symposium on 'Identification and System Parameter Estimation', Budapest, Hungary, July 1991.

25. M. Laban, 'Online aircraft state and parameter estimation', AGARD-CP-519, paper 29, May 1992.

26. M. Laban, 'Online aircraft aerodynamic model identification', Doctoral Dissertation, Delft University of Technology, Department of Aerospace Engineering, To be published 1994.

27. H. Muhammad, 'Identification of turboprop thrust from dynamic flight test measurements', Doctoral Dissertation, Delft University of Technology, Department of Aerospace Engineering, To be published 1994.

28. H.L. Jonkers, J.A. Mulder, K. van Woerkom, 'Measurements in non-steady flight: Instrumentation and analysis', Proceedings of the 7th international aerospace instrumentation symposium, Cranfield, 1972.

29. J.A. Mulder, 'Aircraft control input optimization for aerodynamic estimation in dynamic manoeuvres', 7th IFAC Symposium on 'Identification and System Parameter Estimation', York, UK, July 1985.

30. A.K. Karwal, J.A. Mulder, H. Muhammad, 'Data Analysis in flight testing, 4th symposium of the European chapter of the society of flight test engineers, Rome, Italy, June 1991.

31. R.C. Wingrove, 'Applications of a technique for estimating aircraft states from recorded flight test data', AIAA Paper 72-965, September 1972.

32. R.C. Wingrove, 'Quasi linearization technique for estimating aircraft states from flight data', Jour. Aircraft, May 1973, pp. 303-307.

33. R.C. Wingrove, 'Parameter estimation of powered lift STOL aircraft characteristics including turbulence and ground effects', AGARD CP-172 on 'Methods for Aircraft State and Parameter Identification', Hampton, Virginia, November 1974, chapter 19.

34. B.J. Eulrich, N.D. Weingarten, 'Identification and correlation of the F-4E stall/post stall aerodynamic stability and control characteristics from existing test data', Report AK-5126F-1, Calspan Corp., Buffalo, N.Y., November 1973. Also as AFFDL-TR-73-125, August 1973.

35. J.A. Molusis, 'Analytical study to define a helicopter stability derivative extraction method', Vol. 1, Final Report, Contract NAS1-11613, NASA CR-132372, Sikorsky aircraft, Stratford, Conn., 1973.

36. V. Klein, J.R. Schiess, 'Compatibility check of measured aircraft responses using kinematic equation and Extended Kalman Filter', NASA TN D-8514, 1977.

37. W.E. Hall Jr., J.A. Molusis, 'Data consistency program - Theory and User's Guide', Technical Report No. 3, Contract N00014-72-C-0328, Office of Naval Research, November 1975.

38. T.J. Galbrith, T.J. Petersen, E.C. Roth, 'A computer system for identifying aircraft characteristics from flight test data', The Boeing Co., Seattle, Washington, 1976.

39. D.E. McBrinn, B.B. Brassell, 'Aerodynamic parameter identification for the A-7 airplane at high angles of attack', Proceedings of 3rd Atmospheric flight mechanics conference, Arlington, Texas, 1976.

40. R.E. Bach Jr., 'Variational algorithms for nonlinear smoothing applications', NASA TM-73, 211, 1977.

41. R.E. Bach Jr., 'A variational technique for smoothing flight test and accident data', Jour. Aircraft, July 1982, pp. 546-552.

42. R.E. Bach Jr., R.C. Wingrove, 'Applications of state estimation in aircraft flight data analysis', Jour. Aircraft, Vol. 22, No. 7, July 1985.

43. R.E. Bach Jr., 'A mathematical model for efficient estimation for aircraft motions', 6th IFAC Symposium on 'Identification and System Parameter Estimation', Washington D.C., June 1982.

44. R.S. Hansen, 'DEKFIS User's Guide - Discrete extended Kalman Filter/smoother program for aircraft and rotorcraft data consistency', Contract NAS1-14549, NASA CR-159081, Systems Control Inc., Palo Alto, California, 1979.

45. H.L. Stalford, S. Ramachandran, 'Application of the Estimation Before Modelling (EBM) system identification method to the high angle of attack/side slip flight of T-2C jet trainer aircraft', Vol. II, NADC-76097, 30 June 1978.

46. D.A. Keskar, V. Klein, 'Determination of instrumentation errors from measured data using maximum likelihood method', AIAA Paper 80-1602, 1980.

47. J.A. Mulder, J.G. Hollander, 'Status of dynamic flight test technology - Model identification for flight simulations', SAE Paper 810597, Business aircraft meeting of the society of Automotive Engineers, Wichita, Kansas, April 1981.

48. C. Fratter, 'Determination of aerodynamic coefficients for the avionics research aircraft using the Estimation Before Modelling Technique', M.S.E. Thesis, Aerospace Eng Dept, Princeton University, Princeton, N.J., October 1982.

49. M. Sri Jayantha, R.F. Stengel, 'Data acquisition system and methodology for high angle of attack parameter estimation', SAE Paper 830719, Business and Utility aircraft meeting of the society of Automotive Engineers, Wichita, Kansas, April 1983.

50. R.C. Wingrove, R.E. Bach Jr., 'Analysis of General Aviation Accident using ATC radar records', Jour. Aircraft, October 1983, pp. 872-876.

51. E.K. Parks, R.E. Bach, R.C. Wingrove, 'Analysis of the nature and cause of turbulence upset using airline flight records', Symposium of the society of flight test engineers, New York, September 1982.

52. L.W. Taylor Jr., 'Applications of parameter estimation in the study of spinning airplanes', AIAA Paper 82-1309, 1982.

53. N.E. Nahi, 'Estimation theory and Applications', John Wiley and Sons, 1969.

54. R.D. Grove, R.L. Bowles, S.C. Mayhew, 'A procedure for estimating stability and control parameters from flight test data by using maximum likelihood methods employing a real time digital system', NASA TN D-6735, May 1972.

55. K.W. Iliff, R.E. Maine, 'Practical aspects of using a maximum likelihood estimation method to extract stability and control derivatives from flight data', NASA TN D-8209, April 1976.

56. J.J. Horsten, H.L. Jonkers, J.A. Mulder, 'Flight path reconstruction in the context of non-steady flight testing', Report LR-280, Delft University of Technology, Department of Aerospace Engineering, May 1979.

57. B. Etkin, 'Dynamics of Atmospheric Flight', John Wiley and Sons, 1972.

58. M. Tobak, L.B. Schiff, 'On the formulation of the aerodynamic characteristics in aircraft dynamics', NASA TR R-456, January 1976.

59. W.E. Hall Jr., N.K. Gupta, J.S. Tyler, 'Model structure determination and parameter identification for nonlinear aerodynamic flight regimes', AGARD CP-172 on 'Methods for Aircraft State and Parameter Identification', Hampton, Virginia, November 1974.

60. V. Klein, G. Batterson, 'Determination of airplane model structure from flight data using splines and stepwise regression', NASA TP 2126, March 1983.

61. V. Klein, J.G. Batterson, 'Aerodynamic parameters estimated from flight and wind tunnel data', Jour. Aircraft, Vol. 23, No. 4, April 1986, pp. 306-312.

62. V. Klein, T.P. Ratvasky, B.R. Cobleigh 'Aerodynamic parameters of high angle of attack research vehicle (HARV) estimated from flight data', NASA TM 102692, 1990.

63. J.G. Jones, 'Modelling of systems with a high level of internal fluctuations', AGARD CP-172 on 'Methods for Aircraft State and Parameter Identification', Hampton, Viginia, November 1974.

64. R.F. Antoniewicz, E.L. Duke, B.P. Patterson, 'User's manual for interactive LINEAR, a FORTRAN program to derive linear aircraft models', NASA TP 2835, September 1988.

65. R. Koehler, K. Wilhelm, 'Auslegung von Eingangssignalen für die Kennwert-ermittlung', IB 154-77/40, DFVLR Institut für Flugmechanik, Braunschweig, Germany, December 1977.

66. R.J.A.W. Hosman, 'A method to derive angle of pitch, flight path angle and angle of attack from measurements in nonsteady flight', Report VTH-156, Delft University of Technology, Department of Aerospace Engineering, 1971.

67. R.J.A.W. Hosman, 'Advanced flight test instrumentation: design and calibration', AGARD CP-172 on 'Methods for Aircraft State and Parameter Identification', Hampton, Viginia, November 1974.

68. V. Klein, D.R. Morgan, 'Estimation of bias errors in measured airplane responses using maximum likelihood method', NASA TM 89059, 1987.

69. R.E. Bach Jr., 'State estimation applications in aircraft flight data analysis. A user's manual for SMACK', NASA RP 1252, March 1991.

70. H. Kwakernaak, R. Sivan, 'Linear Optimal Control System', Wiley-Inter Science, 1972.

71. A.P. Sage, J.L. Melsa, 'Estimation Theory with Applications to Communications and Control', McGraw Hill Book Company, 1971.

72. Ch.L. Lawson, R.J. Hanson, 'Solving least squares problems', Prentice-Hall Inc., Englewood Cliffs, N.J., 1974.

73. N.R. Draper, H. Smith, 'Applied Regression Analysis', second edition, John Wiley and Sons, 1981.

74. D.B. Belsley, E. Kuhn, R.E. Welsh, 'Regression Diagnostics, Identifying influential data and sources of collinearity', John Wiley and Sons, 1980.

75. D.C. Montgomery, E.A. Peck, 'Introduction to linear regression analysis', John Wiley and Sons, 1982.

76. P. Eykhoff, 'System Identification', John Wiley and Sons, 1974.

77. W.F. Milliken Jr., 'Progress in dynamic stability and control research', Jour. Aeronautical Sciences, Vol. 14, No. 9, 1947.

78. H. Greenberg, 'A survey of methods for determining stability of an airplane from dynamic flight measurements', NACA TN 2340, 1950.

79. M. Shinbrot, 'On the analysis of linear and nonlinear dynamical systems from transient response data', NACA TN 3288, December 1954.

80. D. DiFranco, 'Inflight parameter identification by the equation of motion technique - Application of the variability stability T-33 airplane', Report No. TC-1921-F-3, Cornell Aeronautical Laboratory, December 1965.

81. G.C. Goodwin, 'Application of curvature methods to parameter and state estimation', IEEE Proceedings, Vol. 16, No. 6, June 1969.

82. L.W. Taylor Jr. et al, 'A comparison of Newton Raphson and other methods for determining stability derivatives from flight data', Third technical workshop on dynamic stability problems, Ames Research Centre, 1968. Also presented at AIAA Third Flight Test, Scientific and Support Conference, Houston, Texas, March 1969.

83. R. Bellman et al, 'Quasilinearization, system identification and prediction', RN3812, RAND corporation, August 1963.

84. K.S.P. Kumar, R. Shridhar, 'On the identification of control systems by the quasilinearization method', IEEE Transactions Automatic Control, Vol. AC-10, April 1964, pp. 151-154.

85. D. Larson, 'Identification of parameters by method of quasilinearization', CAL Report 164, May 1968.

86. D.G. Denery, 'An identification algorithm which is insensitive to initial parameter estimates', AIAA Eigth Aerospace Conference, January 1970.

87. P.C. Young, 'Process parameter estimation and adaptive control', in theory of self adaptive control systems, P.Hammond Ed. Plenum Press, N.Y., 1966.

88. R.D. Shallow, 'Quasilinearization and parameter estimation accuracy', PhD thesis, Syracus University, 1967.

89. B. Dolbin, 'A differential correction method for the identification of airplane parameters from flight test data', University of Buffalo, M.S. Thesis, December 1968.

90. L.S. Lason et al., 'The conjugate gradient method for optimal control problems', IEEE Transactions, G-AL Vol. 12, No. 2, April 1967.

91. W.T. Suit, 'Aerodynamic parameters of the new Navion airplane extracted from flight data', NASA TN D-6643, March 1972.

92. G.S. Steinmetz et al., 'Longitudinal stability and control derivatives of a jet fighter airplane extracted from flight test data by utilizing Maximum Likelihood Estimation', NASA TN D-6532, March 1972.

93. J.S. Tyler, J.D. Powell, R.K. Mehra, 'The use of smoothing and other advanced techniques for VTOL aircraft parameter identification', Final report to Cornell Aeronautical Laboratory under Naval Air systems command contract No. N00019-69-C-0534, June 1970.

94. R.L. Kashyap, 'Maximum Likelihood Identification of Stochastic Linear Dynamic Systems', IEEE Transanctions Automatic Control, Vol. AC, February 1970.

95. R.K. Mehra, 'Identification of stochastic linear dynamic systems using Kalman Filter Representation', AIAA Journal, Vol. 9, No. 1, January 1971.

96. R.K. Mehra, 'Maximum likelihood identification of aircraft parameters', Joint Automatic Control Conference, Atlanta, Georgia, 1970.

97. K.W. Iliff, 'Identification and stochastic control of an aircraft flying in turbulence', Jour. Guidance, Control and Dynamics, Vol. 1, No. 2, 1978, pp. 101-108

98. K.W. Iliff, 'Aircraft Identification Experience', AGARD LS-104 on 'Parameter Identification', Delft, London, November 1979.

99. K.W. Iliff, 'Practical aspects of using a maximum likelihood estimator', AGARD CP-172 on 'Methods for Aircraft State and Parameter Identification', Hampton, Viginia, November 1974.

100. K.W. Iliff, R.E. Maine, 'NASA Dryden's experience in parameter estimation and its use in flight test', AIAA Paper 82-1373, AIAA AFM conference, San Diego, California, August 1982.

101. K.W. Iliff, L.W. Taylor Jr., 'Determination of stability derivatives from flight data using a Newton Raphson minimization technique', NASA TN D-6579.

102. K.W. Iliff, 'Maximum likelihood estimation of lift and drag from dynamic aircraft manoeuvres', Jour. Aircraft, Vol. 14, No. 12, 1977, pp. 1175-1181.

103. R.E. Maine, K.W. Iliff, 'Maximum likelihood estimation of translational acceleration derivatives from flight data', Jour. Aircraft, Vol. 16, No. 10, 1979, pp. 674-679.

104. R.E. Maine, K.W. Iliff, 'User's manual for MMLE3. A general FORTRAN program or maximum likelihood parameter estimation', NASA TP 1563, 1980.

105. R.E. Maine, K.W. Iliff, 'The theory and practice of estimating the accuracy of dynamic flight determined coefficients', NASA RP 1077, 1981.

106. R.E. Maine, K.W. Iliff, 'Identification of dynamic system: Theory and formulation. NASA RP 1138, 1985.

107. R.E. Maine, K.W. Iliff, 'Application of parameter estimation to aircraft stability and control. The output error approach', NASA RP 1168, 1986.

108. R.E. Maine, 'Aerodynamic derivatives for an oblique wing aircraft estimated from flight data by using a maximum likelihood technique', NASA TP 1336, 1978.

109. R.E. Maine, K.W. Iliff, 'Formulation and implementation of a practical algorithm for parameter estimation with process and measurement noise', SIAM Jour. Appl. Math., Vol. 41, No. 3, 1981.

110. R.V. Jategaonkar, E. Plaetschke, 'Maximum likelihood parameter estimation from flight test data for general nonlinear systems', FB-83-14, DFVLR Institut für Flugmechanik, Braunschweig, Germany, 1983.

111. R.V. Jategaonkar, E.Plaetschke, 'Maximum likelihood estimation of parameters in linear systems with process and measurement noise', FB-87-20, DFVLR Institut für Flugmechanik, Braunschweig, Germany, 1987.

112. R.V. Jategaonkar, E. Plaetschke, 'Estimation of aircraft parameters using filter error methods and extended Kalman filter', FB-88-15, DFVLR Institut für Flugmechanik, Braunschweig, Germany, March 1988.

113. R.V. Jategaonkar, E. Plaetschke, 'Algorithms for aircraft parameter estimation accounting for process and measurement noise', Jour. Aircraft, Vol. 26, No. 4, 1989.

114. R.T.N. Chen, 'Input design for aircraft parameter identification using time optimal control formulation', AGARD CP-172 on 'Methods for Aircraft State and Parameter Identification', Hampton, Viginia, November 1974.

115. D.B. Mackie, 'A comparison of parameter estimation results from flight test data using linear and nonlinear maximum likelihood methods', FB-84-06, DFVLR Institut für Flugmechanik, Braunschweig, Germany, 1984.

116. V. Parameswaran, E. Plaetschke, 'Flight path reconstruction using extended Kalman Filtering Techniques', FB-90-41, DLR, Germany, 1990.

117. K.O. Proskawetz, 'Maximum likelihood parameter estimation for general nonlinear systems', IASTED SYMPOSIUM, Grindelwald, 1987.

118. K.O. Proskawetz, 'Robust parameter estimation of nonlinear dynamic systems, Zeitschrift für Flugwissenschaften und Weltraumforschung, Vol. 15, 1991.

119. K.O. Proskawetz, 'System identification of airplanes using Estimation before modelling technique', Zeitschrift für Flugwissenschaften und Weltraumforschung, Vol. 15, 1991.

120. V. Klein, 'Determination of aerodynamic derivatives from steady state measurement of an aircraft'. AIAA Paper 77-1123, 1977.

121. V. Klein, 'Aircraft parameter estimation in the frequency domain', AIAA Paper 78-1344, 1978.

122. V. Klein, 'Maximum likelihood method for estimating airplane stability and control parameters from flight data in frequency domain', NASA TP 1637, 1980.

123. E.A. Morelli, 'Practical input optimization for aircraft parameter estimation experiments', PhD Thesis, The George Washington University, The school of Engg. Science, 1990.

124. G.W. Foster, 'The identification of aircraft stability and control parameters in the presence of turbulence', RAE TR-83025, March 1983.

125. V. Klein, 'Estimation of aircraft aerodynamic parameters from flight data', Proceedings Aerospace Sciences, Vol. 26, 1989, pp. 1-77.

126. W.E. Hall Jr., N.K.Gupta, R.G. Smith, 'Identification of aircraft stability and control coefficients for the high angle of attack regime', Technical Report No. 2, Systems Control Corp., 1974.

127. W.E. Hall Jr., N.K.Gupta, R.S.Hansen, 'Rotorcraft system identification techniques for handling qualities and stability and control evaluation', Preprint No. 78-30, Proceedings 34th annual forum of the American Helicopter Society, Washington, 1978.

128. N.K. Gupta, 'New frequency domain methods for system identification', Joint Automatic Control Conference, San Francisco, June 1977.

129. N.K. Gupta, 'Design and evaluation of sensor systems for state and parameter estimation', Jour. Guidance, Control and Dynamics, Vol. 1, No. 6, November-December 1978.

130. N.K. Gupta, R.K. Mehra, 'Computational aspects of maximum likelihood estimation and reduction in sensitivity function calculations', IEEE Transactions Automatic Control, Vol. AC-19, No. 6, 1974, pp. 774-783.

131. N.K. Gupta, W.E. Hall Jr. T.L. Trankle, 'Advanced model structure determination from test data', Jour. Guidance, Control and Dynamics, Vol. 1, No. 3, May-June 1978.

132. P.G. Hamel, 'A system analysis view of aerodynamic coupling', Jour. Aircraft, Vol. 7, No. 6, November-December 1970, pp. 567-569.

133. P.G. Hamel, 'Aircraft parameter identification methods and their applications - Survey and future aspects' AGARD LS-104 on 'Parameter Identification', Delft, London, November 1979.

134. P.G. Hamel, 'Determination of aircraft dynamic stability and control parameters from flight testing' AGARD LS-I on 'Dynamic stability Parameters', May 1981.

135. P.G. Hamel, B. Krag, 'Dynamic wind tunnel simulation of active control systems' in 'Stability and Control', AGARD CP-260, May 1979.

136. W.R. Wells, S. Ramachandran, 'Flight test design for efficient extraction of aircraft parameters', AIAA 3rd AFM Conference, June 1976.

137. J. Kaletka, M.B. Tischler, W.V. Grünhagen, J.W. Fletcher, 'Time and frequency domain identification and verification of BO-105 Dynamic models', Jour. of the American Helicopter Society, October 1991.

138. J. Kaletka, 'Practical aspects of helicopter parameter identification' AIAA CP-849, No. 84-2081, 1984.

139. M.B. Tischler, 'Advancements in frequency domain methods for rotorcraft system identification', 2nd int. conf. on rotorcraft basic research, University of Maryland, 1988.

140. M.B. Tischler, J. Kaletka, 'Modelling XV-15 Tilt rotor aircraft dynamics by frequency and time domain identification methods', AGARD CP-423, 1987.

141. H. Unbehauen, B. Gohring, 'Test for determining model order in parameter estimation', Automatica, Vol. 10, No. 3, 1974.

142. R. Genesio, M. Milanese, 'Methods for the selection of approximating classes of models. Identification and system parameter estimation', 5th IFAC Symposium, Vol. 1, edited by R. Isermann, 1979.

143. V. Klein, J. Tosovsky, 'General theory of complex random variable and its application to the curve fitting a frequency response', ZPRAVA VZLUZ-11, December 1967.

144. V. Klein, 'On the adequate model for aircraft parameter estimation', Rep. Aero No. 28, Cranfield Inst. Tech., March 1975.

145. D.E. Stepner, R.K. Mehra, 'Maximum likelihood identification and optimal input design for identifying aircraft stability and control derivatives', NASA CR-2200, 1973.

146. L.W. Taylor Jr., 'Application of a new criterion for modelling systems', AGARD CP-172 on 'Methods for Aircraft State and Parameter Identification', Hampton, Viginia, November 1974.

147. K.D. Noderer, 'Analysis of the lateral aerodynamic characteristics of the X-31 model obtained from flight test data', M.S. Thesis, The George Washington University, The school of Engg. Science, July 1992.

148. N.K. Gupta, W.E. Hall Jr., T.L. Trankle, 'Advanced methods of model structure determination from test data', Collection of technical papers, AIAA AFM Conference, August 1977.

149. H.L. Stalford, 'Application of the Estimation Before modelling (EBM) system identification method to high angle of attack/sideslip flight of the T-2C jet trainer aircraft', Volume III, 'Identification of T-2C aerodynamics stability and control characteristics from actual flight test data', NADC-76097-30, US Navy, 1979.

150. V. Klein, J.G. Batterson, P.C.Murphy, 'Determination of airplane model structure from flight data by using modified stepwise regression', NASA TP 1916, October 1981.

151. V. Klein, J.G. Batterson, P.L. Smith, 'On the determination of airplane model structure from flight data', 6th IFAC Symposium on 'Identification and Systems Parameter Estimation', Washington D.C., 1982.

152. M. Idan, 'Nonlinear smoothing identification algorithm with application to data consistency checks', Jour. Guidance, Control and Dynamics, Vol. 16, No. 2, March-April 1993.

153. R.R. Hocking, 'The analysis and selection of variables in linear regression', Biometrics, Vol. 32, 1976.

154. T.C. Hsia, 'System Identification', D.C. Heath and Co., 1977.

155. V. Klein, 'Identification evaluation methods', AGARD LS-104 on 'Parameter Identification', Delft, London, November 1979.

156. V. Klein, 'Two biased estimation techniques in linear regression - Application to aircraft', NASA TM 100649, 1988.

157. V. Klein, B.R. Cobleigh, K.D. Noderer, 'Lateral aerodynamic parameters of the X-29 aircraft estimated frcm flight data at moderate to high angles of attack', NASA TM 104155, 1991.

158. N.K. Gupta, W.E. Hall Jr., 'Input design for identification of aircraft stability and control derivatives', NASA CR-2493, Palo Alto, 1975.

159. N.E. Nahi, 'Optimal inputs for parameter estimation in dynamic systems with white observation noise', Joint Automatic Control Conference, 1969, pp. 506-513.

160. N.E. Nahi, G.A. Napjus, 'Design of optimal probing signals for vector parameter estimation', IEEE Decision and Control Conference, Miami, Florida, 1971.

161. G.C. Goodwin, R.L. Payne, 'Dynamic System Identification: Experimental Design and Data Analysis', Academic Press, 1977.

162. R.Kalaba, K.Spingarn, 'Control, Identification, and Input Optimization', Mathematical Concepts and Methods in Science and Engineering, Vol. 25, Plenum Press, 1982.

163. G. Schulz, 'Entwurf optimaler Eingangssignale für die System Identifizierung', Forschungsbericht FB 76-40, DFVLR Institut für Dynamik der Flugsysteme, Oberpfaffenhofen, Germany, 1976.

164. R.K. Mehra, N.K.Gupta, 'Status of input design for aircraft parameter identification', AGARD CP-172 on 'Methods for Aircraft State and Parameter Identification', Hampton, Virginia, November 1974.

165. R.K. Mehra, 'Frequency-domain synthesis of optimal inputs for multi input-multi output (mimo) systems with process noise', Decision and Control Conference, Phoenix, Arizona, 1974.

166. R.K. Mehra, 'Time-domain synthesis of optimal inputs for system identification', Decision and Control Conference, Phoenix, Arizona, 1974.

167. J. Kiefer, J. Wolfowitz, 'The equivalence of two extremum problems', Canadian Jour. Math., Vol. 12, 1960.

168. J. Kiefer, 'Optimum Designs in Regression Problems, II', Ann. Math. Stat., Vol. 32, 1961.

169. S.E. Dreyfus, 'Dynamic programming and the calculus of variations', Academic Press, 1965.

170. M.J.D. Powell, 'An efficient method for finding the minimum of a function of several variables without calculating derivatives', Computer Journal, Vol. 7, 1964, pp. 155-162.

171. G. Arfken, 'Mathematical methods for physicists', second edition, Academic Press, 1970.

172. D.A. Swick, 'Walsh function generation', IEEE Transactions on Information Theory, IT-15, 1969, p. 167.

173. P. Sonneveld, J.A. Mulder, 'Development and identification of a multi-compartment model for the distribution of adriamycin in the rat', Journal of Pharmacokinetics and Biopharmacentrics, Vol. 9, pp. 577-601, 1981.

174. R. Schmidt, 'Advances in Non-linear parameter optimization', Lecture notes in Control and Information Sciences, Springer-Verlag, 1982.

175. C.J. Kranenburg, P. de Lange, J.A. Mulder, 'Determination of the rigid body inertial characteristics of the De Havilland DHC-2 Beaver experimental aircraft from high accuracy measurements of free oscillations', Report LR-337, Delft University of Technology, Department of Aerospace Engineering, 1982.

176. C.J. Kranenburg, P. de Lange, J.A. Mulder, 'Elementary data processing of measurements in dynamic flight test maneuvers', Report LR-409, Delft University of Technology, Department of Aerospace Engineering, 1986.

177. C.J. Kranenburg, P. de Lange, J.A. Mulder, 'Calibration characteristics and error statistics of a high accuracy flight test instrumentation system for measurements in dynamic flight test maneuvers', Report LR-408, Delft University of Technology, Department of Aerospace Engineering, 1986.

178. A.J. Blok, J.A. Mulder, 'Status of aerodynamic model identification at Delft University of Technology', LR-401, Delft University of Technology, Department of Aerospace Engineering, 1987.

179. B.R. Cobleigh, 'Design of optimal inputs for parameter estimation flight experiments with application to the X-31 drop model', M.S. Thesis, The George Washington University, The school of Engg. Science, July 1991.

180. M. Marchand, 'Untersuchung der Bestimmbarkeit der flugmechanischen Derivative des CCV-Versuchsträgers F-104 G', DFVLR Institut für Flugmechanik, Braunschweig, Germany, March 1977.

181. R.T.N. Chen, 'Input design for parameter identification Part I: A new form and a practical solution', Joint Automatic Control Conference, Austin, Texas, June 1974.

182. J. Durbin, 'Errors in variables', Revue de l'Institut International de Statistique, Vol. 22, 1954, pp. 23-32.

183. T. DeMarco, 'Structured analysis and system specification', Prentice-Hall Inc., Englewood Cliffs, N.J., 1978.

184. E. Yourdon, L.L. Constantine, 'Structured design: Fundamentals of a discipline of computer program and systems design', Prentice-Hall Inc., Englewood Cliffs, N.J., 1975.

185. D.J. Hatley, I.A. Pirbhai, 'Strategies for real time system specification', Dorset House, 1988.

186. W.E. Deskins, 'Basic concepts in algebra', Standard Mathematical Tables, 25th Edition, CRC Press, edited by W.H. Beyer, Chapter II, 1978.

187. R.L. Cannady, W.T.Suit, 'Effects of control inputs on the estimation of stability and control parameters of a light airplane', NASA TP 1043, December 1977.

188. J. Kok, R. van Wijk, 'Evaluation of models describing human operator control of slowly responding complex systems', PhD. Thesis, Delft University Press, November 1978.

189. G.T. Chapman, L.A. Yates, 'Nonlinear aerodynamic parameter estimation and model structure identification', AIAA FMP Conference, Hilton Head, SC, August 1992.

190. R.E. Kalman, 'A new approach to linear filtering and prediction problems', ASME Transactions, Jour. Basic Eng. Series D, 82, 1960.

191. H. Schneider, 'Method of modelling, parameters and state estimation of nonlinear systems', Jour. Guidance, Control and Dynamics, Vol. 3, March-April 1980, pp. 97-98.

192. G.J. Bierman, 'Fixed interval smoothing with discrete measurements', Int. Jour. Control, Vol. 18, No. 1, January 1973.

193. C.M. Brown Jr., 'An extended Kalman filter for estimating aerodynamic coefficients', AFATL-TR-76-158, December 1976.

194. M.A. Efroymson, 'Multiple regression analysis' in 'Mathematical methods for digital computers', Edited by A. Ralston and M.S. Wilff, John Wiley and Sons, 1962.

195. D.J. Denery, 'Identification of system parameters from input-output data with application to air vehicles', NASA TN D-6468, August 1971.

196. D.J. Mook, 'Estimation and identification of nonlinear dynamic systems', AIAA Journal, Vol. 27, No. 7, July 1989.

197. A. Gelb, 'Applied estimation', MIT Press, Cambridge, Masschusets, 1974.

198. L.W. Taylor Jr., K.W. Iliff, 'A modified Newton Raphson method for determining stability derivatives from flight data', Second International Conference on 'Computing Methods on Optimization Problems' San Remo, Italy, September 1968.

199. Anon., 'Methods for Aircraft state and Parameter Identification', AGARD CP-172, Hampton, Virginia, November 1974.

200. R.T.N. Chen, B.J. Eulrich, J.V. Lebacqz, 'Development of advanced techniques for the identification of V/STOL aircraft stability and control parameters', CAL Report No. BM-2820-F-1, August 1971.

201. J.A. Mulder, 'Design and Evaluation of Dynamic Flight Test Manoeuvres', Report LR-497, Delft University of Technology, Department of Aerospace Engineering, Delft, The Netherlands, October 1986.

202. J.H. Vincent, N.K. Gupta, W.E. Hall Jr., 'Recent results in parameter identification for high angle of attack stall regimes', AIAA Paper 79-1640, August 1979.

203. A.J. Ross, G.E.A. Reid, 'The development of mathematical models for a high incidence research model (HIRM). Part 1. Analysis of static aerodynamic data', RAE Technical Report 83037, 1983.

204. A.J. Ross, G.E.A. Reid, 'The development of mathematical models for a high incidence research model (HIRM). Part 2. Analysis of dynamic aerodynamic data', RAE Technical Report 84072, 1984.

205. K. van Woerkom, 'A high accuracy instrumentation system for measurements in dynamic flight conditions', Technical Report, Delft University of Technology, Department of Aerospace Engineering, To be published 1993.

206. A. Pool, D. Bosman, 'Basic Principles of Flight Test Instrumentation Engineering', AGARDograph No. 160, Vol. 1, 1974.

207. J.C. van der Linden, H.A. Mensink, 'Linear and angular position measurement of aircraft components', AGARDograph No. 160, Vol. 8, 1977.

208. W. Wuest, 'Pressure and Flow measurement', AGARDograph No. 160, Vol. 11, 1980.

209. B. Stieler, H. Winter, 'Gyroscopic instruments and their application to flight testing', AGARDograph No. 160, Vol. 15, 1980.

210. D.W. Veatch, R.K. Bogue, 'Analogue signal conditioning for flight test instrumentation', AGARDograph No. 160, Vol. 17, 1980.

211. G.A. Bever, 'Digital signal conditioning for flight test instrumentation', AGARDograph No. 160, Vol. 19, 1980.

212. Anon., 'Guide to in-flight thrust measurement of turbo jets and fan engines by the MIDAP study Group (UK)', AGARD, AG-237, 1979.

213. J.A. Lawford, K.R. Nippress, 'Calibration of air data systems and flow direction sensors', AGARDograph No. 300, Vol. 1, 1983.

214. J.H. Breeman, 'The measurement of the dynamic response of a pressure tubing system', NLR TR 80, National Aerospace Laboratory, Amsterdam, 1980.

215. C.A.A.M. van der Linden, 'Optimal Input design for aircraft parameter estimation', Graduate thesis, Delft University of Technology, Department of Aerospace Engineering, December 1992.

216. C.A.A.M. van der Linden, J.A. Mulder, J.K. Sridhar, 'Recent developments in aircraft parameter identification - Optimal Input Design', Paper presented at the Aerospace Vehicle Dynamics and Control Conference, Cranfield, UK, September 1992.

217. M. van der Wilt, 'Flight path reconstruction in the context of unsteady flight testing', NLR TR 76133 U, National Aerospace Laboratory, Amsterdam, 1976.

218. J. Doekes, J.L. Simons, 'Description of program PIAS (Processing of dynamic manoeuvre measurements with an Interactive Adaptive System)', NLR Memorandum WN-78-006, National Aerospace Laboratory, Amsterdam, 1978.

219. M. Laban, K. Masui, 'Total least squares estimation of aerodynamic model parameters from flight data', Jour. Aircraft, Vol. 30, No. 1, January-February 1993.

220. R.K. Mehra, 'Synthesis of optimal inputs for multi input and multi output (MIMO) systems with process noise', System identification: Advances and case studies. Academic press, N.Y., 1976.

221. R. Rockafeller, 'Convex Analysis', Princeton University Press, Princeton, 1970.

222. S. Platz, E. Bounajem, 'Methodology for the critical evaluation of flight test data', 6th AIAA biennial flight test conference, Hilton head island, August 24-26, 1992.

223. R.C. de Jong, J.A. Mulder, 'Accurate Estimation of Aircraft Inertia Characteristics from a Single Suspension Experiment', Jour. Aircraft, Vol. 24, No. 6, June 1987.

224. F. Aronowitz, 'The Laser Gyroscope', Laser Applications, Vol. 1, Academic Press, New York, 1971.

225. A.V. Oppenheimer, R.W. Schafer, 'Digital Signal Processing', Prentice-Hall Inc., Englewood Cliffs, N.J., 1975.

226. C.T. Leondes, 'Advances in the techniques and technology of the application of nonlinear filters and Kalman filter', AGARDograph No.256, March 1982.

227. L.R. Rabiner, B. Gold, 'Theory and Application of Digital Signal Processing', Prentice-Hall Inc., Englewood Cliffs, N.J., 1975.

228. A. Sen, M. Srivastava, 'Regression Analysis, Theory, Methods and Applications', Springer verlag, 1990.

229. D.M. Allen, 'The prediction sum of squares as a criterion for selecting predictor variables', Technical Report 23, University of Kentucky, 1971.

230. O.H. Golub, C.F. van Loan, 'An analysis of the Total Least Squares Problem', SIAM Jour. of Numerical Analysis, Vol. 17, No. 6, 1980, pp. 883-893.

231. S. Huffel, 'Analysis of the Total Least Squares problem and its use in parameter estimation', PhD Thesis, Leuven University, Leuven, Belgium, 1987.

232. J.K. Sridhar, G.Wulff, 'Multiple input/ multiple output analysis procedures with applications to aircraft', Zeitschrift für Flugwissenschaften und Weltraumforschung, Vol. 16, No. 4, 1992, pp. 208-216.

233. A.E. Bryson Jr., Yu-Chi Ho, 'Applied Optimal Control, Optimization, Estimation and Control', John Wiley and Sons, 1975.

234. R.G. Brown, P.Y.C. Hwang, 'Introduction to Random Signals and Applied Kalman Filtering', John Wiley and Sons, 1992.

235. R.A. Feik, 'On the Application of Compatibility Checking Techniques to Dynamic Flight Test Data', Aeronautical Research Lab., Melbourne, Australia, Aero. Rept. 161, June 1984.

236. J. Blackwell, R.A. Feik, 'Identification of Time Delays in Flight Measurements', Jour. Guidance, Control and Dynamics, Vol. 14, No. 1, 1990.

237. S. Coad, E. Yourdon, 'Object-Oriented Analysis', Yourdon Press, 1991.

238. S. Coad, E. Yourdon, 'Object-Oriented Design', Yourdon Press, 1991.

APPENDIX A - A BRIEF SUMMARY OF MAXIMUM LIKELIHOOD ESTIMATION THEORY

In this appendix a brief overview will be presented of Maximum Likelihood estimation theory and its application to the solution for the parameter-state estimation problem of dynamical systems. The concepts as presented here are referred to in chapter 3 to 5.
A summary of general properties of maximum likelihood estimates is presented in section A.1; see Eykhoff [76] or Nahi [53]. In sections A.2 and A.3 the theory is applied to the solution of the parameter-state estimation problem of nonlinear and linear systems respectively.

A.1 General Properties of Maximum Likelihood Estimates

The joint conditional probability density function of a set of N random vectors $\underline{y}_m(i)$, i = 1(1) N, can be written as:

$$p\left(\underline{y}_m(1), \underline{y}_m(2), \ldots, \underline{y}_m(N) \mid \underline{\theta}\right), \qquad \text{(A.1-1)}$$

where $\underline{\theta}$ denotes the parameter vector of the conditional probability density function.

When sample values of $\underline{y}_m$ (i), i=1(1)N, are substituted (A.1-1) is called the likelihood function $L(\underline{\theta})$. Then a parameter estimate $\hat{\underline{\theta}}$ may be calculated by maximizing (A.1-1) with respect to $\hat{\underline{\theta}}$. When the absolute or global maximum of the likelihood function is reached, the resulting estimate is called the Maximum Likelihood (ML) estimate $\hat{\underline{\theta}}_{ML}$ of $\underline{\theta}$. Instead of maximizing $L(\underline{\theta})$ it is common practice to maximize $\ln L(\underline{\theta})$ instead, usually resulting in an optimization problem which is easier to solve. Since the logarithm is a monotonic function this leads to the same value of $\hat{\underline{\theta}}_{ML}$.

The necessary conditions for a maximum lead to the following set of so-called likelihood equations:

$$\left.\frac{\partial \ln L(\underline{\theta})}{\partial \underline{\theta}}\right|_{\underline{\theta} = \hat{\underline{\theta}}_{ML}} = \underline{0} \,. \qquad \text{(A.1-2)}$$

These equations correspond to the normal equations of linear regression theory. Maximum likelihood estimates have the following attractive properties:

i) ML estimates are asymptotically unbiased,

$$\lim_{N \to \infty} E\{\hat{\underline{\theta}}_{ML}\} = \underline{\theta} \qquad \text{(A.1-3)}$$

ii) ML estimates are asymptotically efficient,

$$\lim_{N \to \infty} E\left\{\left[\hat{\underline{\theta}}_{ML} - \underline{\theta}\right]\left[\hat{\underline{\theta}}_{ML} - \underline{\theta}\right]^T\right\} = C_{\theta\theta} \qquad \text{(A.1-4)}$$

in which $C_{\theta\theta}$ denotes a symmetrical semi positive definite matrix. This matrix is called the Cramer-Rao Lower Bound (CRLB).

iii) ML estimates are consistent; see Eykhoff [76].

Eq. (A.1-4) shows that the covariance matrix of a ML estimate is the best of all conceivable estimates for large sample sizes.

For unbiased estimates the CRLB is:

$$C_{\theta\theta} = M_{\theta\theta}^{-1}, \qquad \text{(A.1-5)}$$

where $M_{\theta\theta}$ is the Fisher information matrix which can be written in two equivalent forms according to:

$$\begin{aligned} M_{\theta\theta} &= E\left\{\frac{\partial \ln L(\underline{\theta})}{\partial \underline{\theta}} \cdot \frac{\partial \ln L(\underline{\theta})}{\partial \underline{\theta}^T}\right\} \\ &= -E\left\{\frac{\partial^2 \ln L(\underline{\theta})}{\partial \underline{\theta}\, \partial \underline{\theta}^T}\right\}, \end{aligned} \qquad \text{(A.1-6)}$$

where the conditional expectation is taken over the sample space of $\underline{y}_m(i)$, i=1(1) N. $M_{\theta\theta}$ is symmetrical and positive semi definite. The importance of the Fisher-information matrix in estimation theory stems from the fact that its inverse yields a lower bound, i.e. a maximally achievable accuracy for any conceivable type of estimate of $\underline{\theta}$.

In the literature on estimation theory the notion 'identifiability' of a parameter vector $\underline{\theta}$ is defined

in several ways. Here 'identifiability' is related directly to the rank of the information matrix as follows:

The parameter vector $\underline{\theta}$ is identifiable from the set of measurements $\underline{y}_m(i)$, i=1(1)N, if and only if $M_{\theta\theta}$ is positive definite for any $\underline{\theta}$ in a neighbourhood of $\underline{\theta}_{ML}$ in parameter space.

A.2 Continuous Time Nonlinear Systems

Let $\underline{x}(t)$ be the n dimensional state vector and $\underline{u}(t)$ the s dimensional input vector of the following nonlinear system:

$$\dot{\underline{x}} = \underline{f}\left(\underline{\theta}, \underline{x}(t), \underline{u}(t)\right), \tag{A.2-1}$$

with initial condition:

$$\underline{x}(0) = \underline{x}_0$$

where $\underline{f}$ denotes a nonlinear vector function, and $\underline{\theta}$ an r dimensional system parameter vector.

It is assumed that $\underline{u}(t)$ is known for $t\in[t_0,t_1]$. At N uniformly spaced time instants $t_i\in[t_0,t_1]$, i=1(1)N, the m-dimensional system output is sampled according to the following model*:

$$\begin{aligned} \underline{y}(i) &= \underline{h}\left(\underline{\theta}, \underline{x}(i), \underline{u}(i)\right), \\ \underline{y}_m &= \underline{y}(i) + \underline{v}(i), \end{aligned} \tag{A.2-2}$$

where $\underline{v}(i)$ represents an additive gaussian measurement error with the following statistics:

$$\begin{aligned} E\{\underline{v}(i)\} &= \underline{0} \\ E\{\underline{v}(i)\underline{v}^T(i)\} &= V_{vv}\cdot\delta_{ij} \end{aligned} \tag{A.2-3}$$

for i,j =1(1)N and in which V_{vv} denotes the covariance matrix of $\underline{v}(i)$. It is assumed that for any $\underline{x}_0\in R^n$ and $\underline{\theta}\in R^r$, Eq. (A.2-1) possesses a unique solution, indicated as $\underline{x}(t)$ and $\underline{y}(t)$, $t\in[t_0,t_1]$.
At one particular sample time instant t_i the conditional probability density function of $\underline{y}_m(i)$ is:

$$p\left(\underline{y}_m(i) \mid \underline{\theta}, \underline{x}_0, V_{vv}\right) = (2\pi)^{-\frac{1}{2}m} (\det V_{vv})^{-\frac{1}{2}} \times \exp\left\{\frac{1}{2}\left[\underline{y}_m(i) - \underline{y}(i)\right]^T V_{vv}^{-1}\left[\underline{y}_m(i) - \underline{y}(i)\right]\right\}.$$

Because of (A.2-3) the joint probability function of $\underline{y}_m(1),\underline{y}_m(2),\ldots,\underline{y}_m(N)$ is the product of the marginal probability density functions. The logarithm of the likelihood function can then be written as:

$$\ln L\left(\underline{\theta}, \underline{x}_0, V_{vv}\right) = -\frac{1}{2} N m \ln(2\pi) - \frac{N}{2} \ln\det(V_{vv}) - \frac{1}{2}\sum_{i=1}^{N}\left[\underline{y}_m(i) - \underline{y}(i)\right]^T V_{vv}^{-1}\left[\underline{y}_m(i) - \underline{y}(i)\right]. \tag{A.2-4}$$

For a given set of observation measurements, the arguments of the likelihood function are the elements of $\underline{\theta}$, $\underline{x}_0$ and V_{vv}. It will be convenient to take the elements of V_{vv}^{-1}, rather than the elements of V_{vv}, as arguments of the likelihood function. This means that the logarithm of the likelihood function will be written below as:

$$\ln L\left(\underline{\theta}, \underline{x}_0, V_{vv}^{-1}\right).$$

According to (A.1-2), the necessary condition for the logarithm of the likelihood function to have a maximum value is that all first order partial derivatives with respect to its arguments are equal to zero. Analytical expressions for these derivatives of the log likelihood function with respect to its arguments are equal to zero. Analytical expressions for these derivatives of the log likelihood function with respect to $\underline{\theta}$, $\underline{x}_0$ and V_{vv} can be obtained from (A.2-4) by applying the rules for differentiation with respect to vectors and matrices as given in Deskins [186]. The results are as follows:

$$\frac{\partial \ln L\left(\underline{\theta}, \underline{x}_0, V_{vv}^{-1}\right)}{\partial \underline{\theta}} = \sum_{i=1}^{N} \frac{\partial \underline{y}^T(i)}{\partial \underline{\theta}} V_{vv}^{-1}\left[\underline{y}_m(i) - \underline{y}(i)\right], \tag{A.2-5a}$$

$$\frac{\partial \ln L\left(\underline{\theta}, \underline{x}_0, V_{vv}^{-1}\right)}{\partial \underline{x}_0} = \sum_{i=1}^{N} \frac{\partial \underline{y}^T(i)}{\partial \underline{x}_0} V_{vv}^{-1}\left[\underline{y}_m(i) - \underline{y}(i)\right], \tag{A.2-5b}$$

$$\frac{\partial \ln L\left(\underline{\theta}, \underline{x}_0, V_{vv}^{-1}\right)}{\partial V_{vv}^{-1}} = \frac{N}{2} V_{vv} - \frac{1}{2}\sum_{i=1}^{N}\left[\underline{y}_m(i) - \underline{y}(i)\right]\left[\underline{y}_m(i) - \underline{y}(i)\right]^T. \tag{A.2-5c}$$

* Note that $\underline{x}(i)$, $\underline{y}(i)$, etc. are simplified notations for $\underline{x}(t_i)$, $\underline{y}(t_i)$.

The so called likelihood equations for $\underline{\theta}$, $\underline{x}_0$ and V_{vv}^{-1} result when each of these derivatives is set equal to zero. The maximum likelihood estimates $\hat{\underline{\theta}}_{ML}$, $\hat{\underline{x}}_{0_{ML}}$ and $(V_{vv}^{-1})_{ML}$ satisfy the likelihood equations.
It is possible to interpret $\underline{\theta}$, $\underline{x}_0$ and the elements of V_{vv}^{-1} as components of an 'augmented' parameter vector $\underline{\theta}_a$ according to:

$$\underline{\theta}_a = \mathrm{col}\left(\underline{\theta}^T, \underline{x}_0^T, [V_{vv}^{-1}]_{11}, [V_{vv}^{-1}]_{12}, \cdots, [V_{vv}^{-1}]_{n_y n_y}\right)$$
$$= \mathrm{col}\left(\underline{\theta}^T, \underline{x}_0^T, \underline{\eta}^T\right),$$

in which $\underline{\eta}$ contains the upper or lower triangular elements of V_{vv}^{-1}. The Fisher information matrix as defined in (A.1-6) may now be partitioned as:

$$M_{\theta_a\theta_a} = \begin{bmatrix} M_{\theta\theta} & \vdots & M_{\theta x_0} & \vdots & M_{0\eta} \\ \cdots\cdots & \cdot\vdots\cdot & \cdots\cdots & \cdot\vdots\cdot & \cdots\cdots \\ M_{x_0\theta} & \vdots & M_{x_0x_0} & \vdots & M_{x_0\eta} \\ \cdots\cdots & \cdot\vdots\cdot & \cdots\cdots & \cdot\vdots\cdot & \cdots\cdots \\ M_{\eta\theta} & \vdots & M_{\eta x_0} & \vdots & M_{\eta\eta} \end{bmatrix}. \qquad \text{(A.2-6)}$$

Using either the first or the second definition of the information matrix in (A-6) it is possible to show that the individual blocks in (A-12) can be written as:

$$M_{\theta\theta} = M_{\theta\theta}^T = \sum_{i=1}^{N} \frac{\partial \underline{y}^T(i)}{\partial \underline{\theta}} V_{vv}^{-1} \frac{\partial \underline{y}(i)}{\partial \underline{\theta}^T}, \qquad \text{(A.2-7a)}$$

$$M_{\theta x_0} = M_{x_0\theta}^T = \sum_{i=1}^{N} \frac{\partial \underline{y}^T(i)}{\partial \underline{\theta}} V_{vv}^{-1} \frac{\partial \underline{y}(i)}{\partial \underline{x}_0^T}, \qquad \text{(A.2-7b)}$$

$$M_{\theta\eta} = M_{\eta\theta}^T = O, \qquad \text{(A.2-7c)}$$

$$M_{x_0x_0} = M_{x_0x_0}^T = \sum_{i=1}^{N} \frac{\partial \underline{y}^T(i)}{\partial \underline{x}_0} V_{vv}^{-1} \frac{\partial \underline{y}(i)}{\partial \underline{x}_0^T}, \qquad \text{(A.2-7d)}$$

$$M_{x_0\eta} = M_{\eta x_0}^T = O. \qquad \text{(A.2-7e)}$$

Let the elements η_h and η_j of $\underline{\eta}$ correspond to the elements $[V_{vv}^{-1}]_{kl}$ and $[V_{vv}^{-1}]_{mn}$ of V_{vv}^{-1} respectively. The element $[M_{\eta\eta}]_{hj}$ of $M_{\eta\eta}$ may then be written as:

$$[M_{\eta\eta}]_{hj} = \frac{N}{4}\left(v_{km}v_{ln} + v_{kn}v_{lm}\right) \qquad \text{(A.2-7f)}$$

in which v_{km}, v_{ln}, v_{kn} en v_{lm} denote the elements $[V_{vv}]_{km}$, $[V_{vv}]_{ln}$, $[V_{vv}]_{kn}$ and $[V_{vv}]_{lm}$ respectively of the covariance matrix V_{vv} of observation measurement errors.

With (A.2-7c) and (A.2-7e) the CRLB can be written as:

$$C_{\theta_a\theta_a} = \begin{bmatrix} \begin{bmatrix} M_{\theta\theta} & \vdots & M_{\theta x_0} \\ \cdots\cdots & \cdot\vdots\cdot & \cdots\cdots \\ M_{x_0\theta} & \vdots & M_{x_0x_0} \end{bmatrix}^{-1} & \begin{matrix} O \\ \cdots\cdots \\ O \end{matrix} \\ \begin{matrix} O & \vdots & O \end{matrix} & M_{\eta\eta}^{-1} \end{bmatrix}. \qquad \text{(A.2-8)}$$

According to (A.1-4), the variance matrix of ML estimation errors approaches asymptotically the CRLB. Eq. (A.2-8) shows that in addition to the estimation errors of the elements of V_{vv}^{-1} are asymptotically uncorrelated with the estimation errors of $\underline{\theta}$ and $\underline{x}_0$. If $\underline{f}(\underline{\theta},\underline{x}(t),\underline{u}(t))$ and $\underline{h}(\underline{\theta},\underline{x}(t),\underline{u}(t))$ are continuously differentiable with respect to $\underline{\theta}$ and $\underline{x}(t)$, the partial derivatives $\partial\underline{y}(i)/\partial\underline{\theta}^T$ and $\partial\underline{y}(i)/\partial\underline{x}_0$ in (A.2-7) can be found by solving the following set of differential equations, the so-called sensitivity equations; see Nahi [53]:

$$\frac{d}{dt}\frac{\partial \underline{x}(t)}{\partial \underline{\theta}^T} = \frac{\partial \underline{f}(\underline{\theta},\underline{x}(t),\underline{u}(t))}{\partial \underline{x}^T(t)} \cdot \frac{\partial \underline{x}(t)}{\partial \underline{\theta}^T} + \frac{\partial \underline{f}(\underline{\theta},\underline{x}(t),\underline{u}(t))}{\partial \underline{\theta}^T},$$
$$\frac{d}{dt}\frac{\partial \underline{x}(t)}{\partial \underline{x}_0^T} = \frac{\partial \underline{f}(\underline{\theta},\underline{x}(t),\underline{u}(t))}{\partial \underline{x}^T(t)} \cdot \frac{\partial \underline{x}(t)}{\partial \underline{x}_0^T}, \qquad \text{(A.2-9)}$$

with initial conditions:

$$\frac{\partial \underline{x}(0)}{\partial \underline{\theta}^T} = O,$$
$$\frac{\partial \underline{x}(0)}{\partial \underline{x}_0^T} = I.$$

The sensitivity equations (A.2-9) can be derived by partially differentiating both sides of the system differential equation in (A.2-1). Subsequently, the order of differentiation in the left hand side of the equation with respect to $\underline{\theta}$ or $\underline{x}_0$ and t respectively, is reversed, for which it must be assumed that $\underline{x}$ is

analytic; see Arfken [171].
Next, partial differentiation of the observation equations in (A.2-2) leads to:

$$\frac{\partial \underline{y}(i)}{\partial \underline{\theta}^T} = \frac{\partial \underline{h}(\underline{\theta}, \underline{x}(i), \underline{u}(i))}{\partial \underline{x}^T(i)} \cdot \frac{\partial \underline{x}(i)}{\partial \underline{\theta}^T} + \frac{\partial \underline{h}(\underline{\theta}, \underline{x}(i), \underline{u}(i))}{\partial \underline{\theta}^T}, \qquad \text{(A.2-10)}$$

$$\frac{\partial \underline{y}(i)}{\partial \underline{x}_0^T} = \frac{\partial \underline{h}(\underline{\theta}, \underline{x}(i), \underline{u}(i))}{\partial \underline{x}^T(i)} \cdot \frac{\partial \underline{x}(i)}{\partial \underline{x}_0^T}.$$

It is noticed here that the partial derivatives $\partial\underline{x}(i)/\partial\underline{\theta}^T$, $\partial\underline{x}(i)\partial\underline{x}_0^T$, $\partial\underline{y}(i)\partial\underline{\theta}^T$ and $\partial\underline{y}(i)\partial\underline{x}_0^T$ depend all on the input signal $\underline{u}(t)$, $t\in[t_0,t_1]$.

According to (A.2-7), $M_{\theta\theta}$, $M_{\theta x_o}$ and $M_{x_o x_o}$ are composed of the latter two derivatives at the sampling times t_i. This means that the CRLB for $\hat{\underline{\theta}}_{ML}$ and $\hat{\underline{x}}_{0_{ML}}$ depends on the system input signal $\underline{u}(t)$ in $[t_0,t_1]$. On the other hand the CRLB for the elements of V_{vv}^{-1} depends only on the number of samples taken, and cannot be influenced by $\underline{u}(t)$. This property of the CRLB may readily be deduced from (A.2-8) and (A.2-7f).

A.3 Continuous Time Linear Systems

As shown in the previous section, the calculation of the information matrix of nonlinear systems requires the solution of nonlinear sensitivity equations. In the case of linear systems, these sensitivity equations reduce to linear equations.
Let the deterministic linear and constant system:

$$\dot{\underline{x}}(t) = F(\underline{\theta})\cdot\underline{x}(t) + G(\underline{\theta})\cdot\underline{u}(t), \qquad \text{(A.3-1)}$$

with initial condition:

$$\underline{x}(t_0) = \underline{x}_0,$$

be observed at discrete instants of time according to the following observation model:

$$\underline{y}(i) = H(\underline{\theta})\cdot\underline{x}(i) + J(\underline{\theta})\cdot\underline{u}(i), \qquad \underline{y}_m(i) = \underline{y}(i) + \underline{v}(i), \qquad \text{(A.3-2)}$$

in which $\underline{v}(i)$ represents again an additive gaussian measurement error (A.2-3). The parameter vector $\underline{\theta}$ contains the unknown elements of the matrices F, G, H and J. The Fisher information matrix and CRLB for $\underline{\theta}$, $\underline{x}_0$ and V_{vv}^{-1} of constant linear systems are identical to the expressions given in (A.2-6) and (A.2-8) for the case of nonlinear systems. The sensitivity equations of linear systems, however, are readily seen to be also linear. Furthermore, if the system and observation models in (A.3-1) and (A.3-2) are constant, i.e. F, G, H and J do not depend on time, then the sensitivity equations are also constant. The sensitivity equations may be written as:

$$\frac{d}{dt}\frac{\partial \underline{x}(t)}{\partial \theta_j} = F(\underline{\theta})\cdot\frac{\partial \underline{x}(t)}{\partial \theta_j} + \frac{\partial F(\underline{\theta})}{\partial \theta_j}\cdot\underline{x}(t) + \frac{\partial G(\underline{\theta})}{\partial \theta_j}\cdot\underline{u}(t), \qquad \text{(A.3-3)}$$

$$\frac{d}{dt}\frac{\partial \underline{x}(t)}{\partial \underline{x}_0^T} = F(\underline{\theta})\cdot\frac{\partial \underline{x}(t)}{\partial \underline{x}_0^T},$$

for j=1(1)r and with initial conditions:

$$\frac{\partial \underline{x}(0)}{\partial \underline{\theta}^T} = O,$$

$$\frac{\partial \underline{x}(0)}{\partial \underline{x}_0^T} = I.$$

The solution of (A.3-3) is used to calculate the derivatives of $\underline{y}$ with respect to $\underline{\theta}$ and $\underline{x}_0$ according to:

$$\frac{\partial \underline{y}(i)}{\partial \theta_j} = H(\underline{\theta})\cdot\frac{\partial \underline{x}(i)}{\partial \theta_j} + \frac{\partial H(\underline{\theta})}{\partial \theta_j}\cdot\underline{x}(i) + \frac{\partial J(\underline{\theta})}{\partial \theta_j}\cdot\underline{u}(i), \qquad \text{(A.3-4)}$$

$$\frac{\partial \underline{y}(i)}{\partial \underline{x}_0^T} = H(\underline{\theta})\cdot\frac{\partial \underline{x}(i)}{\partial \underline{x}_0^T},$$

for j=1(1)r.

It is worth noting that in case $\underline{\theta}$ is known, the estimation problem reduces to a state estimation problem. The corresponding CRLB is:

$$C = \begin{bmatrix} M_{x_0x_0}^{-1} & \vdots & O \\ \cdots\cdots & \cdot & \cdots\cdots \\ O & \vdots & M_{\eta\eta}^{-1} \end{bmatrix}. \qquad \text{(A.3-5)}$$

According to chapter 3, $M_{x_0x_0}$ has full rank if and only if the system (A.3-1) is reconstructible.
The information matrix of the state vector $\underline{x}(i)$ at

time $t_i \in [t_0, t_1]$ can be written analogously to (A.2-7d):

$$M_{x(i)x(i)} = \sum_{i=1}^{N} \frac{\partial \underline{y}^T(i)}{\partial \underline{x}(i)} V_{vv}^{-1} \frac{\partial \underline{y}(i)}{\partial \underline{x}^T(i)} . \qquad \text{(A.3-6)}$$

It is possible to express the information matrix $M_{x(i)x(i)}$ in terms of the information matrix of the initial state $\underline{x}_0$, $M_{x_0x_0}$.

The matrix of partial derivatives $\partial \underline{y}(i)/\partial \underline{x}^T(i)$ can be written as:

$$\frac{\partial \underline{y}(i)}{\partial \underline{x}^T(i)} = \frac{\partial \underline{y}(i)}{\partial \underline{x}_0^T} \cdot \frac{\partial \underline{x}_0}{\partial \underline{x}^T(i)} = \frac{\partial \underline{y}(i)}{\partial \underline{x}_0^T} \cdot \left[\frac{\partial \underline{x}(i)}{\partial \underline{x}_0^T} \right]^{-1} ,$$

in which the matrix of partial derivatives $\partial \underline{x}(i)/\partial \underline{x}_0^T$ may be computed with the sensitivity equations (A.3-3). Substitution of $\partial \underline{y}(i)/\partial \underline{x}^T$ above in the information matrix $M_{x(i)x(i)}$ results in:

$$\begin{aligned} M_{x(i)x(i)} &= \sum_{i=1}^{N} \left[\frac{\partial \underline{x}^T(i)}{\partial \underline{x}_0} \right]^{-1} \frac{\partial \underline{y}^T(i)}{\partial \underline{x}_0} V_{vv}^{-1} \frac{\partial \underline{y}(i)}{\partial \underline{x}_0^T} \left[\frac{\partial \underline{x}(i)}{\partial \underline{x}_0^T} \right]^{-1} \\ &= \left[\frac{\partial \underline{x}^T(i)}{\partial \underline{x}_0} \right]^{-1} M_{x_0x_0} \left[\frac{\partial \underline{x}(i)}{\partial \underline{x}_0^T} \right]^{-1} . \end{aligned} \qquad \text{(A.3-7)}$$

From (A.3-3) and (A.3-4) it follows that partial derivatives of $\underline{y}(i)$ with respect to $\underline{x}_0$ are independent of $\underline{u}(t)$. This means that the ML state reconstruction accuracy as expressed in terms of the CRLB $M_{x(i)x(i)}^{-1}$ is also independent of the time history of the input signal, see (A.3-6).

However, if one or more of the system and observation model parameters must be estimated simultaneously with the reconstruction of the state, the system state reconstruction accuracy is no longer independent of $\underline{u}(t)$. This phenomenon is caused by the fact that the parameter and initial state estimation errors are in principle not uncorrelated i.e.:

$$M_{\theta x_0} = \sum_{i=1}^{N} \frac{\partial \underline{y}^T(i)}{\partial \underline{\theta}} V_{vv}^{-1} \frac{\partial \underline{y}(i)}{\partial \underline{x}_0^T} \neq O .$$

APPENDIX B - CALCULATION OF RECONSTRUCTIBILITY MATRICES Q_i FOR THE OBSERVATIONS $\underline{y}i$ OF THE LONGITUDINAL AND LATERAL LINEAR FLIGHT PATH RECONSTRUCTION PROBLEM

In this appendix, the reconstructibility matrices Q_i of the longitudinal and lateral linear flight path reconstruction problem will be derived for the case of a non-horizontal stationary rectilinear nominal flight condition, $\gamma_o \neq 0$.

B.1 Reconstructibility Matrices of the Longitudinal Flight Path Reconstruction Problem

From (4.1-21) and (4.1-22) it follows that the linear system matrix F of the longitudinal flight path reconstruction model consists of the following elements:

$$F = \begin{bmatrix} 0 & 0 & -g\cos\gamma_0 & 0 & 0 & 1 & 0 & 0 & 0 & 0 \\ 0 & 0 & -\frac{g}{V_0}\sin\gamma_0 & 0 & 0 & 0 & \frac{1}{V_0} & 1 & 0 & 0 \\ 0 & 0 & 0 & 0 & 0 & 0 & 0 & 1 & 0 & 0 \\ \cos\gamma_0 & V_0\sin\gamma_0 & -V_0\sin\gamma_0 & 0 & 0 & 0 & 0 & 0 & 1 & 0 \\ -\sin\gamma_0 & V_0\cos\gamma_0 & -V_0\cos\gamma_0 & 0 & 0 & 0 & 0 & 0 & 0 & 1 \\ 0 & 0 & 0 & 0 & 0 & 0 & 0 & 0 & 0 & 0 \\ 0 & 0 & 0 & 0 & 0 & 0 & 0 & 0 & 0 & 0 \\ 0 & 0 & 0 & 0 & 0 & 0 & 0 & 0 & 0 & 0 \\ 0 & 0 & 0 & 0 & 0 & 0 & 0 & 0 & 0 & 0 \\ 0 & 0 & 0 & 0 & 0 & 0 & 0 & 0 & 0 & 0 \end{bmatrix}, \tag{B.1-1}$$

It is easily verified that:

$$F^2 = \begin{bmatrix} 0 & 0 & 0 & 0 & 0 & 0 & 0 & -g\cos\gamma_0 & 0 & 0 \\ 0 & 0 & 0 & 0 & 0 & 0 & 0 & -\frac{g}{V_0}\sin\gamma_0 & 0 & 0 \\ 0 & 0 & 0 & 0 & 0 & 0 & 0 & 0 & 0 & 0 \\ 0 & 0 & -g & 0 & 0 & \cos\gamma_0 & \sin\gamma_0 & 0 & 0 & 0 \\ 0 & 0 & 0 & 0 & 0 & -\sin\gamma_0 & \cos\gamma_0 & 0 & 0 & 0 \\ 0 & 0 & 0 & 0 & 0 & 0 & 0 & 0 & 0 & 0 \\ 0 & 0 & 0 & 0 & 0 & 0 & 0 & 0 & 0 & 0 \\ 0 & 0 & 0 & 0 & 0 & 0 & 0 & 0 & 0 & 0 \\ 0 & 0 & 0 & 0 & 0 & 0 & 0 & 0 & 0 & 0 \\ 0 & 0 & 0 & 0 & 0 & 0 & 0 & 0 & 0 & 0 \end{bmatrix}, \tag{B.1-2}$$

and:

$$F^3 = \begin{bmatrix} 0 & 0 & 0 & 0 & 0 & 0 & 0 & 0 & 0 & 0 \\ 0 & 0 & 0 & 0 & 0 & 0 & 0 & 0 & 0 & 0 \\ 0 & 0 & 0 & 0 & 0 & 0 & 0 & 0 & 0 & 0 \\ 0 & 0 & 0 & 0 & 0 & 0 & 0 & -g & 0 & 0 \\ 0 & 0 & 0 & 0 & 0 & 0 & 0 & 0 & 0 & 0 \\ 0 & 0 & 0 & 0 & 0 & 0 & 0 & 0 & 0 & 0 \\ 0 & 0 & 0 & 0 & 0 & 0 & 0 & 0 & 0 & 0 \\ 0 & 0 & 0 & 0 & 0 & 0 & 0 & 0 & 0 & 0 \\ 0 & 0 & 0 & 0 & 0 & 0 & 0 & 0 & 0 & 0 \\ 0 & 0 & 0 & 0 & 0 & 0 & 0 & 0 & 0 & 0 \end{bmatrix}, \tag{B.1-3}$$

while fourth and higher powers of F vanish.

The observation matrix H follows from (4.1-23) and (4.1-24) as:

$$H = \begin{bmatrix} 1 & 0 & 0 & 0 & 0 & 0 & 0 & 0 & 0 & 0 \\ 0 & C_{\alpha_1} & 0 & 0 & 0 & 0 & 0 & 0 & 0 & 0 \\ 0 & 0 & 0 & 1 & 0 & 0 & 0 & 0 & 0 & 0 \\ 0 & 0 & 0 & 0 & 1 & 0 & 0 & 0 & 0 & 0 \end{bmatrix}. \tag{B.1-4}$$

With (4.1-25) this leads to the reconstructibility matrices (only the non-empty rows are shown):

$$Q_1 = \begin{bmatrix} 1 & 0 & 0 & 0 & 0 & 0 & 0 & 0 & 0 & 0 \\ 0 & 0 & -g\cos\gamma_0 & 0 & 0 & 1 & 0 & 0 & 0 & 0 \\ 0 & 0 & 0 & 0 & 0 & 0 & 0 & -g\cos\gamma_0 & 0 & 0 \end{bmatrix}, \tag{B.1-5}$$

$$Q_2 = \begin{bmatrix} 0 & C_{\alpha_1} & 0 & 0 & 0 & 0 & 0 & 0 & 0 & 0 \\ 0 & 0 & -\frac{g}{V_0}C_{\alpha_1}\sin\gamma_0 & 0 & 0 & 0 & \frac{1}{V_0}C_{\alpha_1} & C_{\alpha_1} & 0 & 0 \\ 0 & 0 & 0 & 0 & 0 & 0 & 0 & -\frac{g}{V_0}C_{\alpha_1}\sin\gamma_0 & 0 & 0 \end{bmatrix}, \tag{B.1-6}$$

$$Q_3 = \begin{bmatrix} 0 & 0 & 0 & 1 & 0 & 0 & 0 & 0 & 0 & 0 \\ \cos\gamma_0 & V_0\sin\gamma_0 & -V_0\sin\gamma_0 & 0 & 0 & 0 & 0 & 0 & 1 & 0 \\ 0 & 0 & -g & 0 & 0 & \cos\gamma_0 & \sin\gamma_0 & 0 & 0 & 0 \\ 0 & 0 & 0 & 0 & 0 & 0 & 0 & -g & 0 & 0 \end{bmatrix}, \tag{B.1-7}$$

and:

$$Q_4 = \begin{bmatrix} 0 & 0 & 0 & 0 & 1 & 0 & 0 & 0 & 0 & 0 \\ -\sin\gamma_0 & V_0\cos\gamma_0 & -V_0\cos\gamma_0 & 0 & 0 & 0 & 0 & 0 & 0 & 1 \\ 0 & 0 & 0 & 0 & 0 & -\sin\gamma_0 & \cos\gamma_0 & 0 & 0 & 0 \end{bmatrix}. \tag{B.1-8}$$

B.2 Reconstructibility Matrices of the Lateral Flight Path Reconstruction Problem

From (4.1-27) and (4.1-28) it follows that the linear system matrix F of the lateral flight path reconstruction model consists of the following elements:

$$F = \begin{bmatrix} 0 & 0 & \frac{g}{V_0}\cos\gamma_0 & 0 & \frac{1}{V_0} & 0 & -1 & 0 & 0 \\ 0 & 0 & 0 & 0 & 0 & 0 & \frac{1}{\cos\gamma_0} & 0 & 0 \\ 0 & 0 & 0 & 0 & 0 & 1 & \tan\gamma_0 & 0 & 0 \\ V_0 & V_0\cos\gamma_0 & 0 & 0 & 0 & 0 & 0 & 0 & 1 \\ 0 & 0 & 0 & 0 & 0 & 0 & 0 & 0 & 0 \\ 0 & 0 & 0 & 0 & 0 & 0 & 0 & 0 & 0 \\ 0 & 0 & 0 & 0 & 0 & 0 & 0 & 0 & 0 \\ 0 & 0 & 0 & 0 & 0 & 0 & 0 & 0 & 0 \\ 0 & 0 & 0 & 0 & 0 & 0 & 0 & 0 & 0 \end{bmatrix}. \tag{B.2-1}$$

It is easily verified that:

$$F^2 = \begin{bmatrix} 0 & 0 & 0 & 0 & 0 & \frac{g}{V_0}\cos\gamma_0 & \frac{g}{V_0}\sin\gamma_0 & 0 & 0 \\ 0 & 0 & 0 & 0 & 0 & 0 & 0 & 0 & 0 \\ 0 & 0 & 0 & 0 & 0 & 0 & 0 & 0 & 0 \\ 0 & 0 & g\cos\gamma_0 & 0 & 1 & 0 & 0 & 0 & 0 \\ 0 & 0 & 0 & 0 & 0 & 0 & 0 & 0 & 0 \\ 0 & 0 & 0 & 0 & 0 & 0 & 0 & 0 & 0 \\ 0 & 0 & 0 & 0 & 0 & 0 & 0 & 0 & 0 \\ 0 & 0 & 0 & 0 & 0 & 0 & 0 & 0 & 0 \\ 0 & 0 & 0 & 0 & 0 & 0 & 0 & 0 & 0 \end{bmatrix}, \tag{B.2-2}$$

and:

$$F^3 = \begin{bmatrix} 0 & 0 & 0 & 0 & 0 & 0 & 0 & 0 & 0 \\ 0 & 0 & 0 & 0 & 0 & 0 & 0 & 0 & 0 \\ 0 & 0 & 0 & 0 & 0 & 0 & 0 & 0 & 0 \\ 0 & 0 & 0 & 0 & 0 & g\cos\gamma_0 & g\sin\gamma_0 & 0 & 0 \\ 0 & 0 & 0 & 0 & 0 & 0 & 0 & 0 & 0 \\ 0 & 0 & 0 & 0 & 0 & 0 & 0 & 0 & 0 \\ 0 & 0 & 0 & 0 & 0 & 0 & 0 & 0 & 0 \\ 0 & 0 & 0 & 0 & 0 & 0 & 0 & 0 & 0 \\ 0 & 0 & 0 & 0 & 0 & 0 & 0 & 0 & 0 \end{bmatrix}, \tag{B.2-3}$$

while fourth and higher powers of F vanish.

The observation matrix H follows from (4.1-29) and (4.1-30) as:

$$H = \begin{bmatrix} C_{\beta_1} & 0 & 0 & 0 & 0 & 0 & 0 & 1 & 0 \\ 0 & 1 & 0 & 0 & 0 & 0 & 0 & 0 & 0 \\ 0 & 0 & 0 & 1 & 0 & 0 & 0 & 0 & 0 \end{bmatrix}. \tag{B.2-4}$$

With (4.1-25) this leads to the reconstructibility matrices (only the non-empty rows are shown):

$$Q_1 = \begin{bmatrix} C_{\beta_1} & 0 & 0 & 0 & 0 & 0 & 0 & 1 & 0 \\ 0 & 0 & \frac{g}{V_0} C_{\beta_1} \cos\gamma_0 & 0 & \frac{1}{V_0} C_{\beta_1} & 0 & -C_{\beta_1} & 0 & 0 \\ 0 & 0 & 0 & 0 & 0 & \frac{g}{V_0} C_{\beta_1} \cos\gamma_0 & \frac{g}{V_0} C_{\beta_1} \sin\gamma_0 & 0 & 0 \end{bmatrix}, \tag{B.2-5}$$

$$Q_2 = \begin{bmatrix} 0 & 1 & 0 & 0 & 0 & 0 & 0 & 0 & 0 \\ 0 & 0 & 0 & 0 & 0 & 0 & \frac{1}{\cos\gamma_0} & 0 & 0 \end{bmatrix}, \tag{B.2-6}$$

and:

$$Q_3 = \begin{bmatrix} 0 & 0 & 0 & 1 & 0 & 0 & 0 & 0 & 0 \\ V_0 & V_0 \cos\gamma_0 & 0 & 0 & 0 & 0 & 0 & 0 & 1 \\ 0 & 0 & g\cos\gamma_0 & 0 & 1 & 0 & 0 & 0 & 0 \\ 0 & 0 & 0 & 0 & 0 & g\cos\gamma_0 & g\sin\gamma_0 & 0 & 0 \end{bmatrix}, \tag{B.2-7}$$

B.3 Reconstructible Subspaces

A (non-unique) basis U_{1_i} for the reconstructible subspace corresponding to the observation y_i can be formed out of the independent rows in Q_i. The results, in terms of components of $x^*_{1_i}$ are, for $\gamma_0=0$ listed in table 3-1 and table 3-3 for the longitudinal and lateral linear flight path problem respectively.

APPENDIX C - ALGORITHMS FOR FLIGHT PATH RECONSTRUCTION

In this appendix more details are given on the algorithms discussed in chapter 3. In section C.1 the Kalman filter and smoother is applied to a system model which is linearized around a nominal steady condition. In section C.2 the Extended Kalman filter and smoother is applied to a nonlinear system model. Finally in section C.3 the Maximum Likelihood estimation is applied to a deterministic nonlinear system model.
For more details on the algorithms the reader is referred to [71 and 76].

C.1 Kalman Filter/Smoother Applied to a Linear System Model

In this section the kinematical model described by (3.1-4) and (3.1-5) is linearized around a nominal steady flight condition. The linearized kinematical model can be written as:

$$\begin{aligned} \dot{\underline{x}}(t) &= F\underline{x}(t) + G_u\underline{u}_m(t) + G_w\underline{w}(t) \\ \underline{y}(t) &= H\underline{x}(t) + J\underline{u}_m(t) \\ \underline{y}_m(i) &= \underline{y}(i) + \underline{v}(i) \end{aligned} \qquad \text{(C.1-1)}$$

In these equations $\underline{x}$, $\underline{y}_m$ and $\underline{u}_m$ are actually replaced by their deviations from the constant nominal values. F, G_u, G_w, H and J are the partial vector derivatives of $\underline{f}(\underline{x},\underline{u}_m,\underline{w})$ and $\underline{h}(\underline{x},\underline{u}_m)$ with respect to $\underline{x}$, $\underline{u}_m$ and $\underline{w}$.

The system model may next be discretized as:

$$\begin{aligned} \underline{x}(i+1) &= \Phi\underline{x}(i) + \Gamma_u\underline{u}_m(i) + \Gamma_w\underline{w}(i) \\ \underline{y}_m(i) &= H\underline{x}(i) + J\underline{u}_m(i) + \underline{v}(i) \end{aligned} \qquad \text{(C.1-2)}$$

In which the transition matrix Φ, the deterministic input distribution matrix Γ_u and the stochastic input distribution matrix Γ_w are calculated with:

$$\begin{aligned} \Phi &= I + \sum_{q=1}^{Q} \frac{1}{q!} F^q \Delta t^q \\ \Gamma_u &= \left[I + \sum_{q=1}^{Q} \frac{1}{(q+1)!} F^q \Delta t^q \right] G_u \Delta t \\ \Gamma_w &= \left[I + \sum_{q=1}^{Q} \frac{1}{(q+1)!} F^q \Delta t^q \right] G_w \Delta t \end{aligned} \qquad \text{(C.1-3)}$$

where Q is chosen to be sufficiently large to guarantee the accuracy of the calculation.

Assumptions

1) The process and measurement noises are zero mean and white with:

$$\begin{aligned} E\{\underline{w}(i)\} &= \underline{0}, & E\{\underline{w}(i)\underline{w}^T(i)\} &= V_{ww}, \\ E\{\underline{v}(i)\} &= \underline{0}, & E\{\underline{v}(i)\underline{v}^T(i)\} &= V_{vv}, \\ & & E\{\underline{w}(i)\underline{v}^T(i)\} &= O. \end{aligned} \qquad \text{(C.1-4)}$$

2) The initial state vector $\underline{x}_0$ is a random variable vector and $\underline{w}(i)$ and $\underline{v}(i)$ are assumed to be uncorrelated with $\underline{x}_0$:

$$\begin{aligned} E\{\underline{x}_0\underline{w}^T(i)\} &= E\{\underline{w}(i)\underline{x}_0^T\} = O, \\ E\{\underline{x}_0\underline{v}^T(i)\} &= E\{\underline{v}(i)\underline{x}_0^T\} = O. \end{aligned} \qquad \text{(C.1-5)}$$

The Kalman filter provides a way of estimating the state $\underline{x}(i)$ of the model (C.1-2). The filter has the following two interpretations.

1) If the process and measurement noises are Gaussian, the filter gives the minimum variance estimate of the state. That is, it evaluates the conditional mean of $\underline{x}(k)$ given the past measured data $\{\underline{y}_m(i-1), \underline{y}_m(i-2),...\}$; see Sage and Melsa [71].

2) If the Gaussian assumption is removed, the filter gives the linear minimum variance estimate of the state [71] (i.e., having the smallest unconditional error covariance among all linear estimates), but this will not, in general, be the conditional mean.

The Kalman filter has the following results; see [71]:

i) The one-stage prediction algorithm:

$$\begin{aligned} \hat{\underline{x}}(i+1|i) &= \Phi \hat{\underline{x}}(i|i) + \Gamma_u \underline{u}_m(i) \\ \hat{\underline{x}}(0|0) &= E\{\underline{x}_0\} \end{aligned} \tag{C.1-6}$$

ii) The prediction error covariance matrix algorithm:

$$\begin{aligned} P(i+1|i) &= \Phi P(i|i) \Phi^T + \Gamma_w V_{ww} \Gamma_w^T \\ P(0|0) &= E\{\left[\underline{x}_0 - \hat{\underline{x}}(0|0)\right]\left[\underline{x}_0 - \hat{\underline{x}}(0|0)\right]^T\} \end{aligned} \tag{C.1-7}$$

iii) The Kalman gain algorithm:

$$K(i+1) = P(i+1|i) H^T \left[H P(i+1|i) H^T + V_{vv}\right]^{-1} \tag{C.1-8}$$

iv) The measurement update algorithm:

$$\begin{aligned} \hat{\underline{x}}(i+1|i+1) &= \hat{\underline{x}}(i+1|i) + K(i+1) \times \\ &\left[\underline{y}_m(i+1) - H\hat{\underline{x}}(i+1|i) - J\underline{u}_m(i+1)\right] \end{aligned} \tag{C.1-9}$$

v) The posteriori covariance matrix algorithm:

$$\begin{aligned} P(i+1|i+1) &= \left[I - K(i+1)H\right] P(i+1|i) \\ &= \left[I - K(i+1)H\right] P(i+1|i) \left[I - K(i+1)H\right]^T + \\ &+ K(i+1) V_{vv} K^T(i+1) \end{aligned} \tag{C.1-10}$$

The second formula of Eq. (C.1-10) is considered to be numerically more robust than the first one as it cannot result in a non-symmetric covariance matrix; see Bryson and Ho [233].

Once the Kalman filtering is performed, the Kalman smoother may be applied backwards in time to smooth the estimated state trajectory and to find the initial conditions of the system state equation.

The so-called fixed interval Kalman smoother can be written in the following form [71]:

$$\begin{aligned} K_s(i) &= P(i|i) \Phi^T P(i+1|i)^{-1} \\ \hat{\underline{x}}(i|N) &= \hat{\underline{x}}(i|i) + K_s(i) \left[\hat{\underline{x}}(i+1|N) - \hat{\underline{x}}(i+1|i)\right] \\ P(i|N) &= P(i|i) + K_s(i) \left[P(i+1|N) - P(i+1|i)\right] K_s(i)^T \end{aligned} \tag{C.1-11}$$

C.2 Extended Kalman Filter/Smoother Applied to a Nonlinear System Model

Current practice is to use the complete nonlinear kinematical system model of chapter 3 for nonlinear flight path reconstruction. The model can be written in the following general form:

$$\begin{aligned} \dot{\underline{x}}(t) &= \underline{f}\left(\underline{x}(t), \underline{u}_m(t), \underline{w}(t)\right) \\ \underline{y}(t) &= \underline{h}\left(\underline{x}(t), \underline{u}_m(t)\right) \\ \underline{y}_m(i) &= \underline{y}(i) + \underline{v}(i) \end{aligned} \tag{C.2-1}$$

where $\underline{x}(t)$ is an augmented state vector with the unknown parameters as augmented state variables.

The discrete form of the extended Kalman filter is applied to estimate the state variables of this nonlinear system with the same assumptions as given in section C.1, see also [71].

i) The one-stage prediction algorithm:

$$\begin{aligned} \hat{\underline{x}}(i+1|i) &= \hat{\underline{x}}(i|i) + \int_{t_i}^{t_{i+1}} \underline{f}\left(\hat{\underline{x}}(\tau), \underline{u}_m^*(\tau)\right) d\tau \\ \hat{\underline{x}}(0|0) &= E\{\underline{x}_0\} \end{aligned} \tag{C.2-2}$$

where $\underline{u}^*(\tau)$ denotes a linear or higher order interpolation between $\underline{u}_m(i)$ and $\underline{u}_m(i+1)$.

ii) The one-stage prediction covariance matrix algorithm:

$$\begin{aligned} P(i+1|i) &= \Phi(i+1,i) P(i|i) \Phi(i+1,i) + \\ &+ \Gamma_w(i+1,i) V_{ww} \Gamma_w^T(i+1,i) \\ P(0|0) &= E\{\left[\underline{x}_0 - \hat{\underline{x}}(0|0)\right]\left[\underline{x}_0 - \hat{\underline{x}}(0|0)\right]^T\} \end{aligned} \tag{C.2-3}$$

in which the linearized transition matrix $\Phi(i+1,i)$ is calculated from:

$$\Phi(i+1,i) = I + \sum_{q=1}^{Q} \frac{1}{q!} F^{q}(i) \Delta t^{q} \qquad \text{(C.2-4)}$$

$$F(i) = \left. \frac{\partial \underline{f}\left(\underline{x}(t), \underline{u}_m(i), \underline{w}(i)\right)}{\partial \underline{x}^T} \right|_{\substack{\underline{x} = \hat{\underline{x}}(i|i) \\ \underline{w} = \underline{0}}}$$

and the linearized stochastic input distribution matrices $\Gamma_w(i+1,i)$ and $G_w(i)$ are calculated from:

$$\Gamma_w(i+1,i) = \left[I + \sum_{q=1}^{Q} \frac{1}{(q+1)!} F^{q}(i) \Delta t^{q} \right] G_w(i) \Delta t$$

$$G_w(i) = \left. \frac{\partial \underline{f}\left(\underline{x}(t), \underline{u}_m(i), \underline{w}(i)\right)}{\partial \underline{x}^T} \right|_{\substack{\underline{x} = \hat{\underline{x}}(i|i) \\ \underline{w} = \underline{0}}} \qquad \text{(C.2-5)}$$

where Q again is chosen sufficiently large.
It is important to note that F(i) and $G_w(i)$ are calculated at $\underline{x}=\hat{\underline{x}}(i|i)$, i.e. at the the last estimate of $\underline{x}$, instead of on some nominal flight trajectory. This modified form of the Kalman filter is called the *Extended Kalman Filter*.

iii) The Kalman gain algorithm:

$$K(i+1) = P(i+1|i) H^T(i+1) \times \left[H(i+1) P(i+1|i) H^T(i+1) + V_{vv} \right]^{-1} \qquad \text{(C.2-6)}$$

where the linearized observation matrix is calculated with:

$$H(i+1) = \left. \frac{\partial \underline{h}\left(\underline{x}(t), \underline{u}_m(i+1)\right)}{\partial \underline{x}^T} \right|_{\underline{x} = \hat{\underline{x}}(i+1|i)} \qquad \text{(C.2-7)}$$

iv) The measurement update algorithm:

$$\hat{\underline{x}}(i+1|i+1) = \hat{\underline{x}}(i+1|i) + K(i+1) \times \left[\underline{y}_m(i+1) - \underline{h}\left(\hat{\underline{x}}(i+1|i), \underline{u}_m(i+1)\right) \right] \qquad \text{(C.2-8)}$$

v) The posteriori covariance matrix algorithm.

$$\begin{aligned} P(i+1|i+1) &= \left[I - K(i+1) H(i+1) \right] P(i+1|i) \\ &= \left[I - K(i+1) H(i+1) \right] P(i+1|i) \times \\ &\quad \left[I - K(i+1) H(i+1) \right]^T + K(i+1) V_{vv} K^T(i+1) \end{aligned} \qquad \text{(C.2-9)}$$

Again the second formula of Eq. (C.2-9) is considered to be more robust than the first one.

Also for nonlinear system models an extended Kalman smoother may be applied backwards in time to smooth the estimated trajectory and to find the initial conditions of the nonlinear system state equations.

The fixed interval extended Kalman smoother is written as, see also [71]:

$$\begin{aligned} K_s(i) &= P(i|i) \Phi^T(i+1,i) P^{-1}(i+1|i) \\ \hat{\underline{x}}(i|N) &= \hat{\underline{x}}(i|i) + K_s(i) \left[\hat{\underline{x}}(i+1|N) - \hat{\underline{x}}(i+1|i) \right] \\ P(i|N) &= P(i|i) + K_s(i) \left[P(i+1|N) - P(i+1|i) \right] K_s(i)^T \end{aligned} \qquad \text{(C.2-10)}$$

C.3 Maximum Likelihood Estimation Applied to a Deterministic Nonlinear Model

If the system noise $\underline{w}(t)$ is neglected, the flight path reconstruction problem reduces to an output error problem. This can be solved by a Maximum Likelihood algorithm as described below.

In this algorithm, see also Eykhoff [76], the unknown initial conditions $\underline{x}(t_0)$ of the system and the measurement noise covariance matrix V_{vv} are also considered to be unknown parameters together with the set of unknown parameters $\underline{\theta}$ and the Maximum Likelihood estimate of these parameters is computed. The system model to be used in this

case is written in the following form:

$$\begin{aligned} \dot{\underline{x}}(t) &= \underline{f}\left(\underline{x}(t), \underline{u}_m(t), \underline{\theta}\right) \\ \underline{y}(t) &= \underline{h}\left(\underline{x}(t), \underline{u}_m(t), \underline{\theta}\right) \\ \underline{y}_m(i) &= \underline{y}(i) + \underline{v}(i) \end{aligned} \qquad \text{(C.3-1)}$$

where the parameter vector $\underline{\theta}$ consists again of unknown biases and scale factors of the flight test instrumentation system, but now also includes the unknown initial value of $\underline{x}$.

The system is assumed to be deterministic, i.e. the assumption is made here of very small measurement noise from the inertial transducers. Then the joint state and parameter estimation problem can be formulated as a nonlinear optimization problem in which the function to be minimized with respect to $\underline{\theta}$, $\underline{x}(t_0)$ and V_{vv}^{-1} is the negative logarithm of the likelihood function:

$$\begin{aligned} &\ln L\left(\underline{\theta}, \underline{x}_0, V_{vv}^{-1}\right) = \\ &= \frac{1}{2}\sum_{i=1}^{N}\left[\underline{y}_m(i) - \hat{\underline{y}}(i,\underline{\theta})\right]^T V_{vv}^{-1}\left[\underline{y}_m(i) - \hat{\underline{y}}(i,\underline{\theta})\right] + \\ &+ \frac{N}{2}\ln\det V_{vv} \end{aligned} \qquad \text{(C.3-2)}$$

where the covariance matrix of the measurement noise V_{vv} is estimated using:

$$\hat{V}_{vv} = \frac{1}{N}\sum_{i=1}^{N}\left[\underline{y}_m(i) - \hat{\underline{y}}(i,\underline{\theta})\right]\left[\underline{y}_m(i) - \hat{\underline{y}}(i,\underline{\theta})\right]^T \qquad \text{(C.3-3)}$$

The estimated output in Eq. (C.3-3) is obtained by integrating a set of deterministic state equations:

$$\begin{aligned} \hat{\underline{x}}(t_i) &= \underline{x}(t_0) + \int_{t_0}^{t_i} \underline{f}\left(\hat{\underline{x}}(t), \underline{u}_m(t), \underline{\theta}\right) dt \\ \hat{\underline{y}}(i,\underline{\theta}) &= \underline{h}\left(\hat{\underline{x}}(t_i), \underline{u}_m(t_i), \underline{\theta}\right) \end{aligned} \qquad \text{(C.3-4)}$$

The solution algorithm starts by assuming an initial value for $\underline{\theta}$ and using (C.3-4) to calculate a first estimate of $\hat{\underline{x}}(t)$ and $\hat{\underline{y}}(i,\underline{\theta})$. Then $\hat{V}_{vv}$ is estimated using equation (C.3-3) and the log likelihood function is calculated from (C.3-2). A search procedure, such as Gauss-Newton, is then applied to find a better estimate for $\underline{\theta}$. The above procedure is iterated as long as the log likelihood function decreases significantly.

Experience is that from the computational point of view the ML algorithm appears to be more expensive than the extended Kalman filter. Note that the ML method will generate estimates of the measurement error covariance matrix V_{vv} in addition to estimates of the transducer biases and scale factors and the initial state vector. The reader is referred to appendix A for more details of this algorithm.

Annex

AGARD Flight Test Instrumentation and Flight Test Techniques Series

1. Volumes in the AGARD Flight Test Instrumentation Series, AGARDograph 160

Volume Number	*Title*	*Publication Date*
1.	Basic Principles of Flight Test Instrumentation Engineering Issue 1: edited by A. Pool and D. Bosman Issue 2: edited by R.W. Borek and A. Pool	 1974 1994
2.	In-Flight Temperature Measurements by F. Trenkle and M. Reinhardt	1973
3.	The Measurement of Fuel Flow by J.T. France	1972
4.	The Measurement of Engine Rotation Speed by M. Vedrunes	1973
5.	Magnetic Recording of Flight Test Data by G.E. Bennett	1974
6.	Open and Closed Loop Accelerometers by I. Mclaren	1974
7.	Strain Gauge Measurements on Aircraft by E. Kottkamp, H. Wilhelm and D. Kohl	1976
8.	Linear and Angular Position Measurement of Aircraft Components by J.C. van der Linden and H.A. Mensink	1977
9.	Aeroelastic Flight Test Techniques and Instrumentation by J.W.G. van Nunen and G. Piazzoli	1979
10.	Helicopter Flight Test Instrumentation by K.R. Ferrell	1980
11.	Pressure and Flow Measurement by W. Wuest	1980
12.	Aircraft Flight Test Data Processing – A Review of the State of the Art by L.J. Smith and N.O. Matthews	1980
13.	Practical Aspects of Instrumentation System Installation by R.W. Borek	1981
14.	The Analysis of Random Data by D.A. Williams	1981
15.	Gyroscopic Instruments and their Application to Flight Testing by B. Stieler and H. Winter	1982
16.	Trajectory Measurements for Take-off and Landing Test and Other Short-Range Applications by P. de Benque d'Agut, H. Riebeek and A. Pool	1985
17.	Analogue Signal Conditioning for Flight Test Instrumentation by D.W. Veatch and R.K. Bogue	1986
18.	Microprocessor Applications in Airborne Flight Test Instrumentation by M.J. Prickett	1987
19.	Digital Signal Conditioning for Flight Test by G.A. Bever	1991

2. Volumes in the AGARD Flight Test Techniques Series

Number	*Title*	*Publication Date*
AG 237	Guide to In-Flight Thrust Measurement of Turbojets and Fan Engines by the MIDAP Study Group (UK)	1979

The remaining volumes are published as a sequence of Volume Numbers of AGARDograph 300.

Volume Number	*Title*	*Publication Date*
1.	Calibration of Air-Data Systems and Flow Direction Sensors by J.A. Lawford and K.R. Nippress	1983
2.	Identification of Dynamic Systems by R.E. Maine and K.W. Iliff	1985
3.	Identification of Dynamic Systems – Applications to Aircraft Part 1: The Output Error Approach by R.E. Maine and K.W. Iliff Part 2: Nonlinear Model Analysis and Manoeuvre Design by J.A. Mulder, J.K. Sridhar and J.H. Breeman	 1986 1994
4.	Determination of Antenna Patterns and Radar Reflection Characteristics of Aircraft by H. Bothe and D. McDonald	1986
5.	Store Separation Flight Testing by R.J. Arnold and C.S. Epstein	1986
6.	Developmental Airdrop Testing Techniques and Devices by H.J. Hunter	1987
7.	Air-to-Air Radar Flight Testing by R.E. Scott	1988
8.	Flight Testing under Extreme Environmental Conditions by C.L. Henrickson	1988
9.	Aircraft Exterior Noise Measurement and Analysis Techniques by H. Heller	1991
10.	Weapon Delivery Analysis and Ballistic Flight Testing by R.J. Arnold and J.B. Knight	1992
11.	The Testing of Fixed Wing Tanker & Receiver Aircraft to Establish their Air-to-Air Refuelling Capabilities by J. Bradley and K. Emerson	1992

At the time of publication of the present volume the following volumes were in preparation:

Flight Testing of Digital Flight Control Systems
by T.D. Smith

Flight Testing of Terrain Following Systems
by C. Dallimore and M.K. Foster

Reliability and Maintainability
by J. Howell

Testing of Flight Critical Control Systems on Helicopters
by J.D.L. Gregory

Introduction to Flight Test Engineering
edited by F. Stoliker

Space System Testing
by A. Wisdom

Flight Testing of Radio Navigation Systems
by H. Bothe and H.J. Hotop

Simulation in Support of Flight Testing
by L. Schilling

REPORT DOCUMENTATION PAGE			
1. Recipient's Reference	**2. Originator's Reference** AGARD-AG-300 Volume 3 Part 2	**3. Further Reference** ISBN 92-835-0748-7	**4. Security Classification of Document** UNCLASSIFIED/ UNLIMITED
5. Originator	Advisory Group for Aerospace Research and Development North Atlantic Treaty Organization 7 rue Ancelle, 92200 Neuilly sur Seine, France		
6. Title	IDENTIFICATION OF DYNAMIC SYSTEMS – APPLICATIONS TO AIRCRAFT PART 2: NONLINEAR ANALYSIS AND MANOEUVRE DESIGN		
7. Presented on			
8. Author(s)/Editor(s) J.A. Mulder, J.K. Sridhar and J.H. Breeman			**9. Date** May 1994
10. Author(s)/Editor's Address See Flyleaf			**11. Pages** 212
12. Distribution Statement	There are no restrictions on the distribution of this document. Information about the availability of this and other AGARD unclassified publications is given on the back cover.		

13. Keywords/Descriptors

Flight path reconstruction	Nonlinear model identification
Stability and control parameters	Optimal input design
Flight tests	Flight test instrumentation

14. Abstract

This AGARDograph is a sequel to the previous AGARDographs published in the AGARD *Flight Test Techniques Series*, Volume 2 on '*Identification of Dynamic Systems*' and Volume 3 on '*Identification of Dynamic Systems – Applications to Aircraft – Part 1: The Output Error Approach*' both written by R.E. Maine and K.W. Iliff. The intention of the present document is to cover some of those areas which were either absent or only briefly mentioned in these volumes. These areas are *Flight Path Reconstruction, Nonlinear Model Identification, Optimal Input Design and Flight Test Instrumentation.* The present approach to identification is rather different from that presented in the earlier AGARDographs in the sense that the identification problem is decomposed into a state estimation and a parameter identification part. This approach is referred to as the *Two-Step Method* (TSM), although one will find other names like *Estimation Before Modelling* (EBM) in the literature. It will be shown in the present AGARDograph that this approach has significant practical advantages over methods which no attempt is made to decompose the joint parameter-state estimation problem. The two-step method is generally applicable to flight vehicles such as fixed wing aircraft and rotorcraft which are equipped with state of the art inertial reference systems. The theoretical developments in the present AGARDograph will be illustrated with examples of a flight test program with the De Havilland DHC-2 Beaver aircraft, the experimental aircraft of the Delft University of Technology which has been used for almost two decades to test new ideas in the science of aircraft parameter identification.

This AGARDograph has been sponsored by the Flight Mechanics Panel of AGARD.

AGARDograph 300 Volume 3 Part 2
Advisory Group for Aerospace Research and Development, NATO
IDENTIFICATION OF DYNAMIC SYSTEMS – APPLICATIONS TO AIRCRAFT. PART 2: NONLINEAR ANALYSIS AND MANOEUVRE DESIGN
by J.A. Mulder, J.K. Sridhar and J.H. Breeman
Published May 1994
212 pages

This AGARDograph is a sequel to the previous AGARDographs published in the AGARD *Flight Test Techniques Series*, Volume 2 on '*Identification of Dynamic Systems*' and Volume 3 on '*Identification of Dynamic Systems – Applications to Aircraft – Part 1: The Output Error Approach*' both written by R.E. Maine and K.W. Iliff. The intention of the present document is to cover some

P.T.O.

AGARD-AG-300
Volume 3 Part 2

Flight path reconstruction
Stability and control parameters
Flight tests
Nonlinear model identification
Optimal input design
Flight tets instrumentation

AGARDograph 300 Volume 3 Part 2
Advisory Group for Aerospace Research and Development, NATO
IDENTIFICATION OF DYNAMIC SYSTEMS – APPLICATIONS TO AIRCRAFT. PART 2: NONLINEAR ANALYSIS AND MANOEUVRE DESIGN
by J.A. Mulder, J.K. Sridhar and J.H. Breeman
Published May 1994
212 pages

This AGARDograph is a sequel to the previous AGARDographs published in the AGARD *Flight Test Techniques Series*, Volume 2 on '*Identification of Dynamic Systems*' and Volume 3 on '*Identification of Dynamic Systems – Applications to Aircraft – Part 1: The Output Error Approach*' both written by R.E. Maine and K.W. Iliff. The intention of the present document is to cover some

P.T.O.

AGARD-AG-300
Volume 3 Part 2

Flight path reconstruction
Stability and control parameters
Flight tests
Nonlinear model identification
Optimal input design
Flight tets instrumentation

AGARDograph 300 Volume 3 Part 2
Advisory Group for Aerospace Research and Development, NATO
IDENTIFICATION OF DYNAMIC SYSTEMS – APPLICATIONS TO AIRCRAFT. PART 2: NONLINEAR ANALYSIS AND MANOEUVRE DESIGN
by J.A. Mulder, J.K. Sridhar and J.H. Breeman
Published May 1994
212 pages

This AGARDograph is a sequel to the previous AGARDographs published in the AGARD *Flight Test Techniques Series*, Volume 2 on '*Identification of Dynamic Systems*' and Volume 3 on '*Identification of Dynamic Systems – Applications to Aircraft – Part 1: The Output Error Approach*' both written by R.E. Maine and K.W. Iliff. The intention of the present document is to cover some

P.T.O.

AGARD-AG-300
Volume 3 Part 2

Flight path reconstruction
Stability and control parameters
Flight tests
Nonlinear model identification
Optimal input design
Flight tets instrumentation

AGARDograph 300 Volume 3 Part 2
Advisory Group for Aerospace Research and Development, NATO
IDENTIFICATION OF DYNAMIC SYSTEMS – APPLICATIONS TO AIRCRAFT. PART 2: NONLINEAR ANALYSIS AND MANOEUVRE DESIGN
by J.A. Mulder, J.K. Sridhar and J.H. Breeman
Published May 1994
212 pages

This AGARDograph is a sequel to the previous AGARDographs published in the AGARD *Flight Test Techniques Series*, Volume 2 on '*Identification of Dynamic Systems*' and Volume 3 on '*Identification of Dynamic Systems – Applications to Aircraft – Part 1: The Output Error Approach*' both written by R.E. Maine and K.W. Iliff. The intention of the present document is to cover some

P.T.O.

AGARD-AG-300
Volume 3 Part 2

Flight path reconstruction
Stability and control parameters
Flight tests
Nonlinear model identification
Optimal input design
Flight tets instrumentation

of those areas which were either absent or only briefly mentioned in these volumes. These areas are *Flight Path Reconstruction, Nonlinear Model Identification, Optimal Input Design and Flight Test Instrumentation.* The present approach to identification is rather different from that presented in the earlier AGARDographs in the sense that the identification problem is decomposed into a state estimation and a parameter identification part. This approach is referred to as the *Two-Step Method* (TSM), although one will find other names like *Estimation Before Modelling* (EBM) in the literature. It will be shown in the present AGARDograph that this approach has significant practical advantages over methods which no attempt is made to decompose the joint parameter-state estimation problem. The two-step method is generally applicable to flight vehicles such as fixed wing aircraft and rotorcraft which are equipped with state of the art inertial reference systems. The theoretical developments in the present AGARDograph will be illustrated with examples of a flight test program with the De Havilland DHC-2 Beaver aircraft, the experimental aircraft of the Delft University of Technology which has been used for almost two decades to test new ideas in the science of aircraft parameter identification.

This AGARDograph has been sponsored by the Flight Mechanics Panel of AGARD.

ISBN 92-835-0748-7

of those areas which were either absent or only briefly mentioned in these volumes. These areas are *Flight Path Reconstruction, Nonlinear Model Identification, Optimal Input Design and Flight Test Instrumentation.* The present approach to identification is rather different from that presented in the earlier AGARDographs in the sense that the identification problem is decomposed into a state estimation and a parameter identification part. This approach is referred to as the *Two-Step Method* (TSM), although one will find other names like *Estimation Before Modelling* (EBM) in the literature. It will be shown in the present AGARDograph that this approach has significant practical advantages over methods which no attempt is made to decompose the joint parameter-state estimation problem. The two-step method is generally applicable to flight vehicles such as fixed wing aircraft and rotorcraft which are equipped with state of the art inertial reference systems. The theoretical developments in the present AGARDograph will be illustrated with examples of a flight test program with the De Havilland DHC-2 Beaver aircraft, the experimental aircraft of the Delft University of Technology which has been used for almost two decades to test new ideas in the science of aircraft parameter identification.

This AGARDograph has been sponsored by the Flight Mechanics Panel of AGARD.

ISBN 92-835-0748-7

of those areas which were either absent or only briefly mentioned in these volumes. These areas are *Flight Path Reconstruction, Nonlinear Model Identification, Optimal Input Design and Flight Test Instrumentation.* The present approach to identification is rather different from that presented in the earlier AGARDographs in the sense that the identification problem is decomposed into a state estimation and a parameter identification part. This approach is referred to as the *Two-Step Method* (TSM), although one will find other names like *Estimation Before Modelling* (EBM) in the literature. It will be shown in the present AGARDograph that this approach has significant practical advantages over methods which no attempt is made to decompose the joint parameter-state estimation problem. The two-step method is generally applicable to flight vehicles such as fixed wing aircraft and rotorcraft which are equipped with state of the art inertial reference systems. The theoretical developments in the present AGARDograph will be illustrated with examples of a flight test program with the De Havilland DHC-2 Beaver aircraft, the experimental aircraft of the Delft University of Technology which has been used for almost two decades to test new ideas in the science of aircraft parameter identification.

This AGARDograph has been sponsored by the Flight Mechanics Panel of AGARD.

ISBN 92-835-0748-7

of those areas which were either absent or only briefly mentioned in these volumes. These areas are *Flight Path Reconstruction, Nonlinear Model Identification, Optimal Input Design and Flight Test Instrumentation.* The present approach to identification is rather different from that presented in the earlier AGARDographs in the sense that the identification problem is decomposed into a state estimation and a parameter identification part. This approach is referred to as the *Two-Step Method* (TSM), although one will find other names like *Estimation Before Modelling* (EBM) in the literature. It will be shown in the present AGARDograph that this approach has significant practical advantages over methods which no attempt is made to decompose the joint parameter-state estimation problem. The two-step method is generally applicable to flight vehicles such as fixed wing aircraft and rotorcraft which are equipped with state of the art inertial reference systems. The theoretical developments in the present AGARDograph will be illustrated with examples of a flight test program with the De Havilland DHC-2 Beaver aircraft, the experimental aircraft of the Delft University of Technology which has been used for almost two decades to test new ideas in the science of aircraft parameter identification.

This AGARDograph has been sponsored by the Flight Mechanics Panel of AGARD.

ISBN 92-835-0748-7

AGARD
NATO OTAN
7 RUE ANCELLE · 92200 NEUILLY-SUR-SEINE
FRANCE
Télécopie (1)47.38.57.99 · Télex 610 176

DIFFUSION DES PUBLICATIONS
AGARD NON CLASSIFIEES

Aucun stock de publications n'a existé à AGARD. A partir de 1993, AGARD détiendra un stock limité des publications associées aux cycles de conférences et cours spéciaux ainsi que les AGARDographies et les rapports des groupes de travail, organisés et publiés à partir de 1993 inclus. Les demandes de renseignements doivent être adressées à AGARD par lettre ou par fax à l'adresse indiquée ci-dessus. *Veuillez ne pas téléphoner.* La diffusion initiale de toutes les publications de l'AGARD est effectuée auprès des pays membres de l'OTAN par l'intermédiaire des centres de distribution nationaux indiqués ci-dessous. Des exemplaires supplémentaires peuvent parfois être obtenus auprès de ces centres (à l'exception des Etats-Unis). Si vous souhaitez reçevoir toutes les publications de l'AGARD, ou simplement celles qui concernent certains Panels, vous pouvez demander à être inclu sur la liste d'envoi de l'un de ces centres. Les publications de l'AGARD sont en vente auprès des agences indiquées ci-dessous, sous forme de photocopie ou de microfiche.

CENTRES DE DIFFUSION NATIONAUX

ALLEMAGNE
Fachinformationszentrum,
Karlsruhe
D-7514 Eggenstein-Leopoldshafen 2

BELGIQUE
Coordonnateur AGARD-VSL
Etat-Major de la Force Aérienne
Quartier Reine Elisabeth
Rue d'Evere, 1140 Bruxelles

CANADA
Directeur du Service des Renseignements Scientifiques
Ministère de la Défense Nationale
Ottawa, Ontario K1A 0K2

DANEMARK
Danish Defence Research Establishment
Ryvangs Allé 1
P.O. Box 2715
DK-2100 Copenhagen Ø

ESPAGNE
INTA (AGARD Publications)
Pintor Rosales 34
28008 Madrid

ETATS-UNIS
NASA Headquarters
Attention: CF 37, Distribution Center
300 E Street, S.W.
Washington, D.C. 20546

FRANCE
O.N.E.R.A. (Direction)
29, Avenue de la Division Leclerc
92322 Châtillon Cedex

GRECE
Hellenic Air Force
Air War College
Scientific and Technical Library
Dekelia Air Force Base
Dekelia, Athens TGA 1010

ISLANDE
Director of Aviation
c/o Flugrad
Reykjavik

ITALIE
Aeronautica Militare
Ufficio del Delegato Nazionale all'AGARD
Aeroporto Pratica di Mare
00040 Pomezia (Roma)

LUXEMBOURG
Voir Belgique

NORVEGE
Norwegian Defence Research Establishment
Attn: Biblioteket
P.O. Box 25
N-2007 Kjeller

PAYS-BAS
Netherlands Delegation to AGARD
National Aerospace Laboratory NLR
P.O. Box 90502
1006 BM Amsterdam

PORTUGAL
Força Aérea Portuguesa
Centro de Documentação e Informação
Alfragide
2700 Amadora

ROYAUME UNI
Defence Research Information Centre
Kentigern House
65 Brown Street
Glasgow G2 8EX

TURQUIE
Millî Savunma Başkanlığı (MSB)
ARGE Daire Başkanlığı (ARGE)
Ankara

Le centre de distribution national des Etats-Unis ne détient PAS de stocks des publications de l'AGARD.
D'éventuelles demandes de photocopies doivent être formulées directement auprès du NASA Center for Aerospace Information (CASI) à l'adresse suivante:

AGENCES DE VENTE

NASA Center for
Aerospace Information (CASI)
800 Elkridge Landing Road
Linthicum Heights, MD 21090-2934
United States

ESA/Information Retrieval Service
European Space Agency
10, rue Mario Nikis
75015 Paris
France

The British Library
Document Supply Division
Boston Spa, Wetherby
West Yorkshire LS23 7BQ
Royaume Uni

Les demandes de microfiches ou de photocopies de documents AGARD (y compris les demandes faites auprès du CASI) doivent comporter la dénomination AGARD, ainsi que le numéro de série d'AGARD (par exemple AGARD-AG-315). Des informations analogues, telles que le titre et la date de publication sont souhaitables. Veuiller noter qu'il y a lieu de spécifier AGARD-R-nnn et AGARD-AR-nnn lors de la commande des rapports AGARD et des rapports consultatifs AGARD respectivement. Des références bibliographiques complètes ainsi que des résumés des publications AGARD figurent dans les journaux suivants:

Scientifique and Technical Aerospace Reports (STAR)
publié par la NASA Scientific and Technical
Information Program
NASA Headquarters (JTT)
Washington D.C. 20546
Etats-Unis

Government Reports Announcements and Index (GRA&I)
publié par le National Technical Information Service
Springfield
Virginia 22161
Etats-Unis

(accessible également en mode interactif dans la base de données bibliographiques en ligne du NTIS, et sur CD-ROM)

Imprimé par Specialised Printing Services Limited
40 Chigwell Lane, Loughton, Essex IG10 3TZ

AGARD
NATO OTAN
7 RUE ANCELLE · 92200 NEUILLY-SUR-SEINE
FRANCE
Telefax (1)47.38.57.99 · Telex 610 176

DISTRIBUTION OF UNCLASSIFIED AGARD PUBLICATIONS

AGARD holds limited quantities of the publications that accompanied Lecture Series and Special Courses held in 1993 or later, and of AGARDographs and Working Group reports published from 1993 onward. For details, write or send a telefax to the address given above. *Please do not telephone.*
AGARD does not hold stocks of publications that accompanied earlier Lecture Series or Courses or of any other publications. Initial distribution of all AGARD publications is made to NATO nations through the National Distribution Centres listed below. Further copies are sometimes available from these centres (except in the United States). If you have a need to receive all AGARD publications, or just those relating to one or more specific AGARD Panels, they may be willing to include you (or your organisation) on their distribution list. AGARD publications may be purchased from the Sales Agencies listed below, in photocopy or microfiche form.

NATIONAL DISTRIBUTION CENTRES

BELGIUM
Coordonnateur AGARD — VSL
Etat-Major de la Force Aérienne
Quartier Reine Elisabeth
Rue d'Evere, 1140 Bruxelles

CANADA
Director Scientific Information Services
Dept of National Defence
Ottawa, Ontario K1A 0K2

DENMARK
Danish Defence Research Establishment
Ryvangs Allé 1
P.O. Box 2715
DK-2100 Copenhagen Ø

FRANCE
O.N.E.R.A. (Direction)
29 Avenue de la Division Leclerc
92322 Châtillon Cedex

GERMANY
Fachinformationszentrum
Karlsruhe
D-7514 Eggenstein-Leopoldshafen 2

GREECE
Hellenic Air Force
Air War College
Scientific and Technical Library
Dekelia Air Force Base
Dekelia, Athens TGA 1010

ICELAND
Director of Aviation
c/o Flugrad
Reykjavik

ITALY
Aeronautica Militare
Ufficio del Delegato Nazionale all'AGARD
Aeroporto Pratica di Mare
00040 Pomezia (Roma)

LUXEMBOURG
See Belgium

NETHERLANDS
Netherlands Delegation to AGARD
National Aerospace Laboratory, NLR
P.O. Box 90502
1006 BM Amsterdam

NORWAY
Norwegian Defence Research Establishment
Attn: Biblioteket
P.O. Box 25
N-2007 Kjeller

PORTUGAL
Força Aérea Portuguesa
Centro de Documentação e Informação
Alfragide
2700 Amadora

SPAIN
INTA (AGARD Publications)
Pintor Rosales 34
28008 Madrid

TURKEY
Milli Savunma Başkanlığı (MSB)
ARGE Daire Başkanlığı (ARGE)
Ankara

UNITED KINGDOM
Defence Research Information Centre
Kentigern House
65 Brown Street
Glasgow G2 8EX

UNITED STATES
NASA Headquarters
Attention: CF 37, Distribution Center
300 E Street, S.W.
Washington, D.C. 20546

The United States National Distribution Centre does NOT hold stocks of AGARD publications.
Applications for copies should be made direct to the NASA Center for Aerospace Information (CASI) at the address below.

SALES AGENCIES

NASA Center for
Aerospace Information (CASI)
800 Elkridge Landing Road
Linthicum Heights, MD 21090-2934
United States

ESA/Information Retrieval Service
European Space Agency
10, rue Mario Nikis
75015 Paris
France

The British Library
Document Supply Centre
Boston Spa, Wetherby
West Yorkshire LS23 7BQ
United Kingdom

Requests for microfiches or photocopies of AGARD documents (including requests to CASI) should include the word 'AGARD' and the AGARD serial number (for example AGARD-AG-315). Collateral information such as title and publication date is desirable. Note that AGARD Reports and Advisory Reports should be specified as AGARD-R-nnn and AGARD-AR-nnn, respectively. Full bibliographical references and abstracts of AGARD publications are given in the following journals:

Scientific and Technical Aerospace Reports (STAR)
published by NASA Scientific and Technical
Information Program
NASA Headquarters (JTT)
Washington D.C. 20546
United States

Government Reports Announcements and Index (GRA&I)
published by the National Technical Information Service
Springfield
Virginia 22161
United States
(also available online in the NTIS Bibliographic
Database or on CD-ROM)

Printed by Specialised Printing Services Limited
40 Chigwell Lane, Loughton, Essex IG10 3TZ

ISBN 92-835-0748-7